GEORGIA INSTITUTE OF TECHNOLOGY — OFFICE OF CONTRACT ADMINISTRATION

PROJECT ADMINISTRATION DATA SHEET

[X] ORIGINAL [ ] REVISION NO. _____

Project No./(Center No.) E-18-636 (R6287-0A0) GTRC/~~GIT~~ DATE 4 / 7 / 87

Project Director: S.D. Antolovich School/~~Lab~~ MAT Eng.

Sponsor: McDonnell Douglas Corporation
St. Louis, MO

Agreement No.: Standard Research Agreement dated 3/18/87 (Ref. P.O. #Z60511)

Award Period: From 3/16/87 To ~~3/15~~ 9/30/88 (Performance) 3/15/88 Reports

Sponsor Amount:

	New With This Change	Total to Date
Contract Value:	$	$ 50,799
Funded:	$	$ 50,799

Cost Sharing No./(Center No.) _____ Cost Sharing: $ _____

Title: High Temperature Fatigue Behavior of Materials Used in Advanced Airframe Structures

ADMINISTRATIVE DATA

OCA Contact John B. Schonk x4-4820

1) Sponsor Technical Contact:

D.M.Harmon
McDonnell Aircraft Co.
P.O. Box 516
Dept. 337, Bldg. 32
St. Louis, MO 63166

2) Sponsor Issuing Office:

Ken Sutor
McDonnell Douglas Corporation
Box 516
St. Louis, MO 63166

315/232-2010

Military Security Classification: N/A
(or) Company/Industrial Proprietary: N/A

ONR Resident Rep. is ACO: _____ Yes _____ No
Defense Priority Rating: _____

RESTRICTIONS

See Attached N/A Supplemental Information Sheet for Additional Requirements.

Travel: Foreign travel must have prior approval — Contact OCA in each case. Domestic travel requires sponsor approval where total will exceed greater of $500 or 125% of approved proposal budget category.

Equipment: Title vests with Sponsor

COMMENTS:

COPIES TO:

SPONSOR'S I.D. NO. _____

Project Director
Research Administrative Network
Research Property Management
Accounting

Procurement/GTRI Supply Services
Research Security Services
Contract Support Div.(OCA)(2) Pat
Research Communications

GTRC
Library
Project File
Other _____

GEORGIA INSTITUTE OF TECHNOLOGY
OFFICE OF CONTRACT ADMINISTRATION

NOTICE OF PROJECT CLOSEOUT

Closeout Notice Date 04/17/91

Project No. E-18-636 Center No. R6287-0A0

Project Director ANTOLOVICH S D School/Lab MAT ENGR

Sponsor MCDONNELL DOUGLAS CORP/ST LOUIS, MO

Contract/Grant No. Z60511 Contract Entity GTRC

Prime Contract No.

Title STUDY HIGH TEMPERATURE FATIGUE BEHAVIOR OF MATERIALS USED IN ADV. AIRFRAM

Effective Completion Date 891031 (Performance) 891031 (Reports)

Closeout Actions Required:	Y/N	Date Submitted
Final Invoice or Copy of Final Invoice	Y	891205
Final Report of Inventions and/or Subcontracts	Y	891211
Government Property Inventory & Related Certificate	Y	
Classified Material Certificate	N	
Release and Assignment	N	
Other	N	

Comments

Subproject Under Main Project No.

Continues Project No.

Distribution Required:

Project Director	Y
Administrative Network Representative	Y
GTRI Accounting/Grants and Contracts	Y
Procurement/Supply Services	Y
Research Property Managment	Y
Research Security Services	N
Reports Coordinator (OCA)	Y
GTRC	Y
Project File	Y
Other	N
	N

Georgia Tech

Georgia Institute of Technology
Atlanta, Georgia 30332
(404) 894-

November 28, 1988

Dr. Alan H. Rosenstein
Air Force Office of Scientific Research
Building 410
Bolling AFB, D.C. 20332

Dear Dr. Rosenstein:

Enclosed is a brief progress report on AFOSR-87-162 and a request for funding to complete the project. We are now entering the most productive phase of the program and I am expecting exciting and important results.

Should you require further information, please call.

Sincerely

Stephen D. Antolovich, Director
Mechanical Properties Research Lab
Professor and Director
School of Materials Engineering

CYCLIC DEFORMATION, DAMAGE, AND EFFECTS OF ENVIRONMENT IN THE NI_3AL ORDERED ALLOY AT ELEVATED TEMPERATURES

PREPARED BY:

Stephen D. Antolovich

Professor and Director
School of Materials Engineering
Georgia Institute of Technology
Atlanta, Georgia 30332

Progress Report for period 5-1-88 through 12-1-88
Contract No. AFOSR-87-0162

Air Force Office of Scientific Research
Electronic and Material Sciences
Building 410
Bolling AFB, D.C. 20332

Program Manager: Dr. A. H. Rosenstein

Progress Report
AFOSR 87-0162

Prepared by
Stephen D. Antolovich

This project is concerned with the mechanisms of monotonic deformation, cyclic deformation, damage accumulation and fatigue crack propagation in Ni_3Al as affected by composition, temperature and environment. All of these phenomena are important to understand if ordered alloys are to be used in advanced applications.

Based on extensive consultation with other investigators such as C.T. Liu (ORNL) and E.M. Schulson (Darmouth College) the following compositions were chosen:

Nominal Composition (wt. pct)*

Alloy	Al	Ni	Cr	B(ppm)
1	13.28 (25)	86.72 (75)	0	750
2	12.67 (24)	87.33 (76)	0	750
3	10.41 (20)	81.57 (72)	8.02 (8)	750
4	8.64 (17)	83.47 (75)	7.89 (8)	750

* Atomic Pct is shown in brackets. B is in ppm

The alloys were fabricated by Homogeneous Metals, Clayville N.Y., by a PM technique with powders -80 + 400 mesh. Difficulties in maintaining composition were encountered during the initial powder

production phase and some remelting was necessary. The compositions of alloys that were finally supplied are given below.

Actual Composition of Experimental Ni_3Al Alloys (wt. pct.)

Alloy	Al	Ni	Cr	B
1	12.91 (24.34)	87.04 (75.45)	0.00	0.045 (2119)
2	12.41 (23.52)	87.54 (76.24)	0.00	0.048 (2271)
3	10.26 (19.73)	81.51 (72.06)	8.00 (8)	0.046 (2209)
4	8.70 (16.99)	83.55 (74.97)	7.70 (7.80)	0.046 (2242)

These compositions are deemed to be in the range that will yield results consistent with the fundamental thrust of the program as specified in the original proposal.

After some characterization via optical microscopy, SEM and TEM at Georgia Tech, the alloys were sent to Masterson's for machining into tensile, LCF and FCP specimens. To date, we have received LCF and FCP specimens with tensile specimens to follow. Experiments are underway on FCP at 25°C and a graph of crack growth rate vs ΔK is shown in Fig 1.

Since tested specimens of Ni_3Al are only now becoming available, tested specimens of a single crystal Ni base superalloys were used to study deformation mechanisms within the γ' Ni_3Al precipitate. It has been shown that the strength of the alloy at lower temperatures is not only controlled by cross slip of screw segments into cube planes, but also by the formation of faults with the γ'. It will be interesting to see if similar processes are seen

in the pure Ni_3Al.

Dr. Randy Bowman has been responsible for alloy definition, characterization and coordination of specimen fabrication. Dr. Bowman received his Ph.D. in September 1988 working in AFOSR 84-0101 and has accepted a position with NASA-LeRC. He has agreed to stay on to train Mr. Graham Webb in various aspects of TEM and mechanical testing until February 1, 1989. Mr. Webb completed his MS in September 1988 and is currently pursuing his Ph.D. Dr. Bowman has been assisted by both Mr. Webb and Mr. Vessier in various aspects of the project.

As alluded to earlier, good relationships exist with C.T. Liu and E.M. Schulson. Both were consulted in definition of the alloys, and Dr. Schulson did present a seminar at Georgia Tech. In addition, Dr. P. Vessiere of ONERA, France will be at Tech to both present a seminar and to work with Mr. Webb (no funds from the AFOSR grant will be used). Dr. Vessiere is a leading expert on deformation in Ni_3Al and the use of the weak beam TEM technique.

We have now appropriate alloys, specimens and personnel in place and are poised to make rapid progress. Funds in the amount of $112,434 (as stated in the original proposal) are requested to complete the project.

Fig 1. – dadN vs ΔK at R = 0.1 for material "A"

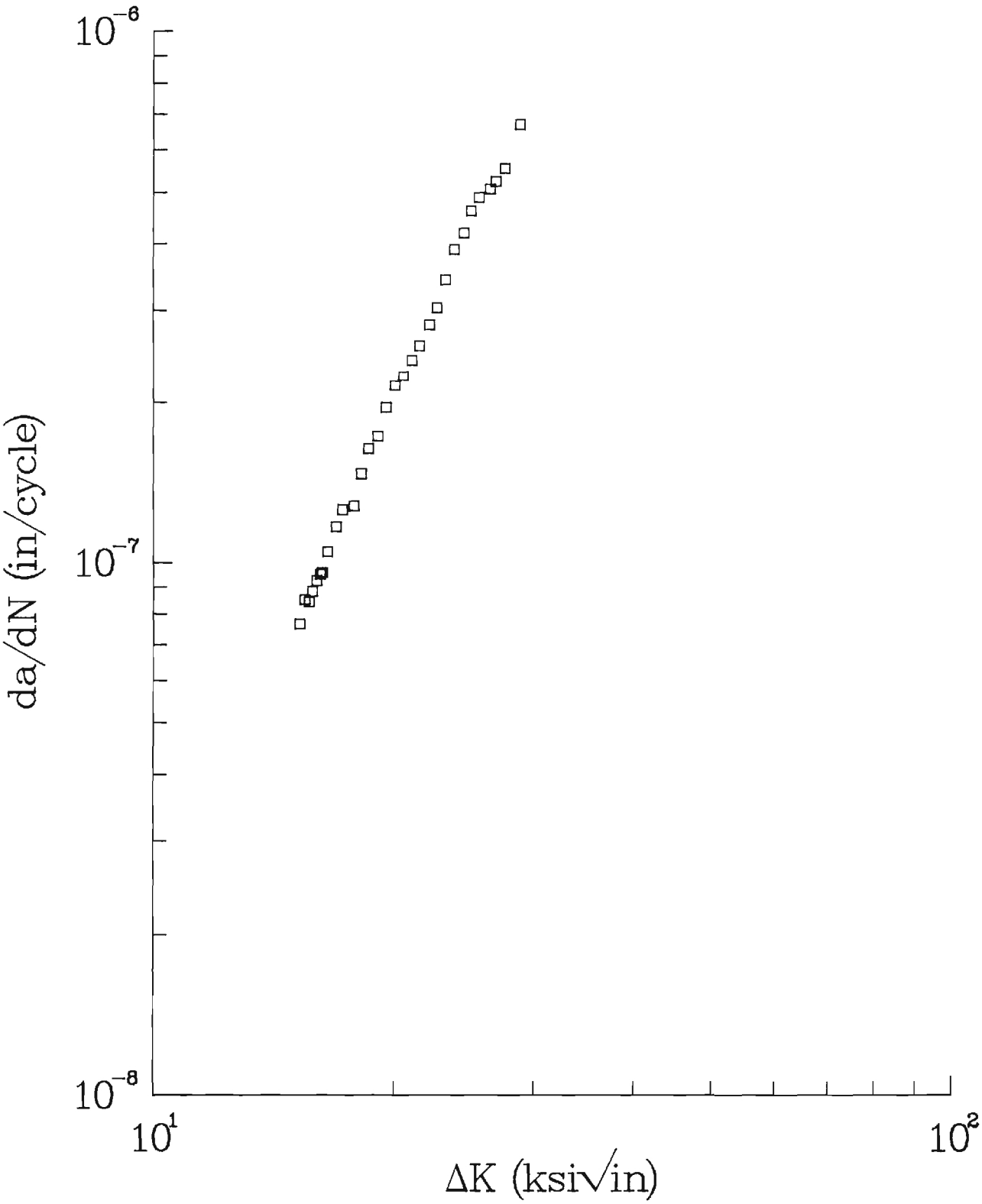

E-18-637

CYCLIC DEFORMATION, DAMAGE, AND EFFECTS OF ENVIRONMENT IN THE Ni_3Al ORDERED ALLOY AT ELEVATED TEMPERATURE

PREPARED BY:

Stephen D. Antolovich

Professor and Director
School of Materials Engineering
Georgia Institute of Technology
Atlanta, Georgia 30332

Graham Webb
Graduate Research Assistant
School of Materials Engineering
Georgia Institute of Technology
Atlanta, Georgia 30332

Progress Report for period 12-1-88 through 6-1-89
Contract No. AFOSR-87-0162

Air Force Office of Scientific Research
Electronic and Material Sciences
Building 410
Bolling AFB, D.C. 20332

Program Manager: Dr. A. H. Rosenstein

Progress Report
AFOSR 87-0162

Prepared by:

Stephen D. Antolovich, P.I.
Graham Webb, Graduate Research Assistant

I. Program Overview

This is the final year of an AFOSR-sponsored program to investigate the mechanisms of cyclic and monotonic deformation in Ni_3Al as a function of composition, temperature, strain rate and environment. In addition to the deformation mechanisms, fatigue crack propagation is also being studied as a function of the same variables. The premise of the program is that it is important to understand these phenomena if ordered alloys are to be used in advanced jet engine components with some degree of confidence.

To date, alloys have been selected, fabricated, processed and machined into specimens. Work has been done in the areas of characterization of the microstructure, tensile testing as a function of temperature composition and strain rate, and FCP testing at room temperature as a function of composition. Details of the studies are given in the subsequent sections and comparisons with information obtained on a previous AFOSR program are given where appropriate.

II. Program Status

A. Material Preparation and Specimen Fabrication

From the extensive consultation with other current investigators in the field such as C. T. Liu (ORNL) and E.M. Schulson (Dartmouth College) nominal alloy compositions were selected as has been reported in previous progress

reports. The materials for the experimental program were produced by Homogeneous Metals, Clayville N.Y. from plasma sprayed powders sized between -80 and +400 mesh. The plasma spray powders were compacted into stainless steel cans, HIPped at 1200° C, then extruded and annealed to produce dense Ni_3Al ingots. The compositions of the alloys obtained from the extruded bars are presented below:

Table I.

Actual Composition of Experimental Ni_3Al Alloys wt. pct. (at. pct.)

Alloy	Al	Ni	Cr	B
A	12.91 (24.34)	87.04 (75.45)	0.00	0.045 (.222)
B	12.41 (23.52)	87.54 (76.25)	0.00	0.048 (.227)
C	10.26 (19.71)	81.69 (72.10)	8.00 (7.97)	0.045 (.221)
D	8.70 (16.99)	83.55 (74.98)	7.70 (7.80)	0.046 (.224)

The composition of alloy A was to be stoichiometric boron modified Ni_3Al which would yield low ductility and intergranular fracture at room temperature. Due to difficulties in maintaining composition during initial powder production, the aluminum content is slightly lower than stoichiometric as revealed by room temperature tensile tests where transgranular fracture and a high strain to failure occurred. With this exception, the compositions of the alloys are deemed satisfactory for the fundamental thrust of the program based upon the chemical analysis and room temperature tensile behavior.

Upon receipt of the extruded bars from Homogeneous Metals, the initial microstructure of each of the alloys was characterized perpendicular and parallel to the extrusion direction by optical metallography Fig. 1. From these photomicrographs it can be seen that the binary alloys (alloy A and alloy B) are predominantly single phase equiaxed Ni_3Al with nominal grain sizes of 26.25 μm

and 20.45 μm respectively. Isolated γ phase precipitates can be seen within grains. Ternary alloy C was found to possess a bimodal distribution of equiaxed grain sizes 3.04μm and 7.56 μm in diameter with disordered γ distributed at grain boundaries indicating heterogeneous nucleation upon cooling. Alloy D was found to be equiaxed single phase γ' grains with a nominal grain size of 10.05 μm. Some indications of a fine lamellar distribution of disordered γ will be verified by TEM. As the grain size of the ternary alloys are significantly smaller than those of the binary alloys, it can be inferred that substitutional chrome acts as a grain refiner of Ni_3Al.

In an effort to characterize the phase structure of the alloys x-ray diffraction was performed at orientations parallel and perpendicular to the extrusion direction of the ingots. The goal of the diffraction experiments was to verify the presence of the $L1_2$ structure in each alloy, determine any preferred orientation due to processing, and examine the effect of the substitutional Cr additions. The results of these experiments are presented as Figs. 2 and 3. Following the diffraction experiments, the presence of the ordered $L1_2$ structure in all alloys was verified by generating a theoretical diffraction pattern using diffraction theory with lattice parameter a = 3.561 Å and space group Pm3m. The comparison between experimental and theoretical diffraction patterns for alloy B in the transverse orientation are presented below:

Table II.

Comparison of Experimental and Theoretical Diffraction Patterns

Index	Experimental		Theoretical	
	d (Å)	I/I_o	d (Å)	I/I_o
100	3.553	6.3	3.564	3.6

110	2.515	3.1	2.520	2.6
111	2.055	100.0	2.057	100.0
200	1.781	37.4	1.782	14.8
210	1.593	2.4	1.594	1.0
211	1.454	1.7	1.454	0.7
220	1.260	15.4	1.260	9.5
300	1.188	0.9	1.188	0.1
310	1.127	0.6	1.127	0.3
311	1.074	9.1	1.074	8.5
222	1.029	5.3	1.029	7.5
320	0.988	0.6	0.988	0.2
321	0.953	0.4	0.953	0.4
400	0.891	4.6	0.891	1.6

From such close correlations between both d-spacing and more importantly relative intensity (within experimental error) the ordered Ll_2 was verified for each of the alloys. From the comparison of <100> family of peaks it was determined that for all alloys, these experimental relative intensities were 2-3 times higher than those predicted. This indicates a preferred <100> texture along the extrusion axis which is consistent with the observations of other investigators at ORNL and NASA for extruded Ni_3Al and NiAl alloys. These observations are to be later verified using crystal orientation techniques by TEM.

Following initial microstructural and phase characterization of all four alloys, the extruded bars of Ni_3Al were shipped to Mastersons Manufacturing Company of Newington, Conn. for producing the specimens for the test program.

The extruded bars of each of the alloys were machined into tensile (Fig. 4), fatigue crack propagation, FCP (Fig. 5), and low cycle fatigue, LCF (Fig. 6), specimens. The exact number of specimens produced for each of the alloys is given below:

Table III.

Specimen number after machining from extruded bars

	Tensile	FCP	LCF
Alloy A	20	12	39
Alloy B	20	12	44
Alloy C	20	12	42
Alloy D	20	12	41

The first shipment of specimens was received on 10-29-88 and the final shipment of specimens was received on 3-31-89.

B. Tensile Behavior

Currently room temperature tensile test have been performed on all alloys in strain control mode at strain rates of 0.5%/min. and 50%/min. on the MTS servohydraulic test machines of the MPRL. In addition, tensile tests have been performed at 600° C at 0.5%/min. also in the strain control mode. The stress-strain curves for the alloys are presented as Figs. 7-9. The results of these tensile tests are summarized below:

Table IV.

Room temperature tensile test results (0.5%/min. and 50%/min.)

	E (ksi)	σ_{ys} (ksi) 0.5%	σ_{uts} (ksi) 0.5%	ϵ_f % 0.5%	σ_{ys} (ksi) 50%	σ_{uts} (ksi) 50%	ϵ_f % 50%
Alloy A	30,000.0	46.0	287.0	49.5	48.9	300.1	51.0

Alloy B	30,000.0	61.0	297.9	55.8	67.4	307.2	42.3
Alloy C	31,000.0	105.5	155.0	16.7	119.0	180.0	13.9
Alloy D	31,000.0	134.4	286.5	39.7	130.9	304.9	39.7

Table V.

600° C tensile test results (all values for 0.5%/min.)

	E (ksi)	σ_{ys} (ksi)	σ_{uts} (ksi)	ϵ_f %
Alloy A	22,000.0	63.7	70.1	1.99
Alloy B	22,000.0	70.5	74.1	0.80
Alloy C	25,000.0	113.7	116.7	10.68
Alloy D	25,000.0	108.7	133.5	22.86

At room temperature all alloys exhibited considerable yield point elongation after an initial "high" yield point which then dropped to the "low" yield value (similar to low carbon steels). The ternary alloys were observed to possess a longer yield point elongation strain range than the binary alloys (6% and 2% respectively). This range of deformation was accompanied by the formation of Luders bands along the gauge length of the specimen. Yield point elongation was then followed by considerable hardening (n = 0.6 to 0.45) to fracture. From Fig. 7 and 8 it can be seen that yield stress increases with decreasing grain size with the exception of alloy C which has a lower yield stress than alloy D even though it possesses a smaller grain size. The inverse relation between yield strength and grain size follows the well known Hall-Petch relation:

$$\sigma_{ys} = \tau_o + Kd^{-\frac{1}{2}} \qquad (1)$$

The deviation of alloy C from Hall-Petch is presently attributed to the bimodal distribution of grain size and the presence of relatively large amounts of disordered γ phase at the grain boundaries, although further TEM investigations on interrupted tests at the onset of yielding are planned to characterize the yielding mechanisms in all of the alloys.

At elevated temperature (T = 600° C) no yield point elongation was observed in any of the alloys. In addition, most alloys did not harden (i.e. perfectly plastic), and in the case of alloy C softened during tensile testing. The binary alloys both fractured after very low elongations (1-2%) where the ternary alloys both retained half of the room temperature elongation. At elevated temperature the Hall-Petch relation between grain size and yield stress is followed in all instances.

Figure 10 demonstrates the trends in failure strain (as determined by reduction in area) vs temperature. As mentioned before the Cr modified alloys retain 50% of room temperature elongation, while the binary alloys fail in a brittle fashion after very little plastic deformation. Figure 11 demonstrates the trend in yield stress vs temperature for the four alloys. From this diagram it can be seen that the yield stress increases with temperature for all but alloy D. This observation is consistent with observations of the deformation response of single crystal Ni_3Al, where the increase in yield strength with temperature is attributed to thermally activated cross slip of screw dislocations from [111] onto [100] planes. As alloy D's yield stress decreased at 600° C (compared to 25° C), the test temperature is obviously beyond the peak temperature for this alloy and cube slip is probably the dominant deformation mode. Figure 12 demonstrates the observed trends in ultimate strength vs temperature for the four alloys. With the notable exception of alloy C, all alloys experienced significant

reduction in ultimate strength at 600° C from that at 25° C. At present the mechanism for this reduction is only known for the binary alloys where oxygen embrittlement at grain boundaries changes the failure mode from transgranular to intergranular fracture. As alloy C experiences brittle intergranular failure at both 25° and 600°C, the ultimate strength is predominantly controlled by extrinsic processing related variables rather than intrinsic changes in material deformation mode. Further TEM investigations are planned to address the decrease in ultimate strength and change in hardening characteristics of the alloys at elevated temperature.

SEM investigations of fractured specimens were used to determine the fracture mode of the alloys at 25° and 600° C. Figure 13 demonstrates the fracture surfaces of the alloys at room temperature. In all cases, a rate dependence on failure mode was not observed. From these photomicrographs it can be seen that alloys A and B fail in a predominantly transgranular fashion. Alloy A was observed to possess a higher area fraction of intergranular fracture than alloy B, which is consistent with the observations of C.T. Liu on the effect of alloy stoichiometry on fracture mode of B doped Ni_3Al at room temperature[1]. The transgranular fracture regions of these alloys were highly crystallographic indicating a high stacking fault energy promoting planar slip.

Alloy C was observed to fail predominately by intergranular cracking along grain boundaries although some regions of transgranular rupture can be observed. The intergranular fracture of alloy C is characteristic of near stoichiometry Ni_3Al, and is desirable for the program's goals. Alloy D was observed to have failed transgranularly by void nucleation, growth and coalescence as is evidenced by the extremely dimpled fracture surface. The extremely non-crystallographic appearance of the fracture surface indicates that the Cr additions serve to

increase the stacking fault energy of the alloy which produces homogeneous or wavy slip.

Figure 14 demonstrates the appearance of the fracture surfaces of the alloys tested at 600° C at 0.5%/min.. From the photomicrographs it can be seen that the binary alloys fail by widespread intergranular rupture. This mode of failure has been attributed (by other investigators) to oxygen weakening of the grain boundaries due to the increased rate of grain boundary diffusion at elevated temperature. The brittle intergranular fracture mode gives rise to the extremely small elongations of these alloys at elevated temperature, and is the primary motivating factor for the substitutional Cr additions to the two ternary alloys. The failure mode of alloy C at elevated temperature is again intergranular with small amounts of transgranular rupture. This failure mode is once again characteristic of near stoichiometric Ni_3Al. The failure mode of alloy D was once again highly transgranular producing a dimpled fracture surface characteristic of void nucleation, growth and coalescence.

C. Fatigue Crack Propagation

In addition to the tensile tests, FCP tests were performed on each of the alloys at room temperature. The tests were conducted in the load control mode with a R ratio (K_{min}/K_{max}) of 0.1 at a frequency of 20 Hz. During the tests the crack lengths were monitored by both visual and potential drop measurements, and good correlation was observed between the two techniques. In addition, laser extensometer measurements were made of the load-line deflection every 25 mils of crack growth to establish closure loads throughout the fatigue tests. The results of these experiments are presented in Figs. 15-17, where the response of the four intermetallic alloys are compared against the results of two superalloys with differing crack growth rates (best and worst) that were

generated during a previous AFOSR program to determine the effect of alloy chemistry on FCP response. Figure 15 demonstrates the applied ΔK vs da/dN behavior of the alloys. From this it can be seen that alloys A, B and D have superior crack growth resistance in the high ΔK regime than both of the superalloys, although the threshold values of both alloy B and D are lower than the best superalloy but better than the worst superalloy. In all cases the crack growth resistance of alloys A, B, and D is superior to that of alloy C. In addition, it should be noted that alloy D has the lowest Paris growth law exponent of all the alloys, which indicates that it is the least sensitive to changes in ΔK in the Paris growth regime. Alloy C was observed to have a threshold ΔK slightly higher than the worst of the superalloys, but has less fatigue crack resistance than the same superalloy in the high ΔK region. In general it can be seen that the resistance to crack growth of all the Ni_3Al is comparable to that of the superalloys.

When modifying the applied ΔK to account for the effect of crack closure (Fig. 16), the same general trends are again observed. The closure measurements revealed that closure occurred only in the binary alloys in the low ΔK regime ($P_{cl} = 0.3P_{max}$), which was observed to decrease with increasing crack growth until no closure was observed at $da/dN \approx 5 \times 10^{-6}$ in/cycle. In all instances no closure effects were observed in the ternary alloys.

Figure 17 contains the crack growth rate of the alloys versus the CTOD. This type of plot gives an indication of the intrinsic damage tolerance of the material at the crack tip (an effective cyclic strain at the crack tip). From this plot it can be seen that the binary alloys are able to accommodate a much higher effective cyclic strain at the crack tip during subcritical crack growth than both of the ternary alloys and both of the superalloys. The high yield

strength of the ternary alloys tends to limit the amount of damage that can be accommodated during cyclic crack growth as the cyclic plastic zone sizes of these alloys are smaller and thus damage is concentrated in a smaller volume ahead of the crack tip. Although much less resistant to crack growth than the lower yield strength binary Ni_3Al alloys, the crack growth resistance of the ternary alloys is comparable to that of the superalloys which both possess lower yield strengths ($\approx$ 90 ksi), thus the intermetallic alloys are better able to accommodate damage ahead of the growing fatigue crack.

SEM investigations of the fracture surfaces of the Ni_3Al alloys were conducted (Fig. 18) to determine the mechanism of crack growth in these alloys. From the photomicrographs it can be seen that the fracture surfaces of all alloys are highly crystallographic due to planar slip. This mode of crack growth has been determined in the previous work on FCP resistance of superalloys to result in highest crack growth resistance as reversible nature of planar slip reduces the interaction between dislocations. As it is the interaction of dislocations which results in the accumulation of damage at the crack tip, this mode of crack growth is highly desirable for fatigue resistance. The only apparent differences between the fracture morphology of any of the four alloys is the roughness of the fracture surface. Alloy D is a notable example in which the degree of roughness is extremely low. These differences can again be linked to relative differences in the stacking fault energy of the alloys which effects the ease at which planar slip occurs. Linear roughness parameter studies are planned for each of the alloys to quantify the roughness of each of the alloys which can then be correlated to differences in crack growth rates in addition to microstructural damage accumulation mechanisms.

III. Program Directions

The experimental program is currently on schedule with the arrival of all the specimens and will progress quite quickly. In this section the remaining tests to be performed will be described in some detail.

A. Tensile

At present half of the tensile tests have been performed in the air environment with tests at 600° C at a strain rate of 50%/min., and 1000° C at 0.5% and 50%/min. remaining. The objective of these tests will be the characterization of the strain rate sensitivity of the alloys at elevated temperature. The tensile high temperature tensile tests are currently underway and will be completed within two weeks.

In addition to these tests, several interrupted tensile tests are to be performed at 25°, 600°, and 1000° C in an effort to characterize the deformation mode and static hardening characteristics of the various alloys using TEM. Due to the rather sensitive characteristics of strain control testing at elevated temperature, these tests will be completed by the end of August using a computer controlled SATEC servohydraulic test machine which will allow extremely accurate interruption of the tensile tests at various elongations of interest (i.e. onset of yielding, within yield point elongation, and during hardening stages of tensile tests).

B. FCP

All room temperature FCP tests have been performed, and all of the FCP specimens have been precracked and have had resistance leads welded on. The completion of the FCP tests at elevated temperatures will proceed rapidly, and is slated for the end of June.

C. LCF

Currently none of the LCF tests have been performed, although the majority of the samples have been electropolished and are ready for testing. LCF tests in air will be run at each of the three temperatures of interest at a constant plastic strain amplitude of 0.1% which is intended to obtain lives of ≈1000 cycles. The LCF tests will be interrupted after 1/4 cycle, stress saturation, and mid-life; and then examined by TEM to determine the cyclic deformation mechanisms that occur during the various phases of fatigue life. The results of the LCF tests will then be correlated to the damage processes occurring ahead of crack tip in the FCP investigations. The LCF tests in air are to be run co-current with the interrupted tensile tests in the computer controlled SATEC servohydraulic test machines with GEMSTAR computer data acquisition, and thus will also be completed by September 1989.

D. Vacuum Experiments

Following the completion of the testing in the air environment, the tensile, FCP, and LCF tests will be replicated on alloy B and D in the vacuum chamber mounted onto a MTS servohydraulic test machine in the MPRL. The goals of these experiments will be to determine the effect of the oxidizing environment on the mechanical response of the two alloys. These tests are quite difficult to perform at elevated temperature and are hoped to be completed by February of 1990.

D. Deformation Characterization By TEM

A number of important microstructural features need characterization by TEM, including the distribution of γ phase within the alloys, as well as the identification of the various static and cyclic deformation characteristics. At present a successful technique has been developed for quickly, and <u>consistently</u> producing foils from the Ni_3Al alloys sufficiently thin to permit

TEM observations. In addition, the techniques necessary for crystal orientation and identification of dislocation character are being perfected. The TEM experiments are to be performed co-current with the mechanical testing as to knowledgeably guide further experimentation.

F. Modelling Activity

The ultimate goal of the program is the completion of physically based model for the predication of cyclic response of Ni_3Al alloys at ambient and elevated temperatures. The model to be developed will be based upon an initial model developed 6 months ago at Georgia Tech by Dr. Walter Milligan during his PhD research. Dr. Milligan investigated the static and cyclic deformation properties of a commercial single crystal nickel based superalloy at ambient and elevated temperatures. The model is fundamental and based upon the thermally aided cross-slip model first proposed by D.P. Pope of the University of Pennsylvania. This model links the cyclic response of ordered intermetallic Ni_3Al to the irreversibility of cross-slip in persistant slip bands during cyclic deformation. The current and remaining mechanical testing as well as the TEM investigations of this experimental program will be directed towards developing a working model based upon this initial premise by the completion date of the program.

IV. Personnel

Dr. Antolovich serves as the P.I. for this program.

Dr. Randy Bowman was responsible for alloy definition and some of the initial testing and characterization. He is presently employed as a Research Scientist by NASA-LeRC in Cleveland where is working on NiAl. He is maintaining close contact with this project and serves as an unofficial consultant with the

agreement of his supervisor, Dr. Hugh Gray.

Mr. Graham Webb is the Graduate Research Assistant supported by this project and working towards his Ph.D. It is anticipated that the completion of this project in May, 1990 will correspond roughly to his completion date.

Mr. Rick Brown is a Research Equipment Specialist in the Mechanical Properties Research Laboratory at Georgia Tech and is involved with experimental set-ups and with assisting and training students.

In addition to the above personnel, clerical assistance is provided by Ms. Janice Coleman. Administrative and financial assistance is provided by Ms. Pat Ledon and by Ms. Judy Lorier, all of the School of Materials Engineering.

V. Interactions and Reporting

Good relationships exist with C.T. Liu (ORNL) and Erland Schulson (Dartmouth College). In addition a good working relationship has been established with Dr. P. Vessiere of ONERA, France. Dr. Vessiere is one of the leading authorities on TEM in ordered compounds and he presented a seminar at Georgia Tech in mid December, 1988.

While there was some delay in obtaining specimens, all specimens are now available and we expect to be publishing a number of articles in the up-coming year. **We will be making a presentation at the International Conference on High Temperature Aluminides and Intermetallics at the Fall TMS meeting in October entitled " High Temperature Fatigue Response of Ni_3Al-Structure Property Relations". The paper is authored by Graham Webb, Stephen D. Antolovich, and Randy Bowman.**

VI. Results From Previous AFOSR Project (83-0101)

A paper was presented and published at the Superalloys 1988 conference. The title of the paper is "**The Effect of Microstructure on the Fatigue Crack Growth Resistance of Ni Base Superalloys**". The paper was authored by Randy Bowman and Stephen D. Antolovich and 2 reprints are enclosed.

Dr. Bowman received his Ph.D. (August, 1988) while working on this project and is presently employed as a Research Scientist at NASA-LeRC in Cleveland, Ohio. Mr. Bowman was selected by NATO to attend a NATO Specialists Meeting in Portugal last year.

As a result of the findings of this study, Dr. Antolovich is working as a consultant to Pratt & Whitney to develop a new, fatigue-resistant disk alloy.

Also directly as a result of this study, SNECMA (a large, French engine manufacturer) is fully supporting a graduate student from France to carry out research on some of the remaining alloys.

VII. References

[1] D.P. Pope, and C.T. Liu, "Strength and Ductility of Intermetallic Coumpounds", , Chapter 18, Superalloys, Composites and Ceramics, Tien and Caulfield Eds., pps. 583-624, book to be published 1989.

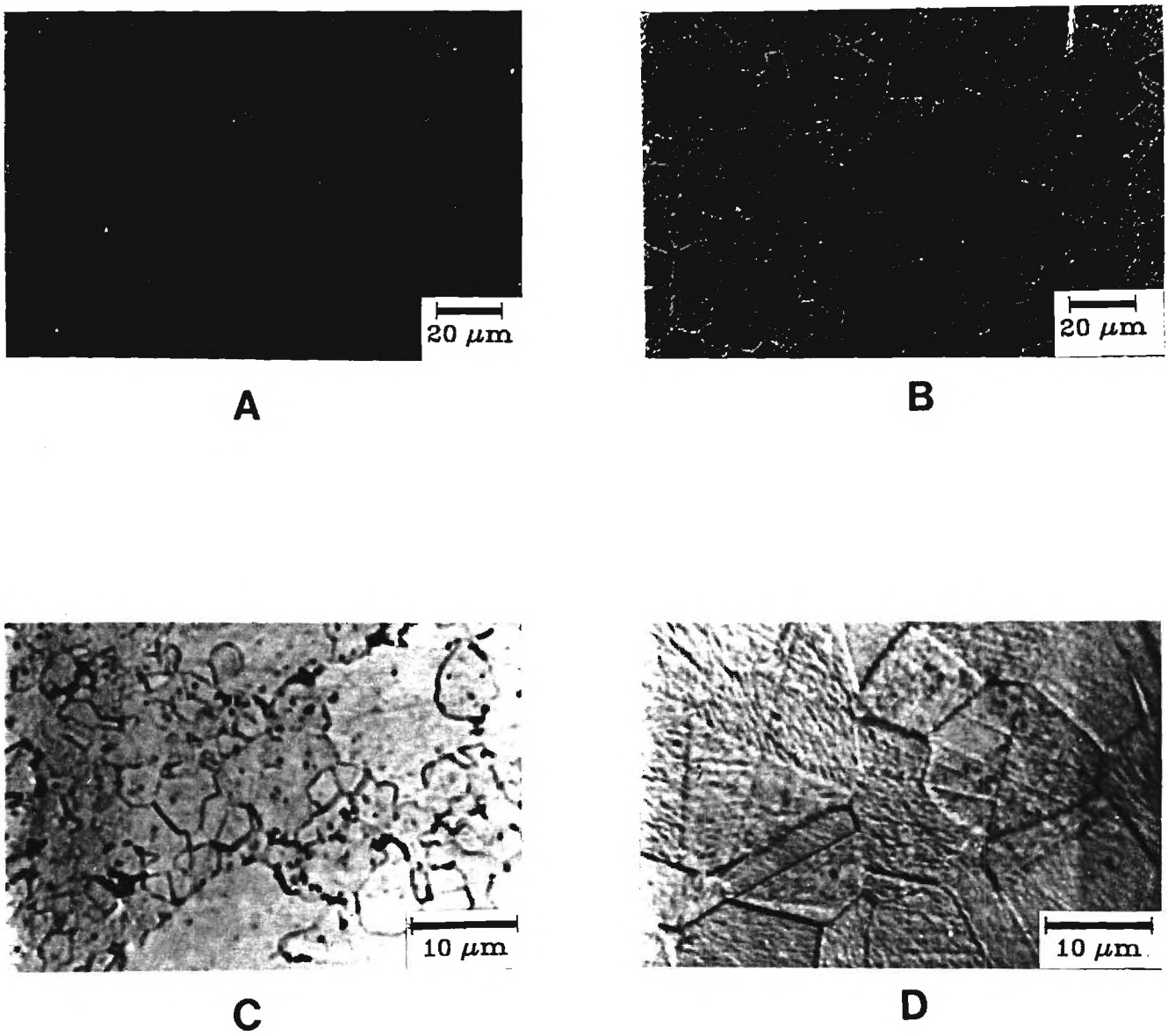

Figure 1. Initial microstructures of Ni_3Al alloys in the transverse orientation, A. Alloy A, B. Alloy B, C. Alloy C, D. Alloy D

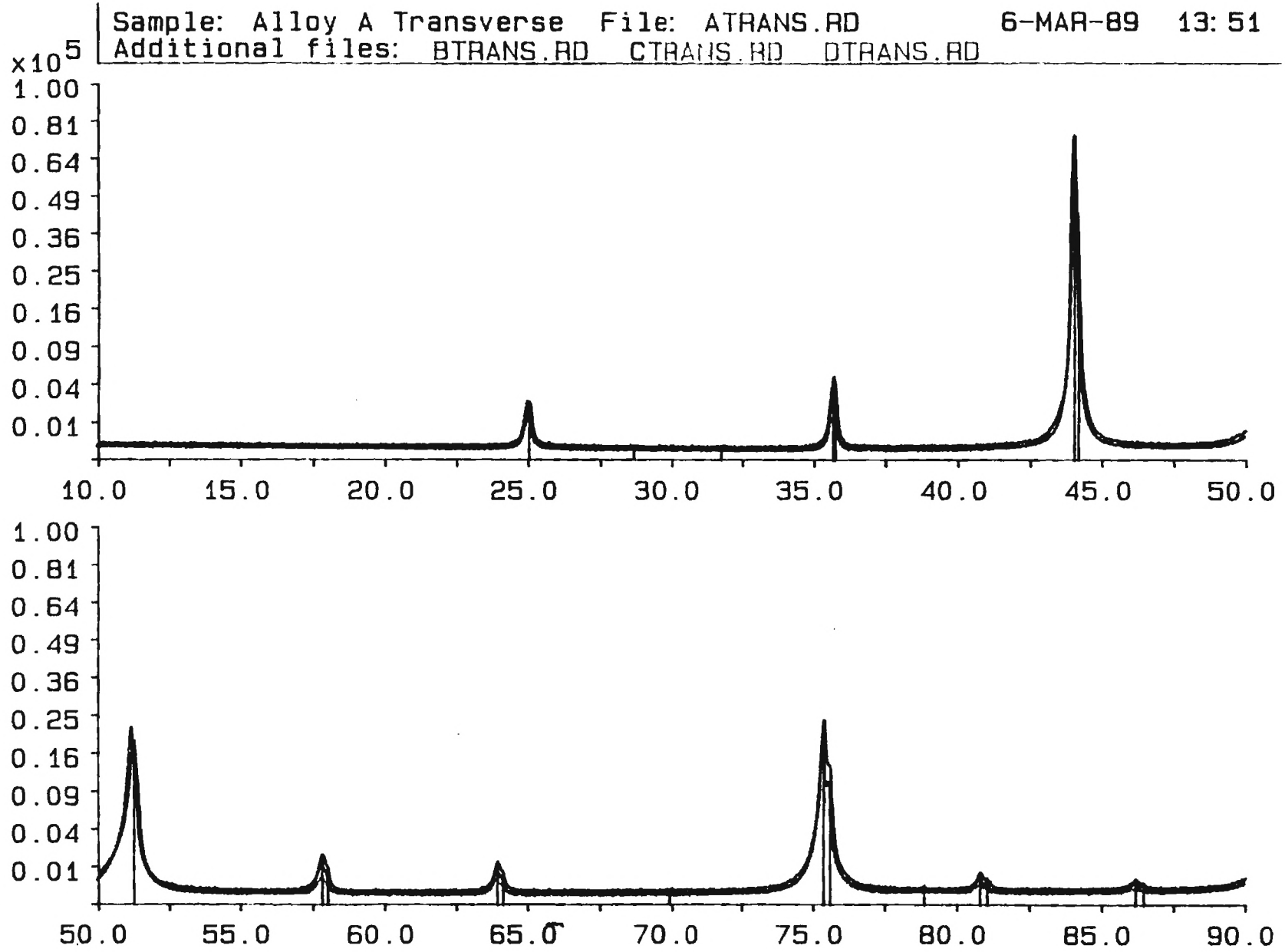

Figure 2. X-ray diffraction patterns for all four alloys in the transverse orientation.

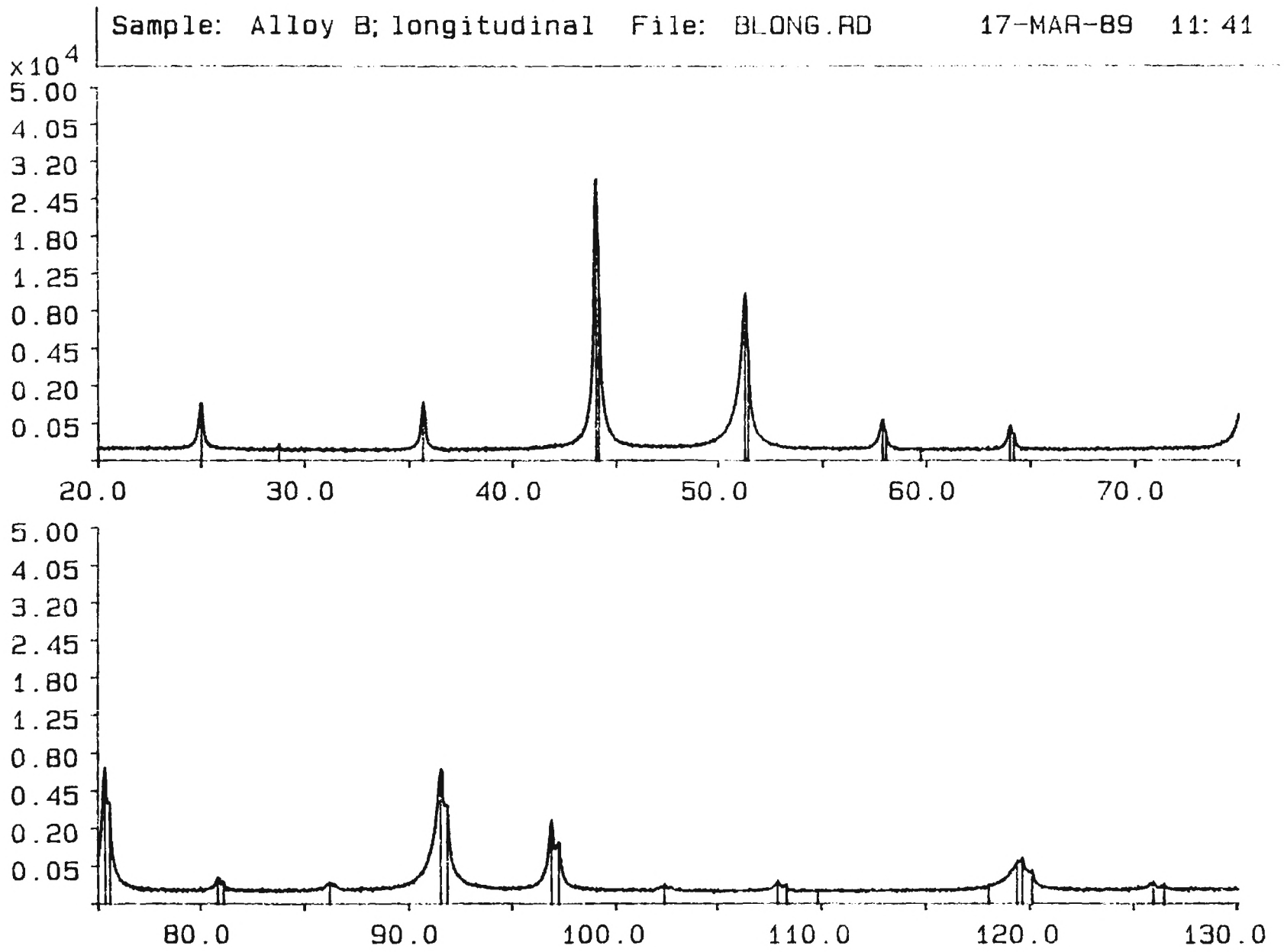

Figure 3. X-ray diffraction pattern for Alloy B in the longitudinal orientation.

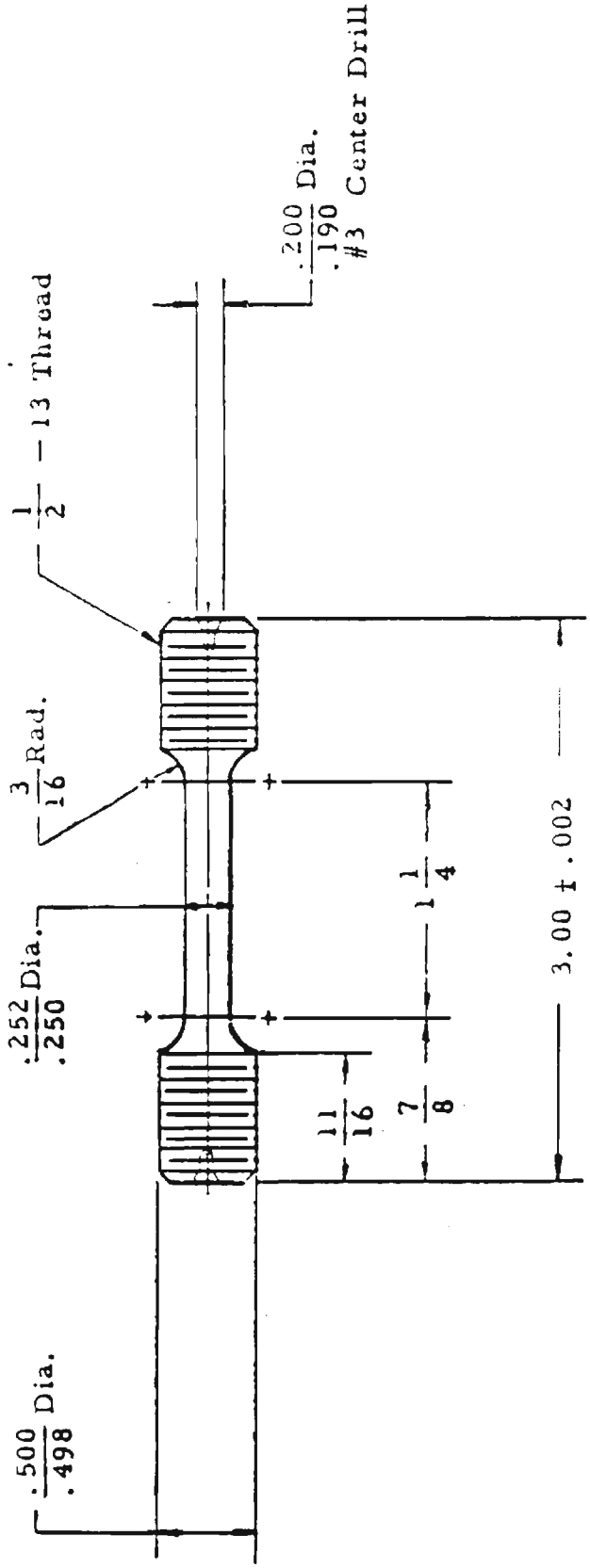

Figure 4. Tensile specimens to be used in the experimental program.

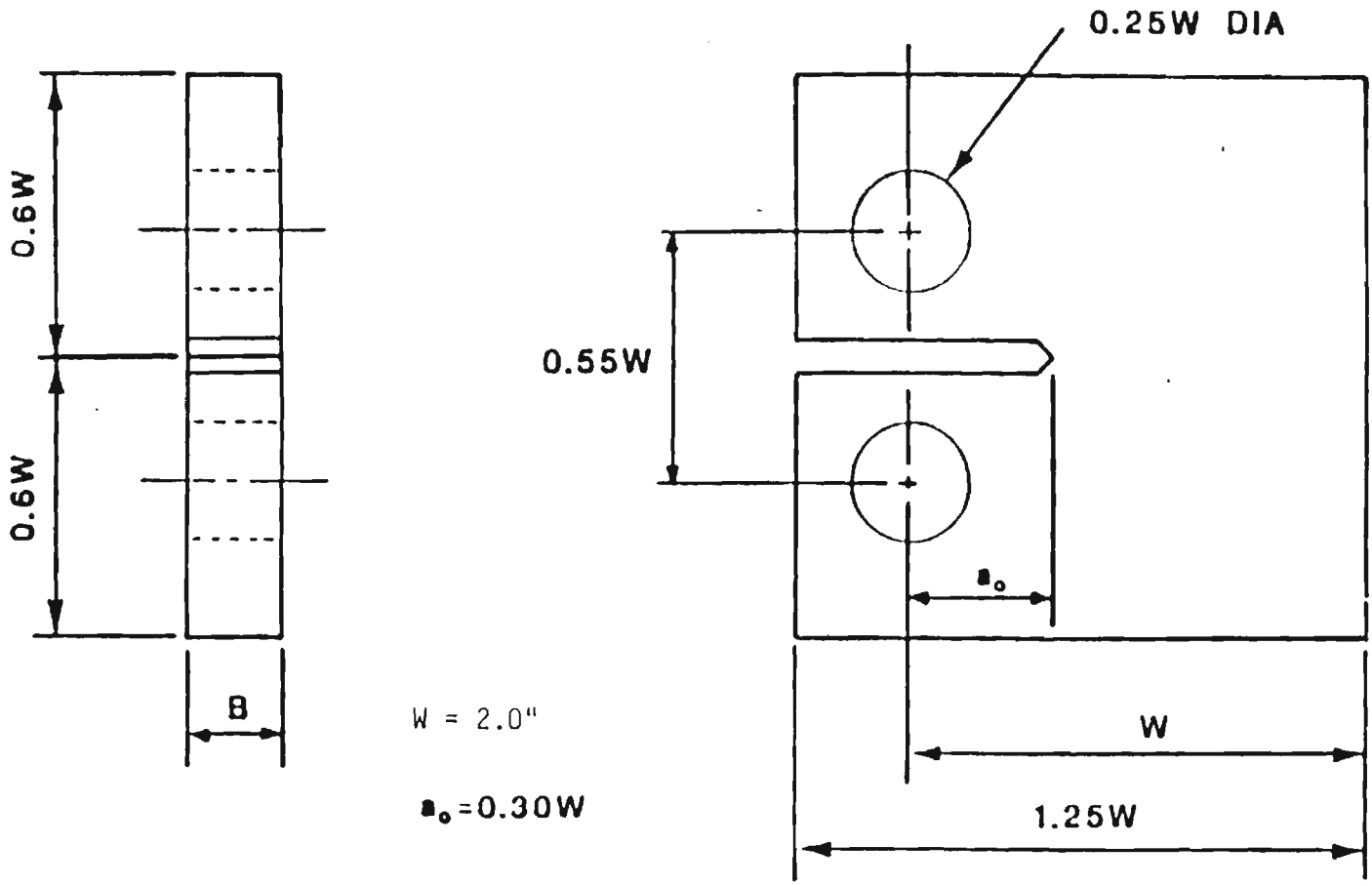

Figure 5. Compact tension type specimen to be employed for fatigue crack propagation studies in the experimental program.

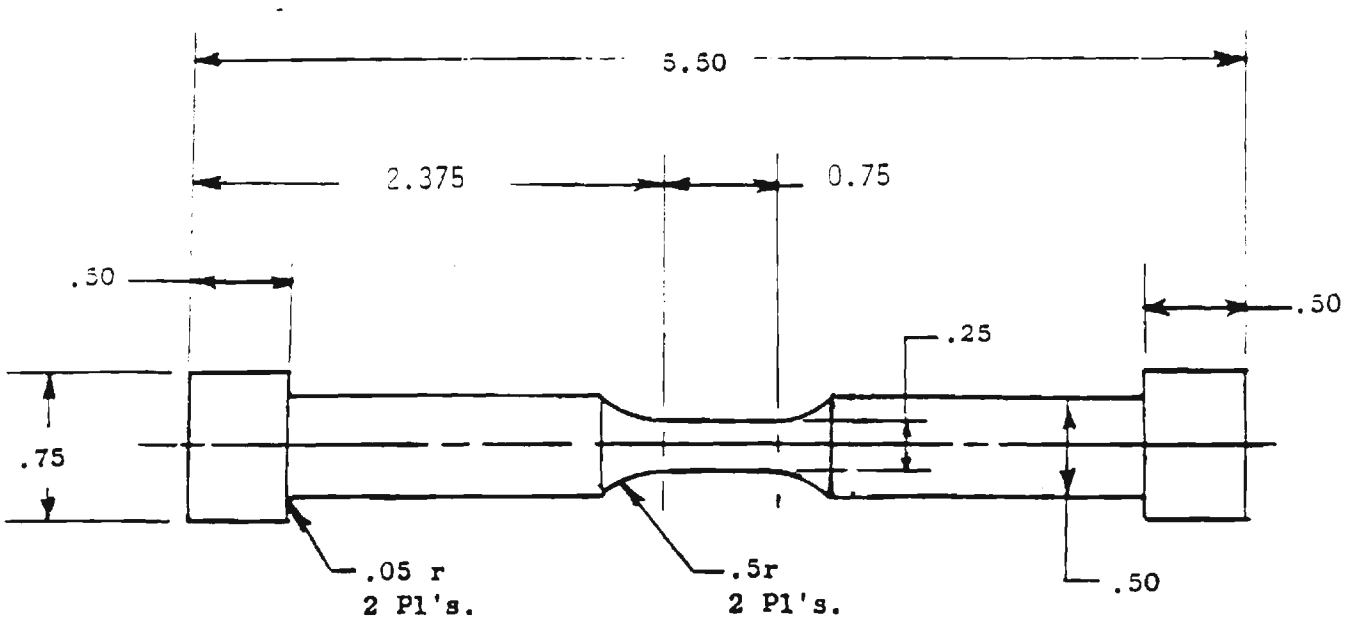

all dimensions in inches

Figure 6. Low cycle fatigue specimens to be employed in the experimental program.

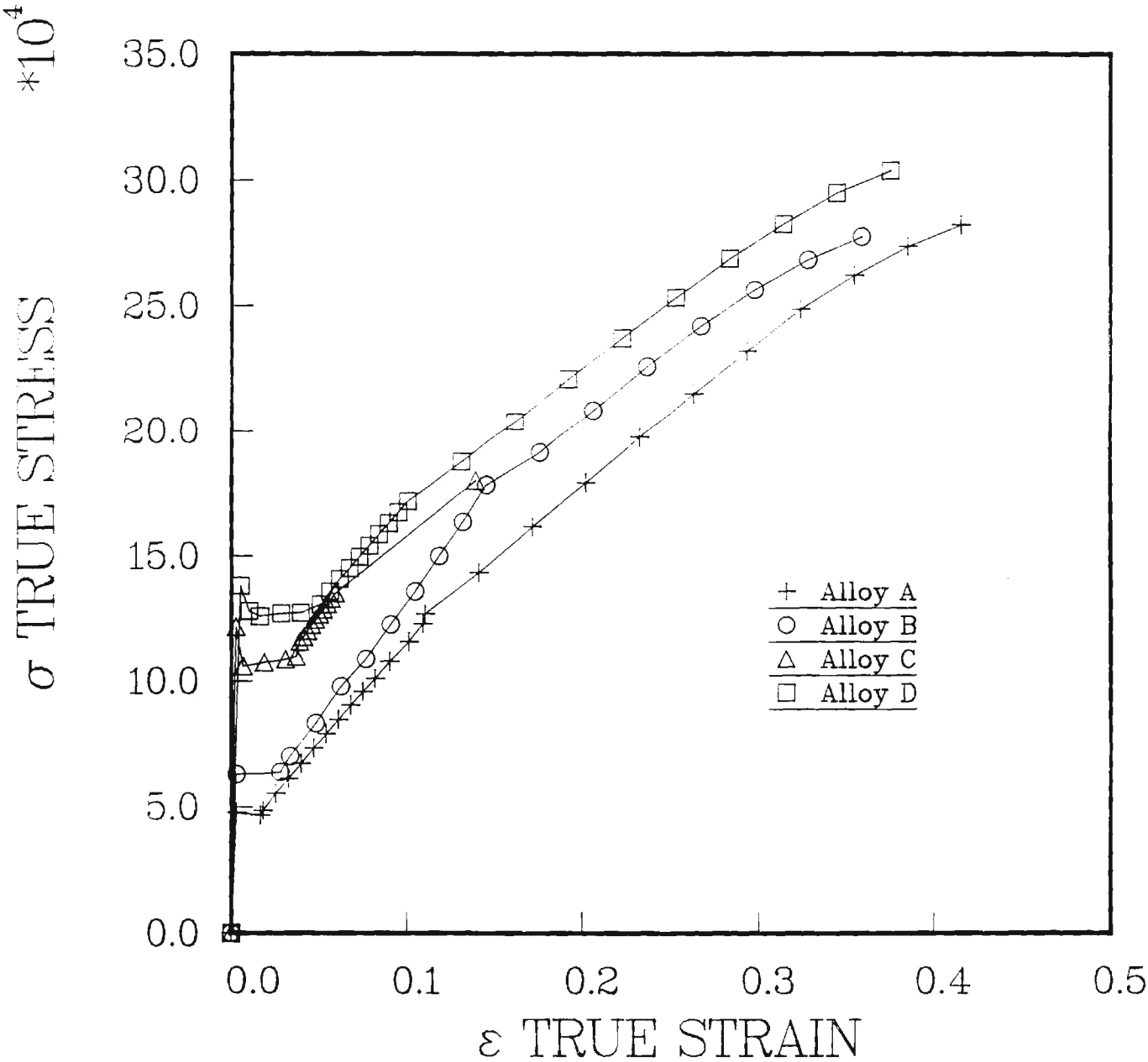

Figure 7. True stress vs true strain curves for the four alloys at room temperature with strain rate 0.5%/min.

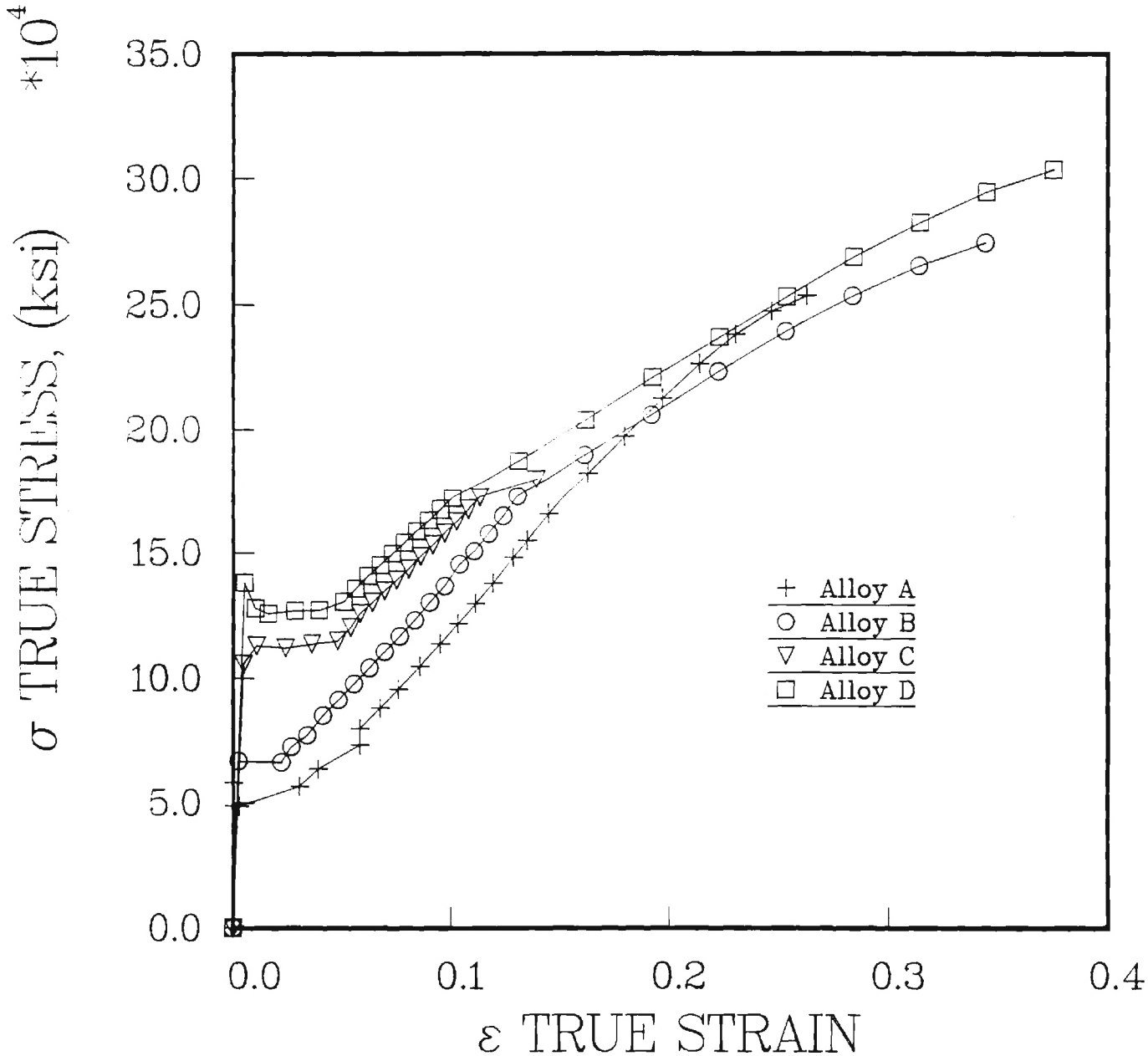

Figure 8. True stress vs true strain for the four alloys at room temperature with a strain rate of 50%/min.

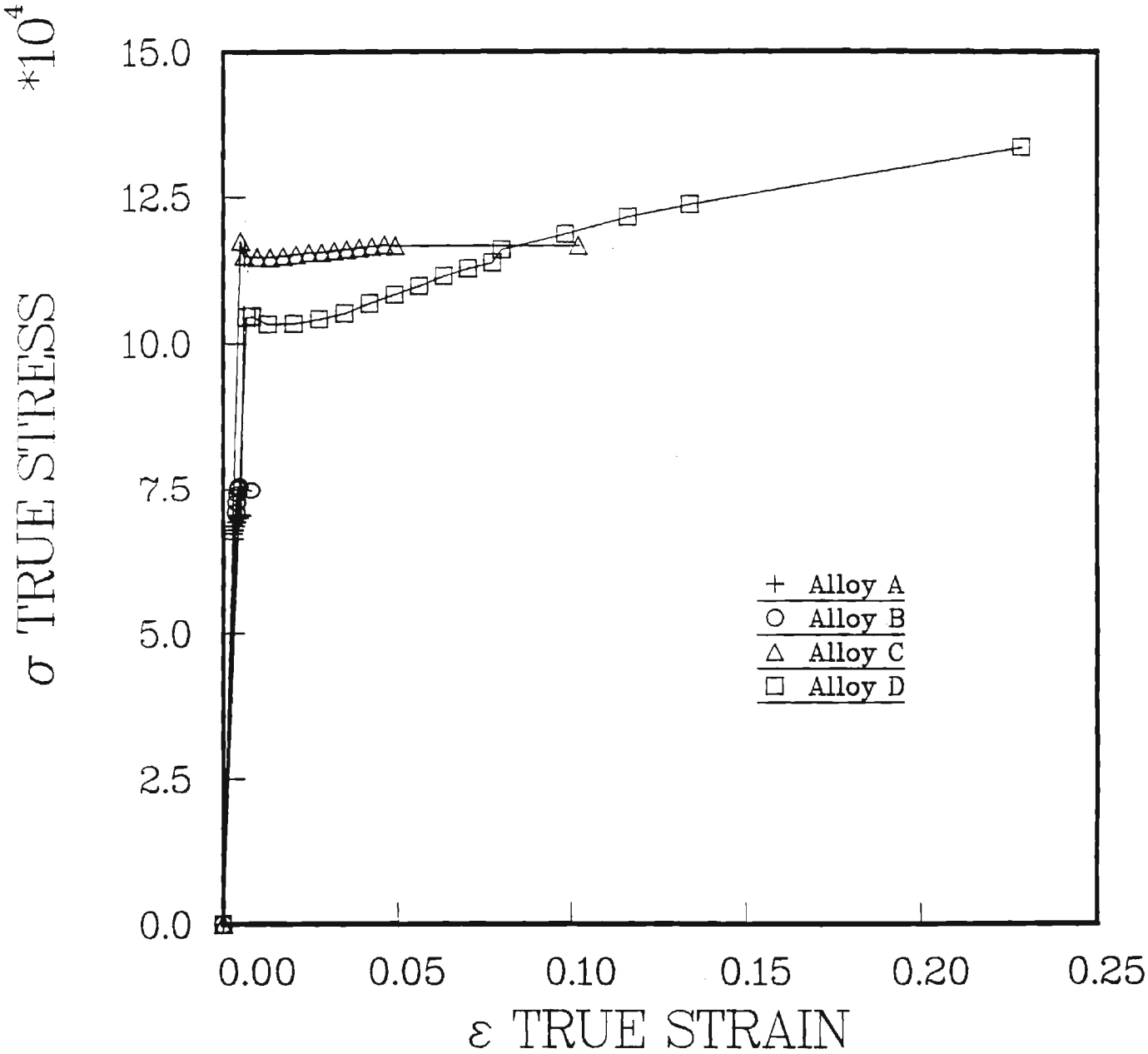

Figure 9. True stress vs true strain for the four alloys at 600° with a strain rate of 0.5%/min.

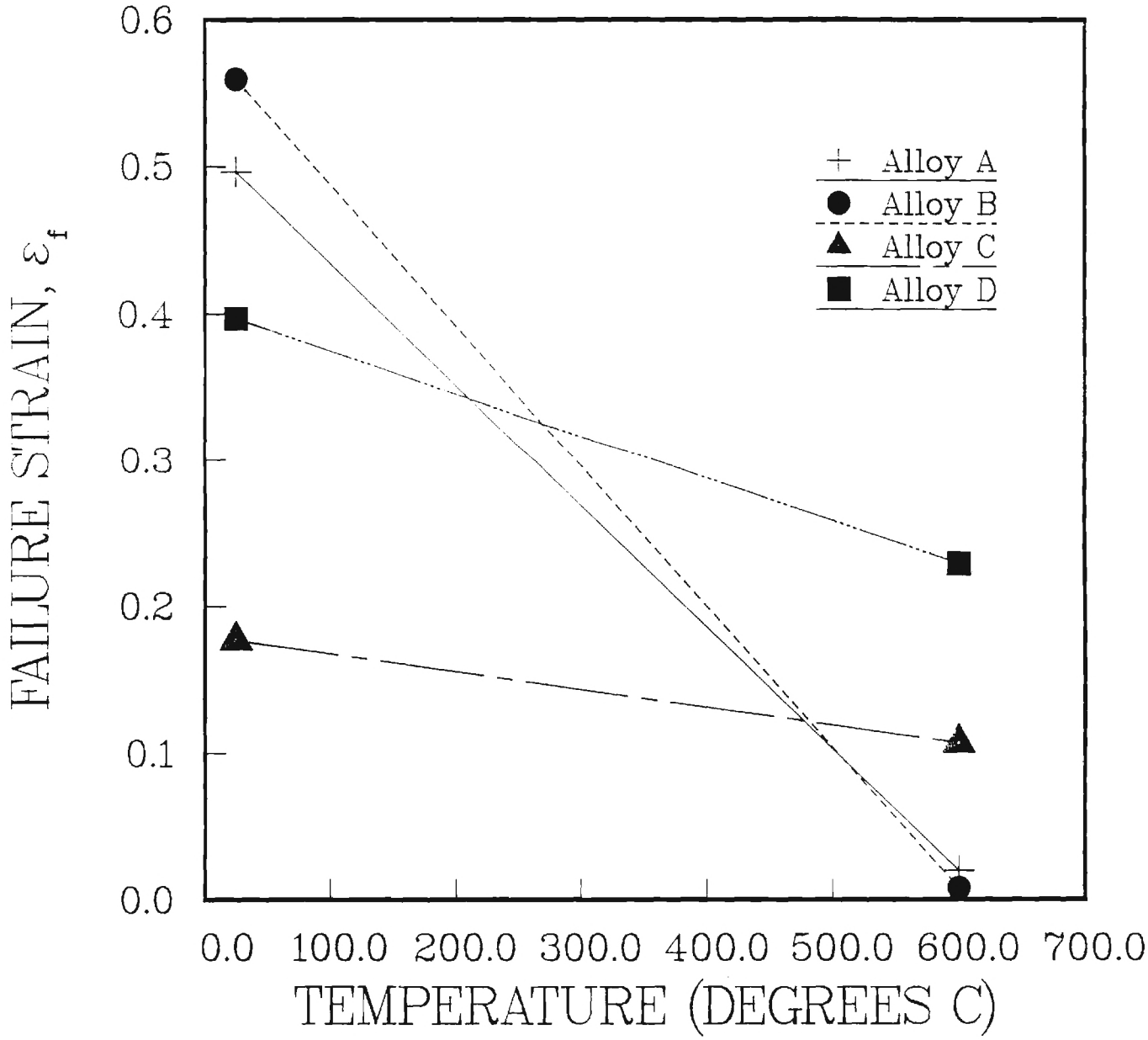

Figure 10. Elongation to failure vs temperature for the four alloys at 0.5%/min..

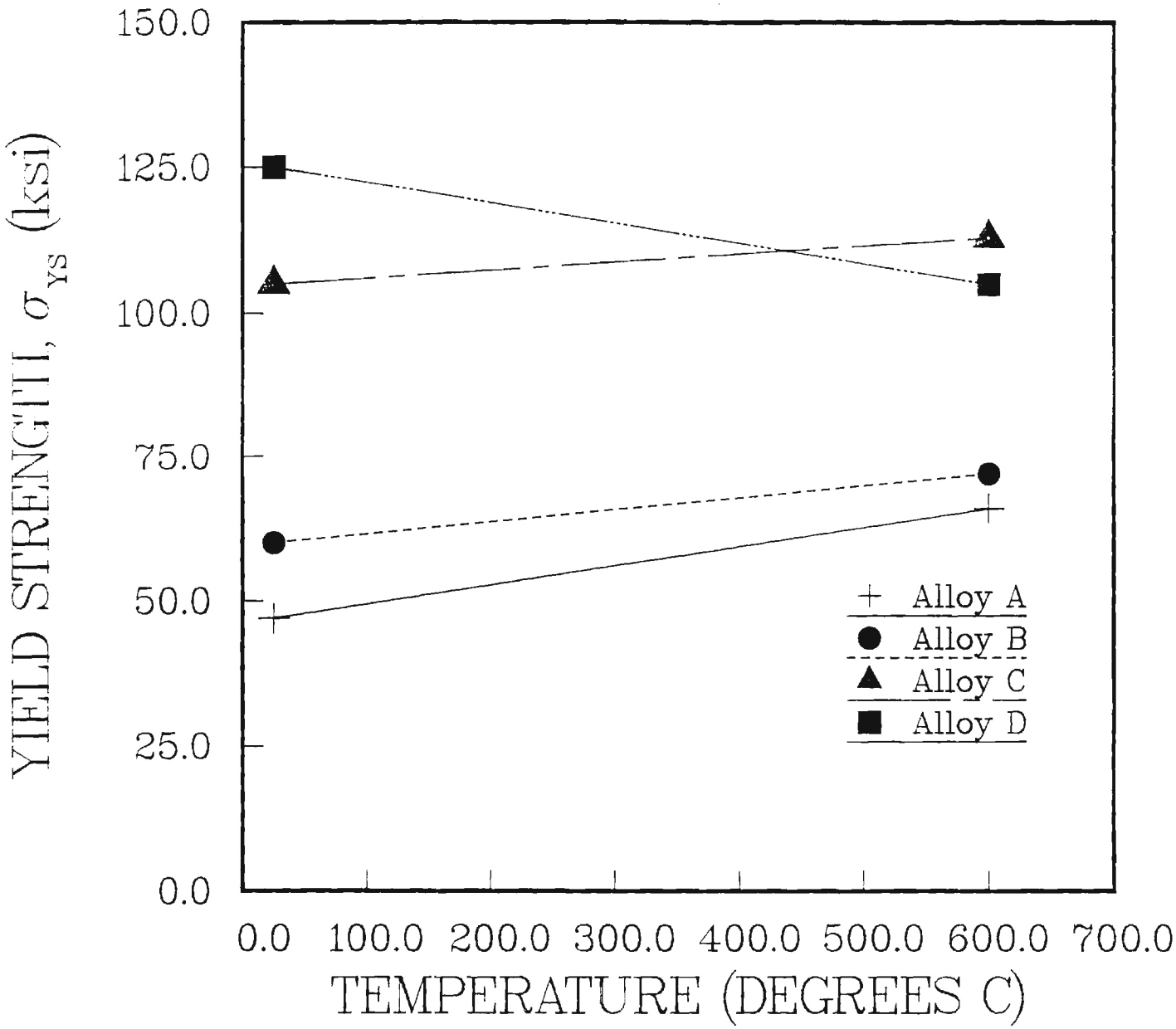

Figure 11. Yield strength vs temperature for the four alloys at 0.5%/min..

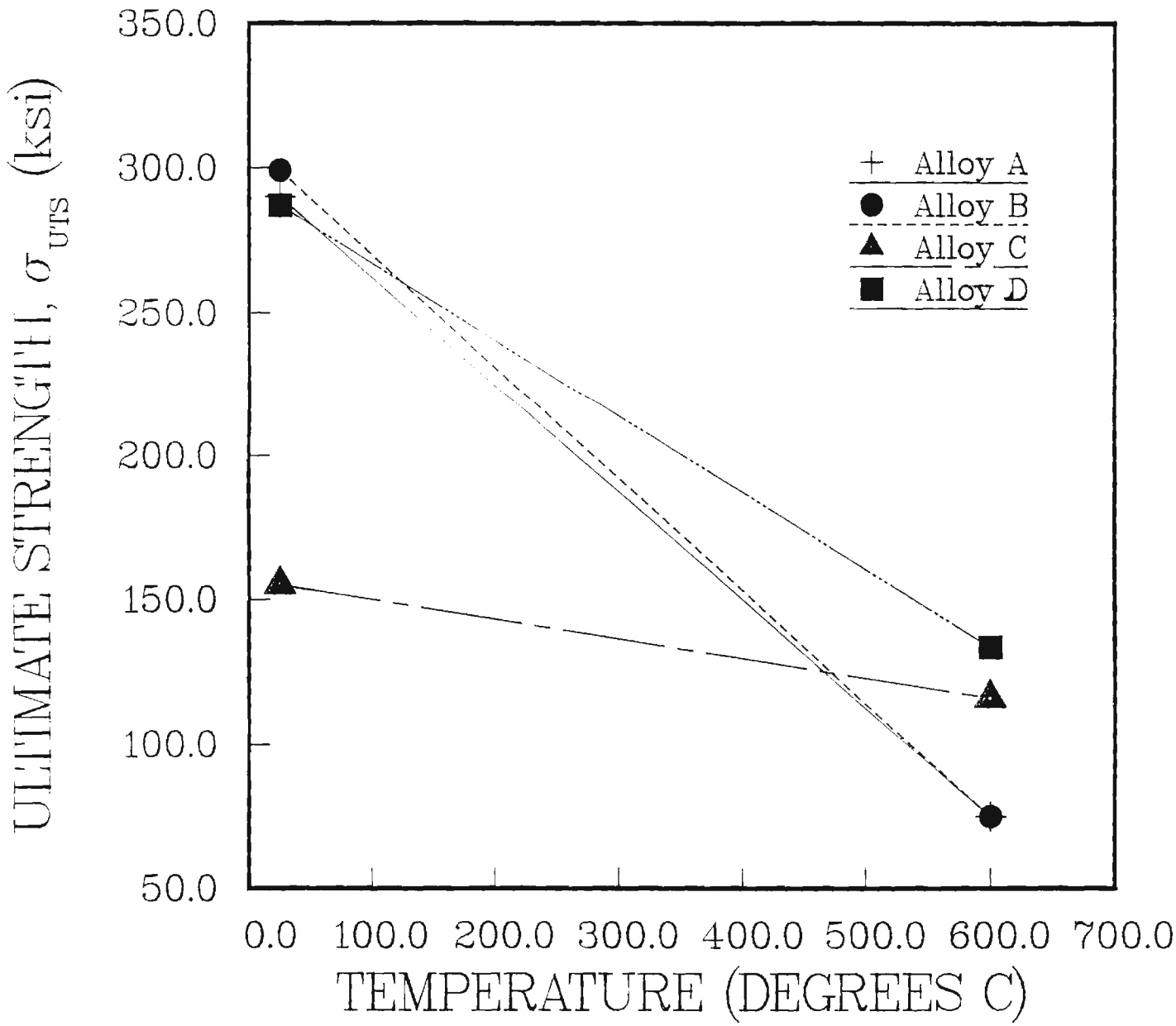

Figure 12. Ultimate tensile strength verse temperature for the four alloys at 0.5%/min..

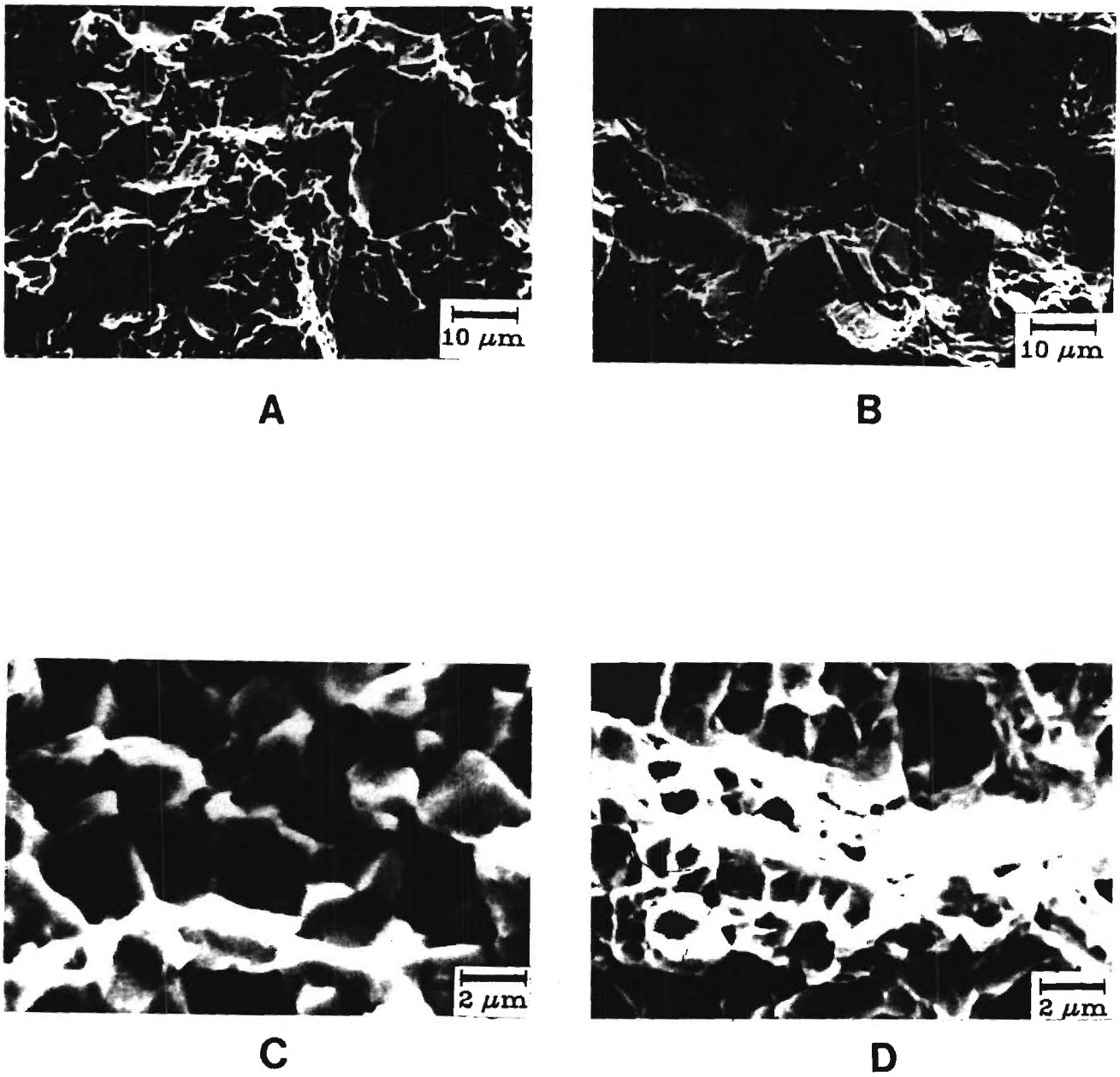

Figure 13. SEM photomicrographs of the four alloys tested at room temperature, A. Alloy A (0.5%/min.), B. Alloy B (50.0%/min.), Alloy C (0.5%/min.), Alloy D (0.5%/min.)

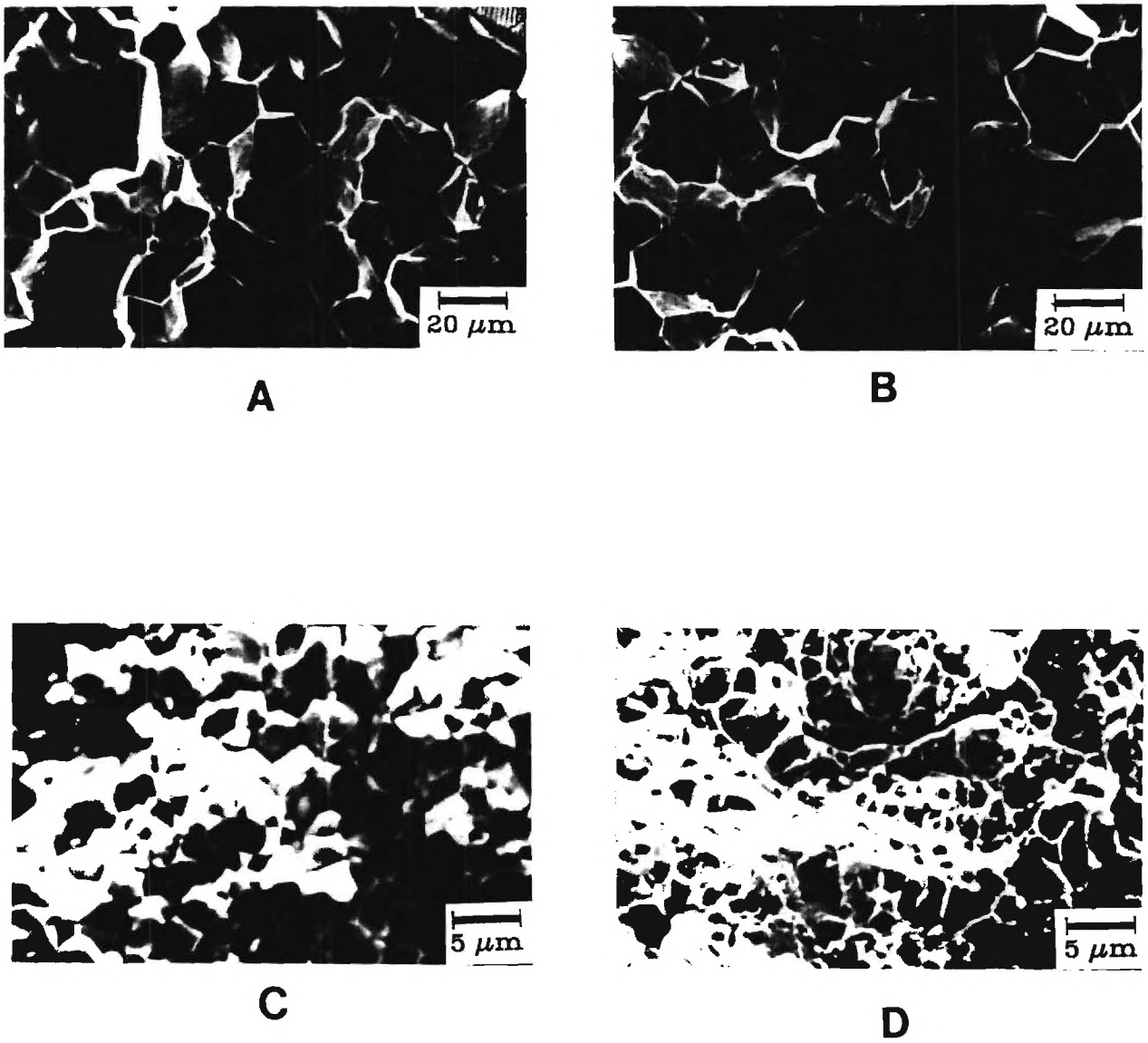

Figure 14. SEM photomicrographs of the four alloys at 600° C at 0.5%/min., A. Alloy A, B. Alloy B, C. Alloy C, D. Alloy D.

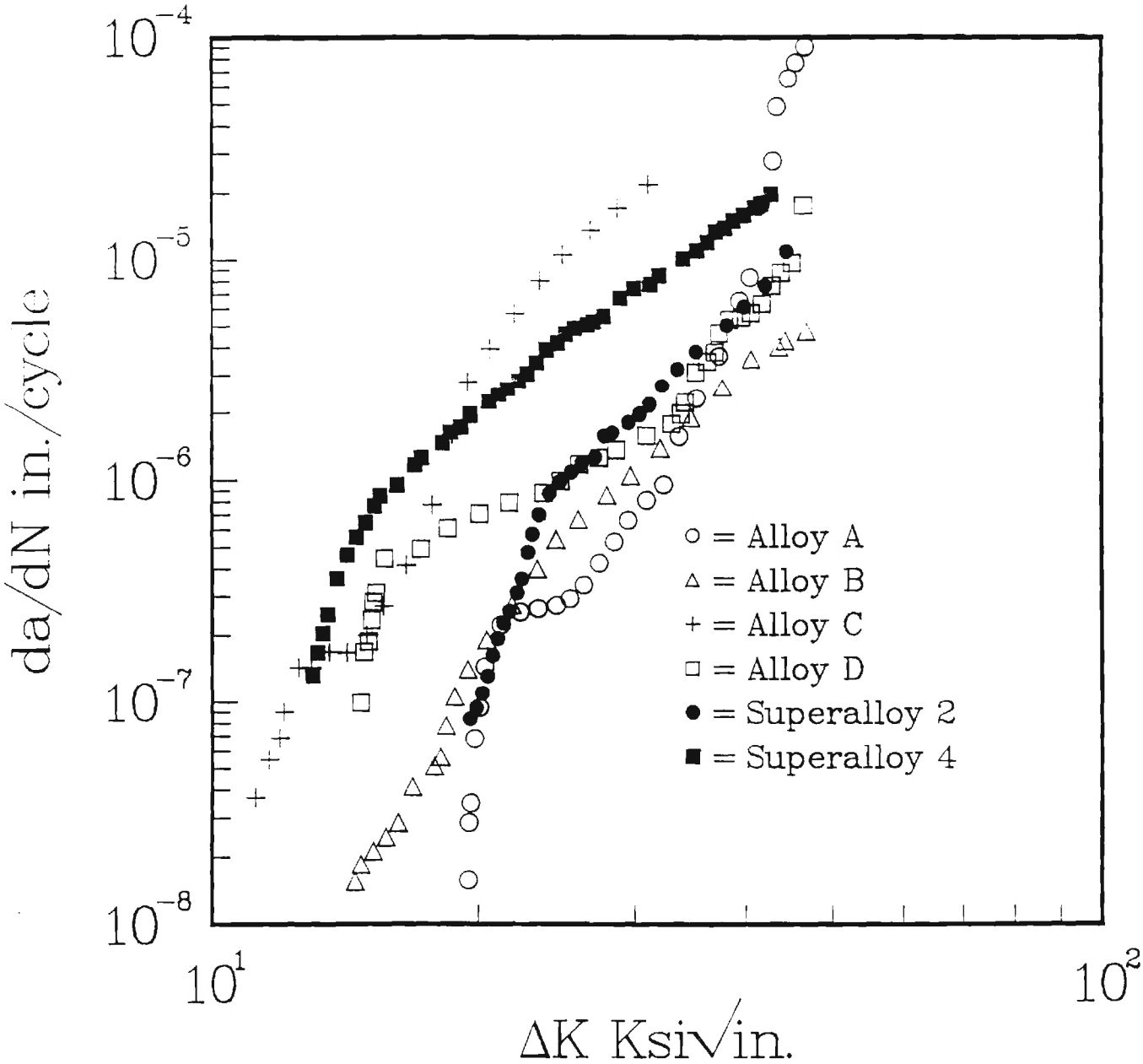

Figure 15 Crack growth rate verse applied ΔK for the four Ni_3Al alloys compared against two superalloys with "best" and "worst" crack growth rates from previous AFOSR program.

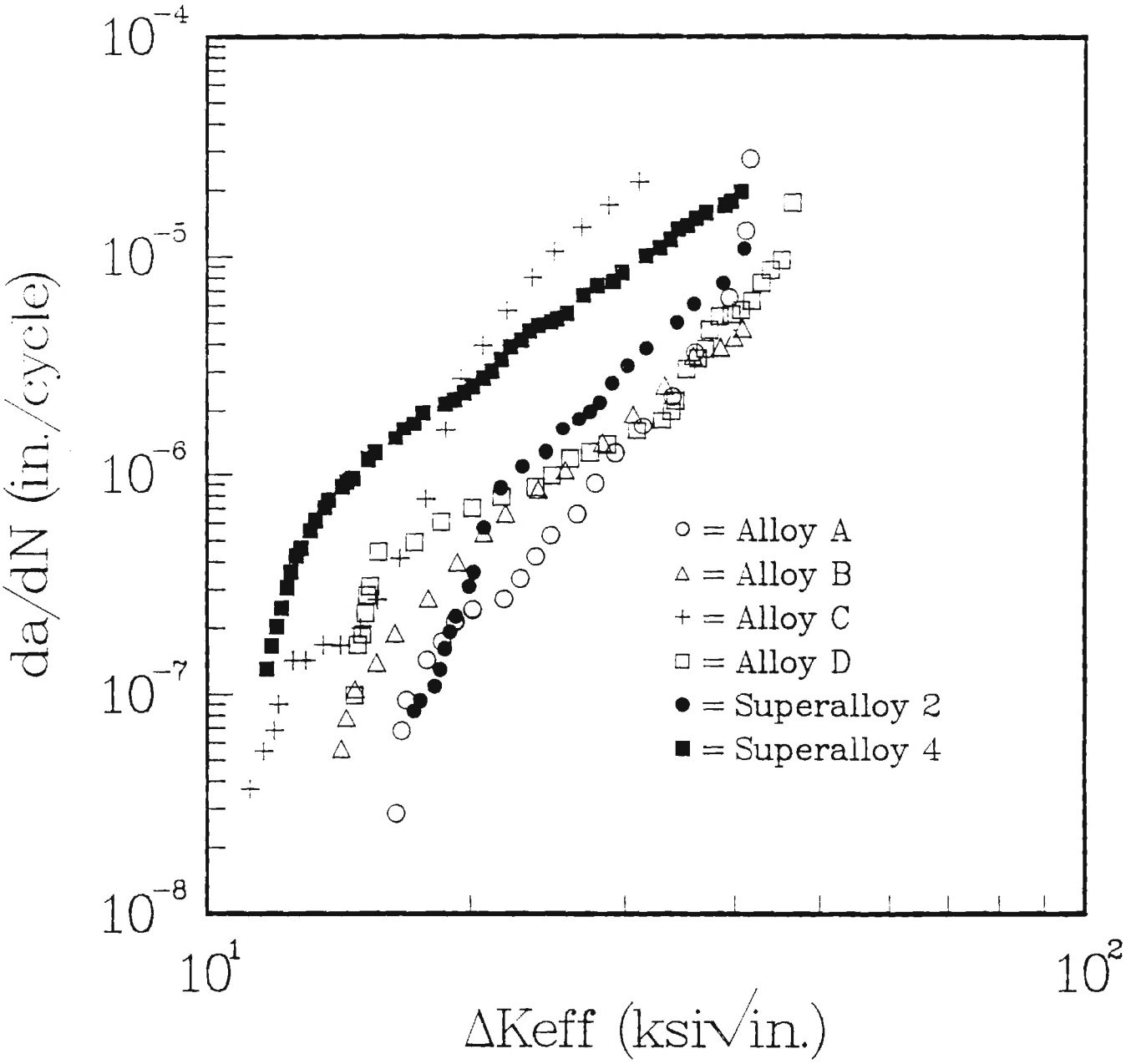

Figure 16. Crack growth rates da/dN verse ΔK_{eff} for the four Ni_3Al alloys compared to "best" and "worst" superalloys.

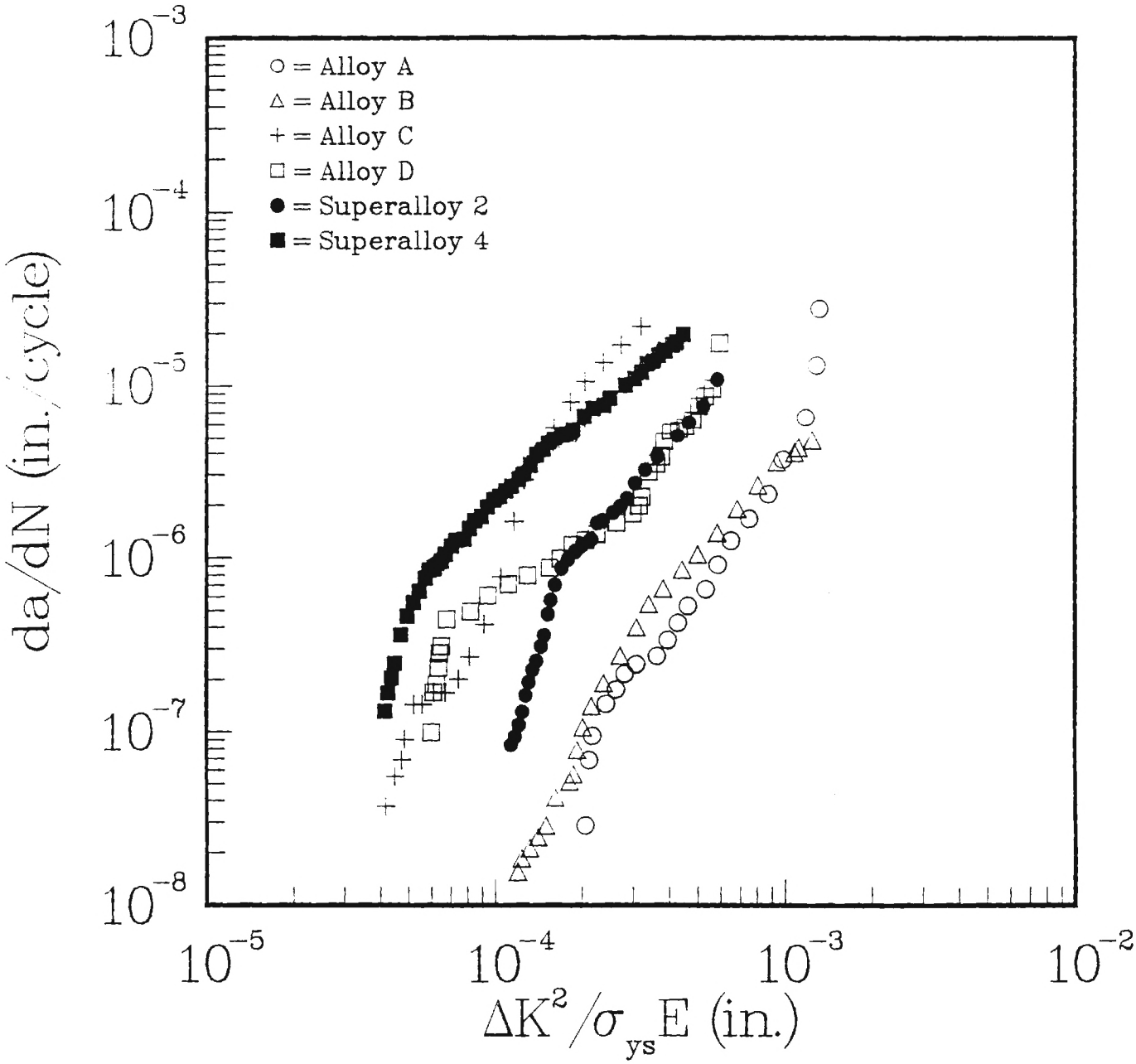

Figure 17. Crack growth rate da/dN verse CTOD ($\Delta K^2/\sigma_{ys}E$) for four alloys as compared to four superalloys.

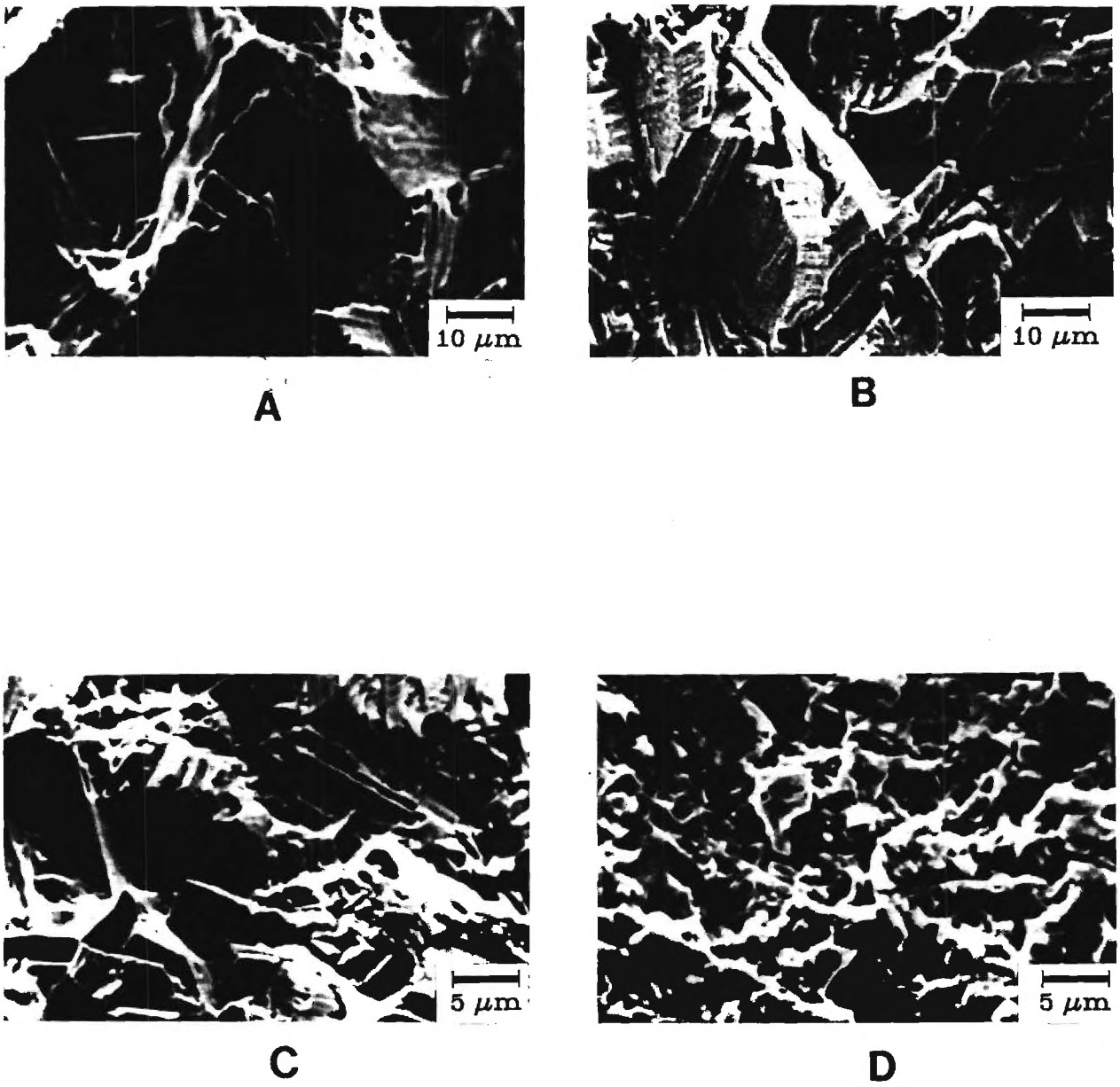

Figure 18. SEM photomicrographs of fatigue crack propagation fracture surfaces, A. Alloy A., B. Alloy B, C. Alloy C, D. Alloy D.

CYCLIC DEFORMATION, DAMAGE, AND EFFECTS OF ENVIRONMENT IN THE NI_3AL ORDERED ALLOY AT ELEVATED TEMPERATURES

PREPARED BY:

Stephen D. Antolovich

Professor and Director
School of Materials Engineering
Georgia Institute of Technology
Atlanta, Georgia 30332

Progress Report for period 5-1-88 through 12-1-88
Contract No. AFOSR-87-0162

Air Force Office of Scientific Research
Electronic and Material Sciences
Building 410
Bolling AFB, D.C. 20332

Program Manager: Dr. A. H. Rosenstein

Progress Report
AFOSR 87-0162

Prepared by
Stephen D. Antolovich

This project is concerned with the mechanisms of monotonic deformation, cyclic deformation, damage accumulation and fatigue crack propagation in Ni_3Al as affected by composition, temperature and environment. All of these phenomena are important to understand if ordered alloys are to be used in advanced applications.

Based on extensive consultation with other investigators such as C.T. Liu (ORNL) and E.M. Schulson (Darmouth College) the following compositions were chosen:

Nominal Composition (wt. pct)*

Alloy	Al	Ni	Cr	B(ppm)
1	13.28 (25)	86.72 (75)	0	750
2	12.67 (24)	87.33 (76)	0	750
3	10.41 (20)	81.57 (72)	8.02 (8)	750
4	8.64 (17)	83.47 (75)	7.89 (8)	750

* Atomic Pct is shown in brackets. B is in ppm

The alloys were fabricated by Homogeneous Metals, Clayville N.Y., by a PM technique with powders -80 + 400 mesh. Difficulties in maintaining composition were encountered during the initial powder

production phase and some remelting was necessary. The compositions of alloys that were finally supplied are given below.

Actual Composition of Experimental Ni_3Al Alloys (wt. pct.)

Alloy	Al	Ni	Cr	B
1	12.91 (24.34)	87.04 (75.45)	0.00	0.045 (2119)
2	12.41 (23.52)	87.54 (76.24)	0.00	0.048 (2271)
3	10.26 (19.73)	81.51 (72.06)	8.00 (8)	0.046 (2209)
4	8.70 (16.99)	83.55 (74.97)	7.70 (7.80)	0.046 (2242)

These compositions are deemed to be in the range that will yield results consistent with the fundamental thrust of the program as specified in the original proposal.

After some characterization via optical microscopy, SEM and TEM at Georgia Tech, the alloys were sent to Masterson's for machining into tensile, LCF and FCP specimens. To date, we have received LCF and FCP specimens with tensile specimens to follow. Experiments are underway on FCP at 25°C and a graph of crack growth rate vs ΔK is shown in Fig 1.

Since tested specimens of Ni_3Al are only now becoming available, tested specimens of a single crystal Ni base superalloys were used to study deformation mechanisms within the γ' Ni_3Al precipitate. It has been shown that the strength of the alloy at lower temperatures is not only controlled by cross slip of screw segments into cube planes, but also by the formation of faults with the γ'. It will be interesting to see if similar processes are seen

in the pure Ni_3Al.

Dr. Randy Bowman has been responsible for alloy definition, characterization and coordination of specimen fabrication. Dr. Bowman received his Ph.D. in September 1988 working in AFOSR 84-0101 and has accepted a position with NASA-LeRC. He has agreed to stay on to train Mr. Graham Webb in various aspects of TEM and mechanical testing until February 1, 1989. Mr. Webb completed his MS in September 1988 and is currently pursuing his Ph.D. Dr. Bowman has been assisted by both Mr. Webb and Mr. Vessier in various aspects of the project.

As alluded to earlier, good relationships exist with C.T. Liu and E.M. Schulson. Both were consulted in definition of the alloys, and Dr. Schulson did present a seminar at Georgia Tech. In addition, Dr. P. Vessiere of ONERA, France will be at Tech to both present a seminar and to work with Mr. Webb (no funds from the AFOSR grant will be used). Dr. Vessiere is a leading expert on deformation in Ni_3Al and the use of the weak beam TEM technique.

We have now appropriate alloys, specimens and personnel in place and are poised to make rapid progress. Funds in the amount of $112,434 (as stated in the original proposal) are requested to complete the project.

Fig 1. – dadN vs ΔK at R = 0.1 for material "A"

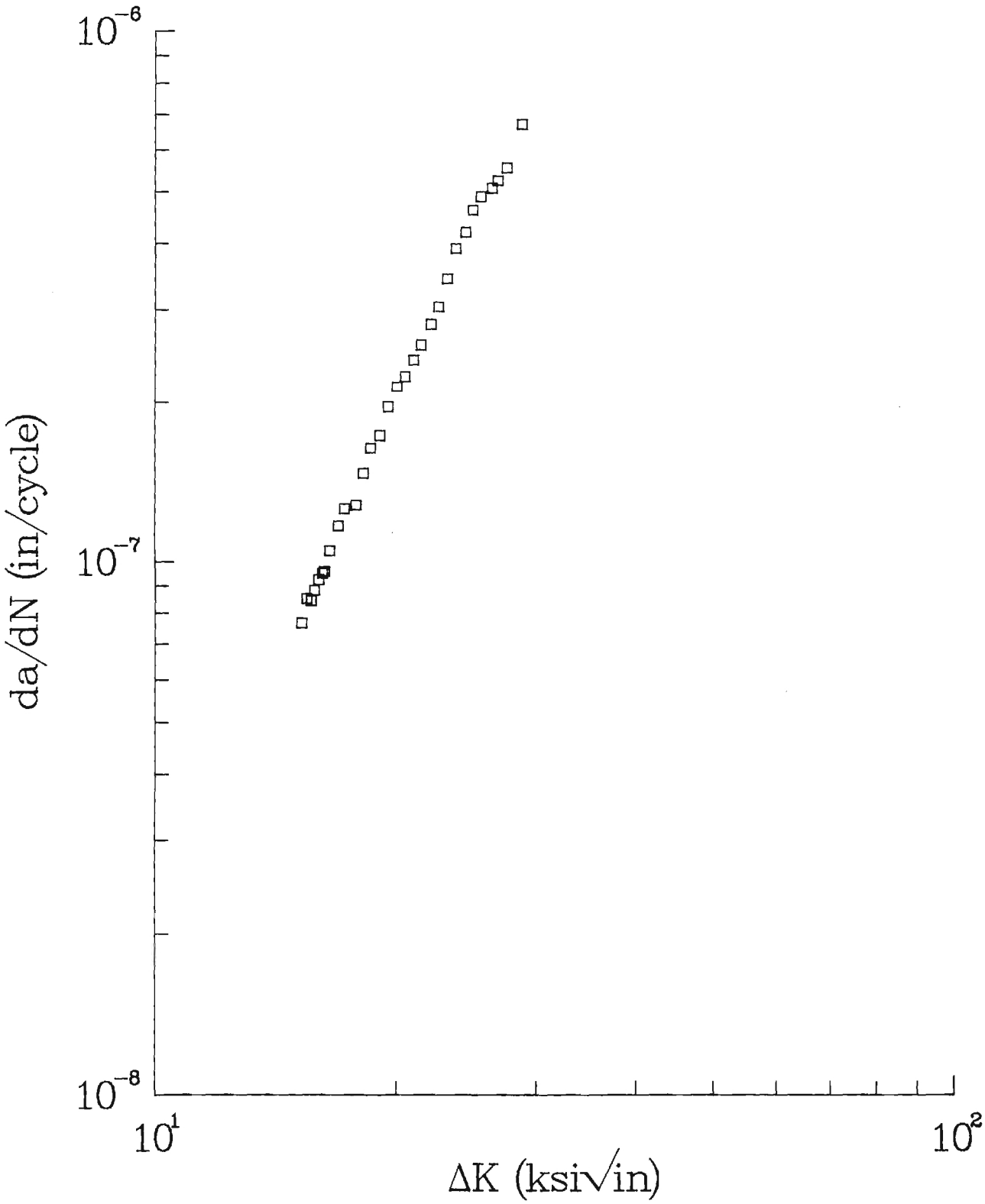

E-18-637

CYCLIC DEFORMATION, DAMAGE, AND EFFECTS OF ENVIORNMENT IN THE Ni_3Al ORDERED ALLOY AT ELEVATED TEMPERATURE

PREPARED BY:

Stephen D. Antolovich
Professor and Director
School of Materials Engineering
Georgia Institute of Technology
Atlanta, Georgia 30332-024

Graham Webb
Graduate Research Assistant
School of Materials Engineering
Georgia Institute of Technology
Atlanta, Georgia 30332-0245

Progress Report for period 6-2-89 through 12-1-89
Contract No. AFOSR-87-0162

Air Force Office of Scientific Research
Electronic and Materials Sciences
Building 410
Bolling AFB, D.C. 20332

Program Manager: Dr. A. H. Rosenstein

I. Summary.

It is now midway through the final year of the AFOSR-sponsored program to investigate the mechanisms of cyclic and monotonic deformation in Ni_3Al as a function of composition, temperature, strain rate and environment. In addition to deformation mechanisms, fatigue crack propagation is also being evaluated as a function of these same variables. The overall goal of the program is to develop a fundamental understanding as to how these materials will perform under conditions similar to those expected in advanced jet engine components.

At present, the alloys have been selected, fabricated, processed, and machined into specimens. In addition, the alloys have been characterized using x-ray and TEM techniques. At present the room temperature tests have been completed and tests at elevated temperature in both air and vacuum environments are ongoing. A presentation at the 2nd Annual ASM/TMS Materials Week was given on the results obtained during the course of the ongoing research. Two other presentations will be given later in the year. Details of these studies are given and comparisons to the results of wrought superalloys are given where appropriate.

II. Program Status.

A. Material Preparation, Fabrication, and Utilization.

As was previously reported, by extensive consultation with other current investigators in the field, the alloy compositions were selected and prepared using powder metallurgy techniques. The powders were then HIPped to produce extruded bars [1]. The compositions of the four alloys obtained from the dense extruded bars are given as Table 1. The original intent of the program was to compare the deformation response and crack growth resistance of hypostoichiometric alloys to completely stoichiometric alloys where boron additions have little beneficial effect (*i.e.* alloy stoichiometry). A second goal was to then compare response between binary and ternary alloys of the same stoichiometry (*i.e.* alloy composition). In calculating the site stoichiometry of the ternary alloys, it is important to remember that half of the Cr atoms occupy Ni sites and half occupy Al sites in the ordered lattice.

Problems in maintaining the desired alloy stoichiometry during processing resulted in two binary hypostoichiometric alloys of essentially identical nickel stoichiometry (75.5 and 76.2 at.%), and two ternary hypostoichiometric alloys of very different nickel stoichiometry (76.1 and 78.9 at.%). As the two binary alloys differ only slightly in composition (and behaved identically during initial tensile, FCP, and LCF testing), the two ternary alloys (Alloy T1 and T2) will be compared to evaluate the effect of Ni stoichiometry. The effect of alloy composition is to be evaluated by comparison of Alloys B1 and T1, as the Ni stoichiometry in these alloys are identical ($\approx$ 76 at. %). The specimens produced from the second binary alloy (B2) are to be utilized in further investigating the effect of strain rate on the intermetallic's deformation response at elevated temperatures (experiments to be described later).

Once received, the extruded bars were fabricated into tensile, low cycle fatigue (LCF), and fatigue crack propagation (FCP) specimens (see previous report for details

[1]). In addition, sections of the bars were removed for characterizing the lattice structure and microstructure of the materials using X-ray diffraction and optical metallography. Results of the diffraction experiments were compared to theoretical predictions with good correlation. The $L1_2$ ordered intermetallic lattice structure was verified for all the experimental alloys. The microstructure of the specimens was characterized as equiaxed (figure 1) from grain size measurements perpendicular and parallel to the extrusion direction. The Alloy B1 and T1 were both single phase γ'. Alloy T2 was found to posess a two phase mixture of primarily γ' with domains of disordered γ. These observations are consistent with the Ni-Cr-Al ternary phase diagram (figure 2).

The grain size of both ternary alloys was found to be 2 (Alloy T2) and 3 (Alloy T1) times smaller than that of the binary alloy ($\approx 20\mu m$). Since all of the alloys were processed identically, it can be concluded that Cr additions refine the grain structure of Ni_3Al. These observations are consistent with the premise that Cr partitions to the grain boundaries in Ni_3Al. As Cr diffuses slowly (compared to Ni and Al), the rate of grain boundary movement is reduced, resulting in finer grain sizes. Such an observation is consistent with the behavior of Cr in Ni-base superalloys.

B. Tensile Deformation Response.

Currently tensile tests have been preformed on all the alloys in air at temperatures of 25°, 300° and 600° C using two strain rates. Additionally, the alloys have been tested at temperatures as high as 1000°C in an effort to select an appropriate upper level temperature for mechanical property comparisons between the binary and ternary alloys. The results of these investigations are tabulated in Table 2, which are discussed below.

1. Low temperature σ-ϵ response.

The low temperature ($< 600^o$ C) tensile response of the alloys is extremely

ductile. Plastic response is characterized by discontinuous yielding and yield point elongation (during which Lüders bands were observed to form) after which considerable hardening occurs. The alloys achieve an ultimate strength and fail with little necking (*i.e.* plastic strain localization). SEM fractography (figure 3) reveals transgranular fracture with the exception of Alloy T1 which exhibits intergranular fracture. The differences in failure modes will be discussed later in some detail. The ductility of all alloys decreased as temperature increased, indicating environmental sensitivity.

2. High Temperature σ-ϵ Response

At elevated temperatures ($\geq$ 600°C), the tensile response of the binary and ternary alloys is quite different than at lower temperatures. The ductility of the binary alloy is nil at temperatures at and above 600°C. At 1000°C the binary alloy regains some ductility. The hardening response of the binary alloy in this range of temperatures is classified as perfectly plastic to failure (T = 600°C), elastic to break (T = 700°–900°C), and continuous softening (T = 1000° C). The fracture surface morphology of the binary alloy at all elevated temperatures is completely intergranular (figure 3). The results of the tensile tests on the binary alloys at elevated temperature indicate brittle response and enviornmental sensitivity.

The ternary alloys were observed to possess both higher strength and ductility than the binary alloy in these range of temperatures. At 600°C the ternary alloys exhibit discontinuous yielding (and Lüders bands) followed by hardening similar to behavior at lower temperatures. At 1000° C the ternary alloys exhibit superplastic response. The fracture surfaces of T1 were completely intergranular at all temperatures tested, while T2 exhibited transgranular failure. Once again ductility of both ternary alloys decreases with increasing temperature until 1000° C.

3. Deformation Response

Lüders band propagation and grain size effects As mentioned previously, the alloys were observed to form Lüders bands on the reduced sections of the specimens. The Lüders bands propagated during yield point elongation until covering the entire gauge length of the specimen. This last event marked the onset of hardening. A thorough discussion of Lüders band propagation and its relationship to yield point elongation has been provided by Schulson and co-workers [2]. In these investigations, the formation and propagation of the Lüders bands is responsible for the discontinuous yielding. Observations of the dislocation structures within the Lüders bands [2] reveal the formation of extrinsic grain boundary dislocations at the intersection of slip bands with grain boundaries. These extrinsic grain boundary dislocations were then observed to nucleate slip in adjacent grains. Thus it was concluded that grain boundaries act as obstacles for dislocation flow in Ni_3Al. Unlocking (and subsequent stress relaxation) occurs from the nucleation of slip within adjacent grains in the Lüders band. The process continues until all grains are saturated. At present, little is understood about the mechanism by which hardening of the material occurs after yield point elongation.

For these and other reasons, the dislocation configurations at grain boundaries under various amounts of plastic deformation are being quantified using new stereological techniques developed at Georgia Tech [3]. These techniques allow simple, accurate, and unbiased measurement of dislocation densities using TEM techniques.

Another important result of Schulson's investigations was the determination of the appropriate Hall-Petch exponent for boron- doped Ni_3Al.

$$\sigma_y = \sigma_o + k_y d^{-0.8} \tag{1}$$

where σ_o and k_y are experimentally determined constants for the stoichiometry and boron content being evaluated. This unusual dependence (*i.e.* an exponent of 0.8) was modeled by a composition independent but grain-size dependent work-hardening description of yielding related to the propagation of Lüders bands [2].

Effect of Composition and Stoichiometry When comparing the response of the binary alloy (B1) to that of the ternary alloy (T1), it is observed that at all temperatures, the yield stress (and Lüders stress) of the ternary alloy is higher than that of the binary alloy (figure 4). These increases in yield strength cannot be solely explained by grain size differences (*i.e.* using Equation 1 and assuming identical experimental constants). Thus Cr increases the lattice resistance to dislocation flow by solid solution strengthening as well as refining the grain boundaries. At elevated temperatures, the ternary alloys can harden considerably, whereas the binary alloy does not.

It is observed that at low temperatures, the ternary alloy T1 is more brittle than its binary equivalent (figure 6). SEM photomicrographs of the fracture surfaces reveal that B1 fails transgranularly while T1 fails intergranularly (figure 3). This indicates that Cr weakens the grain boundaries in Ni_3Al. It is further interesting to note that T2 (high Ni Stoichiometry) has elongations comparable to that of the binary alloy and also fails transgranularly. From these observations it can be concluded that, Cr bearing alloys require higher Ni site stoichiometry than equivalent binary alloys to obtain comparable low temperature elongations. This observation can also be explained by the mechanism of Cr segregation to grain boundaries.

Numerous studies [2,4,5] on the effect of boron doping of hypostoichiometric and stoichiometric alloys have determined that in hypostoichiometric alloys, the grain boundaries are enriched in both Ni and B compared to the bulk composition. Undoped

and/or stoichiometric alloys showed no such enrichment. Thus Ni and B enrichment of the grain boundaries was attributed to the observed increased ductility. Although it is widely recognized that the boundaries are enriched, the effect of this enrichment is still a subject of considerable debate (*i.e.* cohesive strengthening [4,6] versus slip enhancement by disordering grain boundaries [7,8]).

As Cr substitutes for both Ni and Al sites and segregates to grain boundaries, the grain boundary chemistry of Cr bearing alloys are bound to be much different than that of a comparable binary alloy. In general, the number of Ni atoms at the grain boundaries in ternary alloys should be lower (relative to the binary alloy), which could lead to the observed grain boundary weakening of the Cr bearing alloy. This view is further supported by noting that as the concentration of Ni in the ternary alloy increases from 72.1% in T1 to 75.0% in T2, transgranular fracture and high ductility result. In order to evaluate the effect of Cr partitioning to grain boundaries as a function of Ni stoichiometry, several Auger studies are being conducted.

At elevated temperatures, the ternary alloy T1 possesses far greater ductility than the binary alloy even though failure is intergranular for both alloys. Intergranular failure and low ductility are characteristic of binary Ni_3Al at elevated temperature [2,5]. Liu [5] attributes this characteristic response to environmentally assisted "dynamic embrittlement" of the grain boundaries. Dynamic embrittlement occurs as a result of the simultaneous application of stress in the presence of oxygen at elevated temperatures. By this mechanism cracks form at grain boundaries near free surfaces where exposure to oxygen results in the reduction in the boundary strength. Intergranular failure results from continuous embrittlement of the freshly exposed surfaces at the crack tips which subsequently cause the crack to propagate along the weakened boundaries. Schulson [2] also acknowledges the deleterious role of oxygen at elevated temperature but also points out that grain boundary sliding and cavitation

also contribute to the embrittling mechanism.

Dynamic embrittlement can be avoided by refining the grain size such that cracks are less than supercritical, lengthening the aspect ratio of the grains (*i.e.* grain diameter parallel to stress axis/grain diameter parallel to stress axis) reduce the total grain boundary area normal to the direction of applied stress, or by the addition of $\approx$ 8% Cr. In this program the latter approach was applied to increase high temperature ductility. As ternary alloy T1 exhibits good elevated temperature ductility while possessing the same fracture morphology as the binary alloy, it can be concluded that ductility loss due to dynamic embrittlement is a much more severe mechanism than Ni depletion. The enhanced ductility of the Cr-bearing alloy is due to the rapid formation of Cr_2O_3 in the presence of oxygen. This oxide coats the exposed crack surfaces and reduces boundary weakness.

Yield Strength. Examination of figure 4 reveals several interesting trends. The yield strength of alloys B1 and T1 both increase with temperature until $T > 600^o$ after which the strength decreases as T increases. This anomolous increase in strength is characteristic of most Ni_3Al alloys [2,9,10,11]. Conversely, the yield strength of ternary alloy T2 is observed to decrease with temperature, with greater decreases occurring at the low strain rate (0.5%/min.). This behavior is inconsistent with the cross-slip mechanism [12] of hardening widely accepted to explain the deformation response of Ni_3Al. The observed discrepancy is currently the subject of a TEM investigation, and is related to the domains of disordered γ present within this alloy.

The strain rate effect of the binary and ternary alloys at elevated temperatures is extremely interesting. At low temperatures, there is relatively little strain rate effect on the yield strength of both binary and ternary alloys. At 600°C, the yield strength is significantly higher for the faster strain rate (50%/min.) for both binary and ternary

alloys. This is a significant observation in that it is in apparent contridiction to the predictions of the cross-slip model (PPV model) [12]. According to this model, increasing temperature increases the likelihood of a screw dislocation segment cross-slipping from octahedral to cube planes. These cross-slipped segments act as pinning points which impede dislocation flow on the octahedral planes. For this reason, the higher the temperature (for constant $\dot{\gamma}$) the greater the number of pinning points, which results in a higher yield strength.

According to this mechanism, the effect of strain rate should be the **inverse** of the temperature effect. That is, the higher the strain rate (for a constant T), the lower the number of cross-slip events (and thus pinning points) that occur before yielding. The reduction in the number of pinning points should result in a lower yield strength. As this type of strain rate effect is not observed for either single crystal [11] or polycrystalline [10] Ni_3Al, the PPV model does not completely describe this important aspect of intermetallic deformation. In view of this apparent discrepancy, it can be argued that a second thermally activated process is present which competes with the cross-slip mechanism to give rise to a net positive strain rate effect. As the strain rate effect is observed to increase as grain size decreases (figure 7), it is expected that this second mechanism will involve the grain boundaries.

To better understand the strain rate effect in polycrystalline Ni_3Al, a series of experiments is planned which utilize the specimens produced from the unused binary alloy (Alloy B2). In these experiments, the 0.2% yield strength of the alloy is to be measured at temperatures ranging from 300° to 800°C at three strain rates 0.5%, 50%, and 500%/min.. The specimens will be tested in strain control in compression (due to relatively low tensile ductility at elevated temperature). The dislocation structures will then be studied in the TEM. The results of the investigation will then be evaluated in light of the PPV model and pertinent modifications suggested.

Ultimate Strength and Hardening Characteristics. For all alloys, σ_{uts} is observed to decrease with increasing temperature with the greater loss in yield strength occurring for binary alloys (figure 5). This decrease can be directly related to an apparent change in the hardening characteristics of the alloys. At lower temperatures, all alloys harden considerably until failure. As temperature increases, the amount of hardening decreases (Table 2) until eventually perfectly plastic response occurs. It should be noted that the binary alloy shows perfectly plastic response before the ternary alloys. At extremely high temperatures (*i.e.* 1000° C), the alloys soften after yielding instead of harden. Strain rate does not appear to affect ultimate strength significantly until at $T > 600^o$ C, after which greater strength occurs at faster strain rates. For these cases, little to no hardening occurs, and the increase in yield strength can account for the observed increase in ultimate strength. When hardening does occur, increasing strain rate slightly increases the hardening exponent. These observed trends further suggest a second thermally activated process which controls deformation in polycrystalline Ni_3Al. It is apparent from the observed trends in hardening response as a function of temperature and strain rate that microstructural stress relaxation (such as grain boundary sliding) occurs at a faster rate at elevated temperatures. This view can also be used to understand the effect of strain rate, as this mechanism is thermally activated, and thus can have a greater effect at lower strain rates. As the Cr modified alloys harden more at higher temperatures than the binary alloy, it can also be inferred that Cr reduces the rate stress relaxation, most likely by reducing the rate of boundary diffusion.

Failure Strain. By examining the data for the trend in failure strain with temperature (figure 6), it can be seen that ductility decreases with temperature until 1000^oC where ductility increases significantly. In comparing binary to ternary, it can

be seen that both ternary alloys retain more ductility at elevated temperatures than the binary alloy. The binary alloy is extremely brittle at elevated temperatures and tends to exhibit more ductility at higher strain rates. Ternary alloys also tend to have higher failure strain at the faster strain rate but the effect is much smaller. These observations are consistent with a dynamic embrittlement mechanism as discussed previously. At extremely high temperatures ($\approx$ 1000°C) the ternary materials become superplastic. Alloy T2 exhibited much more superplasticity than Alloy T1, and did not fail during the test.

C. Low Cycle Fatigue Testing

Currently low cycle fatigue tests have been performed on all the alloys at room temperature. The tests were conducted in plastic strain control mode using a SATEC servohydraulic test machine with a CATS controller containing combinatorial feedback. The combinatrial feedback option allowed the test endpoints to be determined by the formula:

$$\epsilon_{pl} = \epsilon_{tot} - \sigma/E \tag{2}$$

using the current values of the load and strain channels to determine ϵ_{tot}, σ and thus ϵ_{pl}. All specimens were cycled at a plastic strain range, $\frac{\Delta\epsilon_{pl}}{2} = 0.3\%$ at strain rates of 0.5% and 50%/min..

1. Macroscopic Cyclic Deformation Response

The first specimens of each alloy were tested to failure to determine relative capabilities to absorb plastic work. These initial tests resulted in the cumulative glide plots (figure 8) which present the cyclic hardening and softening characteristics of the three alloys. In this figure, alloys B1 and T2 initially cyclicly harden, reach a peak value, then soften continuously to failure. Alloy T1 fails in the hardening range of cyclic life before the onset of softening. Representative initial hysterisis loops are presented in figure 9. The ternary alloys both maintain a higher cyclic stress than

the binary alloy which cyclicly harden more, and at a faster rate than both of the ternary alloys. Ternary alloy T2 hardens more than alloy T1 (due to earlier failure of T1 in the hardening range), but at the same approximate rate. The binary alloy was able to survive twice as many reversals (Alloy B1, $2N_f = 7940$) as the best ternary alloy (Alloy T2, $2N_f = 4100$), and over two orders of magnitude greater than the equivalent ternary alloy (Alloy T1, $2N_f = 44$). Thus the binary alloy is better able to accumulate plastic work than the ternary alloys. In comparing ternary alloy T1 to T2, the effect of increased Ni stoichiometry is to increase LCF life by 2 orders of magnitude.

It is also interesting to note that a small ($\approx 5\%$) compressive flow stress asymmetry exists for all but alloy T1. The asymmetry remains relatively constant during the cyclic life of all alloys. This is indicative of some preferred crystallographic orientation. It is widely known [9] that the cyclic deformation response of Ni_3Al exhibits a tension-compression asymmetry which is dependent upon crystallographic orientation with respect to the stress axis. All specimens were machined such that the stress axis is parallel to the extrusion direction, such perferred orientation can be expected. TEM crystal orientation of numerous grains (≈ 50) has not revealed the presence of any preferred crystallographic orientation, a more statistically representative sampling of the samples orientation is needed. To this end, experiments are underway to determine the bulk crystallographic orientation of the specimens by x-ray texture measurements. Through these experiments the presence or lack of crystallographic orientation within the samples can be determined.

2. Microscopic deformation response.

Binary alloy-crack initiation. Figure 10 is a replica of the binary alloys surface (which was electropolished prior to testing) near a site of microcrack initiation. From

this figure it is clear that crack initiation is associated with the formation of cracks at the intersection of persistent slip bands (PSBs) with grain boundaries. PSB formation is highly indicative inhomogeneous planar slip which is a desirable cyclic deformation mechanism as it limits the damage to a smaller volume of the material. It is observed that in most cases, the intersection of a PSB with a grain boundary results in the formation of a PSB of different orientation within adjacent grains. Slip bands were not observed to intersect within individual grains. In this photomicrograph, a Stage I crack is seen on the order of 9-10 grains (*i.e.* $\approx 300\mu$m) in length.

Binary alloy-TEM observations of cyclic deformation response. Figure 11 is a photomicrograph of deformation structure of the binary alloy after 100 reversals of plastic strain control with $\frac{\Delta\epsilon_{pl}}{2} = 0.3\%$. This corresponds to the life where maximum hardening occurs. In this photomicrograph several interesting features have been identified and related to the material's cyclic deformation response. The deformation structure consists of large numbers of APB coupled superdislocations lying on parallel overlapping slip bands. Due to the tilting conditions under which the photmicrograph was taken, overlapping slip bands result in a Moire interference pattern from overlapping APB. In addition, cyclic deformation has resulted in the formation of large numbers of intrinsic $\frac{a}{3}(111)$ dislocation loops. Such loops have been observed during cyclic deformation of hypostoichiometric Ni_3Al single crystals at room temperature [13]. Stoloff [13] has proposed a mechanism for loop and dipole formation during cyclic deformation of Ni_3Al at room temperature.

The mechanism proposes that during cyclic deformation Kear-Wilsdorf locks impede dislocation flow on octahedral planes. To accommodate the applied strain, flow of unconstricted dislocation segments leads to jog formation. Dislocation dipoles and loops are subsequently pinched off as the dislocation moves away. The presence of

intrinsic loops and dipoles was proposed to increase the vacancy concentration within the PSBs of Ni_3Al single crystals, resulting in expansion during cyclic deformation. To relieve the accumulating strain, microvoids and cracks were observed to form and lead to crack initiation [13].

In the experimental polycrystalline binary alloy, jogs were also observed after cyclic loading (Figure 12). Figure 13 further shows a region of high loop and dipole density. From these preliminary observations, it appears that the deformation mechanisms in single crystal and polycrystal are similar.

Ternary alloy-crack initiation. Figure 14 is a SEM photomicrograph of ternary alloy T2 near the fracture surface. It can be seen that PSBs do not form in this alloy, and slip is expected to be more homogeneous. This is a less preferred cyclic deformation mechanism as damage is less contained than in the case of planar slip. The crack size corresponding to the change from Stage I crack growth to Stage II (*i.e.* Paris law growth) is expected to be very small (on the order of the grain size). In examining the failure specimen surface, a few extremely large cracks were observed. Figure 15 shows an initiation site from which several cracks oriented at 45° to the stress axis originate. It was observed that most cracks were oriented along the plane of maximum shear, unlike the binary alloy (figure 10) in which cracks of crystallographic nature eventually result in macro-cracks oriented 90° to the principal stress axis of the specimen.

D. Fatigue Crack Propagation.

Currently all fatigue crack propagation (FCP) measurements have been made on all alloys at 25°C and 600° C. In addition, FCP tests have also been conducted on Alloy B1 and T2 at 300° C.

All tests were conducted at an R-ratio of 0.1 at a cyclic frequency of 10 Hz. The

results of these experiments are presented as figure 16, from which the Paris Growth law constants (Table 3) were derived. FCP experiments have also been attempted on the binary alloy at 900°C and 1000°C. In both cases the specimens fractured upon initial loading similar to a fracture toughness experiment. As no stable crack growth was observed at these temperatures, no FCP data could be generated.

1. Effect of composition and stoichiometry

The room temperature FCP results for all alloys have been thoroughly discussed in the previous progress report [1].

At 300°C, the threshold of Alloy T2 is reduced significantly more than the threshold of the binary alloy from the 25°C value. At this temperature, the ternary alloy possesses a lower Paris growth law exponent than the binary alloy. Regardless, the binary alloy possesses a lower crack growth rate than alloy T2 for most values of ΔK. In the binary alloy, the onset of stage 3 crack growth occurs at $\approx$ 40 MPa$\sqrt{\text{m}}$, but in Alloy T2, stage 3 crack growth initiates at $\approx$ 80 MPa$\sqrt{\text{m}}$. Thus the ternary alloy is expected to have twice the fracture toughness of the binary alloy at this temperature.

At 600°C, the threshold values of the alloys again decrease, with Alloy B1 and T1 possessing the same approximate value ($\approx$ 10 MPa$\sqrt{\text{m}}$), although stable crack growth occurs at a much higher rate in the binary alloy. In comparing T1 to T2, it can be seen that T2 possesses a much lower threshold. It is interesting to note that in the binary alloys, the onset of stable crack propagation occurs at faster rates as temperature increases (i.e. pre-exponential term increases). In the ternary alloys, stable crack propagation occurs at the same rate for all temperatures, although the threshold decreases significantly.

2. Comparison to Waspalloy.

Figure 17 is a comparison of the FCP resistance of the binary and ternary alloys to that of Waspalloy at room temperature (from the results of Clavel et al [14]). From this, it can be seen that Alloys B1 and T2 have FCP resistance comparable to that of Waspalloy. Alloy T1 has a much lower threshold ΔK than Waspalloy, and is thus inferior to the wrought superalloy at ambient temperatures.

In figure 18, the FCP resistance of Waspalloy at 550°C and 650°C is compared to the Ni_3Al alloys at 600°C. As the data for Waspalloy is identical at both temperatures, it can be safely assumed that the response at 600°C is identical also. At elevated temperatures (*i.e.* 600° C) the Waspalloy is far superior to all intermetallic alloys.

III. Program Directions.

The experimental program is currently well underway with major portions of the mechanical testing completed. The final period of the contract will focus on completing the few remaining mechanical tests as well as microscopy and theoretical modelling of observed deformation response. In this section of the report, the remaining experiments to be performed are described.

A. Testing.

1. Tensile tests.

The vast majority of the tensile tests have been performed in air. The only remaining task is the selection of the appropriate high temperature (*i.e.* $T > 600^o$) for comparison of the binary and ternary alloy. The binary alloy is extremely brittle in this range of temperature until 1000° C, and the ternary alloys are superplastic at 1000^oC. Because of this response it is difficult to select an appropriate upper limit temperature.

As previously described, a series of strain controlled tensile tests is to be performed to determine the strain rate effect in binary Ni_3Al as a function of temperature. The results of this experiment will be used to evaluate the PPV [12] deformation model, and is of particular interest from the viewpoint of processing and working these materials. These experiments are to follow the elevated temperature LCF tests and should be completed by the end of the program.

2. Low cycle fatigue tests.

LCF tests at elevated temperature are currently in progress with expected completion of the matrix by February. LCF tests at 600^oC in the vacuum environment will follow the tensile tests and should be completed by March.

3. FCP tests.

One replication of FCP tests has been completed up to 600°C. Elevated temperature FCP tests will be completed within 2 weeks. Computer data acquisition and control software has been designed to allow generation of data by both decreasing and increasing ΔK techniques. This will allow generation of the full curve from threshold to unstable crack growth, and verify the validity of the current data. In addition, a new technique for measuring crack closure using resistance drop techniques is being evaluated. If the validity of the technique can be verified at room temperature (by comparison to other established techniques), it will be used to measure closure loads at elevated temperature. Following these tests, FCP tests are to be run on each alloy in the vacuum environment. Completion of these tests is scheduled for the end of Febuary.

B. Microscopy.

At present there is a considerable amount of microscopy that remains to be completed before the end of the experimental program.

Preliminary results are encouraging and can be correlated to the response of single crystals. Recent collaboration between Dr. Randy Bowman and Graham Webb at NASA-Lewis has laid the foundations for the TEM investigations, particularly in the use of the "weak beam" technique. The majority of the TEM studies will focus upon the cyclic deformation structures present within the alloys at various life fractions of interest. TEM study of the interaction of dislocations at grain boundaries is expected to yield answers for the observed strain rate effects at elevated temperature, as well as play an important role in the crack initiation process. Jog formation and the reversibility of cross slip will also be studied. The TEM investigation has begun and is expected to be finished near the completion of the final report.

C. Modelling Activity.

At present, the controlling aspects of the alloy's static and cyclic deformation

response are being determined. The results of the investigations will then be used to derive appropriate constitutive descriptions. The effect of environment on behavior is also being determined. Preliminary response of the alloys has indicated discrepancies with the PPV [12] model for describing the response of ordered Ni_3Al as a function of temperature. At present these discrepancies are believed to be associated with a second thermally activated stress relaxation mechanism involving the grain boundaries. Once the important aspects of cyclic deformation response have been determined, a physically based model for describing fatigue crack propagation similar to that of Saxena and Antolovich [15] will be developed.

I.V. Personnel.

Dr. Antolovich serves as the Principal Investigator (P.I.) for this program.

Dr. Randy Bowman was responsible for alloy definition and some initial testing and characterization. In addition, he has provided guidance and training in TEM deformation characterization techniques. He is presently employed as a Research Scientist by NASA-LeRC in Cleveland where he is working on NiAl and NiAl matrix composites. He is maintaining close contact with this project and serves on the Ph.D. committee for Mr. Webb under agreement of his supervisor, Dr. Hugh Gray.

Mr. Graham Webb is the Graduate Research Assistant supported by this project and is working towards his Ph.D. It is anticipated that the completion date of this project will correspond roughly to his completion date.

Mr. Rick Brown is a Research Equipment Specialist in the Mechanical Properties Research Laboratory at Georgia Tech and is involved with experimental set-ups and with assisting and training students.

In addition to the above personnel, clerical assistance is provided by Ms. Janice Coleman. Administrative and financial assistance is provided by Ms. Pat Ledon and by Ms. Judy Lorier, all of the School of Materials Engineering.

V. Interactions and Reporting

Good relationships exist with C.T. Liu (ORNL), Erland Schulson (Dartmouth College), and D.P. Pope (University of Pennsylvania), as several informal discussions and seminar presentations have taken place.

As was reported previously, a presentation was given by Graham Webb at the 2nd annual ASM-TMS materials week in Indianapolis, Ind. on Oct 1-5 of 1989. The presentation was entitled "The Strain Rate Dependence of Polycrystalline Ni_3Al", co- authored by Graham Webb, Stephen D. Antolovich, and Randy Bowman. We will be making two more presentations this year including one at the ASM yearly meeting in Anaheim, CA. on February 22, entitled "Fatigue Crack Propagation of Polycrystalline Ni_3Al as a Function of Temperature and Composition". The paper is co-authored by Graham Webb and Stephen D. Antolovich. The second paper is to be presented at the ASM international Aeromat-90, entitled "Cyclic Deformation of Ni_3Al as a function of Temperature, Composition, and Strain Rate" authored by Graham Webb and Stephen D. Antolovich.

In addition to the presentations, it is expected that a publication on the results of the strain rate experiments will be prepared later in the year. Publication of fatigue results is also anticipated upon completion of microscopy experiments.

Table 1: Composition of Ni_3Al Alloys in Atomic Percent

Alloy	Ni	Al	Cr	B
Binary 1, B1	76.3	23.5	0.0	0.22
Binary 2, B2	75.5	24.3	0.0	0.23
Ternary 1, T1	72.1	19.7	8.0	0.22
Ternary 2, T2	75.0	17.0	7.8	0.22

Table 2: Tensile Properties of Ni_3Al Alloys at Ambient and Elevated Temperature in Air

Alloy	T (°C)	$\dot{\epsilon}$ (%/min.)	$\sigma_{0.2\%}$ (MPa)	σ_{uts} (MPa)	ϵ_f (%)	n
Alloy B1	25	0.5	413	1404	56	0.61
Alloy T1			725	1065	17	0.56
Alloy T2			861	1519	39	0.54
Alloy B1		50	468	1416	42	0.62
Alloy T1			817	1237	14	0.58
Alloy T2			893	1475	39	0.55
Alloy B1	300	0.5	413	766	12	0.54
Alloy T2			831	1375	33	0.48
Alloy B1		50	463	810	27	0.56
Alloy T1			815	1381	38	0.49
Alloy B1	600	0.5	536	545	2	*
Alloy T1			791	802	11	*
Alloy T2			701	747	23	*
Alloy B1		50	617	545	4	*
Alloy T1			829	955	15	*
Alloy T2			812	918	24	0.23
Alloy B1	800	0.5	370	370	1.1	†
Alloy B1	1000	0.5	137	137	10	†
Alloy T1			32	40	52	†
Alloy T2			20	38	>100	‡

Notes:

All stress values reported are based upon initial specimen area.

*No hardening, perfectly plastic response.

† Softening after yield.

‡ Perfectly plastic response, did not fail in calibrated stroke range.

Table 3: Paris Growth Law Constants of Ni_3Al Alloys at Ambient and Elevated Temperature, R=0.1, ν = 10 Hz

Alloy	Temperature (° C)	ΔK_{th} (MPa$\sqrt{m}$)	C (m/cycle)	m
B1	600	10.8	5.0×10^{-9}	2.64
T1		10.0	7.0×10^{-13}	5.13
T2		8.1	1.8×10^{-12}	4.16
B1	300	14	4.0×10^{-13}	3.86
T2		10	1.0×10^{-11}	2.87
B1	25	16	1.1×10^{-13}	3.64
T1		11	1.0×10^{-15}	5.79
T2		17	5.0×10^{-11}	1.57

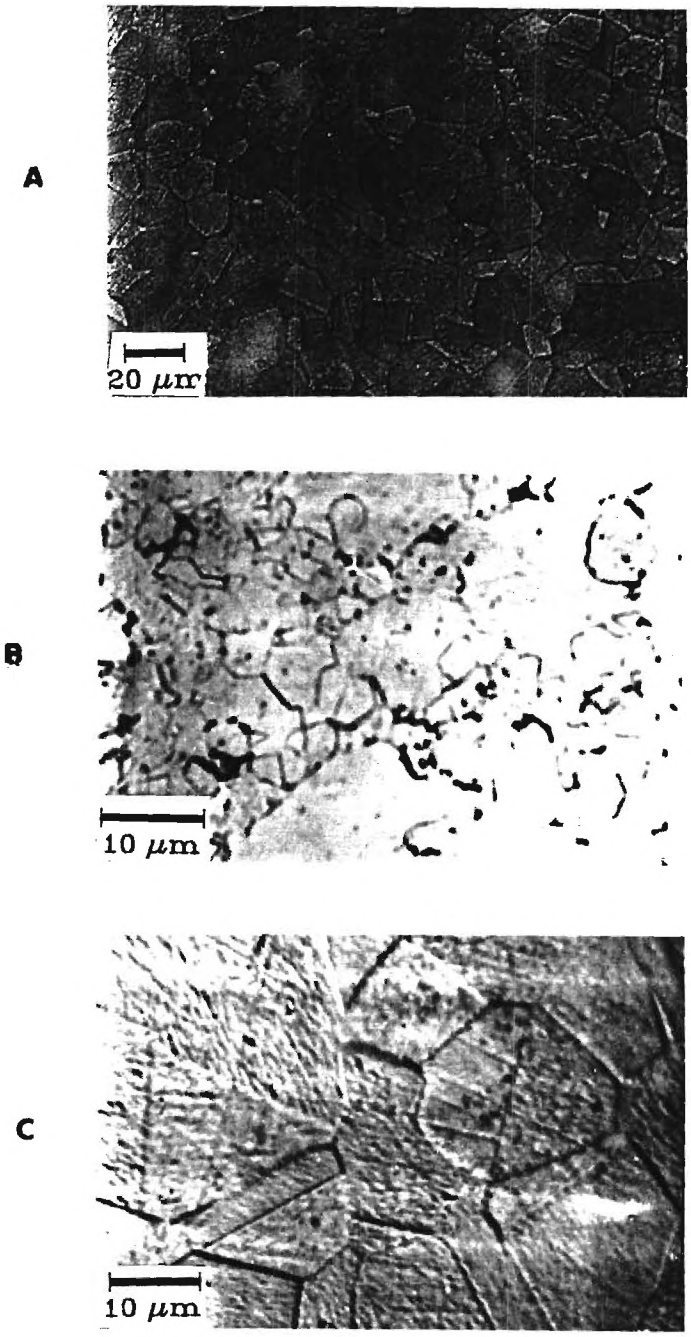

Figure 1: Initial microstructures of Ni_3Al in the transverse orientation, A.) Alloy B1, B.) Alloy T1, C.) Alloy T2.

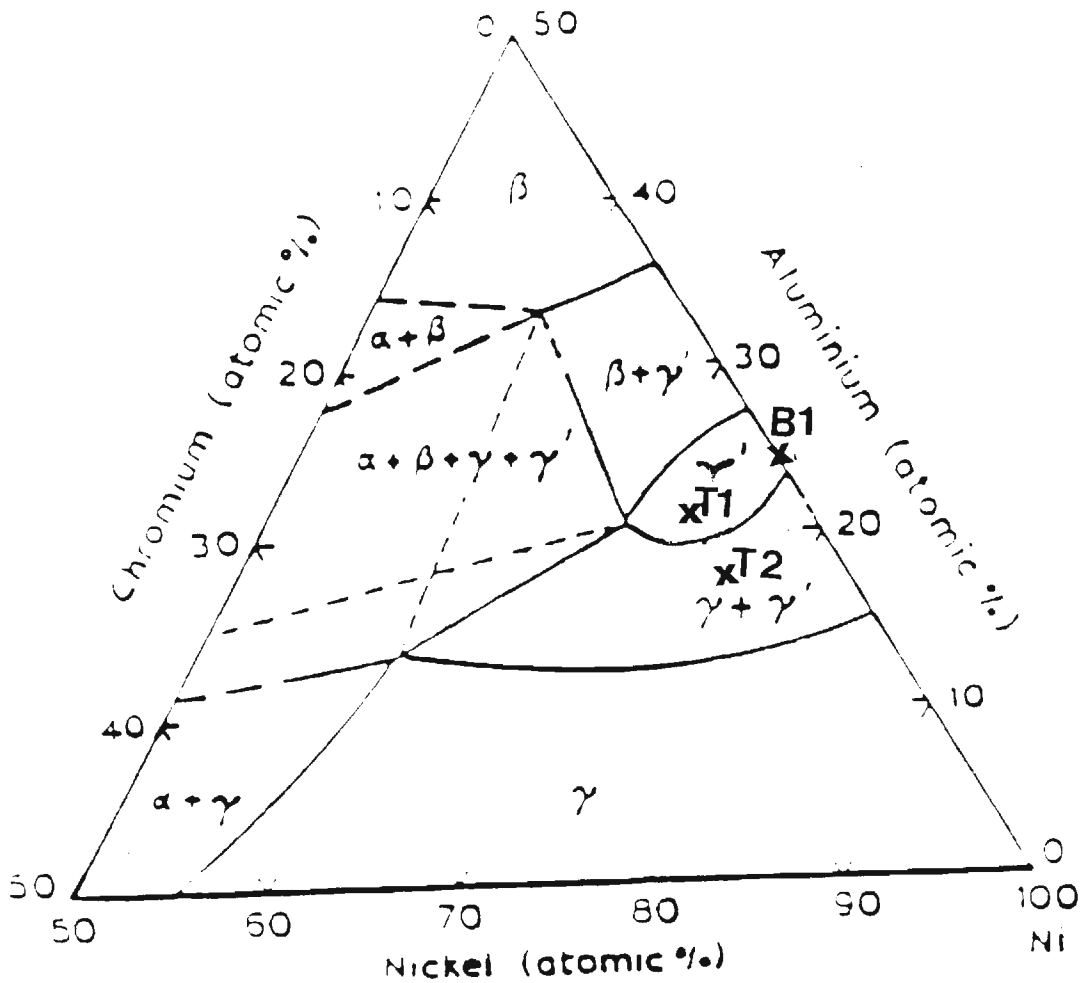

Figure 2: A reproduction of Taylor's diagram upon which the compostions of the alloys under study are marked [16] .

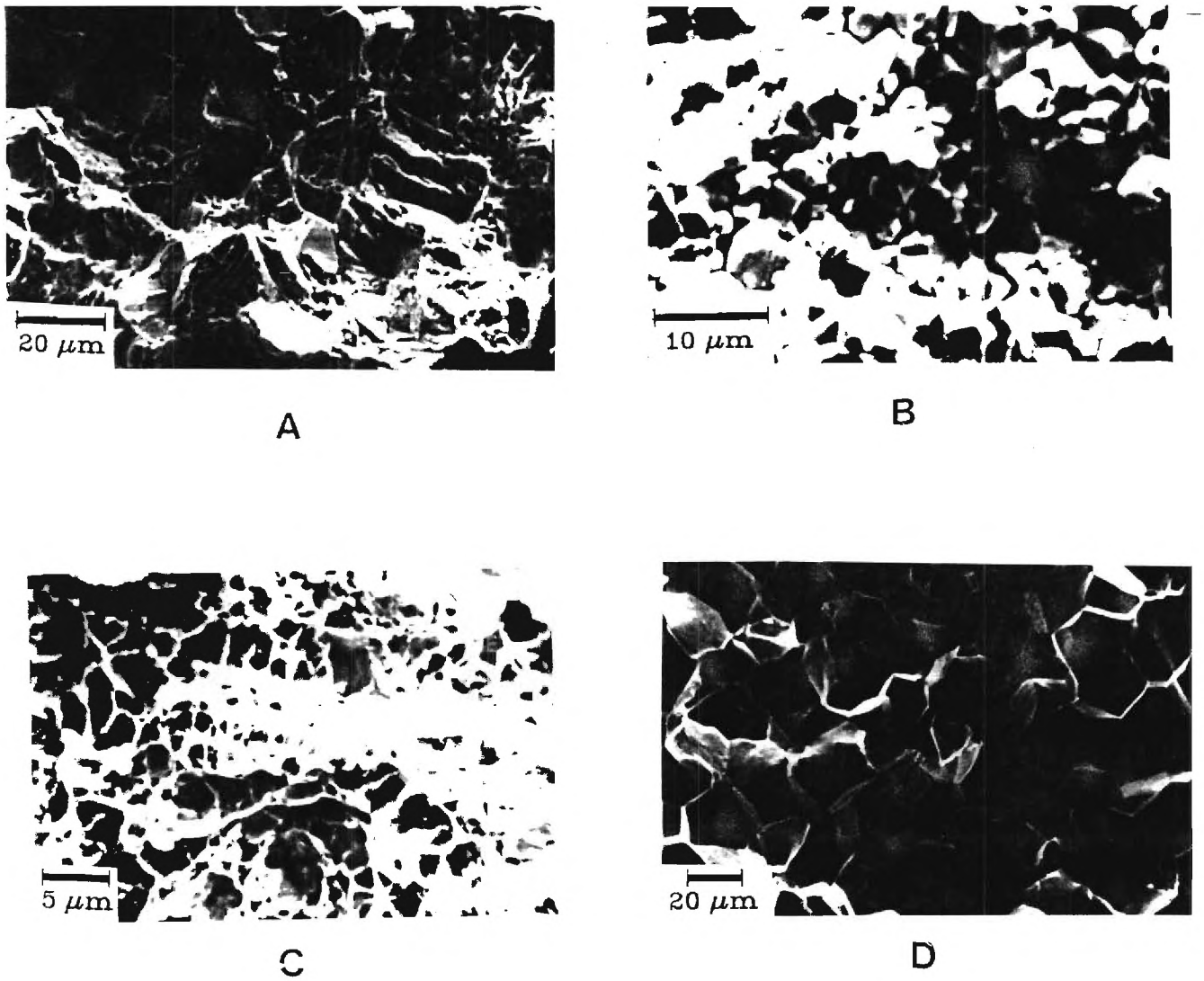

Figure 3: SEM photomicrographs of tensile fracture surfaces. A.) Alloy B1, 25°C. B.) Alloy T1, 25°C. C.) Alloy T2, 25°C. D.) Alloy B1 600°C.

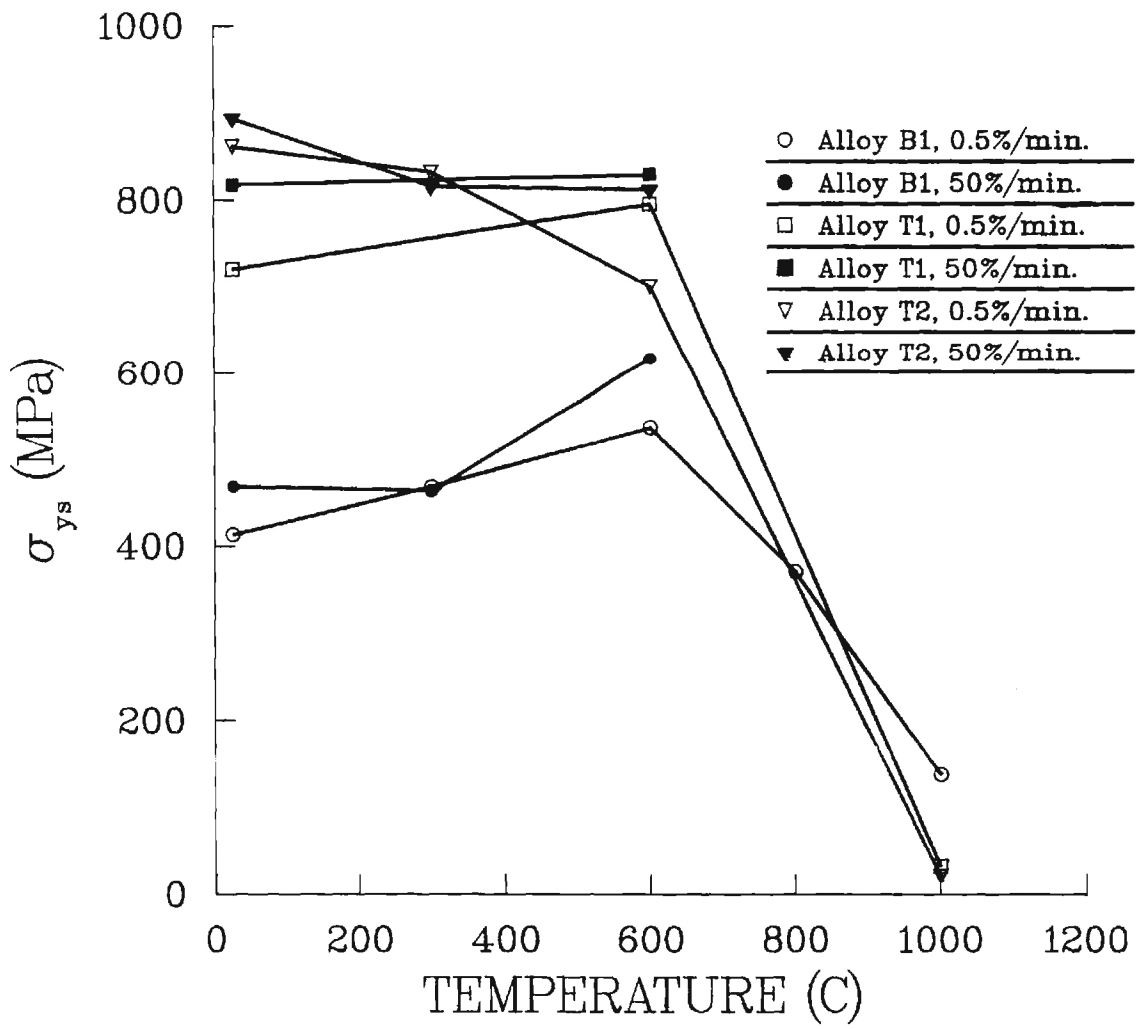

Figure 4: $\sigma_{0.2\%}$ as a function of temperature for the three experimental alloys. Data was obtained at $\dot{\epsilon} = 0.5\%/\text{min.}$ and $50\%/\text{min.}$

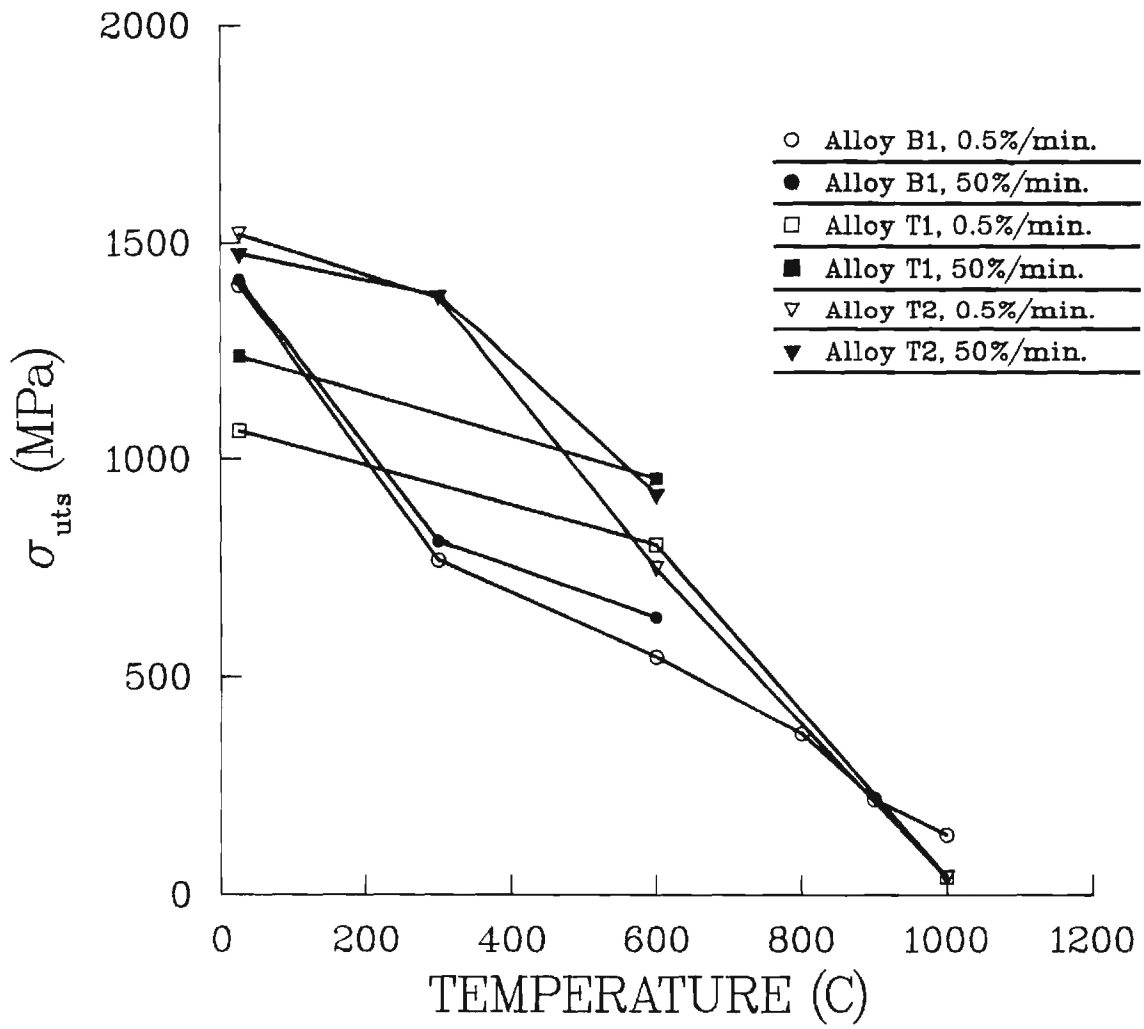

Figure 5: σ_{uts} as a function of temperature for the three experimental alloys. Data was obtained at $\dot{\epsilon} = 0.5\%/\text{min.}$ and $50\%/\text{min.}$

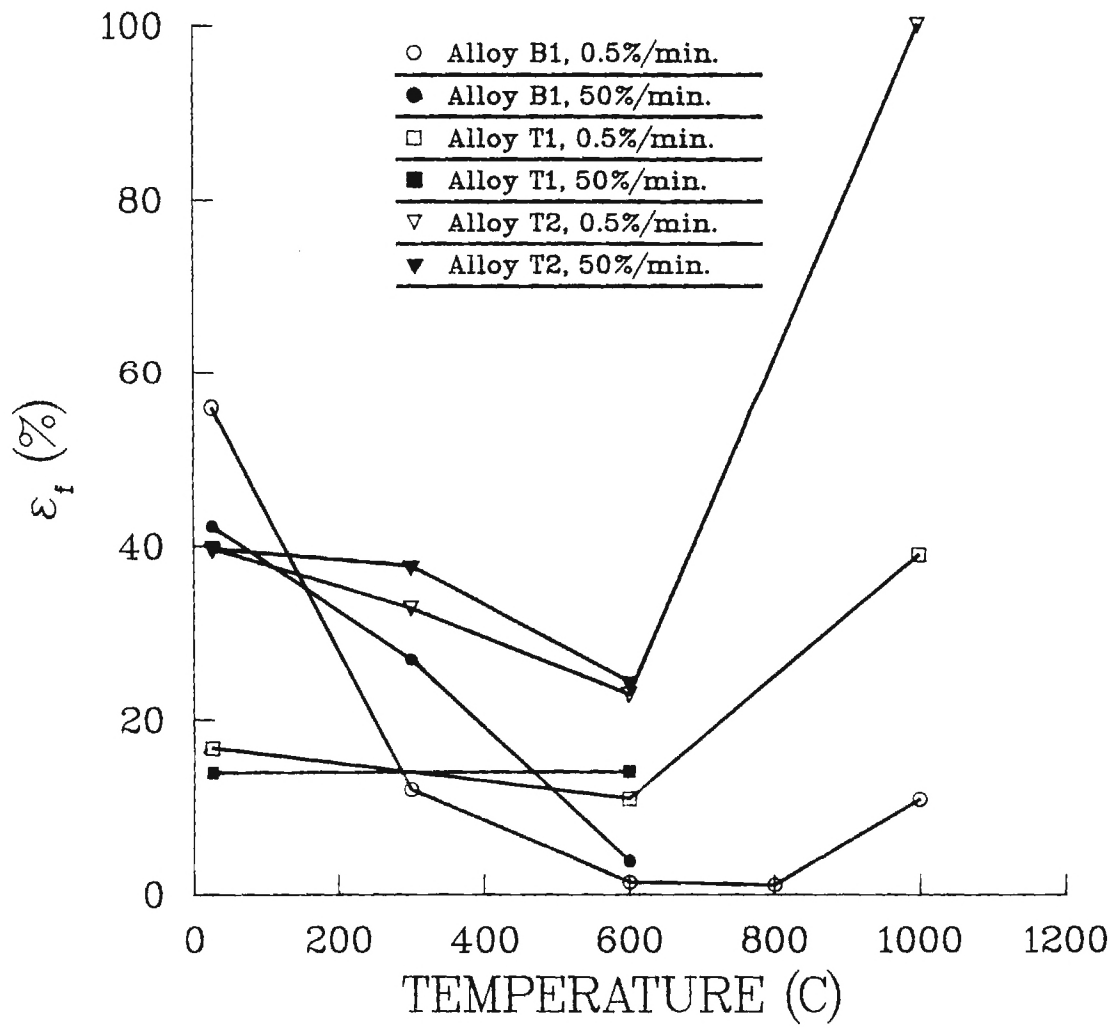

Figure 6: ϵ_f as a function of temperature for the three experimental alloys. Data was obtained at $\dot{\epsilon} = 0.5\%/\text{min.}$ and $50\%/\text{min.}$

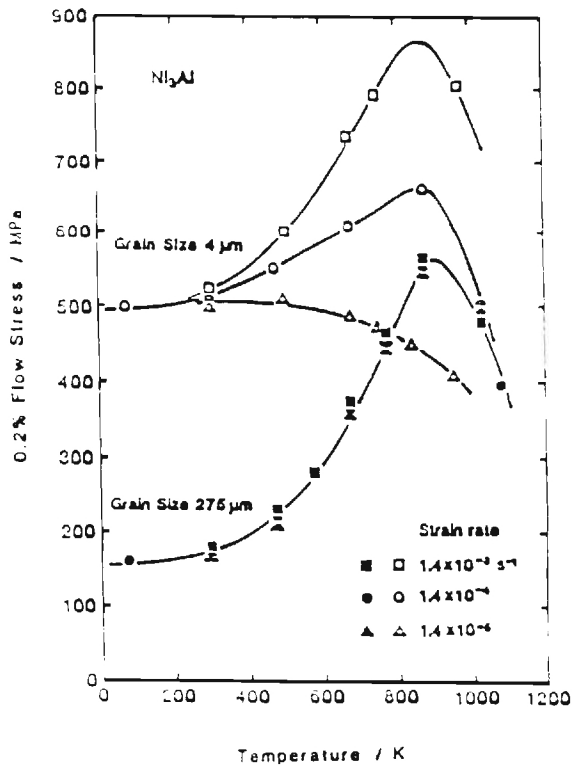

Figure 7: Temperature and strain rate dependence of flow stress in polycrystalline Ni_3Al with two different grain sizes [11]

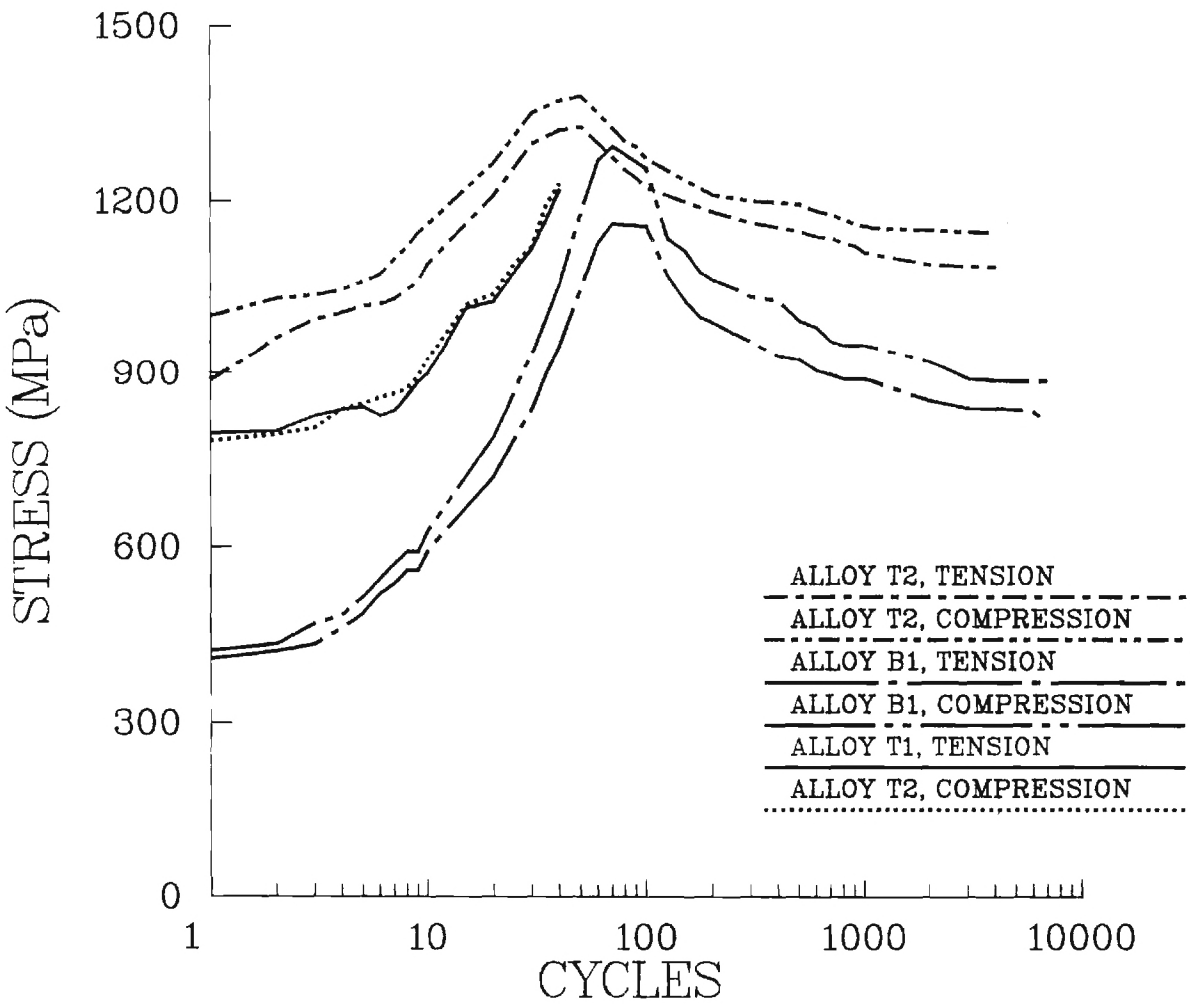

Figure 8: Cumulative glide plot of the three experimental Ni_3Al alloys at 25° C, $\dot{\epsilon}$ = 50%/min.

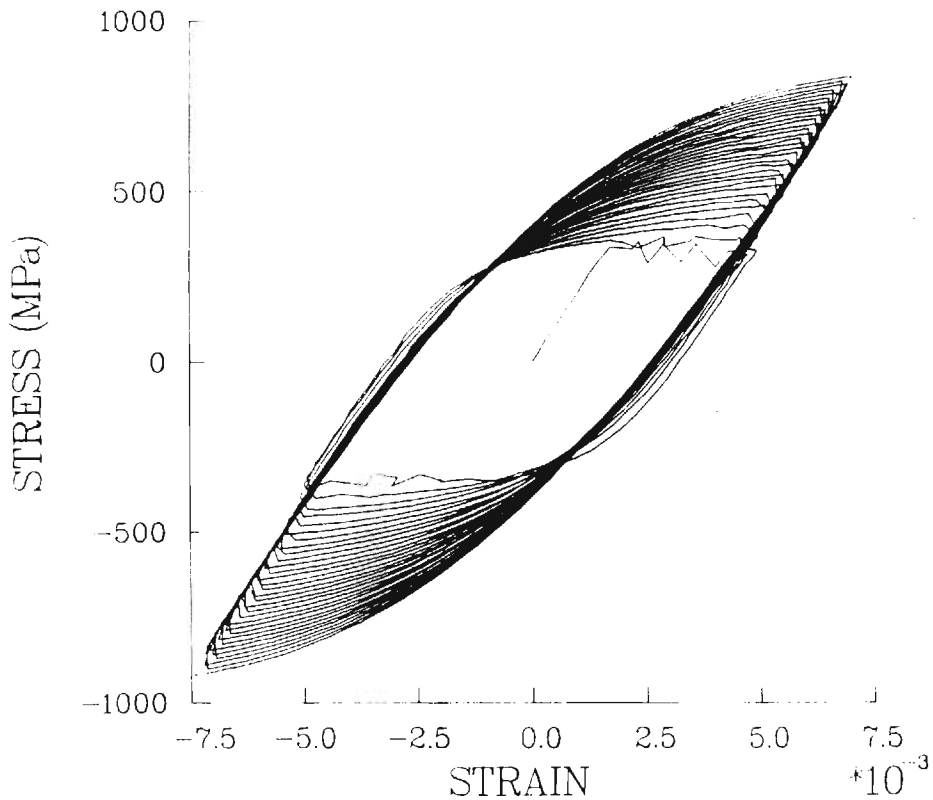

Figure 9: Representative initial plastic strain control ($\frac{\Delta\epsilon}{2} = 0.3\%$) hysterisis loops for binary alloy at $25°C$, $\dot{\epsilon} = 50\%/\text{min}$.

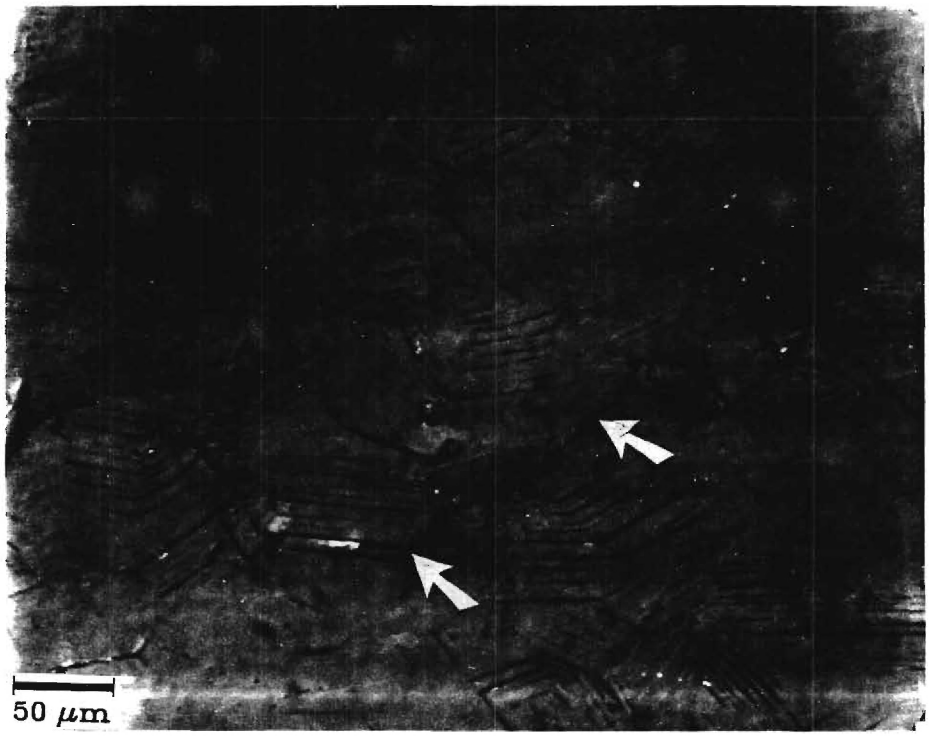

Figure 10: Replica of Alloy B1 LCF specimen (N_f = 7940) indicating the presence of PSBs leading to the formation of a Stage 1 crack (arrow)

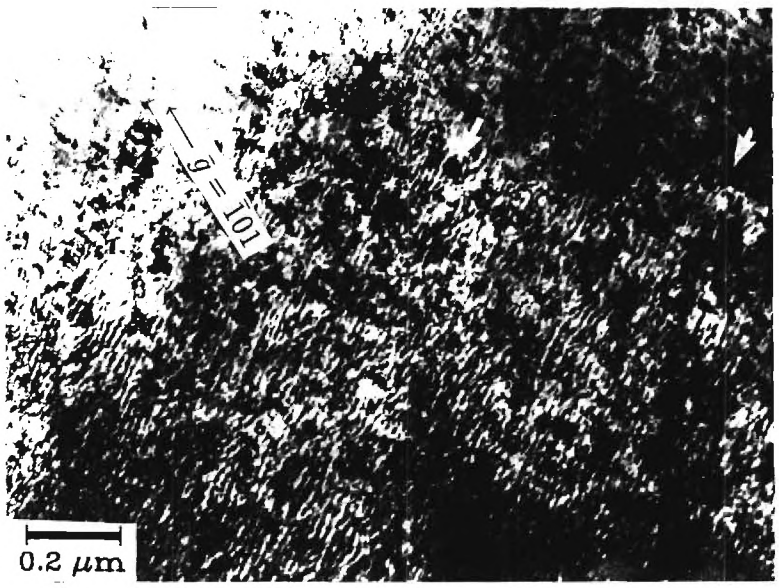

Figure 11:
TEM Photomicrograph of Deformation Substructure in Binary Ni_3Al subjected to 100 reversals of $\frac{\Delta\epsilon}{2} = 0.3\%$. Note the presence of numerous intrinsic $\frac{a}{3}(111)$ dislocation loops (arrows). $\bar{g} = \bar{1}10$

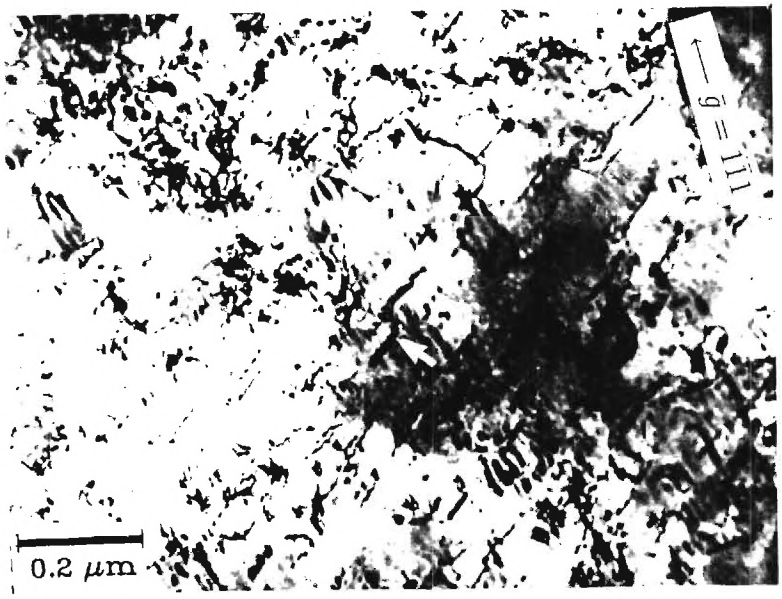

Figure 12: TEM photomicrograph of deformation substructure of Alloy B2 subjected to 100 reversals of $\frac{\Delta\epsilon_{pl}}{2} = 0.3\%$. Cross slip of a screw dislocation lying on octahedral to cube planes has resulted in the formation of a jog (arrow).$\bar{g} = \bar{1}\bar{1}1$

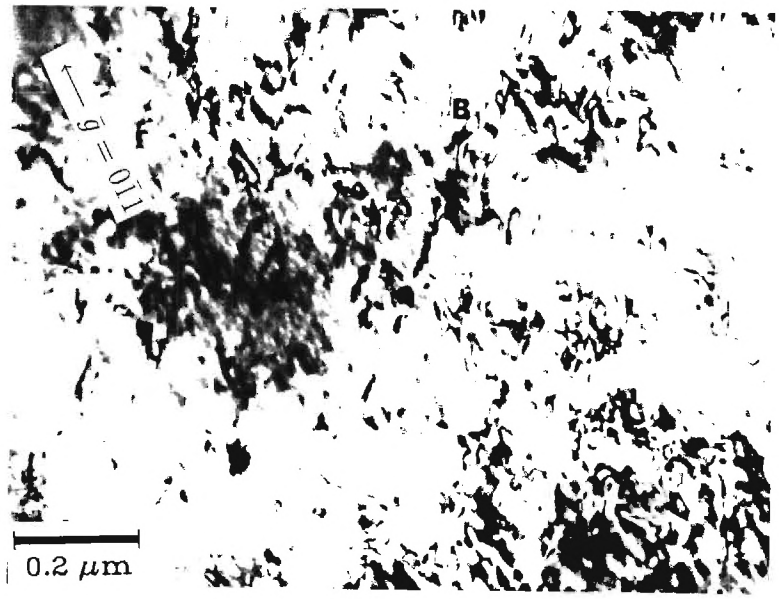

Figure 13: TEM photomicrograph of deformation substructure of Alloy B2 subjected to 100 reversals of $\frac{\Delta\epsilon_p}{2} = 0.3\%$. Flow of screw dislocations on octehedral planes within slip bands has resulted in the formation of dislocation loops (A) and dipoles (B). $\bar{g} = 0\bar{1}1$

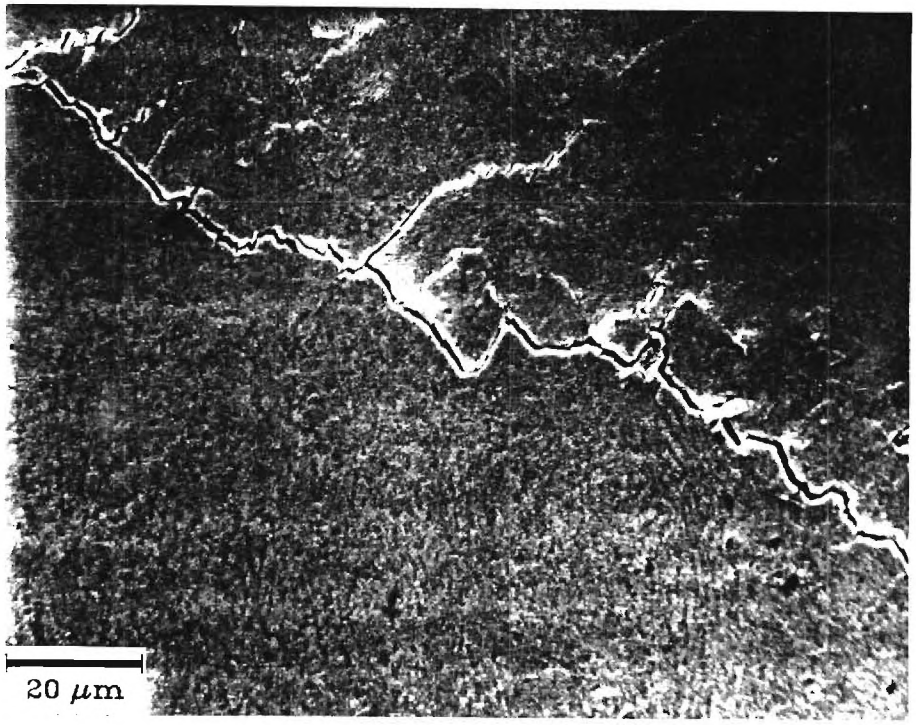

Figure 14: SEM photomicrograph of a large crack present on the surface of a specimen of Alloy T2 subjected to $N_f = 4100$ reversals.

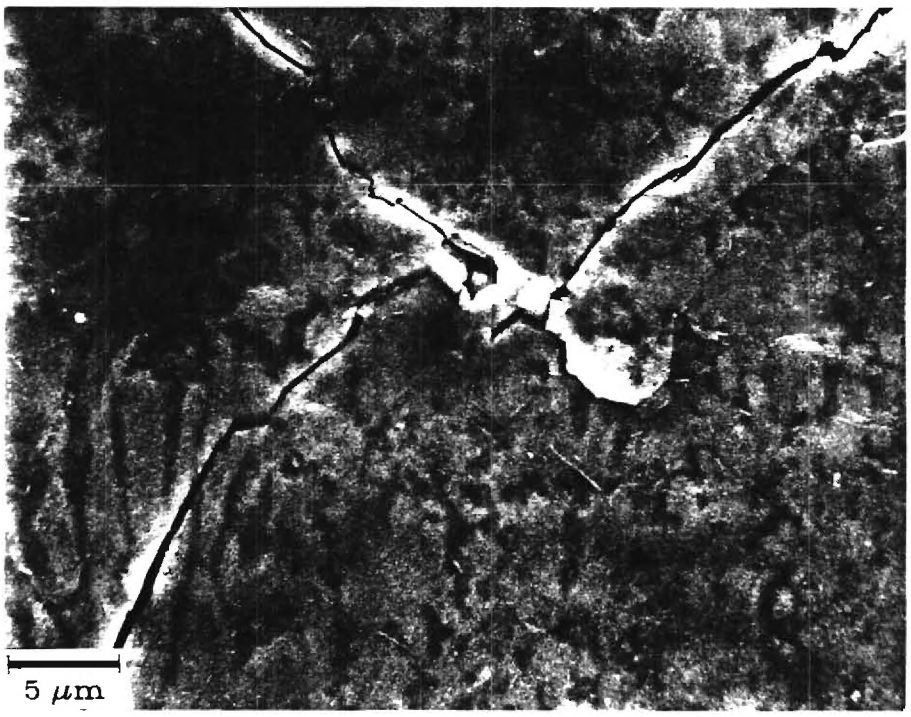

Figure 15: SEM photomicrograph of inititation site of crack in figure 14.

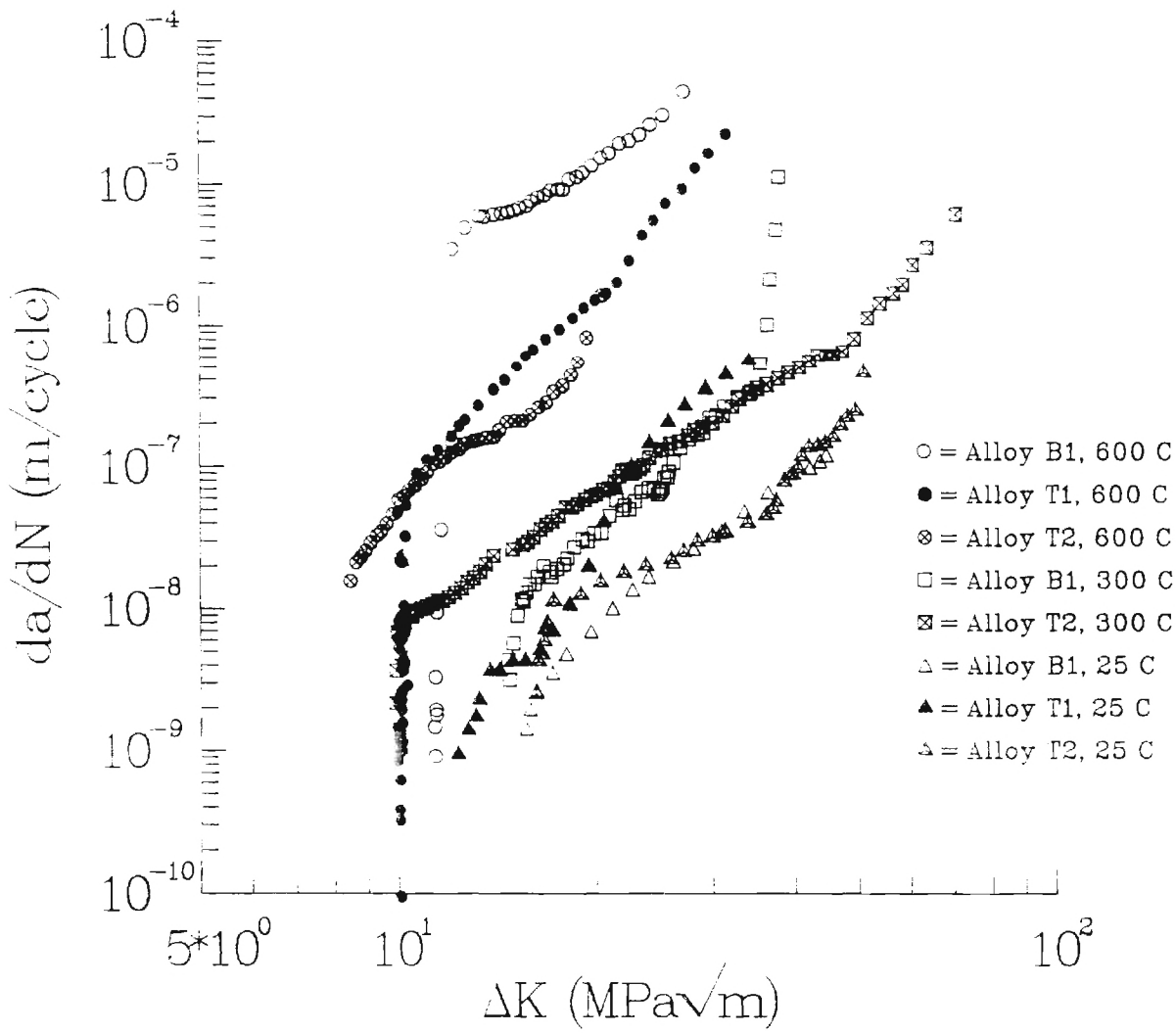

Figure 16: Master FCP plot for the three experimental alloys. R=0.1, ν = 10 Hz, air enviornment.

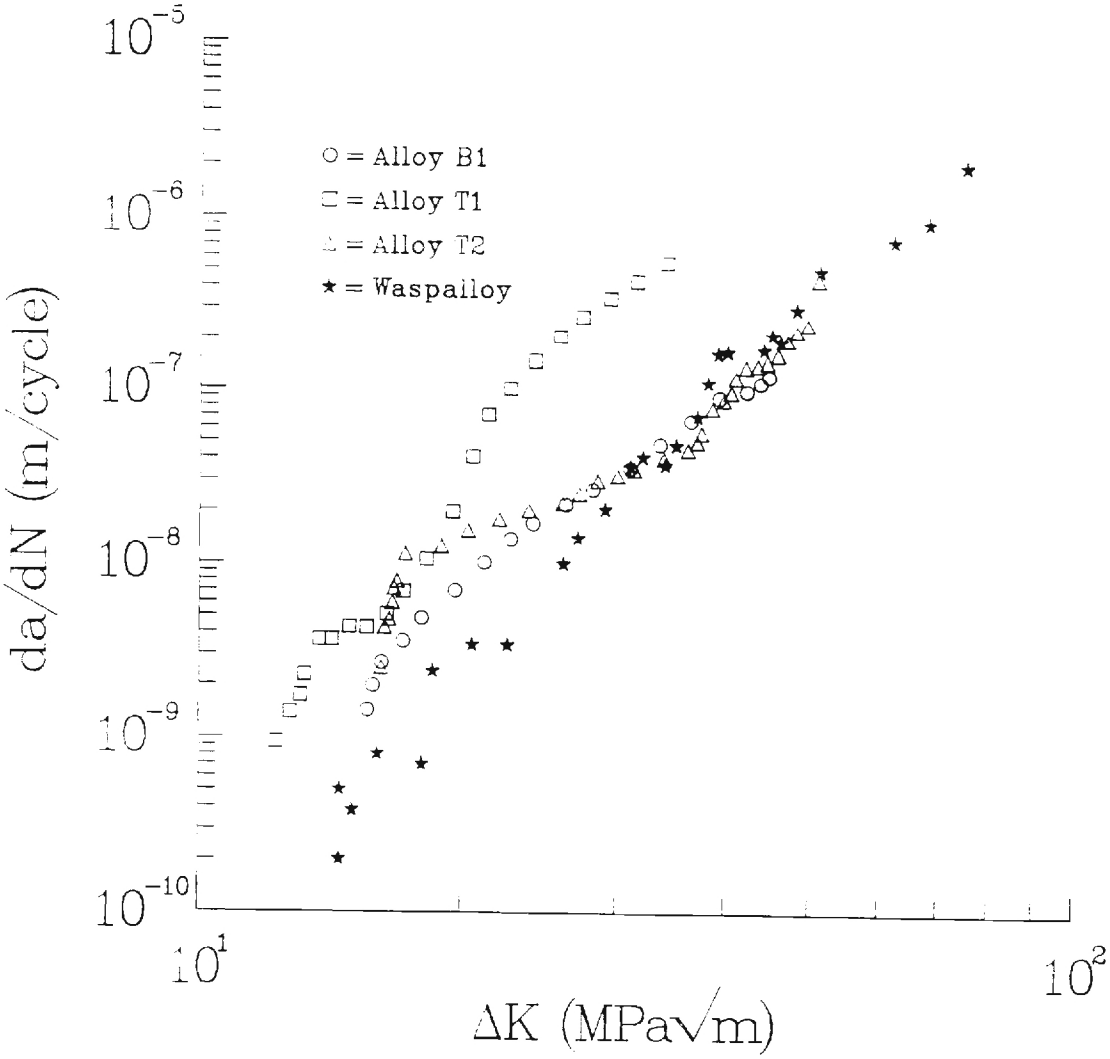

Figure 17: Comparison of the FCP response of the experimental Ni_3Al alloys to that of Waspalloy at 25° C, R=0.1, ν = 10 Hz. (Waspalloy data obtained from [14]

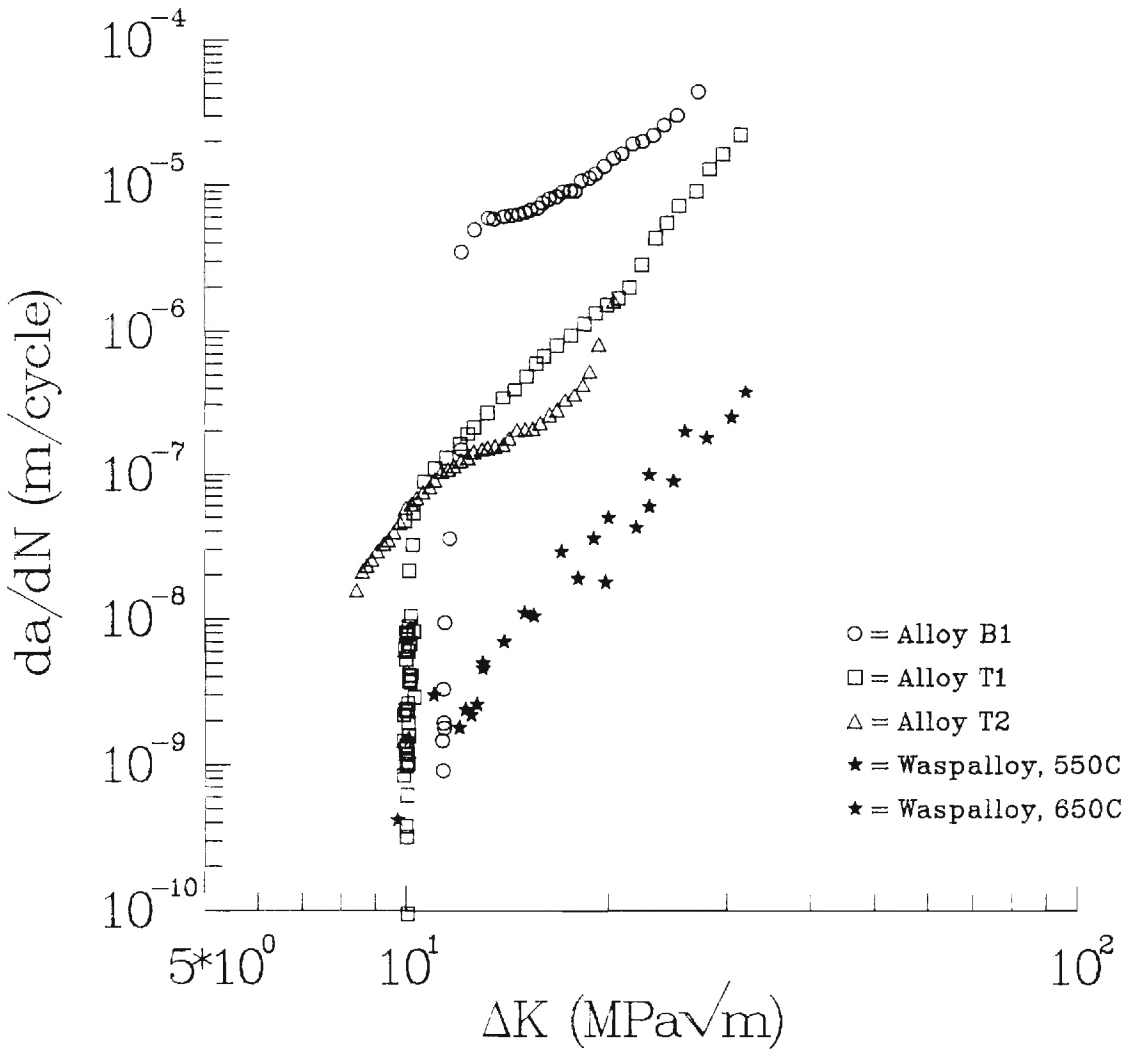

Figure 18: Comparison of the FCP response of the experimental Ni_3Al alloys to that of Waspalloy at 600° C, R=0.1, ν = 10 Hz. As the FCP data of the Waspalloy is identical at 550°C and 650°, it is expected that the 600°C is also represented (Waspalloy data obtained from [14]

References

[1] Stephen D. Antolovich and Graham Webb. *Cyclic Deformation, Damage, and Effects of Enviornment in the Ni_3Al Ordered Alloy At Elevated Temperature.* Technical Report, Georgia Institute of Technology, June 1989. Progress Report for 12-1-88 through 6-1-89 for AFOSR-87-0162.

[2] E.M. Schulson, I. Baker, and H.J. Frost. The Strength and Ductility of Intermetallic Compounds: Grain Size Effects. In C.C. Koch, C.T. Liu, and N.S. Stoloff, editors, *High Temperature Ordered Intermetallic Alloys*, pages 195–205, Materials Research Society Symposium, 1985.

[3] A. M. Gokhale. Unbiased Estimation of Curve Length in 3D Using Vertical Slices. *Journal of Microscopy*, in press.

[4] D.N. Sieloff, S.S. Brenner, and Hua Ming-Jian. The Microchemistry of Grain Boundaries in Ni_3Al. In C.T.Liu, A.I.Taub, N.S. Stoloff, and C.C. Koch, editors, *High Temperature Ordered Intermetallic Alloys III*, pages 155–160, Materials Research Society Symposium, 1989.

[5] C.T.Liu, C.L.White, and J.A. Horton. Effect of Boron Grain-Boundaries in Ni_3Al. *Acta Metall*, 33:213–229, 1985.

[6] C.T. Liu. Ductility and Fracture Behavior of Polycrystalline Ni_3Al Alloys. In N.S. Stoloff, C.C. Koch, C.T.Liu, and O.Izumi, editors, *High Temperature Ordered Intermetallic Alloys II*, pages 355–367, Materials Research Society Symposium, 1987.

[7] E.M.Schulson, T.P.Weihs, I.Baker, H.J.Frost, and J.A.Horton. Grain Boundary Accommadation of Slip in Ni_3Al Containing Boron. *Acta Metall*, 34:1395–1399, 1986.

[8] A.H. King and M.H. Yoo. Dislocation Reactions at Grain Boundaries in $l1_2$ Ordered Alloys. In N.S. Stoloff, C.C. Koch, C.T.Liu, and O.Izumi, editors, *High Temperature Ordered Intermetallic Alloys II*, pages 99–104, Materials Research Society Symposium Proceedings, 1987.

[9] D.P. Pope and C.T. Liu. Strength and Ductility of Intermetallic Compounds. In J. Tien and Caulfield, editors, *Superalloys, Composites, and Ceramics*, pages 583–624, American Society of Materials, 1989.

[10] J.K. Tien, S. Eng, and J.M. Sanchez. An Overview of the Temperature Dependence of the Strength of the Ni_3Al System. In N.S. Stoloff, C.C. Koch, C.T.Liu, and O.Izumi, editors, *High Temperature Ordered Intermetallic Alloys II*, pages 183–193, Materials Research Society Symposium Proceedings, 1987.

[11] S. Miura, S. Ochiai, Y. Oya, Y. Mishima, and T. Suzuki. Effect of Strain Rate on the Plastic Behaviour of $L1_2$ Compounds Based on Ni_3Al. In C.T.Liu, A.I.Taub, N.S. Stoloff, and C.C. Koch, editors, *High Temperature Ordered Intermetallic Alloys III*, pages 341–346, Materials Research Society Symposium Proceedings, 1989.

[12] V.Paidar, D.P. Pope, and V.Vitek. A Theory of the Anomalous Yield Behavior in $L1_2$ Ordered Alloys. *Acta Metall*, 32:435–48, 1984.

[13] L.M. Hsiung and N.S. Stoloff. Electron Microscopy Study of Fatigue Crack Intiation in Ni_3Al Single Crystals. In C.T.Liu, A.I.Taub, N.S.Stoloff, and C.C.Koch, editors, *High Temperature Ordered Intermetallic Alloys III*, pages 261–267, Materials Research Society Symposium Proceedings, 1989.

[14] M. Clavel, C. Levaillant, and A. Pineau. Influence of the Micromechansims of Cyclic Deformation at Elevated Temperature on Fatigue Response. In *Deformation at Elevated Temperatures*, pages 24–45, American Society for Testing of Materials, 1978.

[15] S.D. Antolovich, A. Saxena, and G.R. Chanani. A Model for Fatigue Crack Propagation. *Engineering Fracture Mechanics*, 7:649–652, 1975.

[16] A. Taylor and R.W. Floyd. Experimental Determination of Phase Equilibria Within the System Ni-Cr-Al. *Journal of the Institute of Metals*, 81:451, 1953.

GEORGIA TECH 1885-1985

DESIGNING TOMORROW TODAY

Georgia Institute of Technology
School of Materials Engineering
Atlanta, Georgia 30332-0245
(404) 894- 2816

May 31, 1988

Dr. Alan H. Rosenstein
Air Force Office of Scientific Research
Electronic and Materials Sciences
Building 410
Bolling AFB, D.C. 20332-6448

Dear Dr. Rosenstein:

Enclosed you will find 6 copies of the annual technical progress report for AFOSR-87-0162. If you need additional information, please give me a call.

Sincerely,

Stephen D. Antolovich, Director
Mechanical Properties Research Lab
Professor and Director
School of Materials Engineering

SDA/ptl

CYCLIC DEFORMATION, DAMAGE, AND EFFECTS OF ENVIRONMENT IN THE NI_3AL ORDERED ALLOY AT ELEVATED TEMPERATURES

PREPARED BY:

Stephen D. Antolovich

Professor and Director
School of Materials Engineering
Georgia Institute of Technology
Atlanta, Georgia 30332

Progress Report for period 5-1-87 through 5-1-88
Contract No. AFOSR-87-0162

Air Force Office of Scientific Research
Electronic and Material Sciences
Building 410
Bolling AFB, D.C. 20332

Program Manager: Dr. A. H. Rosenstein

I. Program Overview

In this study, a basic program is defined to investigate cyclic deformation, damage accumulation, and fatigue crack propagation (FCP) in the ordered Ni_3Al system as affected by composition, temperature, and environment. While this class of ordered alloys shows great promise for elevated temperature applications in jet and rocket engines, problems of brittleness and damage by hostile environments have been encountered in monotonic tensile deformation. The basic mechanisms of cyclic deformation and fatigue crack propagation have not been fully investigated; yet they must be understood if these materials are to be used in advanced applications.

II. Program Status

A. Material Preparation

To investigate the role of boron in improving the ductility of this class of material two compositions were chosen, one which exhibits brittle behavior and the other which exhibits non-brittle behavior. Two other compositions, one subject to environmental influences and the other possessing relative insensitivity to environment will be used will be used to study the mechanisms of environmental embrittlement under conditions of cyclic loading.

Powder metallurgy techniques were used for the production of the above mentioned alloys by Homogeneous Metals, Inc. Each of the four alloys was produced by atomization of the melt resulting

in power particles having identical chemistries. The powder alloys were then screened to +80-400 and extruded to produce 12' long bars approximately 2" in diameter which yielded nearly 200 lbs. of usable material of each of the four compositions. In addition, 50 lbs. of excess powder material for each of the four alloys was obtained which can be used in future investigations.

The compositions of the alloys are as follows;

			Atomic Percent					
Alloy	Ni	Al	Cr	B	C	S	N_2 (ppm)	O_2 (ppm)
A	Bal	12.91	0.0	.045	.0099	<.001	4	170
B	Bal	12.41	0.0	.048	.0066	<.001	5	72
C	Bal	10.26	8.0	.046	.0075	<.001	3	84
D	Bal	8.70	7.7	.046	.0060	<.001	3	84

In addition to the +80-400 powder, a small section attach to the end of each extrusion consisting of -400 mesh powder was produced providing an opportunity to fabricate a limited number of samples from very fine powder material.

Optical metallagraphy of the extruded material reveals a fine grain material, ~80 μm, in both the transverse and longitudinal directions as shown in Fig. 1. Orientation studies utilizing the transmission electron microscope are currently underway to determine if any crystallographic texturing occured as the result of the extrusion process. The grains consist of both a dendritic and a lamellar structure with different lamellar spacings present within a given alloy.

Because Ni_3Al can exist over a range of compositions it is possible that the microstructure consists of a partially ordered solid solution whose composition varies in a systematic fashion. It is also possible that two phases are present, one being the strongly ordered Ni_3Al and the other a random solid solution of nickel. X-ray diffractometery studies of the alloys are underway to establish the degree of order in each alloy by measuring the intensity of the superlattice reflections. A typical structure as seen in the TEM is shown in Fig. 2.

Low cycle fatigue, Tensile, and FCP specimens will be machined from the extruded rods. Machining is to be performed by Mastersons Manufacturing and is expected to be completed by June 1988.

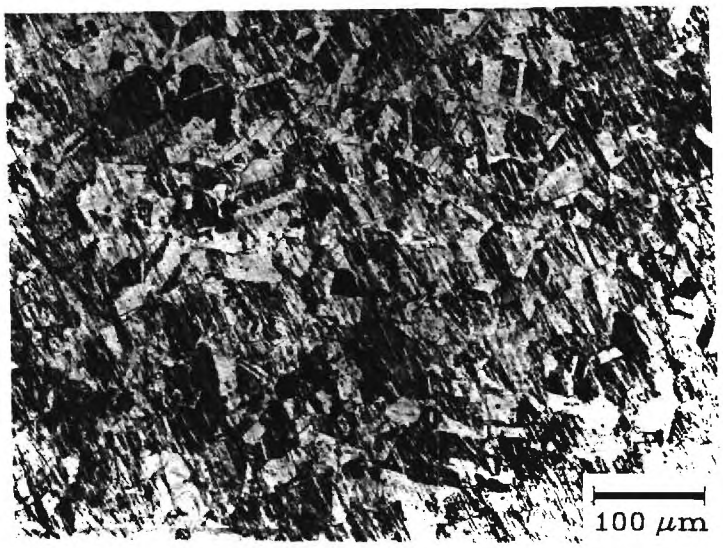

(a)

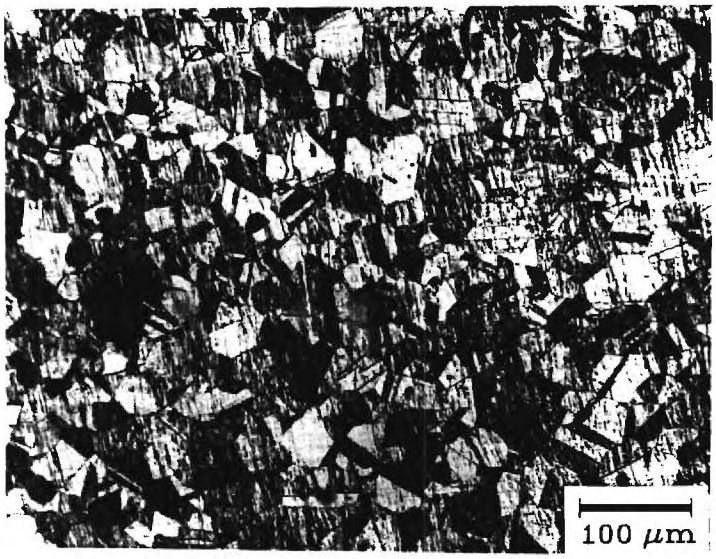

(b)

Figure 1 - Optical micrograph of specimen C, -80/+400 mesh along a) longitudinal and b) transverse direction.

Figure 2 - TEM micrograh of specimen C, -400 mesh showing low dislocation density and small grain size due to rapid cooling during atomization.

U-10-636

GEORGIA TECH 1885-1985

DESIGNING TOMORROW TODAY

Georgia Institute of Technology
School of Materials Engineering
Atlanta, Georgia 30332-0245
(404) 894-

June 8, 1988

Mr. David Harmon
McDonnel Douglas Corporation
McDonnel Aircraft Company
Box 516
St. Louis, Missouri 63166

Dear Dave,

Enclosed please find test results for fatigue experiments of Ti 6242 at 1000F, R=0.5 and a 30s hold. As usual, I have included graphs and all of the raw data. If you have any questions, just give me a call.

I hope all is going well with you. Again, please call if you have any questions or need more information.

Sincerely,

Stephen D. Antolovich, Director
Mechanical Properties Research Lab
Professor and Director
School of Materials Engineering

SDA/ptl

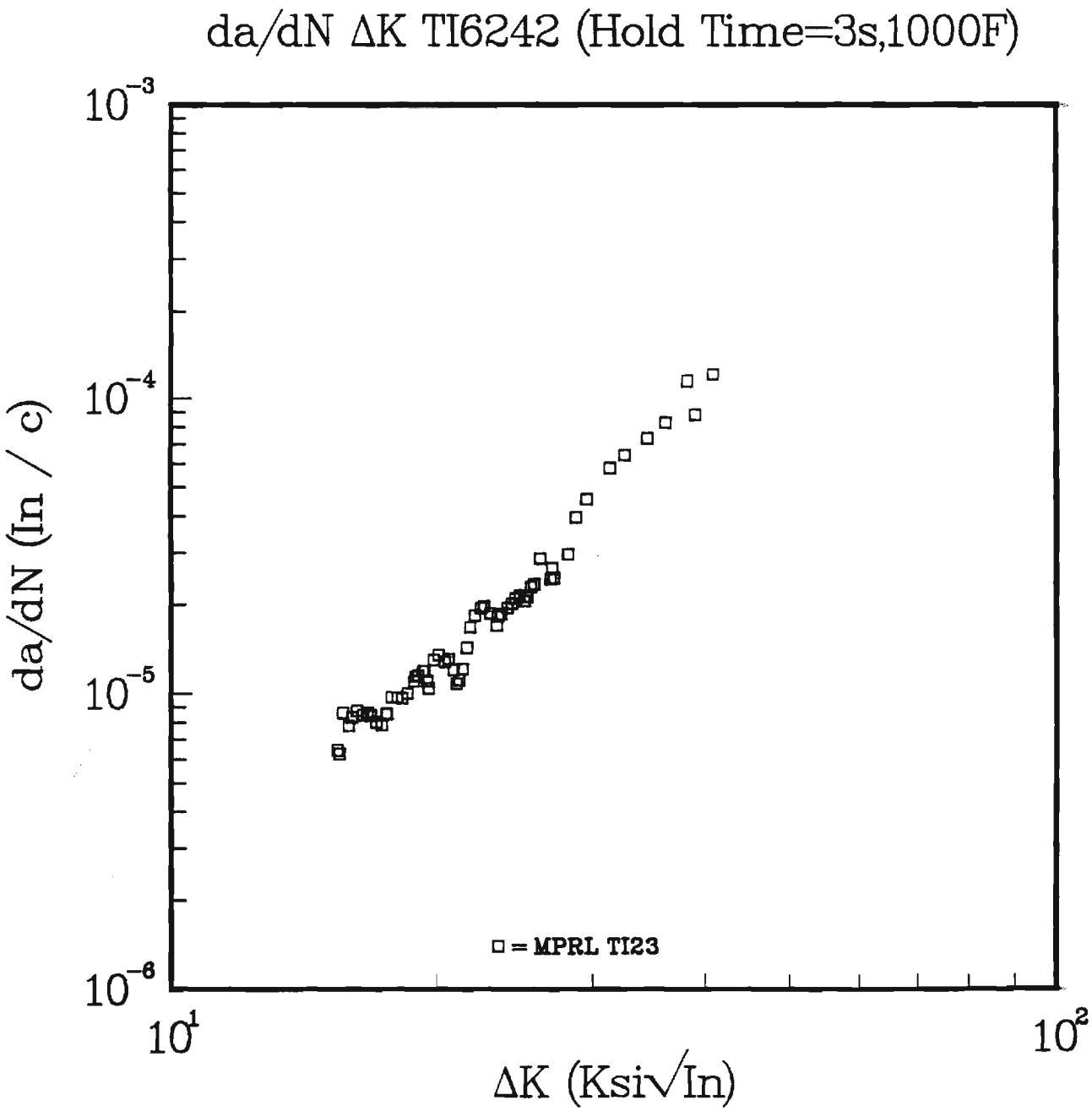
da/dN ΔK TI6242 (Hold Time=3s,1000F)
10^-3
10^-4
10^-5
10^-6
da/dN (In / c)
10^1
10^2
ΔK (Ksi√In)
□ = MPRL TI23

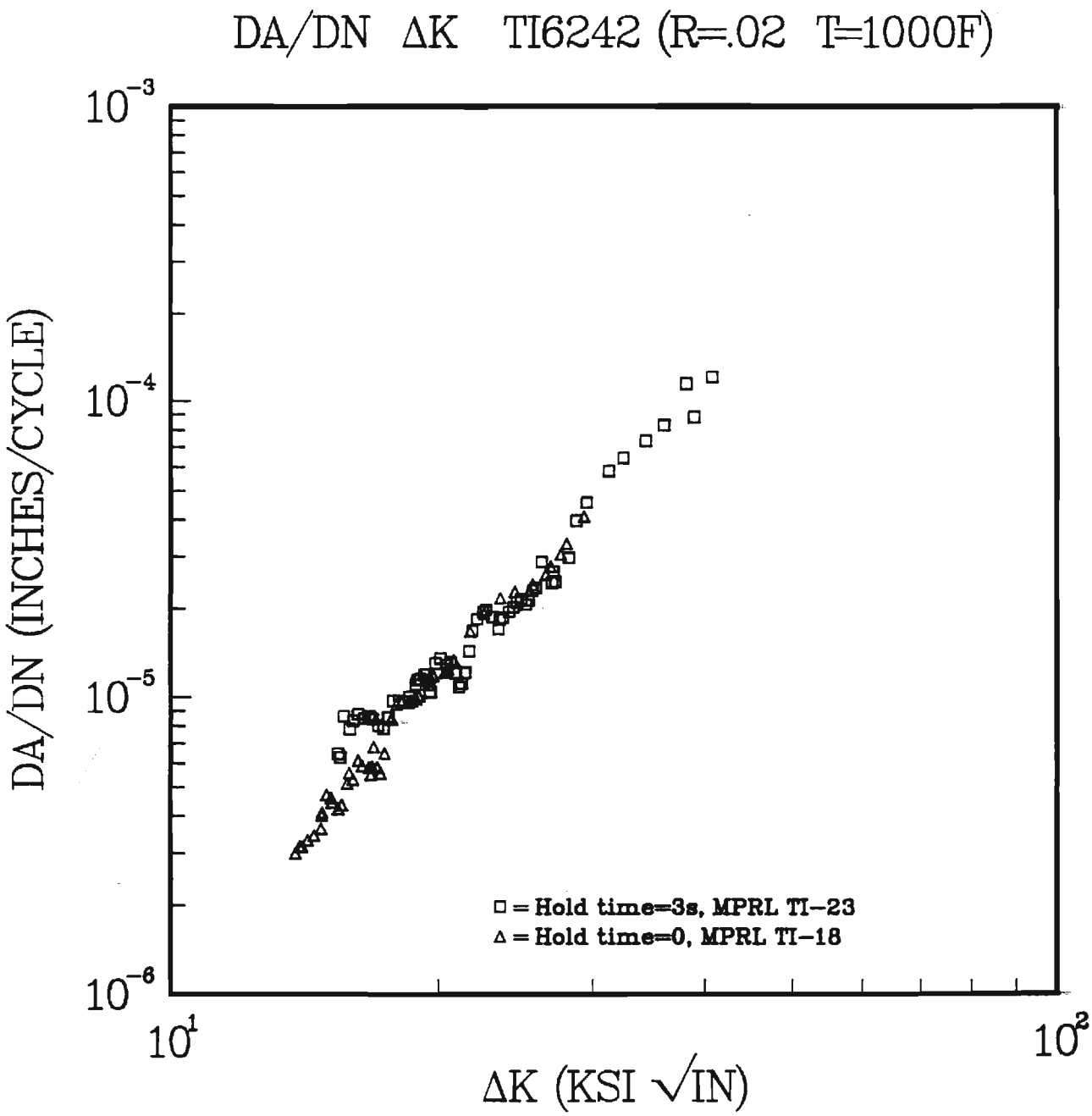
DA/DN ΔK TI6242 (R=.02 T=1000F)
DA/DN (INCHES/CYCLE)
10^-3
10^-4
10^-5
10^-6
10^1
10^2
ΔK (KSI √IN)
□ = Hold time=3s, MPRL TI-23
△ = Hold time=0, MPRL TI-18

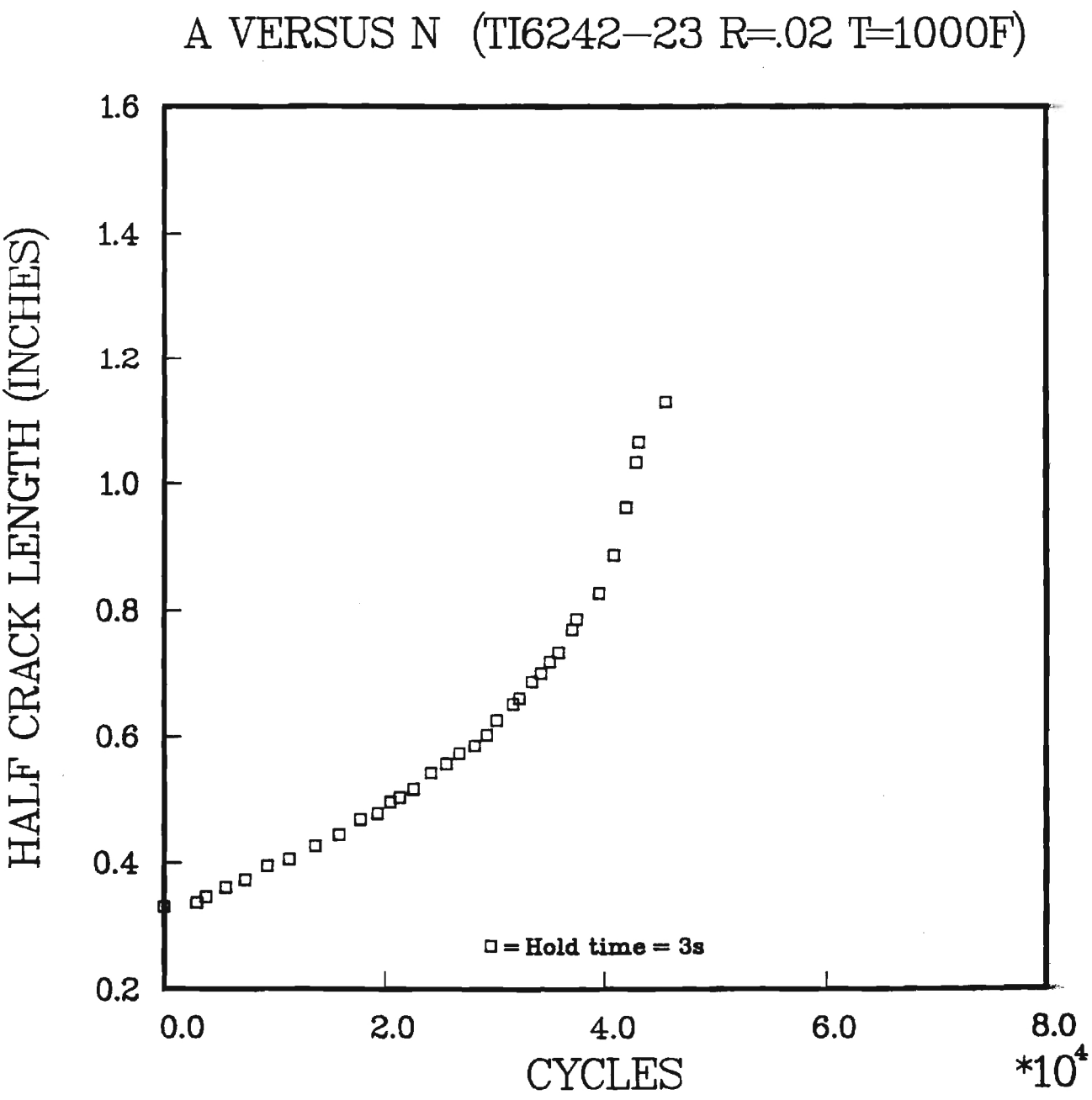
A VERSUS N (TI6242–23 R=.02 T=1000F)
HALF CRACK LENGTH (INCHES)
1.6
1.4
1.2
1.0
0.8
0.6
0.4
0.2
0.0
2.0
4.0
6.0
8.0
CYCLES
*10^4
□ = Hold time = 3s

N POINT INC.POLYNOMIAL METHOD FOR DET. DA/DN

SPECIMEN IDENTIFICATION >> TI-23
LOG BOOK REFERENCE >>
MATERIAL TESTED >> TI6242
DATE TESTED >> 5-17-88
INITIALS OF THE TESTOR >> LV
TODAY'S DATE >> 5-21-88

NO. POINTS= 68 HOLD TIME = 3 s

CT SPECIMEN B= 0.185 IN. W= 3.000 IN. AM= 0.000 IN.

Pmin= 0.163Kips Pmax= 8.163Kips R= 0.020 Test Freq= 0.250Hz.

TEMP.= 538.C Environment= AIR Yield Strength= 140.00 ksi

OBS.NO.	CYCLES	A (Half crack) (")	DELK (Ksi*In**1/2)	DA/DN ("/c)
1	0.	0.3295		
2	880.	0.3327		
3	2980.	0.3358		
4	3300.	0.3390	15.38	0.642E-05
5	3800.	0.3449	15.47	0.624E-05
6	4350.	0.3480	15.61	0.859E-05
7	5570.	0.3598	15.85	0.778E-05
8	6450.	0.3630	15.99	0.830E-05
9	7340.	0.3717	16.19	0.874E-05
10	8490.	0.3799	16.47	0.846E-05
11	9340.	0.3941	16.67	0.859E-05
12	10050.	0.3969	16.81	0.843E-05
13	11340.	0.4047	17.06	0.800E-05
14	12700.	0.4154	17.30	0.782E-05
15	13700.	0.4256	17.51	0.855E-05
16	14800.	0.4335	17.75	0.972E-05
17	15850.	0.4433	18.03	0.972E-05
18	16780.	0.4531	18.26	0.964E-05
19	17750.	0.4677	18.51	0.100E-04
20	19000.	0.4748	18.83	0.110E-04
21	19320.	0.4772	18.90	0.114E-04
22	19910.	0.4866	19.05	0.115E-04
23	20490.	0.4957	19.27	0.119E-04
24	20820.	0.4980	19.36	0.119E-04
25	21340.	0.5028	19.50	0.110E-04
26	21700.	0.5071	19.57	0.104E-04
27	22600.	0.5161	19.84	0.130E-04
28	23200.	0.5248	20.09	0.135E-04
29	24190.	0.5421	20.45	0.128E-04
30	24700.	0.5504	20.64	0.131E-04
31	25600.	0.5567	20.92	0.120E-04
32	26200.	0.5630	21.08	0.108E-04

33	26800.	0.5732	21.23	0.111E-04
34	27400.	0.5791	21.42	0.121E-04
35	28200.	0.5850	21.66	0.143E-04
36	28750.	0.5949	21.84	0.168E-04
37	29300.	0.6028	22.12	0.184E-04
38	29890.	0.6181	22.47	0.195E-04
39	30200.	0.6256	22.65	0.198E-04
40	30880.	0.6370	23.03	0.187E-04
41	31700.	0.6516	23.41	0.170E-04
42	31920.	0.6551	23.49	0.183E-04
43	32280.	0.6606	23.68	0.186E-04
44	33000.	0.6728	24.07	0.195E-04
45	33450.	0.6870	24.34	0.202E-04
46	33830.	0.6921	24.57	0.210E-04
47	34280.	0.7004	24.85	0.215E-04
48	34790.	0.7122	25.16	0.206E-04
49	35060.	0.7189	25.34	0.213E-04
50	35500.	0.7287	25.60	0.230E-04
51	35850.	0.7335	25.83	0.235E-04
52	36400.	0.7465	26.23	0.287E-04
53	37070.	0.7697	26.95	0.244E-04
54	37220.	0.7728	27.06	0.266E-04
55	37450.	0.7862	27.19	0.246E-04
56	38950.	0.8039	28.19	0.297E-04
57	39500.	0.8272	28.76	0.397E-04
58	40000.	0.8449	29.54	0.456E-04
59	40850.	0.8874	31.32	0.581E-04
60	41330.	0.9303	32.52	0.643E-04
61	41950.	0.9626	34.45	0.734E-04
62	42390.	0.9953	36.08	0.829E-04
63	42840.	1.0339	38.18	0.114E-03
64	42880.	1.0425	38.95	0.881E-04
65	43090.	1.0657	40.79	0.120E-03
66	43420.	1.1177		
67	45470.	1.1295		
68	43550.	1.1535		

Rupture at N = 43620 c

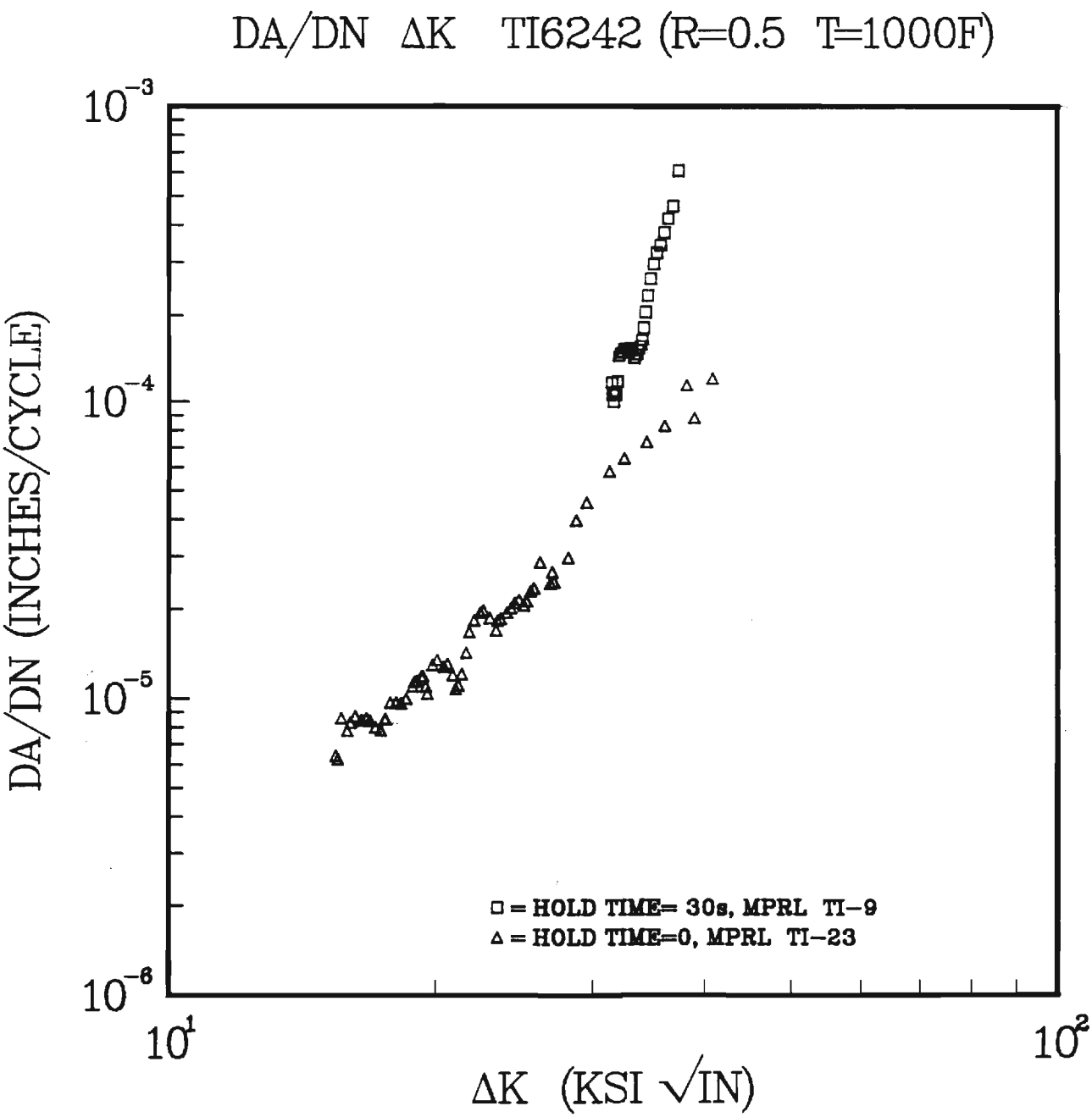
DA/DN ΔK TI6242 (R=0.5 T=1000F)
DA/DN (INCHES/CYCLE)
10^-3
10^-4
10^-5
10^-6
10^1
10^2
ΔK (KSI √IN)
□ = HOLD TIME= 30s, MPRL TI-9
△ = HOLD TIME=0, MPRL TI-23

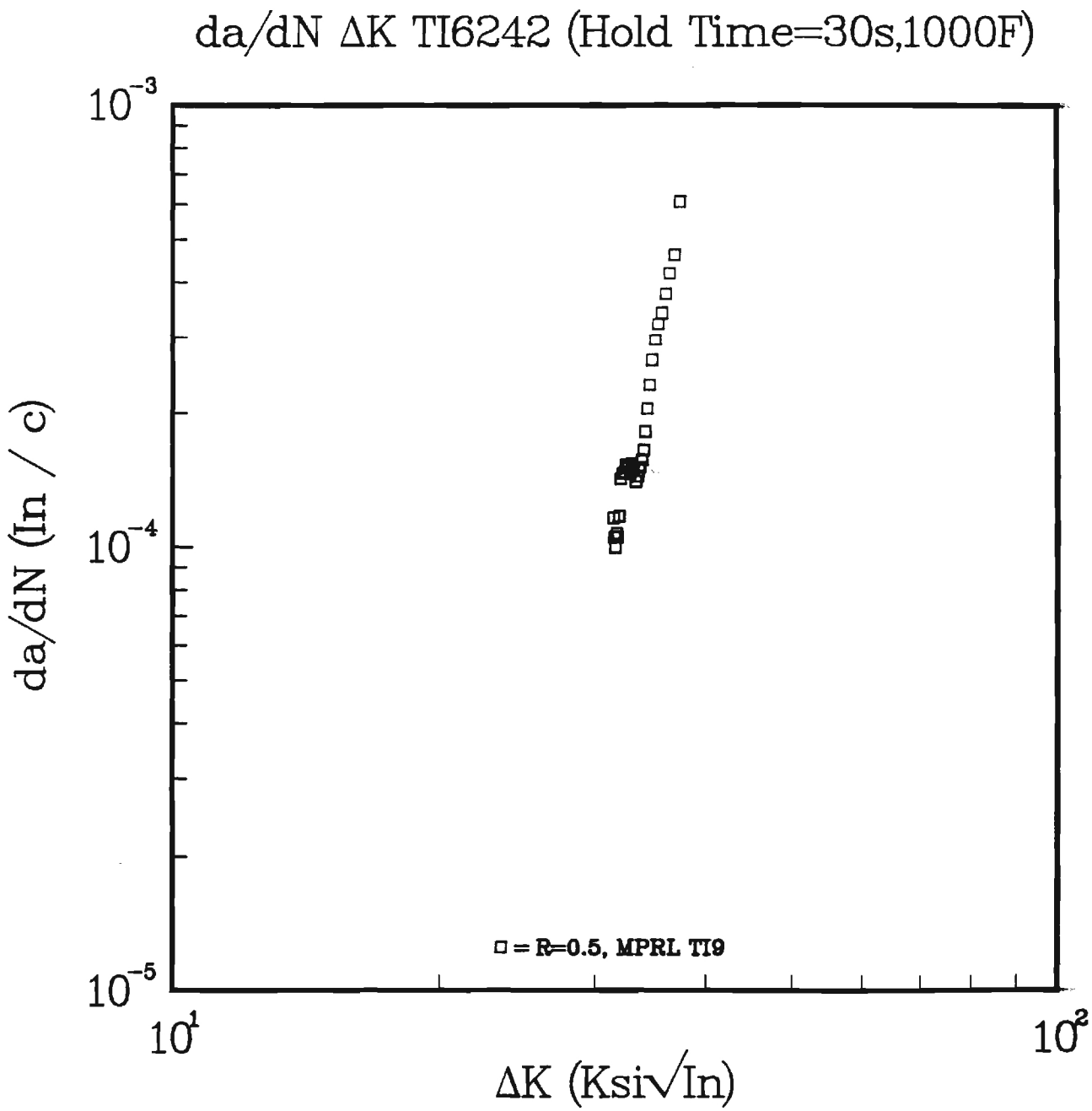
da/dN ΔK TI6242 (Hold Time=30s,1000F)
10^{-3}
10^{-4}
10^{-5}
da/dN (In / c)
□ = R=0.5, MPRL TI9
10^{1}
10^{2}
ΔK (Ksi√In)

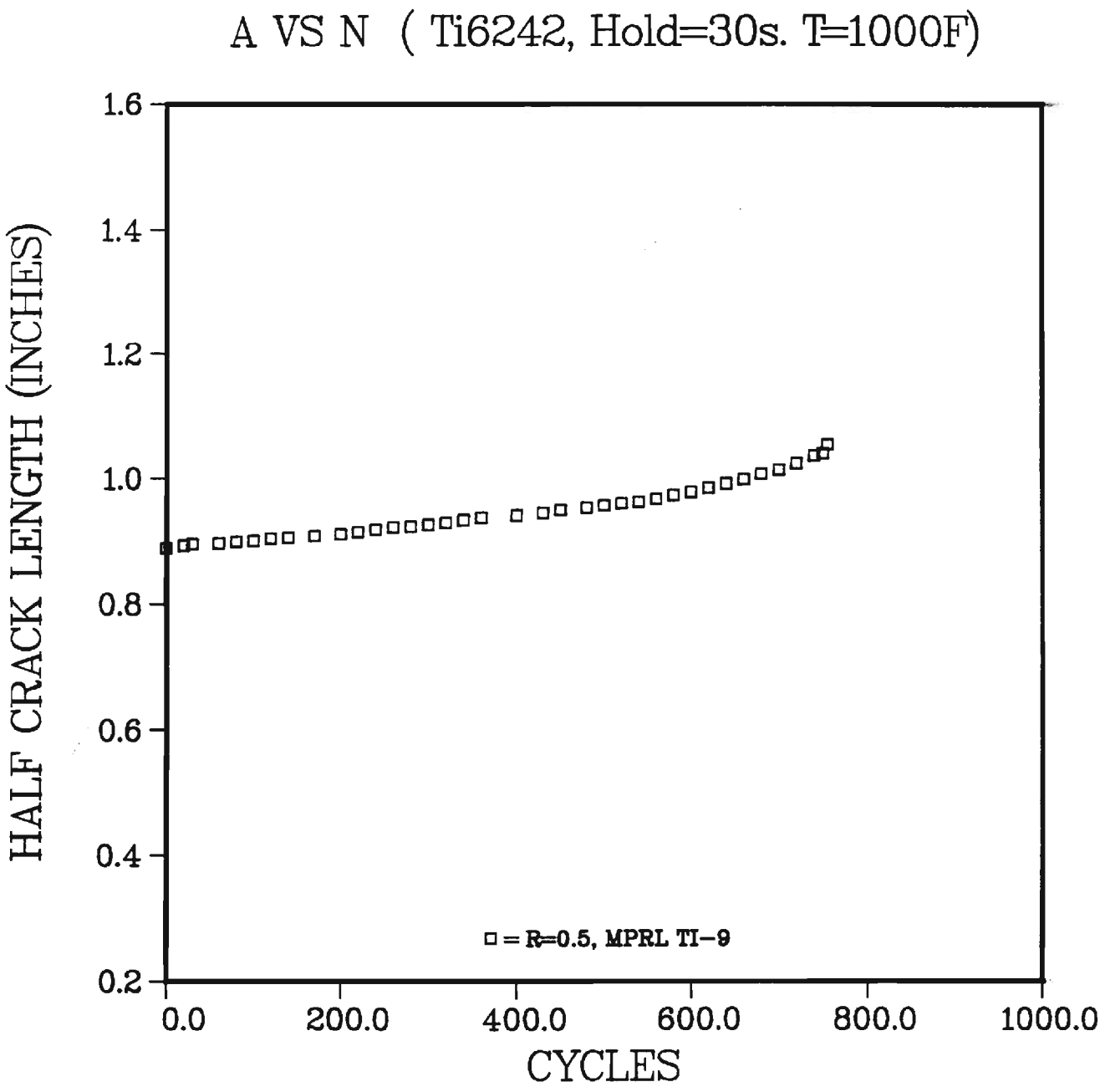
A VS N (Ti6242, Hold=30s. T=1000F)
HALF CRACK LENGTH (INCHES)
1.6
1.4
1.2
1.0
0.8
0.6
0.4
0.2
0.0
200.0
400.0
600.0
800.0
1000.0
CYCLES
□ = R=0.5, MPRL TI-9

N POINT INC.POLYNOMIAL METHOD FOR DET. DA/DN

SPECIMEN IDENTIFICATION >> TI-9
LOG BOOK REFERENCE >>
MATERIAL TESTED >> TI6242
DATE TESTED >> 5-30-88
INITIALS OF THE TESTOR >> LV
TODAY'S DATE >> 6-2-88

NO. POINTS= 37 Hold time = 30 s.

CT SPECIMEN B= 0.185 IN. W= 3.000 IN. AM= 0.000 IN.

Pmin= 8.000Kips Pmax=16.000Kips R= 0.500 Test Freq= 0.032Hz.

TEMP.= 538.C Environment= AIR Yield Strength= 140.00 ksi

OBS.NO.	CYCLES	A (")	DELK (Ksi*In**1/2)	DA/DN ("/c)
1	0.	0.8886		
2	20.	0.8925		
3	30.	0.8953		
4	60.	0.8965	31.50	0.116E-03
5	80.	0.8992	31.57	0.105E-03
6	100.	0.9004	31.66	0.996E-04
7	120.	0.9043	31.76	0.107E-03
8	140.	0.9055	31.83	0.105E-03
9	170.	0.9083	31.95	0.117E-03
10	200.	0.9110	32.08	0.142E-03
11	220.	0.9146	32.22	0.146E-03
12	240.	0.9185	32.36	0.147E-03
13	260.	0.9224	32.50	0.153E-03
14	280.	0.9236	32.61	0.151E-03
15	300.	0.9264	32.73	0.153E-03
16	320.	0.9299	32.88	0.146E-03
17	340.	0.9339	33.02	0.154E-03
18	360.	0.9374	33.14	0.149E-03
19	400.	0.9409	33.37	0.140E-03
20	430.	0.9449	33.55	0.144E-03
21	450.	0.9496	33.67	0.151E-03
22	480.	0.9531	33.90	0.157E-03
23	500.	0.9567	34.05	0.165E-03
24	520.	0.9602	34.18	0.182E-03
25	540.	0.9626	34.35	0.205E-03
26	560.	0.9673	34.55	0.232E-03
27	580.	0.9732	34.78	0.264E-03
28	600.	0.9780	35.07	0.296E-03
29	620.	0.9846	35.36	0.323E-03
30	640.	0.9913	35.69	0.342E-03
31	660.	0.9980	36.05	0.377E-03
32	680.	1.0067	36.42	0.420E-03
33	700.	1.0134	36.88	0.462E-03

34	720.	1.0240	37.39	0.608E-03
35	740.	1.0362		
36	750.	1.0402		
37	755.	1.0543		

Rupture at N = 760 c.

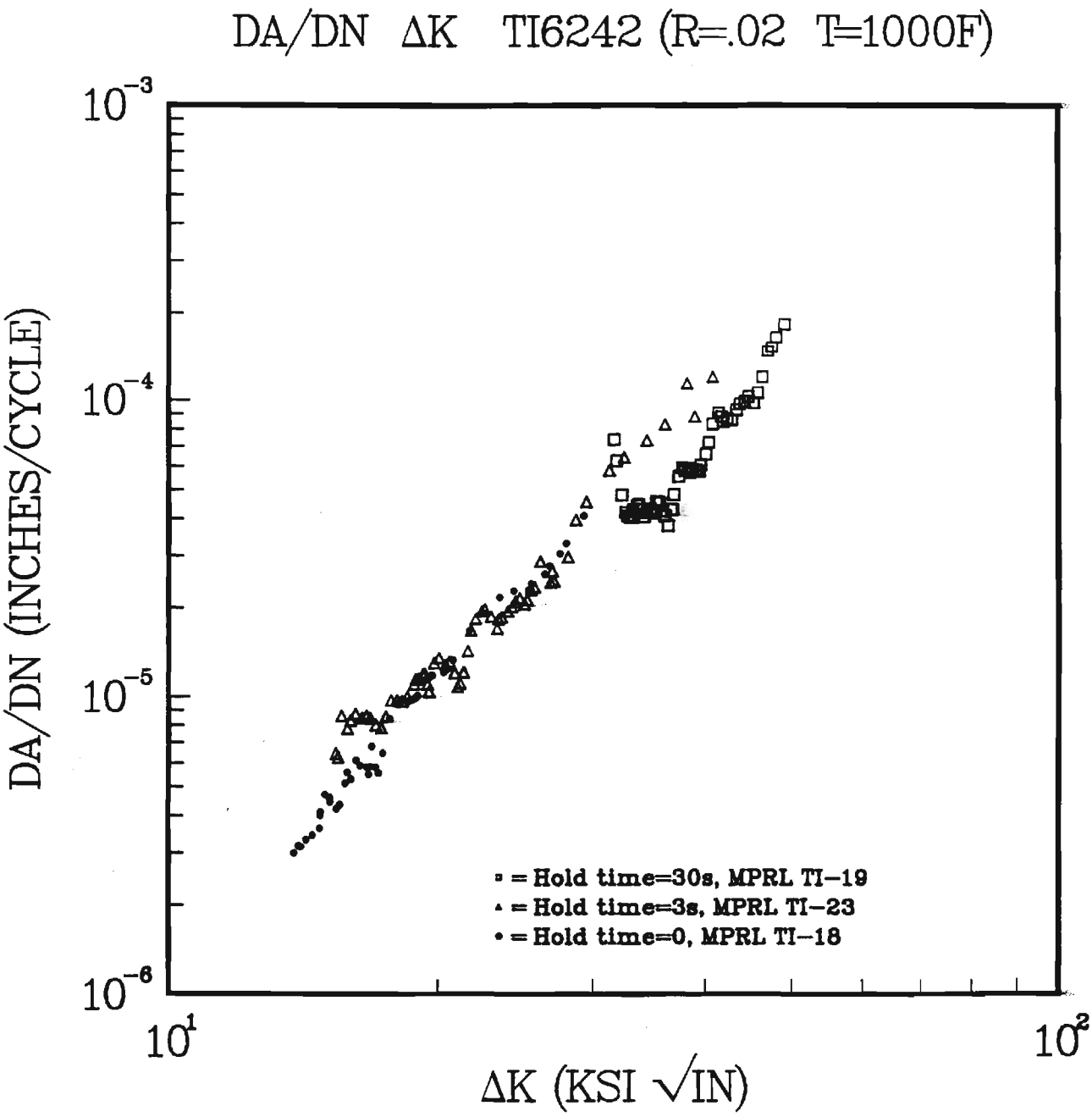
DA/DN ΔK TI6242 (R=.02 T=1000F)
DA/DN (INCHES/CYCLE)
ΔK (KSI √IN)
10^-3
10^-4
10^-5
10^-6
10^1
10^2
▫ = Hold time=30s, MPRL TI-19
▵ = Hold time=3s, MPRL TI-23
• = Hold time=0, MPRL TI-18

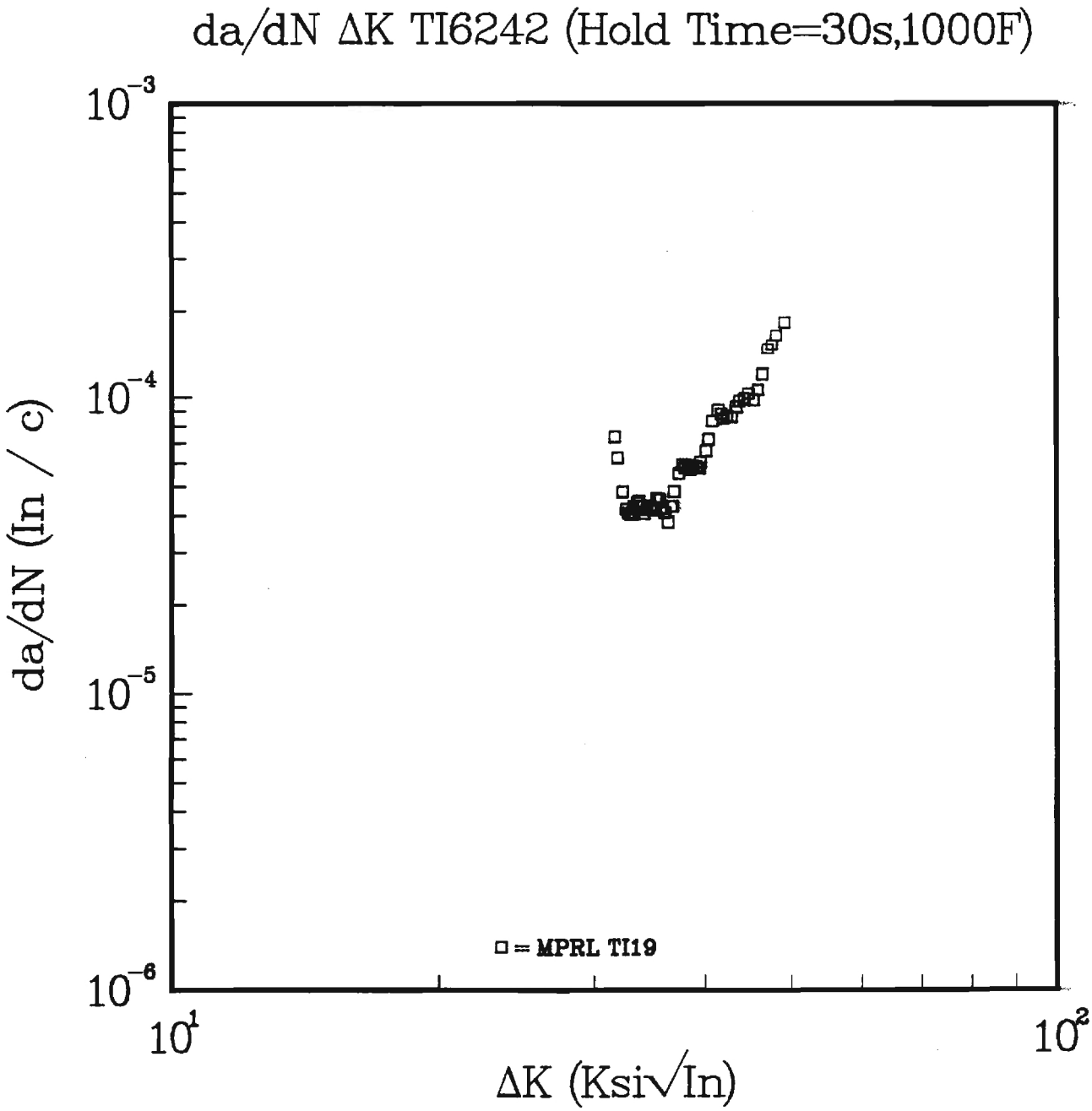
da/dN ΔK TI6242 (Hold Time=30s,1000F)
da/dN (In / c)
10^-3
10^-4
10^-5
10^-6
10^1
10^2
ΔK (Ksi√In)
□ = MPRL TI19

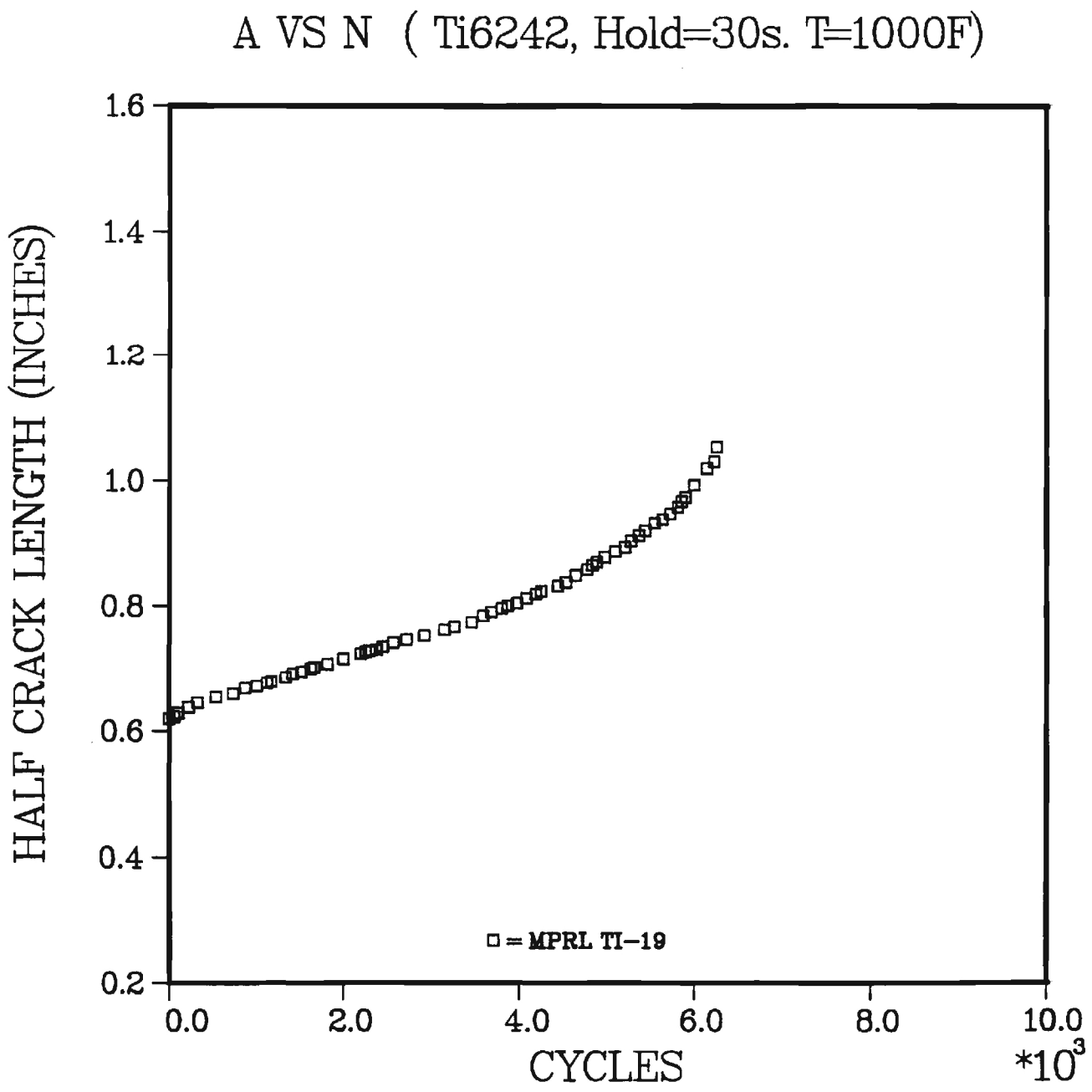
A VS N (Ti6242, Hold=30s. T=1000F)
HALF CRACK LENGTH (INCHES)
1.6
1.4
1.2
1.0
0.8
0.6
0.4
0.2
0.0
2.0
4.0
6.0
8.0
10.0
CYCLES
*10^3
□ = MPRL TI-19

VEN POINT INC.POLYNOMIAL METHOD FOR DET. DA/DN

SPECIMEN IDENTIFICATION >> TI-19
LOG BOOK REFERENCE >>
MATERIAL TESTED >> TI6242
DATE TESTED >> 5-23-88
INITIALS OF THE TESTOR >> LV
TODAY'S DATE >> 5-26-88

NO. POINTS= 59 Hold time = 30s.

CCT SPECIMEN B= 0.185 IN. W= 3.000 IN. AM= 0.000 IN.

Pmin= 0.225Kips Pmax=11.241Kips R= 0.020 Test Freq= 0.032Hz.

TEMP.= 538.C Environment= AIR Yield Strength= 140.00 ksi

OBS.NO.	CYCLES	A (Half crack) (")	DELK (Ksi*In**1/2)	DA/DN ("/c)
1	0.	0.6185		
2	60.	0.6224		
3	105.	0.6280		
4	225.	0.6374	31.69	0.736E-04
5	325.	0.6449	31.91	0.624E-04
6	535.	0.6539	32.32	0.480E-04
7	730.	0.6594	32.62	0.420E-04
8	865.	0.6685	32.82	0.408E-04
9	1000.	0.6720	33.04	0.403E-04
10	1120.	0.6772	33.24	0.430E-04
11	1170.	0.6791	33.31	0.404E-04
12	1340.	0.6858	33.61	0.442E-04
13	1420.	0.6913	33.75	0.447E-04
14	1520.	0.6945	33.94	0.429E-04
15	1630.	0.6996	34.13	0.430E-04
16	1670.	0.7016	34.19	0.405E-04
17	1820.	0.7067	34.44	0.419E-04
18	2000.	0.7150	34.74	0.431E-04
19	2200.	0.7232	35.10	0.417E-04
20	2260.	0.7264	35.22	0.425E-04
21	2300.	0.7283	35.28	0.457E-04
22	2380.	0.7299	35.45	0.455E-04
23	2450.	0.7346	35.59	0.452E-04
24	2570.	0.7413	35.80	0.423E-04
25	2720.	0.7461	36.05	0.409E-04
26	2920.	0.7524	36.37	0.379E-04
27	3150.	0.7618	36.72	0.430E-04
28	3260.	0.7665	36.93	0.482E-04
29	3460.	0.7740	37.39	0.554E-04
30	3590.	0.7846	37.72	0.593E-04
31	3680.	0.7909	37.98	0.580E-04

32	3800.	0.7969	38.34	0.590E-04
33	3870.	0.8012	38.50	0.572E-04
34	3970.	0.8055	38.76	0.586E-04
35	4080.	0.8130	39.10	0.583E-04
36	4190.	0.8201	39.40	0.576E-04
37	4250.	0.8244	39.54	0.606E-04
38	4440.	0.8327	40.09	0.660E-04
39	4530.	0.8386	40.36	0.722E-04
40	4640.	0.8496	40.78	0.832E-04
41	4770.	0.8591	41.40	0.907E-04
42	4830.	0.8657	41.70	0.881E-04
43	4880.	0.8709	41.94	0.848E-04
44	4970.	0.8787	42.33	0.866E-04
45	5090.	0.8878	42.83	0.859E-04
46	5200.	0.8945	43.35	0.930E-04
47	5270.	0.9043	43.71	0.973E-04
48	5360.	0.9130	44.26	0.992E-04
49	5430.	0.9205	44.72	0.103E-03
50	5540.	0.9327	45.31	0.981E-04
51	5630.	0.9386	45.81	0.106E-03
52	5720.	0.9476	46.38	0.120E-03
53	5810.	0.9583	47.05	0.147E-03
54	5855.	0.9673	47.54	0.152E-03
55	5900.	0.9740	48.06	0.165E-03
56	6000.	0.9933	49.11	0.183E-03
57	6150.	1.0193		
58	6230.	1.0303		
59	6260.	1.0535		

Rupture at N = 6320 c.

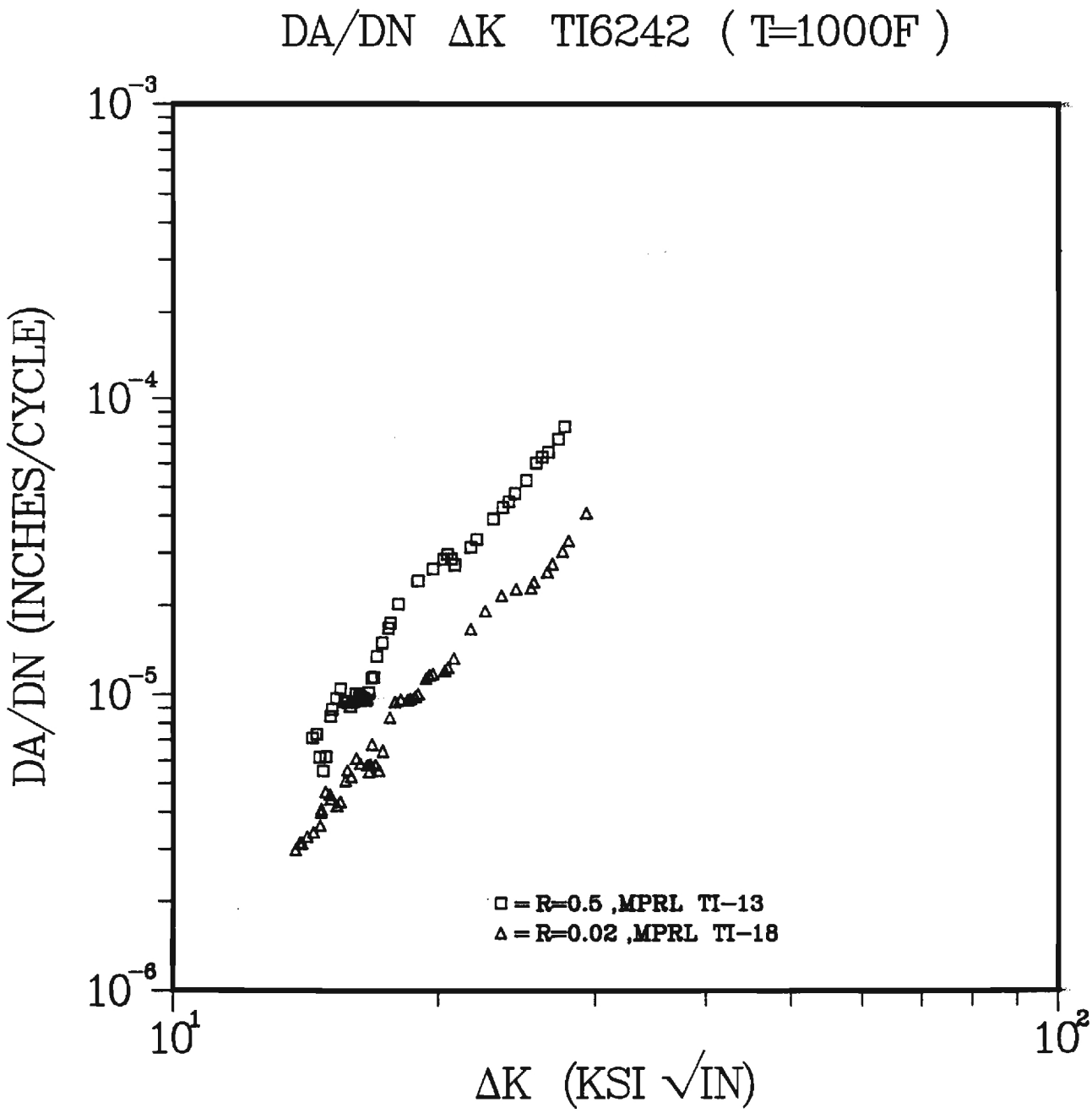
DA/DN ΔK TI6242 (T=1000F)
DA/DN (INCHES/CYCLE)
ΔK (KSI √IN)
10^-3
10^-4
10^-5
10^-6
10^1
10^2
□ = R=0.5 ,MPRL TI-13
△ = R=0.02 ,MPRL TI-18

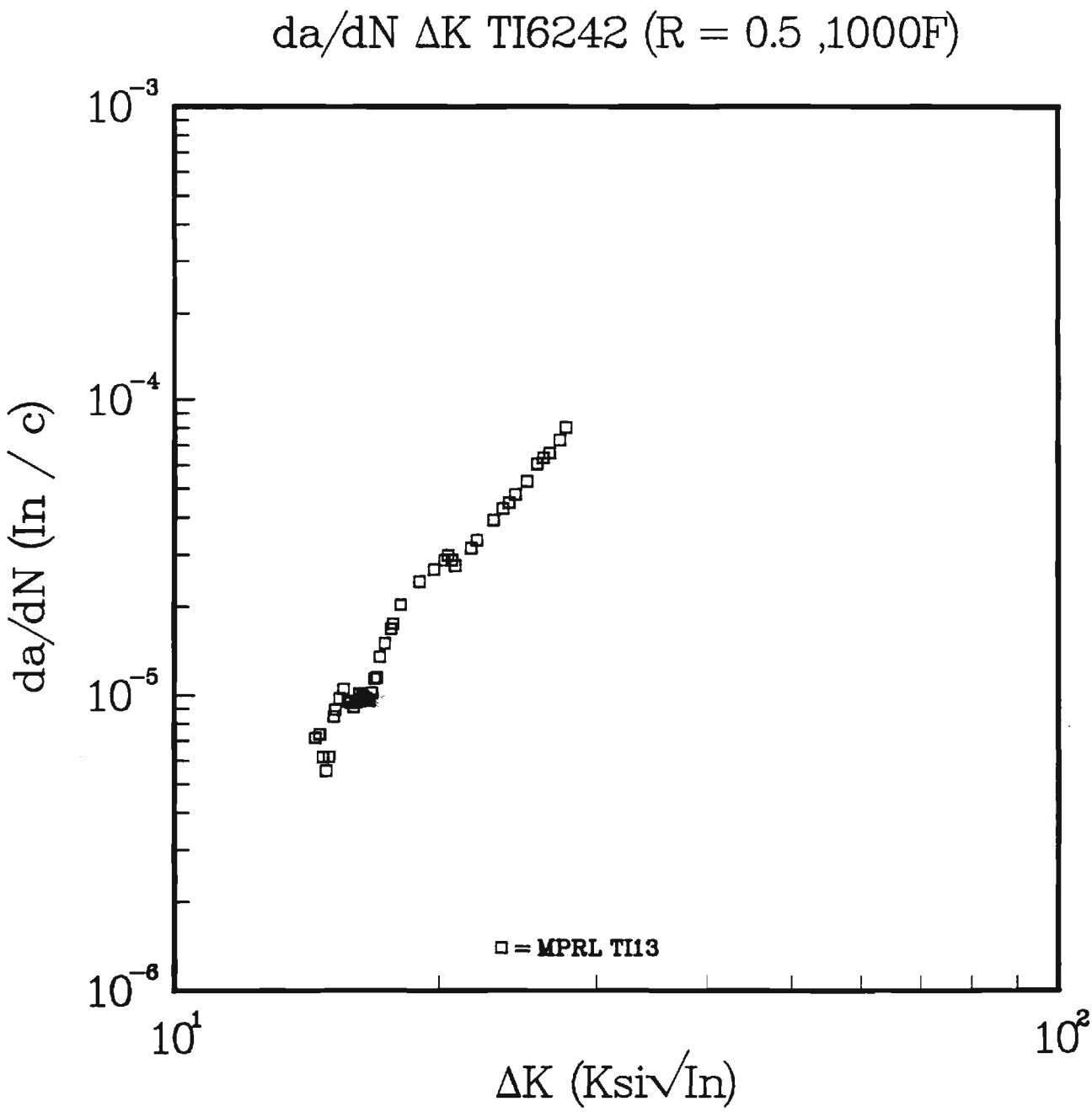
da/dN ΔK TI6242 (R = 0.5 ,1000F)
10^-3
10^-4
10^-5
10^-6
da/dN (In / c)
10^1
10^2
ΔK (Ksi√In)
□ = MPRL TI13

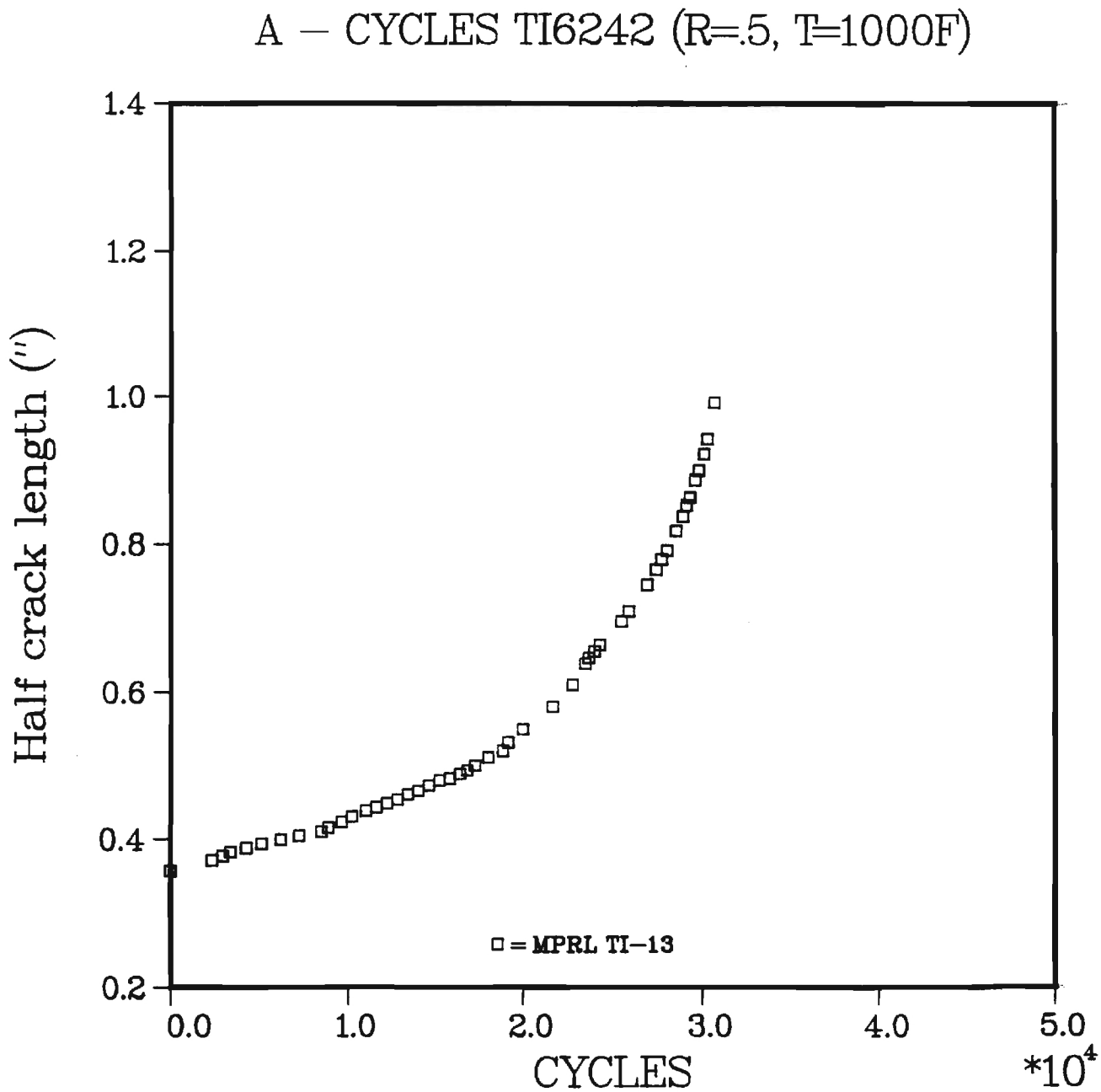
A – CYCLES TI6242 (R=.5, T=1000F)
Half crack length (")
1.4
1.2
1.0
0.8
0.6
0.4
0.2
0.0
1.0
2.0
3.0
4.0
5.0
CYCLES
*10^4
□ = MPRL TI–13

/EN POINT INC.POLYNOMIAL METHOD FOR DET. DA/DN

SPECIMEN IDENTIFICATION >> TI-13
LOG BOOK REFERENCE >>
MATERIAL TESTED >> TI6242
DATE TESTED >> 5-27-88
INITIALS OF THE TESTOR >> LV
TODAY'S DATE >> 5-29-88

NO. POINTS= 49

CCT SPECIMEN B= 0.184 IN. W= 3.000 IN. AM= 0.000 IN.

Pmin= 7.000Kips Pmax=14.000Kips R= 0.500 Test Freq= 8.000Hz.

TEMP.= 538.C Environment= AIR Yield Strength= 140.00 ksi

OBS.NO.	CYCLES	A (Half crack) (")	DELK (Ksi*In**1/2)	DA/DN ("/c)
1	0.	0.3563		
2	2300.	0.3709		
3	2890.	0.3768		
4	3300.	0.3823	14.44	0.712E-05
5	4200.	0.3878	14.60	0.733E-05
6	5050.	0.3933	14.72	0.615E-05
7	6150.	0.3988	14.85	0.552E-05
8	7200.	0.4043	14.96	0.618E-05
9	8480.	0.4094	15.14	0.846E-05
10	8870.	0.4150	15.20	0.893E-05
11	9625.	0.4228	15.37	0.974E-05
12	10200.	0.4303	15.53	0.105E-04
13	11000.	0.4382	15.70	0.951E-05
14	11600.	0.4429	15.82	0.942E-05
15	12200.	0.4480	15.94	0.912E-05
16	12800.	0.4531	16.05	0.947E-05
17	13400.	0.4602	16.18	0.101E-04
18	14000.	0.4650	16.33	0.991E-05
19	14600.	0.4724	16.46	0.977E-05
20	15200.	0.4795	16.59	0.959E-05
21	15800.	0.4819	16.71	0.102E-04
22	16400.	0.4886	16.83	0.114E-04
23	16800.	0.4933	16.94	0.115E-04
24	17250.	0.5000	17.07	0.135E-04
25	18000.	0.5114	17.31	0.150E-04
26	18850.	0.5201	17.60	0.168E-04
27	19150.	0.5311	17.69	0.175E-04
28	20000.	0.5491	18.06	0.203E-04
29	21700.	0.5801	18.99	0.243E-04
30	22800.	0.6101	19.73	0.267E-04
31	23500.	0.6390	20.28	0.287E-04

32	23700.	0.6465	20.47	0.298E-04
33	24000.	0.6555	20.67	0.288E-04
34	24300.	0.6642	20.85	0.275E-04
35	25500.	0.6957	21.73	0.315E-04
36	25900.	0.7094	22.05	0.335E-04
37	26900.	0.7453	23.02	0.392E-04
38	27400.	0.7657	23.59	0.429E-04
39	27700.	0.7795	23.96	0.448E-04
40	28000.	0.7913	24.35	0.478E-04
41	28500.	0.8177	25.09	0.529E-04
42	28900.	0.8374	25.76	0.606E-04
43	29100.	0.8524	26.17	0.634E-04
44	29300.	0.8630	26.59	0.658E-04
45	29600.	0.8866	27.29	0.729E-04
46	29800.	0.8992	27.74	0.804E-04
47	30100.	0.9217		
48	30300.	0.9417		
49	30700.	0.9917		

rupture at N = 30830 c.

UNCLASSIFIED
SECURITY CLASSIFICATION OF THIS PAGE

REPORT DOCUMENTATION PAGE

Form Approved OMB No. 0704-0188

1a. REPORT SECURITY CLASSIFICATION UNCLASSIFIED	1b. RESTRICTIVE MARKINGS
2a. SECURITY CLASSIFICATION AUTHORITY	3. DISTRIBUTION / AVAILABILITY OF REPORT APPROVED FOR PUBLIC RELEASE: distribution is unlimited
2b. DECLASSIFICATION / DOWNGRADING SCHEDULE	
4. PERFORMING ORGANIZATION REPORT NUMBER(S)	5. MONITORING ORGANIZATION REPORT NUMBER(S)
6a. NAME OF PERFORMING ORGANIZATION Georgia Institute of Technology 6b. OFFICE SYMBOL (If applicable)	7a. NAME OF MONITORING ORGANIZATION Air Force Office of Scientific Research
6c. ADDRESS (City, State, and ZIP Code) School of Materials Engineering Atlanta, Georgia 30332	7b. ADDRESS (City, State, and ZIP Code) Electronic and Materials Sciences Building 410 Bolling AFB D.C. 20332
8a. NAME OF FUNDING / SPONSORING ORGANIZATION AFOSR 8b. OFFICE SYMBOL (If applicable)	9. PROCUREMENT INSTRUMENT IDENTIFICATION NUMBER
8c. ADDRESS (City, State, and ZIP Code) Electronic and Materials Sciences Building 410 Bolling AFB D.C. 20332	10. SOURCE OF FUNDING NUMBERS PROGRAM ELEMENT NO. / PROJECT NO. / TASK NO. / WORK UNIT ACCESSION NO.

11. TITLE (Include Security Classification)
Cyclic Deformation, Damage, and Effects of Environment in the Ni_3Al Ordered Alloy at Elevated Temperature

12. PERSONAL AUTHOR(S)
Stephen D. Antolovich and Graham Webb

13a. TYPE OF REPORT	13b. TIME COVERED	14. DATE OF REPORT (Year, Month, Day)	15. PAGE COUNT
Technical Report	FROM 12-1-87 TO 12-1-90	March 29, 1991	103

16. SUPPLEMENTARY NOTATION

17. COSATI CODES		
FIELD	GROUP	SUB-GROUP

18. SUBJECT TERMS (Continue on reverse if necessary and identify by block number)
Dynamic Embrittlement
Cr Effect
Grain boundary cracking
Cr-B particles
Fatigue Crack Propagation
Thermal reversibility

19. ABSTRACT (Continue on reverse if necessary and identify by block number)

The objective of this study is an experimental determination of the effect of composition, temperature, and environment on the fatigue crack propagation resistance of Ni_3Al polycrystalline alloys. The experimental portion of the report describes these results in which the important metallurgical variables were identified. In addition, an analytical model for yielding based upon the concept of cross-slip equilibria is introduced. Th model utilizes a thermodynamic framework which is consistent with all presently observed characteristics of yielding in Ni_3Al, including strain rate independence and thermal reversibility. Complete thermal reversibility was experimentally observed in polycrystalline Ni_3Al which lends futher credence to the model.

Two alloy compositions were evaluated with the same equivalent stoichiometry and processing history. Both alloys were single phase, substoichiometric B-doped compositions, one binary Ni-Al, one ternary Ni-Al-Cr. Following initial processing, the

20. DISTRIBUTION / AVAILABILITY OF ABSTRACT ☐ UNCLASSIFIED/UNLIMITED ☐ SAME AS RPT. ☐ DTIC USERS	21. ABSTRACT SECURITY CLASSIFICATION UNCLASSIFIED
22a. NAME OF RESPONSIBLE INDIVIDUAL Stephen D. Antolovich	22b. TELEPHONE (Include Area Code) 404-894-3012 22c. OFFICE SYMBOL

DD Form 1473, JUN 86 Previous editions are obsolete. SECURITY CLASSIFICATION OF THIS PAGE

UNCLASSIFIED

Block 19 cont.

mean linear intercept grain size of the ternary alloy was 3 times smaller than that of the binary alloy. An additional heat treatment was used to grow identical grain sizes i the binary and ternary alloys. These alloys were then used to evaluate the Cr effect o the elevated temperature deformation properties. The materials were subjected to tensi low cycle fatigue and fatigue crack propagation testing at ambient and elevated tempera in both air and vacuum environments. The results from static and cyclic testing indicated that the grain boundary cohesive strength of the Ni-Al-Cr ternary alloys was lower than that of the Ni-Al alloys at ambient temperatures. At elevated temperatures, stress-assited oxygen diffusion along grain boundaries significantly reduces the grain boundary strength of the Ni-Al alloys and results in degredation of the mechanical properties. This effect is far less pronounced in the ternary alloy as the Cr addition were found to reduce the degradation of grain boundary strength at elevated temperature This occurs by reduction of the grain boundary diffusivity of oxygen in the Cr_2O_3 oxide which is extremely dense and resistant to spalling.

CYCLIC DEFORMATION, DAMAGE, AND EFFECTS OF ENVIRONMENT IN THE Ni_3Al ORDERED ALLOY AT ELEVATED TEMPERATURE

PREPARED BY:

Stephen D. Antolovich

Professor and Director
School of Materials Engineering
Georgia Institute of Technology
Atlanta, Georgia 30332

Graham Webb
Graduate Research Assistant
School of Materials Engineering
Georgia Institute of Technology
Atlanta, Georgia 30332

Technical Report

Final Report for period 12-1-87 through 12-1-90
Contract No. AFOSR-87-0132

Air Force Office of Scientific Research
Electronic and Materials Sciences
Building 410
Bolling AFB, D.C. 20332

Program Manager: Dr. A.H. Rosenstein

ABSTRACT

The objective of this study is an experimental determination of the effect of composition, temperature and environment on the fatigue crack propagation resistance of Ni_3Al polycrystalline alloys. The experimental portion of the report describes these results in which the important metallurgical variables were identified. In addition, an analytical model for yielding based upon the concept of cross-slip equilibria is introduced. The model utilizes a thermodynamic framework which is consistent with all presently observed characteristics of yielding in Ni_3Al, including strain rate independence and thermal reversibility. Complete thermal reversibility was experimentally observed in polycrystalline Ni_3Al which lends further credence to the model.

Two alloy compositions were evaluated with the same equivalent stoichiometry and processing history. Both alloys were single phase, substoichiometric B doped compositions, one binary Ni-Al, one ternary Ni-Al-Cr. Following initial processing, the mean linear intercept grain size of the ternary alloy was 3 times smaller than that of the binary alloy. An additional heat treatment was used to grow identical grain sizes in the binary and ternary alloys. These alloys were then used to evaluate the Cr effect on the elevated temperature deformation properties. The materials were subjected to tensile, low cycle fatigue and fatigue crack propagation testing at ambient and elevated temperature, in both air and vacuum environments. The results from static and cyclic testing indicated that the grain boundary cohesive strength of the Ni-Al-Cr ternary alloys was lower than that of the Ni-Al alloys at ambient temperatures. At elevated temperatures, stress-assisted oxygen diffusion

along grain boundaries significantly reduces the grain boundary strength of the Ni-Al alloys and results in degredation of mechanical properties. This effect is far less pronounced in the ternary alloy as the Cr additions were found to reduce the degradation of grain boundary strength at elevated temperature. This occurs by reduction of the grain boundary diffusivity of oxygen in the Cr_2O_3 oxide which is extremely dense and resistant to spalling.

TABLE OF CONTENTS

LIST OF TABLES

1. INTRODUCTION

Currently high temperature, high stress applications in the aerospace industry are almost entirely dominated by the use of superalloys. It is widely recognized that the development of conventional nickel superalloys has reached a point of diminishing returns. Further increases in use temperature (resulting in increased efficiency) will be achieved through the development of new higher temperature material systems. Towards this end, material systems that possess long range order (LRO) have been selected. The term LRO implies that the atoms in these alloys occupy specific sublattice sites and form superlattice structures. In general, the strength of these alloys does not degrade rapidly with increasing temperature, and in some cases the flow stress actually increases. Long range order produces stronger binding and closer packing between atoms which restricts atomic mobility leading to slower diffusion and perhaps better creep resistance. Ordered intermetallics such as aluminides and silicides are generally resistant to both oxidation and corrosion due to the ability to form dense, adherent, oxide surface films.

Although possessing several desirable characteristics, ordered intermetallic alloys are, in general, brittle. It is this characteristic that has limited their application. The brittleness is attributable to low crystallographic symmetry and/or grain boundary weakness. Low crystallographic symmetry limits the number of permissible slip systems which results in brittle intergranular fracture rather than plastic flow. Grain boundary weakness occurs from low grain boundary coherent strength, due to differences in electronegativity and atom size, limited mobility of grain boundary dislocations, or a combination of both of these mechanisms.

Recently, increases in intermetallic ductility have been demonstrated through control of metallurgical variables. One well known example is the ability of small B additions to ductilize ordered Ni_3Al [1]. Such demonstrations have increased interest for the use of such materials for high temperature applications.

In the present study, the Ni_3Al ordered material system is examined. This material possesses the $L1_2$ (FCC derivative) structure with Ni atoms on face centered lattice sites and Al atoms on corners (figure 1.1). Binary Ni_3Al is ductile as a single crystal, but brittle as a polycrystal [2]. Examination of polycrystal fracture surfaces reveal intergranular fracture. These observations imply that grain boundary weakness controls the ductility of this material system. As alluded to previously, small additions of B (0.028 wt%) in Ni rich (hypostoichiometric) alloys have resulted in large ambient temperature elongations and transgranular fracture [1]. At elevated temperatures in vacuum environments, the compositional modifications continue to ductilize Ni_3Al up to its melting point [3]. However, in the presence of oxygen, intergranular fracture and low ductility again result [4]. These observations imply that at elevated temperature environmental attack of the grain boundaries produces low ductility and intergranular fracture. It has since been discovered that the elevated temperature environmental sensitivity can be reduced by Cr additions [5].

Based upon these preliminary results, it appears that Ni_3Al alloys show promise for consideration as high temperature structural materials. At this point, further evaluation of the mechanical properties of these materials (specifically creep, oxidation and fatigue) must be evaluated before implementation in structural applications. At present, understanding of the effect of cyclic loading at ambient and elevated temperatures is limited. In addition,

the effects of environment on cyclic deformation are not well understood. Such information is essential if the goal of utilizing intermetallics in structural components is to be met.

Towards this end, the current research program was conducted. The program combined mechanical testing, microscopy, and analytical studies to identify mechanisms which determine the fatigue response of polycrystalline Ni_3Al alloys. The experimental program variables were composition, temperature, strain rate, and environment. Such testing enabled evaluation of the important metallurgical variables which control cyclic deformation. In addition, new advances were made in modeling the deformation response of Ni_3Al alloys at elevated temperatures. This information will be indispensable in developing LRO alloys to their maximum usefulness, as well as providing further insight into the deformation response of Ni-base superalloys which are strengthened by Ni_3Al precipitates.

2. BACKGROUND

2.1 Dislocations in Ni_3Al

There are several important differences between the deformation characteristics of ordered and disordered materials that can be directly related to the presence of long range atomic order. In the specific case of ordered $L1_2$ materials, the superlattice structure constrains the flow of the dislocations, by controlling core characteristics [6]. In Ni_3Al and like $L1_2$ alloys, several different combinations of dislocations and faults have been proposed [7]. The nature of these dissociation are dependent upon both alloy composition and temperature.

Computer simulations of the core configuration of dislocations in $L1_2$ ordered materials [6,8,9] have determined that non-planar core configurations exist in $L1_2$ ordered materials. The most important implication of this results is that components of the stress tensor which do not exert a resolved shear stress on the dislocation can have a large effect on the flow properties by altering the core dissociation [10-12]. Such an effect has been shown to be very important in determining the flow properties of Ni_3Al alloys.

A given dislocation in a $L1_2$ superlattice can dissociate in a number of ways, depending upon which faults are stable and how long the Burgers vectors are. Here only faults on {111} and {010} planes are considered as these are the important slip planes in $L1_2$ materials [11]. On {111} (octahedral) planes many different fault dissociations and associated dislocation configurations can occur (figure 2.1) [7], while on {010} (cube) planes, only one type of dissociation occurs [13].

It is well known that unit dislocations in disordered lattices are only partial

dislocations in the superlattice of ordered materials. These partials must either combine to form larger dislocations with Burgers vector equal to a primitive lattice translation, or occur in pairs separated by a strip of antiphase boundary (APB). The latter type of dislocation is known as a "superdislocation". APB coupled dislocations can occur on either octahedral or cube planes and are demonstrated in figure 2.1(a). It was further noted that each of the paired dislocations joined by APB on {111} (termed superpartials) can additionally dissociate into two Shockley partials of Burgers vector a/6<121> (figure 2.1(b)) connected by a stacking fault. As the stacking fault is super-imposed onto the existing antiphase boundary, the resulting combined fault is called a complex stacking fault (CSF). A third fault that can occur on {111} in $L1_2$ structures results from the dissociation of the unit dislocation by the shear vector a/3<112> (figure 2.1(c)) which produces a fault known as the superlattice intrinsic stacking fault (SISF) bound by two partial dislocations. All three of these faults can occur simultaneously according to the scenario demonstrated in figure 2.1(d). A final possibility occurs when two SISF bound partial dislocation pairs overlap on adjacent {111} planes (figure 2.1(e)) resulting in a fault known as a superlattice extrinsic stacking fault (SESF). Direct observations of dislocations using both TEM and HREM techniques have revealed dislocations dissociated in Ni_3Al by all of the above scenarios [10,12,14-22].

2.2 Deformation in Single Crystal Ni_3Al

In most crystalline, dislocation flow dictates material plasticity, which in turn controls fatigue properties. Due to this, a through understanding of dislocation mechanisms is

essential for understanding fatigue processes. The strength of Ni_3Al has been observed to possess three different deformation regimes as temperature increases (figure 2.2), where each regime is associated with a change in the sign of $d\tau/DT$ [10,11,20,23-25]. The initial regime is associated with a decreasing flow stress with temperature. The second regime is characterized by a positive increase in shear stress with temperature. The third and final regime is once again characterized by negative $d\tau/DT$ which is separated from regime II by a peak value. The temperatures where the various regimes end and begin are observed to depend on composition and crystallographic orientation. The principal operating slip system in regime I and II is $\{111\}<110>$ (primary octahedral slip). The principal operating slip system in regime III is $\{010\}<110>$ (primary cube slip).

In regime I, the observed variation in shear stress with temperature is considered to be related to the variation in shear modulus with temperature [10,11,20,23-25]. When tested at very low temperatures, the dislocation substructures are observed in the form of tangled edge and mixed dipoles [10,20,21,23] and SISF bound dislocation loops [10,20,21]. In this regime, deformation is considered to occur similar to that observed in FCC materials.

Regime II, where the flow stress increases with temperature (*i.e.* anomolous flow) covers the largest range of temperatures and has received the greatest amount of attention. In this temperature regime the material possesses several unusual deformation characteristics including:

1. Schmid's law is not obeyed [10].
2. Orientation dependent tension-compression asymmetry [11].
3. Strain rate independence [14].
4. Thermal reversibility [2].

Observations of samples deformed in this region have noted long, straight dislocations of screw orientation [7,10,11,14-21,23]. Due to the ability of screw dislocations to cross-slip during glide, several theories have been proposed to describe the motion of screw dislocations in Regime II. These models propose that the observed anamolous behavior is related to thermally activated cross-slip from glissile to sessile planes during deformation [10-12,26,27]. These theories and others will be discussed in section IV.

Deformation in region III obeys Schmid's law and is strain rate sensitive [10,25]. Deformation in the high temperature regime is observed to occur by both edge, screw and mixed dislocations gliding on non-close packed planes {100} [10,28]. In this regime deformation can be thought of as a normal slip process on an abnormal slip plane.

2.3 Deformation of Polycrystalline Ni_3Al

Although it is known that single crystals of Ni_3Al are highly ductile, polycrystalline materials were observed to be extremely brittle, fracturing in an intergranular fashion [2]. The brittle behavior was observed to be an intrinsic material property (*i.e.* not due to impurities) related to grain boundary weakness [29]. The intrinsic brittleness was determined to be related to differences in valency, electronegativity, and atom size between nickel and aluminum atoms in Ni_3Al [30-33]. It was this fundamental brittleness which was the major obstacle to the development of Ni_3Al as a structural material.

Aoki and Izumi [1], first determined that manipulation of material variables can increase the ductility of Ni_3Al. They observed that micro-alloying Ni_3Al with B imparts substantial ductility. Liu *et al* [3] later determined that the optimum ductility is obtained

using 0.25 wt % B in hypo-stoichiometric (*i.e.* Ni rich) Ni_3Al. The ductility increase is associated with a change in fracture morphology from transgranular to intergranular.

2.3.1 Ductilization Mechanisms

Auger Electron Spectrophscopy (AES) [3,29-33] and other techniques [34-37] were used to determine the composition of grain boundaries in B ductilized alloys. These investigations revealed that B segregates to grain boundaries [3,30,33-35,37], substitutes interstitially [3,32,36,37], and that the concentration of Ni is higher within grain boundaries [3,33,34].

Although there is general agreement as to the composition of grain boundaries in Ni_3Al, there are essentially two different mechanisms to explain ductilization of Ni_3Al by boron additions and changes in alloy stoichiometry. The first mechanism, as first proposed by Liu *et al* [3] contends that the boron additions change grain boundary chemistry and increases their cohesive strength. This theory has received validation from various calculations of grain boundary cohesive strength as a function of boron content and stoichiometry [38-40], which predict strong, highly directional atomic bonding within the strongly ordered lattices of Ni_3Al. The directional bonding places compatibility requirements upon the lattice which are best satisfied in the presence of B in Ni rich Ni_3Al [39,40] for which the boundary is stronger than the bulk lattice.

A second mechanism for explaining the observed ductility is that the B disorders the boundaries. This disordering facilitates grain-boundary slip and dislocation transmission [37,41]. This effectively reduces slip band stress concentration at grain-boundary intersections. Ductility is enhanced as the stress applied to the grain boundary is lowered

[41]. Problems with this theory are due to lack of unambiguous evidence for a change from the ordered $L1_2$ structure to a disordered phase at grain boundaries.

2.3.2 Elevated Temperature Environmental Effects

Although Ni_3Al alloys exhibit good oxidation resistance, elevated temperature ductility is sensitive to environments at elevated temperatures [4,42-46]. When tested in air environments, it was determined that ductility increases initially with temperature, then degrades, reaching nil-ductility at 500-750°C (figure 2.3). The ductility drop with temperature was associated with a gradual change in fracture morphology from initially transgranular at low temperatures to totally intergranular at the ductility minimum. Liu *et al* [4,42-46] later determined that the high ductility and transgranular fracture characteristic of ambient temperature deformation were maintained at 600°C in vacuum environments, but not in air [42-46] or relatively low oxygen partial pressure [4]. A dynamic embrittlement mechanism was proposed involving:

1. Localized grain boundary stress concentration
2. Elevated temperature
3. The presence of gaseous oxygen.

By this mechanism, at elevated temperatures, oxygen is chemisorbed within grain boundary crack tips. This weakens the atomic bonding there and decreases the crack growth resistance of the material. The lack of overall ductility is caused by continuous embrittlement of fresh crack tip material which subsequently propagates the crack along the boundary. It is important to note that this mechanism does not involve oxidation, or even oxygen diffusion as the degree of embrittlement has been observed to be solely dependent upon the presence of oxygen when stress is applied at elevated temperatures [43,44].

Currently there are two known techniques for overcoming elevated temperature environmental embrittlement of Ni_3Al [5,46]. The first is to eliminate grain boundaries oriented perpendicular to the stress axis (i.e. eliminate the normal stress across the boundaries) [46]. This was demonstrated by testing Ni_3Al with columnar grain structure produced by a directional solidification technique. When tested with grain boundaries oriented parallel to the stress axis, high ductility and transgranular fracture was observed up to 700° C [46].

The second technique to create high temperature ductility is to alloy with moderate amounts of the strategic element Cr [5]. Figure 2.4 demonstrates the effect of Cr additions on the elevated temperature tensile elongation of Ni_3Fe alloys which behave similarly to Ni_3Al. Cr additions are thought to promote the formation of dense tenacious oxide at the grain boundaries which reduces exposure to gaseous oxygen and thus environmental embrittlement at elevated temperatures.

2.4 Fatigue of $L1_2$ Ordered Alloys

Currently, there is only a small body of knowledge regarding the deformation and fatigue crack growth mechanisms that occur in polycrystalline Ni_3Al. Cyclic deformation studies are primarily for single crystals of $L1_2$ alloys [47-51], with only one investigation for polycrystal behavior at elevated temperatures [21]. Several FCP investigations for polycrystalline materials [52-55] have been conducted with the results presented in the form of Paris-growth law curves for ambient and elevated temperatures.

2.4.1 Characteristics of Cyclic Deformation

Cyclic deformation experiments on various single crystal $L1_2$ alloys [47-50] have revealed that the orientation dependent tension-compression asymmetry is stable during cyclic deformation at temperatures below peak strength [47-50]. For most experiments, significant cyclic hardening was observed. The rise in cyclic stress was dependent upon temperature, crystal orientation and strain range applied [47-49]. In general, cyclic hardening continued to failure except for low cyclic strain amplitudes or for temperatures beyond peak (*i.e.* Regime III), where a saturation stress was achieved prior to failure. Cyclic softening was not observed during cyclic deformation of the single crystals.

During cyclic loading, deformation was observed to be inhomogeneously distributed within slip bands. These slip bands then initiated final fracture from the stress concentration. TEM observations of the deformed specimens revealed the presence of long straight screw dislocations [48,51], as well as dislocation debris from dislocation interactions. Bonda *et al* [51] reported the debris to be in the form screw and edge dipoles. Hsiung *et al* [48] reported a/3[111] Frank loops within slip bands presumably generated by intersection of mobile dislocations during cyclic loading. The loops were assumed to form by coalesence of defect clusters which reduced the volume decrease within slip bands. The change in volume was reported to place the slip bands in a state of residual tension which resulted in crack nucleation.

Dowling [28] investigated the cyclic response of boron-modified hypostoichiometric polycrystals with 0.5% Hf at 600° C in air and vacuum environments. During plastic strain control cycling it was observed that the cyclic strength in compression was always greater

than in tension. Cyclic hardening to saturation occurred independent of environment, although when tested in air, fracture preceded saturation in some cases. Increasing the strain rate by an order of magnitude (from 0.001/s to 0.01/s) doubled the fatigue life at a given plastic strain range. When tested in vacuum environments, the fatigue life increased by two orders of magnitude. Slip band traces were observed in samples tested to stress saturation, indicating that deformation was inhomogeneous. TEM observations revealed the presence of long straight screw dislocations. When tested in vacuum significant amounts of dislocation debris were also observed, which were not present in specimens tested in air. In air, fracture initiated at grain boundaries, with an intergranular fracture morphology. In vacuum, cracks were observed to nucleate at Hf rich islands located at grain boundaries which which then propagated in a transgranular fashion. It was concluded that fatigue in air was controlled by environmental embrittlement of the grain boundaries. The large improvement in life when tested in vacuum was attributed to the removal of gaseous oxygen and the subsequent elimination of dynamic embrittlement [4].

2.4.2 Fatigue Crack Propagation

In recent years several investigations have measured the crack growth rates of Ni_3Al at both ambient and elevated temperatures [51-54]. These investigations have revealed that fatigue crack growth rates increase with increasing temperature. This increase was consistent with a fracture morphology that continuously evolved from transgranular at ambient temperature to completely intergranular at 500-600° C [52-54]. When tested in vacuum environments, transgranular fracture was observed when tested at 600° C [54]. Crack

growth rate was found to be frequency dependent at elevated temperature, with increase growth rate for lower frequencies [53,54]. It was determined that at ambient temperatures Cr bearing alloys have a higher crack growth rate than comparable binary alloys. When tested at elevated temperatures, the crack growth rates of the Cr bearing alloys were lower than binary alloys when tested in both air and vacuum environments.

From these observations, an environmental mechanism assisted by increased temperature in the presence of the crack tip was described (identical to Liu's mechanism [4]). All investigators [52-54] accounted for changes in crack growth rates to an ever increasing amount of grain boundary embrittlement that occurred as temperature increased. As transgranular fracture is expected to absorb more plastic work then intergranular fracture, the increase in crack growth rates at elevated temperature is related to an increase in the amount of intergranular fracture. At present little is understood of the relationship between crack tip deformation and crack growth at both ambient and elevated temperatures.

3. EXPERIMENTAL VARIABLES

3.1 Program Variables

The experimental variables selected for evaluating the static and cyclic deformation characteristics of the polycrystalline alloys were; composition (Ni-Al-B and Ni-Al-Cr-B), temperature (25°, 300°, 600°C), strain rate (10^{-4}/sec and 10^{-2}/sec), and environment (air and vacuum). These variables were studied in tensile, low cycle fatigue (LCF) and fatigue crack propagation (FCP) testing. The tensile tests were designed to provide initial material property information which was utilized to select fatigue load and strain amplitudes as well as anticipate material fatigue response. The low cycle fatigue tests were designed to determine the evolution of fatigue deformation and damage. These test were not used to generate fatigue life data (Coffin-Manson data), but were intended to evaluate the deformation substructure occurring ahead of growing fatigue cracks. This information was then used to understand the fatigue crack propagation behavior.

Following mechanical testing, deformation and fracture mechanisms were evaluated by a variety of microscopy techniques, including SEM, TEM and optical metallography. SEM was used primarily to examine the fracture morphology of failed specimens. TEM microscopy was used to evaluate initial microstructures as well as to characterize the evolution of fatigue damage. Optical metallography was used to characterize the initial microstructures and also used to view replicas of the specimen surfaces.

X-ray diffraction was used to verify the existence of the L12 ordered lattice in the experimental alloys.

3.2 Material Description

In the experimental program two different alloy compositions were selected for experimental evaluation. One was a binary Ni-Al+B alloy similar to alloy IC-15 initially developed by Oak Ridge National Laboratory. The second alloy selected was a ternary alloy containing 8 at.% Cr and identical B content as the binary alloy. The stoichiometry of Ni and Al in the ternary alloy was adjusted to achieve an equivalent stoichiometry as that of the binary alloy. This was achieved following the criteria for ternary site substitution initially determined by Guard and Westbrook [56] based upon the direction of the solubility lobe in the ternary phase diagram of Ni-Al-Cr (figure 3.1). As the direction of the Cr solubility lobe is in a direction bisects the quasi-binary sections Ni_3Al-Ni_3Cr and Ni_3Al-Cr_3Al, it is presumed that Cr substitutes in equal amounts on Ni and Al sites. Using this idea the compositions of the alloys were specified. After specification, the alloys were produced from plasma sprayed powders. The powders were sieved and particle sizes between -180 and +400 mesh were placed into stainless steel cans. Consolidation was achieved by extrusion of the cans at 1100° C, then annealed at 1200° for 1 hour in argon. Once manufactured, the alloy compositions were characterized (Table I), and microstructures, substructures, and diffraction characteristics were evaluated [57].

These characterization procedures revealed two hypo-stoichiometric B modified Ni_3Al, one binary alloy and one ternary alloy containing Cr. The mean linear intercept grain size of the as-received binary alloy was determined to be 10.2μm, while the ternary alloy had a grain size of 3.5μm. In this alloy, the microstructure consisted of recrystallized (8μm) and partially recrystallized grains of smaller size (1μm). In order allow direct comparison

between the binary and ternary alloy, the grain size of a portion of the ternary alloy was increased to 10.1μm by heat treating at 1000° C for 128 hrs in Ar. The alloys were machined into specimens suitable for tensile (figure 3.2), low cycle fatigue (figure 3.3) and fatigue crack propagation (figure 3.4) testing.

4. ANALYTICAL MODEL FOR ANOMALOUS YIELDING IN NI_3AL

4.1 Background

As mentioned in the previous chapter, in the range of temperatures where the strength is anomolous (Regime II, figure 2.2) there have been numerous attempts to provide a theoretical basis for predicting the numerous unusual characteristics of deformation in Ni_3Al alloys [11-15,26,27]. These models are, in one way or another, based upon the concept of thermally activated pinning of screw superdislocations during deformation. This approach was originally suggested by Kear and Wilsdorf [58] to explain work hardening in Cu_3Au. The mechanism is thermally activated cross slip of APB bound screw superdislocations from {111} planes to {010} planes which shared the common <110> burgers vector (figure 4.1). This work was first extended to describe anomolous yielding in $L1_2$ alloys by Takeuchi and Kuramoto [10]. In their theory, pinning of the dislocation line occurred by cross-slip from {111} to {010} in small localized regions. The pinning process was assumed to be thermally activated and was modelled in an Arrenhius framework. Additional work [6,8,11,59] extended these basic ideas to what has become well known as the Cross-Slip Pinning (CSP) model [12,59]. A separate earlier, but less well known approach, with nearly identical results was developed by Greenberg and co-workers [26-27,60-65]. In these models, a physical description of the yielding process in $L1_2$ alloys is provided whereby screw dislocations experience transformations from glissile to sessile forms by localized cross-slip from {111} to {010} slip planes. Glide of the glissile portions of the dislocation is hindered by the sessile portions which increases the stress necessary to cause

screw dislocations. The density of the sessile portions is dependent upon temperature which thus results in an increasing the flow stress with temperature.

From this basic mechanism, several forms of stress modified activation enthalpy were proposed [10-12,26,27,60-65] for characterizing cross-slip kinetics. In these models, the activation enthalpy for cross-slip is altered by the stresses which affect the cross-slip process. The models based upon cross-slip pinning have experienced considerable success in providing a theoretical basis for various understanding deformation in Ni_3Al including:

1. Increasing strength with temperature.
2. Violation of Schmid's law.
3. Orientation dependent tension-compression asymmetry.

Although extremely successful in several regards, the models are unable to describe all aspects of deformation, most notably the observed independence of the flow stress on strain rate. As all of the models mathematically assume a kinetic framework, a rate effect opposite to that of temperature is implicit.

During the course of the experimental work on the current project, the time dependency of cross-slip kinetics were evaluated [66]. It was discovered that cross-slip is a virtually instantaneous process. This suggests that deformation in Ni_3Al is more properly described in the context of thermodynamic equilibrium [67]. Following the theoretical developments, several experiments were conducted to test the validity of the model with the programs alloys which was met with remarkable success. In this section of the report, both the analytical and experimental developments will be reported

4.2 MODEL FORMULATION

In Ni_3Al alloys, the rate of cross-slip segment accumulation on the cube cross-slip plane (010) is determined by the balance of cross-slip rate in both directions. Using a simple energy diagram argument (figure 4.2), this can be expressed as:

$$dx/dt = (dx/dt)_{(111)\rightarrow(010)} - (dx/dt)_{(010)\rightarrow(111)} \tag{4.1}$$

Or, using Maxwell-Boltzmann statistics:

$$dx/dt = \nu\ (1-x)\ \exp(-G_{pin}/kT) - \nu\ x\ \exp(-G_{unpin}/kT) \tag{4.2}$$

where x = fraction of a screw dislocation that is cross-slipped on (010),
ν = attempt frequency,
G_{pin} = activation energy for cross-slip,
G_{unpin} = activation energy for reverse cross-slip,
k = Boltzmann's constant,
T = absolute temperature.

From this kinetic equation, an equilibrium cross-slipped fraction of the dislocation line can be defined as the length fraction x_{max} which corresponds to the steady-state condition:

$$dx/dt|_{x\ =\ xmax} = 0 \tag{4.3}$$

Combining equations (2) and (3):

$$x_{max} = [1 + \exp(\Delta G/kT)]^{-1} \tag{4.4}$$

where $$\Delta G = G_{pin} - G_{unpin} \tag{4.5}$$

If the activation energies G_{pin} and G_{unpin} are assumed to be independent of x, G_{unpin} can be eliminated in equation (4.2) using equation (4.4). This leads to:

$$dx/dt = \nu\ (1 - x/x_{max})\ \exp(-G_{pin}/kT) \tag{4.6}$$

4.2.1 Calculation of Enthalpy and Strain Rate Independence

Before continuing with the analysis G_{pin} will be evaluated and used to confirm that

cross-slip kinetics are virtually instantaneous. This will be accomplished by ignoring the entropy contribution to Gpin. This assumption is valid in that the configurational entropy will not limit cross-slip kinetics, although it can be expected to influence thermodynamic equilibrium. This can be accomplished using the physical picture illustrated in figure 4.3. to describe the dislocation segment in its highest energy state. From this the following expression is derived:

$$G_{pin} \approx H_{pin} = [Q_{con} - (\tau_{pe}b)bd] + [\Gamma_{010}b^2 - (\tau_{010}b)b2 \qquad (4.7)$$

or:

$$H_{pin} = Q - \tau_{111}V \qquad (4.8)$$

where:

H_{pin} = activation enthalpy for cross-slip,
Q_{con} = energy to constrict the Shockley partials on a length b,
τ_{pe} = constriction on edge component of Shockley partials,
d = equilibrium spacing of Shockley partials,
Γ_{010} = antiphase boundary energy on (010),
τ_{010} = resolved stress on (010),
τ_{111} = resolved stress on (111),
Q = $Q_{con} + \Gamma_{010}b^2$, and
V = $(\tau_{pe}/\tau_{111})db^2 + (\tau_{010}/\tau_{111})b^3$.

V is therefore a function of orientation, and is different in tension and compression due to τ_{pe}. The configuration presented here for the dislocation in its highest energy state is similar to that previously proposed by Paidar et al [12].

It will be shown later that the yield stress is a linear function of x, and that it implies:

$$\tau_{111} = (x/x_{max})\ \tau_{ys} \qquad (4.9)$$

where τ_{ys} is the critical resolved shear stress on (111). The activation energies are therefore not strictly independent of x. However, in equation (4.6), the correction for the x-dependence of activation energies would only change the linear function $(1 - x/x_{max})$ to a more complex function ranging from 1 (at x = 0) to 0 (at x = x_{max}), and is thus only a

second order correction.

The attempt frequency ν can also be estimated. For face-centered cubic structure, an evaluation would be $\nu = \nu_D/12$, where ν_D is Debye's atomic frequency. This was considered reasonably appropriate for use in $L1_2$ ordered structures.

An iterative algorithm was then used for numerical integration of (4.6), which resulted in x vs time curves such as that reproduced in figure 4.4. From these curves, an intrinsic characteristic time for cross-slip kinetics, t_o, was defined as the time needed to achieve 63% of x_{max}. For reference, this time is equal to $3x10^{-12}$ s for Q=0.1 eV, T=400° C, τ_{ys}=400 MPa and [123] tensile orientation.

A second time which is characteristic of extrinsic deformation, t_y, can be defined as the time necessary to achieve a characteristic deformation γ_{ch} (e.g. 0.2%) at a given strain rate $\dot{\gamma}$:

$$t_y = \gamma_{ch}/\dot{\gamma} \tag{4.10}$$

$$\text{For } \dot{\gamma} = 100\%/\text{s}, \; t_y = 2x10^{-3} \text{ s.}$$

Comparing t_o and t_y and referring to figure 4.4 leads one to conclude that for strain rates that have been applied, the extrinsic characteristic time for yielding are much greater than the intrinsic characteristic time for cross-slip (i.e. $t_y > t_o$). Therefore, the fraction of the dislocation line on (010) achieves its equilibrium value x_{max} quasi-instantaneously independent of the strain rate applied.

As has been demonstrated, screw dislocation segments alternate from (111) to (010) at extremely high frequencies. The equilibrium state is the state for which segments cross-slip in both directions at the same rate. This implies that the dislocation will experience an

average friction stress from these pinning points. Due to this, screw dislocations are expected to remain straight when moving. At equilibrium, the applied force per unit length of dislocation (i.e. $\tau_{111}b$) is balanced by the drag force which arises from the presence of the pinning points:

$$\tau_{111}b = C_o\,(x/b) \tag{4.11}$$

or:

$$\tau_{111} = (C_o/b^2)\,x = \tau_o\,x \tag{4.12}$$

where C_o = drag force per cross-slipped segment,
x/b = segments per unit dislocation length,
$\tau_o = C_o/b^2$.

The resolved shear stress on (111) is therefore linearly related to x as was assumed previously. Using equation (4.11), figure 4.4 can be transformed into figure 4.5, where the yield stress is plotted vs the logarithm of time. The characteristic times corresponding to experimentally obtainable strain rates are indicated. Thus, for strain rates that have been experimentally applied, the characteristic times for yielding are much larger than t_o, such that the equilibrium density of pinning points x_{max} is achieved independently of strain rate. Here it is important to realize that C_o is simply the drag force exerted on the dislocation by a single pinning point and is thus independent of dislocation velocity. Indeed, it is proposed that the velocity dependence is related to the number of pinning points which forms on the dislocation line. Here it has been demonstrated that the equilibrium state is achieved quasi-instantaneously and as:

$$\tau_{ys} = \tau_o\,x_{max} \tag{4.13}$$

The observed strain rate independence of yielding in Ni_3Al [10,68,69], can be explained on the basis that dislocations move at a velocity consistent with the drag force

exerted by the equilibrium density of pinning points for the specific temperature/stress scenario.

4.2.2 A Thermodynamically Based Model for Yielding in Ni_3Al

Having demonstrated that the cross-slip kinetics are virtually instantaneous, it is the present contention that thermal strengthening in Ni_3Al is better described using a thermodynamic framework. Using equations (4.4) and (4.13), the following expression is easily derived:

$$\tau_{ys} = \tau_0/[1 + \exp(\Delta G/kT)] \tag{4.14}$$

The functional form of τ_{ys} implies that τ_{ys} increases with temperature only if $\Delta G > 0$. In this case, the barrier height for pinning is larger than that for unpinning. It also implies that the unpinning process is favored over the pinning process and the majority of the dislocation line is therefore unpinned.

For larger values of ΔG, the exponential term in equation (4.14) is much greater than 1, and the equation can be simplified to:

$$\tau_{ys} = \tau_0 \exp(-\Delta G/kT) \tag{4.15}$$

This provides the exponential temperature dependence of yield stress that has been widely used to correlate experimental data [10-12,26,27]. However, to correctly describe the temperature dependence of yielding, it is demonstrated here that the driving force (i.e. ΔG) should be considered instead of the activation energy G_{pin}.

Previous formulations have always focused on the activation barrier for pinning in order to describe yielding. This energy G_{pin} is certainly important, but to describe the kinetics of pinning. Using it implicitly implies a time-related process. Therefore, strain rate

independence of yielding can not be predicted using a kinetic framework.

When considering ΔG however, we are not interested in kinetics but also in the thermodynamics of pinning (i.e. the final or equilibrium state). Because the kinetics are extremely fast, the equilibrium state is achieved quasi-instantaneously, and therefore controls deformation. As a consequence, no time-dependence is expected. This provides a physical justification for the stain rate independence of yielding.

It may seem perplexing that the model implies a positive ΔG for the pinning process. A chemical analogy may help to understand the meaning of this positive sign. Indeed, in the case of the reaction:

$$A \rightleftarrows B$$

the sign of the standard free energy change ΔG^o decides whether the reaction is favored in direction 1 ($\Delta G^o < 0$), or in direction 2 ($\Delta G^o > 0$). However, even if the reaction is favored in direction 1 because ΔG^o is negative, some B will be present at equilibrium. The reason is that the free energy of the system (ΔG_{sys}) will be minimized by transforming some A into some B. The sign and magnitude of ΔG^o will determine what fraction of A will be transformed.

Similarly, the sign and magnitude of the driving force for core transformations decides what fraction of the dislocation line will be pinned. The free energy of the system will be minimized for pinning of small segments if ΔG is positive, and for pinning of most of the dislocation if ΔG is negative.

In summary, although the core transformation of the entire dislocation may not be energetically favorable (if $\Delta G > 0$), the system minimizes its free energy ΔG_{sys} by core

transformation of a fraction of the dislocation line. In this model, no particular assumption was made regarding the sign of ΔG, but a positive ΔG is found to be consistent with the observed temperature dependence of yielding.

The orientation dependence and tension-compression asymmetry of the yield stress have been well described by both Grinberg [26,27] and Paidar, Pope, and Vitek [12,59]: They considered the modification of the activation enthalpy due to stresses on (111) and (010) planes. Here, the similar modification is proposed for G_{pin} and G_{unpin}, which leads to:

$$\Delta G = G_{pin} - G_{unpin} = Q - (\tau_{(010)}V_1 + \tau_{pe(111)}V_2 + ...) \quad (4.16)$$

or

$$\Delta G = Q - \tau_{(111)}V \quad (4.17)$$

where V is a function of orientation, and is different in tension and compression.

4.3 Thermal Reversibility

The implications of the model presented here will now be discussed relative to known deformation characteristics of Ni_3Al. Using this model, the following deformation characteristics may be quantitatively predicted: increasing strength with temperature, orientation dependence, tension-compression asymmetry, and strain rate independence. Unfortunately, like the CSP model, the current model cannot account for the deformation substructures that have been observed in deformed Ni_3Al, most notably screw dislocations completely dissociated on {010} planes in the form of Kear-Wilsdorf (KW) locks (figure 4.1) [15,16,18,20,21]. In order to investigate this apparent discrepancy the concept of thermal reversibility was examined.

4.3.1 Cottrell-Stokes Experiments

The first determination of thermal reversibility in Ni_3Al was provided by Davies and Stoloff

[2] who conducted Cottrell-Stokes experiments on Ni_3Al alloys. These tests consisted of an initial straining at elevated temperature followed by cooling to some significantly lower temperature after which the specimen was further strained. The results of this experiment were then compared to the results of another test on identical material deformed to the same strain as the first specimen, but entirely at the lower temperature. Such comparisons provide an indication of the reversibility of deformation with respect to temperature, and as such are highly useful for evaluating the validity of deformation models in Ni_3Al.

At present there have been a number of such studies that have been conducted on Ni_3Al alloys [20,21,70]. The results of these experiments all indicate that deformation at elevated temperature only slightly affects subsequent low temperature strength. This indicates that deformation in Ni_3Al is "thermally reversible". The amount of irreversibility (i.e. strengthening after high temperature deformation) varied between the various investigations which is not surprising due to the differences in experimental conditions employed (i.e. crystal orientation, temperature, and strain amplitude). One of these investigators [70] attributed the irreversibility as evidence for the development of a dislocation substructure. At this point what must be determined is whether *initial* yielding in these alloys is completely reversible (as would be suggested by the current model) or significantly irreversible (as suggested by the presence of KW locks). Until now there has been no systematic evaluation of the characteristics of thermal reversibility. In the following section, the results from a series of Cottrell-Stokes experiments on polycrystalline Ni_3Al are presented. In these experiments, the effects of strain amplitude and initial test temperature on thermal reversibility are evaluated. The results of these experiments are then discussed

with regard to the newly proposed model as well as to mechanisms which describe the generation, glide and subsequent interaction of KW locks.

4.3.2 Experimental Procedure

The Cottrell-Stokes experiments were performed on the binary hypostoichiometric boron-modified binary Ni_3Al alloy with a 12μm mean linear intercept grain size. The testing was conducted on LCF specimens (figure 3.4) suitable for loading in either tension or compression. The Cottrell-Stokes tests were conducted in strain control using a SATEC CATS servohydraulic test machine. The specimens were induction heated in air between water cooled grips. The induction coil was adjusted such that a temperature distribution of $\pm$ 2 C was obtained in the gauge section of the coil. The initial elevated test temperatures selected were 400° and 600°C. These temperatures were chosen to be in the regime where strength is anomalous (i.e. Regime II). At 600°C, thermal activation is sufficient for some primary cube slip to occur which is not expected at 400°C [10,11,14]. The tests at 400°C were conducted in tension, and the tests at 600°C were conducted in compression as dynamic embrittlement of the grain boundaries limits the tensile failure strain at this temperature (ϵ_f < 1%) [4]. The low temperature portion of all Cottrell-Stokes tests was 25°C (room temperature). Following the elevated temperature testing, the specimens were rapidly cooled between the water cooled grips and retested within 10 minutes of achieving room temperature. The average elapsed time between the elevated temperature test and the low temperature test was 20 minutes. The specimens were strained to either 2% (1% at each temperature) or 4% (2% at each temperature) total strain. In addition to the Cottrell-Stokes tests, tension and compression tests were conducted at ambient temperature

on identical material to 4% total strain for comparison to the results of the Cottrell-Stokes tests.

4.3.3 Results and Discussion

The results of the three Cottrell-Stokes tests are presented as figure 4.6-4.8. In examining figure 4.6, note that the deformation is completely thermally reversible. This is an important result; it indicates that the deformation at the elevated temperature has virtually no effect upon the subsequent deformation at the lower temperature. This complete thermal reversibility is obviously consistent with the newly proposed model. However, this result is in conflict to the results of previous experiments conducted on single crystals on Ni_3Al which all showed some irreversibility [20,21,70]. In these latter tests, the upper test temperatures were closer to T_p ($T \geq 500°C$) and larger strains were applied (generally 2% at each test temperature). Figure 4.8 presents the data for a Cottrell-Stokes test run under identical temperature conditions to those in figure 4.6, but in this case to a higher strain level. Here the flow stress of the material is slightly increased (10%) by the previous deformation at the elevated temperature. The amount of increase corresponds to the degree of hardening experienced during deformation at 400° C.

When performing Cottrell-Stokes experiments with temperatures closer to T_p (600°C), the flow stress is also raised when retested at ambient temperature. Here the observed irreversibility can be attributed to dislocations present on cube slip planes. Although 600°C is below T_p, there is sufficient thermal activation to permit some primary cube glide although octahedral slip is still dominant. Since these dislocations are present on non-close packed planes, they require significant thermal activation to overcome the large Pierels

stresses. At ambient temperature, these dislocations become sessile from the lack of thermal activation and thus impede further glide on the favored octahedral system.

To summarize the results of the three Cottrell-Stokes tests, deformation in polycrystalline Ni_3Al exhibits full thermal reversibility under the following conditions:

(1) Low ($<1\%$) total strains before significant hardening accumulates.

(2) Temperatures where primary cube slip can not operate.

If larger strains or temperatures are applied, the material demonstrates partial irreversibility. The amount of observed irreversibility was greatest when the elevated temperature deformation was close to T_p. Larger strains were also observed to increase the flow stress, but not nearly as dramatically as by elevating the temperature. The results of these experiments tend to support the current models predictions. At present it is uncertain whether any deformation process involving the thermally activated formation of KW locks can be consistent with thermal reversibility. If indeed KW locks occur by a thermally activated process, then a high density of such dislocations would be generated during the deformation at elevated temperature. These dislocations would then be present when retested at the lower temperature and give rise to the same flow stress level measured at the initial elevated temperature. Since this does not occur, there is a strong indication that if deformation in Ni_3Al is indeed controlled by KW locks, they must be much weaker obstacles to octahedral glide then previously envisioned. A second plausible explanation is that KW locks are an artifact of TEM investigations and as such are not a result of the deformation process.

5. CHARACTERISTICS OF MONOTONIC DEFORMATION

5.1 Experimental Procedures

Prior to tensile testing, all specimens were electro-polished in a solution of 80% methanol and 20% perchloric acid at -20° C using a current of 1.35 amps to eliminate machining defects. Following the electro-polishing procedure the diameter of all specimens were carefully measured to within 0.0254 mm. The tensile tests were conducted in the displacement control mode of an MTS servo-hydraulic test machine. The ramp rate was selected to achieve nominal strain rates of 10^{-2}/sec and 10^{-4}/sec during plastic deformation. These tests were conducted in both air and ultra-high vacuum ($< 10^{-8}$ MPa) environments. The vacuum environment was obtained in a Perkin-Elmore Vacuum chamber which was fitted to an MTS servo-hydraulic test machine. To obtain the ultra-high vacuum, two cryo-absorption pumps were used to achieve a vacuum of $< 10^{-4}$ MPa, then a compressed helium cryogenic pump was engaged to achieve the ultra-high vacuum levels utilized during testing. Elevated temperature (300° and 600° C) in the air environment was accomplished by heating the specimen and load train in a three-zone resistance furnace. In vacuum, the specimens were heated by a circular dense alumina single zone resistance heater with exposed elements which surrounded the specimen and portions of the load train in the vacuum chamber (figure 5.1). Specimen temperature was measured by one (air) or three (vacuum) type K thermocouple placed into contact with the specimen surface. Specimens were allowed to equilibrate at temperature for 1 hr prior to testing. The three-zone furnace permitted control of the specimen temperature to within $\pm 1°$ C during testing in air, while the single zone furnace controlled the temperature to within $\pm 5°$C in the vacuum environment.

The output signals from the load cell and ram displacement were recorded by analog X-Y recorder and computer data acquisition. Following testing the diameter of the failed specimen was remeasured in the vicinity of the fracture surface. The data was reduced to obtain 0.2% offset yield strength, ultimate strength, and elongation to fracture. As all specimens were observed to experience discontinuous yielding accompanied by the development of Lüders bands, the reported yield strength was taken as the average stress during Lüders band propagation at the 0.2% strain offset. The failure strain reported was determined from the relationship:

$$\epsilon_f = \ln(A_i/A_f) \tag{5.1}$$

where A_i, and A_f are the initial and final area of the sample.

5.2 Yield Behavior

In Figure 5.2 (a) the experimental data obtained from measurement of 0.2% offset yield strength as a function of temperature. These results indicate that the yield strength (figure 5.2 (a)) of all alloys increases with temperature, reaching a peak value beyond 600°C. The yield strength of the binary and ternary alloy with 10μm grain size are virtually identical. For both alloys, the yield strength is observed to be slightly higher when tested at a strain rate of 10^{-2}/sec then for 10^{-4}/sec. The effect is more pronounced at elevated temperatures (>300°C). The ternary alloy with 3.5μm grain size is observed to be approximately twice as strong as with the larger grain size. A Hall-Petch analysis of the yield data was conducted using the equation:

$$\sigma_{ys} = \sigma_o + k_y(d)^{-1/2} \tag{5.2}$$

provided values of k_y = 1525 MPa·μm$^{-0.5}$ and σ_o = 67 MPa for the ternary alloy (Ni-Al-Cr).

These values were compared to values of k_y = 740 MPa·$\mu m^{-0.5}$ and σ_o = 184 MPa reported for binary Ni_3Al+B of similar stoichiometry (*i.e.* 76 At.% Ni and 24 At.% Al with 0.1 At.% B) and processing history (powder extruded) tested at identical strain rates [71]. These values correlate fairly well with the binary alloy which was measured to have a 10.2μm grain size (*i.e.* σ_y = 410 MPa measured vs 414 MPa calculated). The constant k_y provides a measure of the grain-boundary's resistance to the transmission of slip from one grain to the next, and is related to the stress concentration required to operate dislocation sources at or near grain boundaries in unyielded grains. The constant σ_o is the frictional stress of dislocations on their slip planes which can be related to the yield stress of single crystals by division of a Taylor factor (2.75). From this description it can be seen the Cr additions significantly impede slip transmission to adjacent grains, while weakening the lattice resistance to slip.

5.3 Ductility

Figure 5.2 (b) and 5.2 (c) reports the trends in failure strain verse temperature for air and vacuum environments respectively. The binary alloy (Ni-Al-B) was observed to possess a high elongation (≈50%) to fracture at ambient temperature which degraded with increasing temperature. Increasing the strain rate was observed to increase the failure strain significantly at elevated temperatures, but not at ambient temperature. Accompanying the degradation in ductility was a gradual change in fracture mode (figure 5.3 (c) and (d)) from completely transgranular at ambient temperature to completely intergranular at 600° C. When examining the tensile behavior of the alloys tested in vacuum, there was no such

degradation in the failure strain and fracture surfaces were completely transgranular. Such behavior is consistent with dynamic embrittlement of the grain boundaries by oxygen at elevated temperature [4].

Examination of this same data for the ternary alloys (Ni-Al-Cr-B) with 3.5μm and 10.1μm grain size reveals that in both cases the ductility is lower than that of the binary alloy at ambient temperature, but is superior at elevated temperatures. The reduction at ambient temperature is accompanied by a very different fracture morphology (figure 5.3 (a) vs 5.4 (a)). Fracture in the binary alloy is transgranular while the fracture surfaces of the ternary alloy are completely intergranular. This observation can be related to the presence of weak grain boundaries in the ternary alloys. The increased resistance to slip transmission also increases the tendency for low enery intergranular fracture by raising the grain boundary stress. The combination of these two properties results in intergranular fracture and a reduced ductility.

Examination of the results of the tensile tests conducted in the vacuum environment (figure 5.2 c) reveal that although there is a very strong influence of environment on the failure strain of the binary alloy, there is only a very slight reduction for the ternary alloy. The Cr additions in the ternary alloy have effectively reduced if not eliminated environmental embrittlement at elevated temperature. One likely mechanism for the observed superiority of the ternary alloy is that the presence of Cr promotes the formation of a dense tenacious Cr_2O_3 oxide which protects the grain boundaries from environmental attack by reducing boundary diffusivity.

Comparison of the ductilities of the 10.2μm and 3.5μm grain size ternary alloys

reveals that the larger grain size increases the ductility at low temperatures ($T < 0.5\ T_m$). This behavior is in direct contrast to the behavior of binary alloys where grain refinement increases the ductility at both ambient and elevated temperatures [73,74]. There, the observed results were explained from the viewpoint of reducing the critical crack size present within the alloys and reduction in grain boundary stress from slip band pile ups at grain boundaries. In the ternary alloys with Cr, the observed behavior is interpreted to be consistent with difficulty of slip transmission across grain boundaries. The larger grain size imparts a higher average dislocation path length which imparts higher ductility in a material in which slip transmission across grain boundaries is difficult. In addition, examination of figure 5.4 (a) and (b) reveals significant differences in the appearance of intergranular fracture at ambient temperature between the two grain sizes. In the large grain size material, the grain boundary facets are decorated with particles. Such particles have been observed at the grain boundaries of similar intermetallic alloys [72] and were identified as chromium borides by microdiffraction analysis.

These particles were only rarely observed on the fracture surface of the small grain size material and their size was considerably smaller. The site preference of the particles indicates that nucleation was heterogeneous, and occurred during elevated temperature processing. These particles can be expected to exert a Zener drag force on the advancing boundary (which explains the relatively slow kinetics of grain growth in the Cr alloyed material with respect to the binary material). The elevated temperature processing to increase the grain size can be expected to both nucleate additional particles, and grow existing particles to larger sizes. As B and Cr both seggregate to the particles and away from

interstitial sites in the grain boundaries, these particles can reduce the grain boundary strength. The role of these particles on both ambient and elevated temperature deformation and crack growth will be examined more thoroughly in subsequent discussions.

At 600°C ($T > 0.5\ T_m$), the failure strains of the two alloys are virtually identical. This can be explained on the basis that as temperature increases the effectiveness of grain boundaries in impeding slip is reduced due to thermal activation. In this situation the ductility of the two grain sizes should converge in the absence of dynamic embrittlement and grain boundary sliding. Grain boundary sliding has been reported to significantly reduce the ductility of binary alloys with large grain sizes ($\approx 40\mu m$) at temperatures as low as 400° C [73,74]. Comparison of the fracture surfaces for the two different grain size ternary alloys at 600° (figure 5.4 (c) and (d)) indicates that significant plasticity occurs at the grain boundaries in the case of the large grain size material. Enhanced mechanical locking of the boundaries by the chromium boride particles reduces the tendency to form wedge cracks and provides the observed grain size independent ductility.

6. CHARACTERISTICS OF CYCLIC DEFORMATION

6.1 Experimental Procedures

Prior to low cycle fatigue testing all specimens were electro-polished using similar conditions as for the tensile specimens to remove machining defects. Prior to fatigue testing, translational (two perpendicular directions) and rotational alignment of the load train was achieved to within 0.0254 mm. This was accomplished to minimize bending moments and guarantee a uniform stress state within gauge section of the specimen. Low cycle fatigue testing was conducted in plastic strain control mode utilizing a SATEC CATS servo-hydraulic test machine. Elongation at both ambient and elevated temperature was measured using a MTS displacement gauge attached to alumina rods spring loaded onto the specimen. Plastic strain control was obtained using the combinatorial feedback output of the machine and the relationship:

$$\epsilon_p = \epsilon_t - P/A_o/E \tag{6.1}$$

where

ϵ_t = strain conditioner output signal.
ϵ_p = plastic strain combinatorial output signal.
P = load conditioner output signal.
A_o = initial specimen diameter.
E = measured elastic modulus for current temperature.

Plastic strain control was obtained by generating total strain control ramps which were programmed to end on desired plastic strain output signals (typically $\epsilon_p = \pm 0.003$). Upon attaining the plastic strain endpoint of a given ramp, a sequencer was utilized to initiate a second total strain control ramp in the reverse sense. In this way a series of hysterisis loops could be generated with a constant loop width at zero stress regardless of hardening or softening characteristics.

Low cycle fatigue testing was conducted at temperatures of 25° and 600° C. Specimen heating was obtained by a Lepel 1200 Watt induction heater utilizing a well calibrated coil. The coil was adjusted to repeatedly obtain a temperature gradient of $\pm$ 5° C in the gauge section of a calibration specimen. During fatigue testing, specimen temperature was controlled by an Omega PID controller from thermocouples spot welded to the upper and lower shoulders. Shoulder temperature was chosen to correlate to the desired temperature distribution in the gauge section of the specimen. During elevated temperature testing the grips were water cooled. Specimens were equilibrated at temperature for 30 minutes prior to fatigue testing to ensure uniform heating throughout the gauge section of the specimen.

During fatigue testing, output signals of the load cell and displacement gauge were monitored using an analog strip chart recorder which continuously recorded the endpoints of each hysterisis loop. The output signals of the load cell, displacement gauge and combinatorial feedback channels were recorded by both analog X-Y recorder and computer data acquisition. This was conducted during selected fractions of the total fatigue life of the specimen.

Plastic strain ranges were selected to provide specimen life between 100 and 10000 cycles (ranging from 0.3% to 0.6%). In most cases the specimens failed suddenly without any prior tensile load drop. Initial tests were conducted to failure. Subsequent testing was also conducted under identical conditions then interrupted at life fractions where significant changes in the deformation response had previously occurred. The surfaces from these interrupted tests were replicated. The specimens were subsequently sectioned for TEM

microscopy to determine the evolution of cyclic damage during low cycle fatigue testing.

6.2 Deformation at 25°C

Figure 6.1 shows the cyclic hardening behavior for $\Delta\epsilon_p = 0.006$ at ambient temperature for the binary and ternary alloys tested at 10^{-2}/sec. From this it can be seen that the characteristics of deformation of the binary and ternary alloy with 10μm grain size are very similar. During cyclic deformation, cyclic hardening was rapid, achieving a peak value (≈300% higher than the initial stress) followed by gradual softening. In the ternary alloy with a 3.5μm grain size, significant hardening is also observed, but failure occurs prior to achieving a peak value.

6.2.1 Cyclic Hardening

TEM investigation of samples interrupted in the regime of cyclic hardening (figure 6.2) revealed several types of dislocations. These were (1) APB coupled screw dislocations with **b** = <110>, (2) Mixed and edge dipoles with **b** = <110> on {111} planes, and (3) Faulted dislocations. The latter were observed to increase in density of with increasing accumulated plastic strain (figure 6.6), until at peak hardening reaching such large densities that separation of individual defects was difficult if not impossible. These dislocations were observed to be homogeneously distributed throughout all grains, predominantely on the primary <110>{111} slip system (as determined from Schmid factor analysis). Using standard BF and DF techniques for defect analysis [75] the faults were determined to be intrinsic in nature with a fault vector **R** = {111}. Utilizing the invisibility criterion the dislocations bounding the fault were both **b** = <121>. Trace analysis indicated the faulted

loops to be oriented along <110> directions. From these investigations the defects were characterized as SISF loops residing on the octahedral glide plane.

SISF loops have been observed in Ni_3Al deformed at low to intermediate temperatures [10,19,20,21,22,75]. At present the role of such dislocations in deformation is presumed to be minimal as they possess a highly non-planar core structure [6] and are presumed to be sessile. Until now there has been no reported observation of such loops resulting in cyclic hardening of Ni_3Al, although it has been recognized that such loops could serve as barriers to the glide of the a/2<110> screw dislocation [22].

These dislocations arise from one of two mechanisms; (1) dissociation of unit superdislocation into two a/3<112> partials [7] (using the notation of Thompson's tetrahedron);

$$\mathbf{2AB} \rightarrow \mathbf{2A\delta} + \mathbf{2\delta B} \qquad (6.2)$$

or (2) shear dissociation of a/2<110> superpartial dislocations via the reaction [22];

$$<110> \rightarrow a/2<110> + a/2<110> \rightarrow a/6<110> + a/6<112> + a/3<112> \qquad (6.3)$$

which is energetically unfavorable in terms of self energy, but is realistic when considering that the a/3<112> partial is subjected not only to the attractive forces of both the Shockley partial and the SISF, but also to the repulsion of the a/2<110> partial. For the first mechanism to occur, it has been demonstrated that the ratio of the APB energy to SISF energy must be sufficiently large (in the range 25-35) [6,8]. For the second mechanism to occur, the APB/SISF energy ratio must be 10 [22]. For the range of APB and SISF energies observed (105-130 mJm^{-2} and 5 - 15 mJm^{-2}) [16,21] and predicted (140 mJm^{-2} and 13mJm^{-2}) [78] for Ni_3Al, the later mechanism is more favorable. Direct observation of this mechanism

was accomplished during in-situ deformation in the TEM [77]. Such dislocations were observed to nucleate from a/2<110> screw superpartial which had become pinned locally under the influence of an applied stress.

It is proposed that during cyclic deformation of the substoichiometric polycrystalline Ni_3Al alloys, cyclic deformation results in glide of a/2<110> APB coupled dislocations in screw orientation. Intersection of these dislocations on intersecting glide planes leads to the formation of dipoles and SISF bound dislocation loops. As the density of the sessile SISF loops on the octahedral glide planes increases, the induced strain field interacts with glissile dislocations resulting in higher stresses required to achieve the imposed plastic strain. As cycling continues, the density of the loops increases resulting in the observed hardening.

6.2.2 Cyclic Softening

As was previously described, rapid hardening to a peak value was followed by cyclic softening. Although observed in a variety of precipitate hardened materials, cyclic softening is not typically observed in homogeneous single phase materials (in the absence of sufficient thermal activation to allow recovery). Coincident with the occurrence of cyclic softening was the appearance of slip traces on specimen surfaces (figure 6.3). These slip traces were observed to increase in number with increased plastic work, becoming more closely spaced, at times resulting in microcracks. In the TEM, the slip bands were observed to exist within a background of SISF loops (figure 6.4). The SISF loops are observed to be oriented in <110> directions consistent with the primary slip system. The slip bands are aligned in <110> directions on {111} planes, which were generally not the primary active slip systems for the given grain (*i.e.* not highest Schmid factor). Slip bands were observed to nucleate

additional slip bands in adjacent grains (figure 6.4-(b)). At larger amounts of cyclic work, the slip band spacing decreases and occurs on intersecting <110>{111} slip systems (figure 6.4 (c)). Within these slip bands no SISF loops were observed, although the dislocation density is higher than that in the surrounding matrix.

It is proposed that once a critical density of SISF loops has accumulated during cyclic hardening, slip on the primary octahedral slip system requires a higher shear stress than that necessary to cause glide on the secondary octahedral slip system (due to a lower density of barriers). The slip bands are paths of least resistance for gliding dislocations. Where these slip bands intersect grain boundaries, the increased stress resulting from the dislocation pile ups nucleates additional slip bands. As cycling continues, the number of slip bands increases. These slip-bands through the heavily work-hardened matrix apear to be similar to persistant slip bands (described by Laird for single phase metals) in which deformation occurs more easily.

6.3 Cyclic Deformation at 600° C

At elevated temperatures, the characteristics of cyclic deformation were quite different than at ambient temperature. The materials behaved quite differently for different strain rates unlike at ambient temperature where the deformation response and substructures were similar. During cyclic deformation both creep and environmental attack were found to play a significant role in determining the life at a given plastic strain range.

Figure 6.5 indicates the cumulative glide behavior of the alloys at a strain rates of 10^{-2}/sec and 10^{-4}/sec. When tested at 10^{-2}/sec, all materials hardened significantly, while when tested at the lower strain rate (10^{-4}/sec) the materials all soften significantly. The

ability of both materials to absorb plastic work was found to be at least an order of magnitude higher for the lower strain rate. This effect was particularly pronounced for the binary alloy in which the life increased by 3 orders of magnitude when strained at a rate of 10^{-4}/sec. As could be expected from the results of the tensile tests (section 4), the cyclic stress amplitude for a given plastic strain was higher for the 10^{-2}/sec strain rate.

In all cases, crack initiation and propagation occurred by intergranular fracture. Slip traces were not observed on the specimen surfaces. TEM observations of the deformation substructures of the alloys at the two different strain rates (figure 6.6) reveal very different deformation characteristics between the two strain rates.

The predominant features of the deformation substructures at 600° C were homogeneous distributions of long straight a/2<110> screw dislocations. Although isolated SISF loops were observed, the density of these dislocations was insufficient for wither deformation or hardening. The virtual absence of such faults is consistent with previous observations of SISF loops [19-22]. In one of these studies, it was proposed that the increased thermal activation permits recombination of the a/3<121> partials [22]. At the higher strain rate the density of dislocation debris was considerably higher. The dislocation debris was in the form of mixed a/2<110> loops and dipoles resulting from the intersection of the glissile dislocations. When tested at a rate of 10^{-4}/sec, the deformed material contained a much lower density of dipoles, and relatively no loops or defect clusters. An additional feature of the deformation substructure when tested at the lower strain rate is considerable bowing of predominantly screw oriented dislocations in the cube plane. Figure 6.7 (a) is a weak-beam photomicrograph taken with the the beam direction **B** = [010] which

indicates examples (arrows) of bowed dislocations. Bowing of screw dislocations onto cube planes at elevated temperature has been correlated to non-conservative creep deformation in Ni_3Al [70]. In addition, dislocation networks (figure 6.7 (b)) were observed at the grain boundaries of specimens tested at the lower strain rate.

These observations indicate that at 600° C, deformation again occurs from the motion of a/2<110> APB bound screw dislocations. Intersection of these dislocations during reversed loading leads to the formation of dislocation debris in the form of defect clusters, loops and dipoles. This debris interferes with the movement of the glissile dislocations, with continued cycling results in significant cyclic hardening. At the lower strain rate, the dislocation density remains relatively low as the defects are either swept to the grain boundaries, or migrate to the glissile dislocations. In addition, there is considerable evidence for thermally activated glide of these dislocations on cube planes. The combination of these two mechanisms results in the observed softening observed during elevated temperature cyclic deformation.

Failure occurs at lower levels of plastic work in the harder (10^{-2}/sec) material due to higher stress levels that enhance dynamic embrittlement of the grain boundaries. The dynamic embrittlement mechanism is thus responsible for crack nucleation. When tested at the lower strain rate, cycling results in softening and crack nucleation is consequently delayed.

7. FATIGUE CRACK PROPAGATION

7.1 Experimental Procedures

Prior to fatigue crack propagation, the specimens were ground and polished. The final polishing was conducted with 1μm diamond paste. Following polishing, stainless steel resistance leads were welded onto the specimens. Fatigue loading was conducted in the load control mode of a MTS servo-hydraulic test machine in both air and ultra-high vacuum ($< 10^{-9}$ MPa) environments. The vacuum environment was obtained in the vacuum chamber described in Chapter 4. An R-ratio (K_{min}/K_{max}) of 0.1 was utilized for all tests. Test frequency was 10 Hz. Cracking was initiated in the near threshold regime.

Testing was conducted at temperatures of 25° and 600° C. The elevated temperatures were obtained in air by heating the specimen and portions of the load train in a three zone resistance furnace. Specimen temperature was measured by two type K thermocouples spot welded onto the specimen slightly below the anticipated plane of cracking. In vacuum, a rectangular, single zone dense ceramic resistance heater with exposed elements was used to heat the specimen (figure 7.1). It was determined that this specimen to heater geometry induced a temperature gradient of 20° C across the anticipated path of crack growth. Three type K thermocouples were spot welded onto the specimens directly below the anticipated plane of cracking. During testing, the furnace temperature was adjusted to provide the desired temperature at the current location of the crack tip to within $\pm$5° C.

Crack length was continuously monitored by dc potential drop method. Data was recorded using analog strip chart recorders and via computer data acquisition. The

technique was initially calibrated from visually monitoring crack length during testing with travelling microscopes. Precracking of all specimens was conducted in the temperature/environment in which the actual test was to be conducted.

At ambient temperature, crack closure was evaluated utilizing a technique developed in the MPRL laboratory [79]. A Zygo laser extensometer with 10^{-8} mm resolution was focused onto the machine slot at the load line of the compact test specimens. Prior to closure measurements, a linear output from the apparatus was obtained from an uncracked specimen. The results of these measurements revealed that the measured closure loads were typically lower than P_{min}. Thus closure mechanisms did not alter test results.

7.2 Results at Ambient Temperature

The results from the fatigue crack propagation testing in air are presented in figure 7.2. These results indicate that the fatigue crack growth resistance (FCGR) of the binary alloy is greater than that of the ternary alloy. The FCGR of the ternary alloy with the smaller (3.5μm) grain size less than that with the 10.2μm grain size by over an order of magnitude. The difference between crack growth rates for the binary (Ni-Al + B) and ternary (Ni-Al-Cr + B) alloy with identical grain sizes was over 3 orders of magnitude. The reproducibility of data was confirmed with the large grain size ternary alloy.

Crack growth in the binary alloy was observed to occur by transgranular fracture. Planar slip deformation was revealed from the highly crystallographic facets (figure 7.3 (a)). Such morphology is characteristic of a material experiencing planar slip consistent with the deformation observations (section 6.2.2). The crack path in the ternary alloy was observed

to be predominantly intergranular for both grain sizes (figure 7.3 (b) and (c)). The fracture surface of the smaller grain size ternary material was observed to have 30%-50% transgranular crack growth (figure 7.3 (b)) (indicates planar slip deformation). The areal fraction of intergranular fracture increased with increasing ΔK. The fracture surfaces of the ternary alloy with the large grain size were observed to be completely intergranular (figure 7.3 (c)). The grain boundaries in both alloys were observed to possess numerous parallel ledges from emergence of active slip planes.

These observations were interpreted to be consistent with the prior mechanical behavior (tensile and LCF). The grain boundaries in the binary alloy are stronger (greater cohesive strength) and better able to initiate/transfer slip in/to adjacent grains than for the ternary alloys. Between the large and small grain sizes in the ternary alloy, the smaller grain size had stronger grain boundaries. Chromium-boride precipitates observed on the fractured grain boundaries of the material with the 10.1μm indicate weakening by B depletion. This weakening subsequently enhances crack growth as intergranular fracture absorbs far less work than transgranular fracture. In intergranular fracture, the applied normal stress exceeds the grain boundary cohesive strength allowing for crack propagation. Variation in the grain boundary cohesive strength will result in different intergranular crack growth rates. For these reasons, the observed differences in FCGR are correlated to ratio of transgranular to intergranular crack growth.

6.3 Crack Growth at 600°

At elevated temperatures, the crack growth rates increase substantially for all alloys

(figure 7.4). The crack growth resistance of the ternary alloy at elevated temperature is greater than that of the binary alloy (figure 7.5). The crack growth resistance of the binary alloy decreases by over 5 orders of magnitude from that possessed at room temperature. In vacuum (figure 7.6), the crack growth rate increases by 2 orders of magnitude (3 orders of magnitude smaller than the rate measured in air). These results are accompanied by differences in crack path. In air, the material cracks along the grain boundaries, but in vacuum the fracture morphology is predominantly transgranular (figure 7.7). These results indicate that oxygen diffusion along grain boundaries in the presence of an applied stress field results in reduction of grain boundary cohesive strength. These observations indicate that environmentally assisted crack growth controls the temperature dependence of the FCGR of the binary alloy.

Examination of the results for the ternary alloy reveals an order of magnitude increase in crack growth rate from that observed at ambient temperature (figure 7.4 (a) and (b)). The increase was greatest for the smaller grain size material. The fracture surfaces were almost completely intergranular in both cases (figure 7.8). Once again, the crack growth resistance of the 10.1μm grain size material was lower than that with a 3.5μm grain size. The difference in these rates is attributed to a lower grain boundary cohesive strength in the 10.1μm material caused by the growth of chromium boride particles. These results indicate that environmental attack does occur along the grain boundaries, but it has a lower influence upon the crack growth rate in the Cr alloys.

8. CONCLUSIONS

1. An analytical examination of the kinetics of thermally activated strengthening during deformation of Ni_3Al indicated that they are sufficiently rapid to give rise to an equilibrium substructure in time intervals much less than those associated with normal strain rates.

2. This concept was used to demonstrate the strain rate independence of Ni_3Al alloys and develop a model based upon thermodynamic considerations for yielding in Ni_3Al. The model prdicts all experimental observations for Ni_3Al.

3. For the model to predict the increase in strength with temperature, a positive driving force for cross-slip is required.

4. Experimental observations of complete thermal reversibility were made and used to provide additional justification for the theoretical model.

5. The degree of thermal reversibility was experimentally demonstrated to be a function of prior strain and deformation temperature. The higher the temperature or strain, the less the reversibility.

7. The yield strength of the binary and ternary alloys was found to be virtually identical for

similar grain size, stoichiometry and temperature.

8. A Hall-Petch analysis indicated that Cr additions increase the difficulty of slip transmission between adjacent grains while decreasing the lattice resistance to slip relative to binary alloys.

9. Cr additions resulted in the nucleation and growth of chromium boride precipitates at the grain boundaries of Ni_3Al alloyed with 8 at.% Cr and 0.25% B during elevated temperature processing.

10. Chromium boride precipitates degrade the grain boundary cohesive strength by a reduction in the boron concentration at the grain boundaries.

11. Cyclic deformation of Ni_3Al occured by planar slip, at times resulting in the formation of persistent slip bands which led to softening.

12. An increasing density of dislocations on the slip bands increases both slip band and grain boundary stress. This results in either transgranular or intergranular crack initiation depending upon the grain boundary strength.

13. Diffusion of gaseous oxygen aided by crack tip stress fields was demonstrated to control high temperature deformation properties by degradation of the grain boundary cohesive

strength.

14. At elevated temperature, Cr decreases the rate of environmental attack along the grain boundaries.

REFERENCES

1. K. Aoki and O. Izumi, "On the Ductility of the Intermetallic Compound Ni_3Al", *Nippon Kinzoka Gakkaishi*, 1979, vol. 43, p. 1190.

2. R.G. Davies and N.S. Stoloff, "On the Yield Stress of Aged Ni-Al Alloys", *Transactions of the Metallurgical Society of AIME*, 1965, vol. 233, p. 714.

3. C.T. Liu, C.L. White and J.A. Horton, "Effect of Boron on Grain-Boundaries in Ni_3Al", *Acta Metallurgica*, 1985, vol. 33, p. 213.

4. A.I. Taub, K.M. Chang and C.T. Liu, "Effects of Environment on the Elevated Temperature Ductility of Boron-Doped Ni_3Al","Nickel Aluminides for Structural Use", *Scripta Metallurgica*, 1986, vol. 20, p. 1613.

5. C.T. Liu and V.K. Sikka, "Nickel Aluminides for Structural Use", *Journal of Metals*, 1986, vol. 38, p. 19.

6. V. Paidar , M. Yamaguchi, D.P. Pope and V. Vitek, "Dissociation and Core Structure of <110> Screw Dislocations in $L1_2$ Ordered Alloys-II. Effects of Applied Shear Stress", *Philosophical Magazine A*, 1982, vol. A45, p. 883.

7. B.H. Kear, A.F. Giamei, J.M. Silock and R.K. Ham, "Slip and Climb Processes in γ' Precipitation Hardened Nickel-Base Alloys", *Scripta Metallurgica*, 1968, vol. 2, p. 287.

8. M. Yamaguchi, V. Paidar, D.P. Pope and V. Vitek, "Dissociation and Core Structure of <110> Screw Dislocations in $L1_2$ Ordered Alloys-I.Core Structure in an Unstressed Crystal", *Philosophical Magazine A*", 1982, vol.A45, p. 867.

9. T.A. Parthasarathy, D.M. Dimiduk, D. Woodward, and D. Diller, "Computer Simulation of a_0<110> Screw Dislocations in Ni3Al", To be Published in J.O. Stiegler, D.P. Pope, C.T. Liu editors High-Temperature Ordered Intermetallic Alloys IV, Materials Research Society.

10. S. Takeuchi and E. Kuramoto, "Temperature and Orientation Dependence of the Yield Stress in Ni_3Ga Single Crystals",
Acta Metallurgica, 1973, vol. 21, p. 415.

11. C. Lall, S. Chin and D.P. Pope, "The Orientation and Temperature Dependence of the Yield Stress of $Ni_3(Al,Nb)$ Single Crystals", *Metallurgical Transactions A*, 1979, vol. 10A, p. 1323.

12. V. Paidar, D.P. Pope and V. Vitek, "A Theory of the Anomalous Yield Behavior in $L1_2$ Ordered Alloys", *Acta Metallurgica*, 1984, vol. 32, p.435.

13. P.A. Flinn, "Theory of Deformation in Superlattices", *Transactions of the Metallurgical Society of AIME*, 1968, vol. 218, p. 145.

14. P.H. Thorton, R.G. Davies, and T.L. Johnston, "The Temperature Dependence of the Flow Stress of the γ' Phase Based Upon Ni_3Al", *Metallurgical Transactions*, vol. 1, 1970, p.207.12.

15. Y.Q. Sun and P.M. Hazzledine, "A TEM Weak-Beam Study of Dislocations in γ' in a Deformed Superalloy", *Philosophical Magazine A*, 1988, vol. A58, p. 603.

16. P. Véyssiere, J. Douin and P. Beauchamp, "Observations of Dislocations in Ni_3Al", *Philosophical Magazine A*, 1985, vol. A53, p. 469.

17. P. Veyssiere, "Transmission Electron Microscope Observation of Dislocations in Ordered Intermetallic Alloys and the Flow Stress Anomaly", In C.T. Liu and A.I. Taub and N.S. Stoloff and C.C. Koch editors High Temperature Ordered Intermetallic Alloys III, Materials Research Society, 1989, p. 175.

18. M. A. Crimp, "HREM Examination of [101] Screw Dislocations in Ni_{3Al}", *Philosophical Magazine Letters*, 1989, vol. 60, p. 45.

19. I. Baker and E.M. Schulson, "The Effect of Temperature on Dislocation Structures in Ni_3Al", *Physical States of Solids (a)*, 1985, vol. 89, p.163.

20. D. Dimiduk, "Strengthening by Substitutional Solutes and the Temperature Dependence of the Flow Stress in Ni_3Al", WRDC-TR-89-4106, 1989.

21. W.E. Dowling, Oxidation and Its Influence on the Mechanical Behavior of Ni_3Al, Ph.D. dissertation, University of Michigan-Ann Arbor, 1989.

22. P. Véyssiere, J. Douin, and P. Beauchamp, "On the presence of superlattice intrinsic stacking faults in plastically deformed Ni_3Al", *Philosophical Magazine A*, 1985, vol. 51, p. 469.

23. R. A. Mulford and D.P. Pope, "The Yield Stress of $Ni_3(Al,W)$", *Acta Metallurgica*, vol. 21, 1973, p. 1375.

24. Y. Mishima, Y. Oya, T. Suzuki, "Characteristic Mechanical Properties and Phase Stability of $L1_2$ Intermetallic Compounds", In C.C. Koch, C.T. Liu, and N.S. Stoloff editors, High Temperature Intermetallic Alloys, 1985, Materials Research Society, p. 227.

25. T. Suzuki, Y. Mishima, S. Miura, "Plastic Behavior in $Ni_3(Al,X)$ Single Crystal-Temperature, Strain Rate, Orientation, and Composition, *ISIJ International*, vol. 29, 1989, 1, p.1.

26. B.A. Greenberg, M.A. Ivanov, Y.N. Gornostirev, and L.E. Karkina, "Phenomenalogical Theory of Plastic Deformation with Several Types of Mobile and Immobile Dislocations II. An Analysis of the Features of Plastic Deformation of Ordered Alloys With a Superstructure $L1_2$", *Physical States of Solids A*, vol. 49, 1978, p. 517.

27. B.A. Greenberg, M.A. Ivanov, YU.N. Gornostryrev, and L.E. Karkina, *Physical States of Solids A*, vol. 38, 1976, p. 653.

28. P.M. Hazzledine, M.H. Yoo, and Y.Q. Sun, "The Geometry of Glide in Ni_3Al at Temperatures Above the Flow Stress Peak", *Acta Metallica*, vol. 37, 12, p.3255.

29. T. Ogura, S. Hanada, T. Masumoto and O. Izumi,"Grain Boundary Fracture of $L1_2$ Type Intermetallic Compound Ni_3Al", *Metallurgical Transactions A*, vol. 16A, 1985, p. 441.

30. A.I. Taub and C.L. Briant, "Grain Boundary Chemistry and Ductility in Ni-Base $L1_2$ Intermetallic Compounds", In N.S. Stoloff and C.C. Koch and C.T. Liu and O. Izumi editors High Temperature Ordered Intermetallic Alloys II, Materials Research Society, 1987, 343.

31. O.Izumi and T. Takasugi, "Deformability Improvements of $L1_2$-Type Intermetallic Compounds", In N.S. Stoloff and C.C. Koch and C.T. Liu and O. Izumi editors High Temperature Ordered Intermetallic Alloys II, Materials Research Society, 1987, p. 173.

32. C.L. White and A. Choudhury,"Grain Boundary and Surface Segregation in Boron Doped Ni_3Al", In N.S. Stoloff, C.C. Koch, C.T. Liu, and O. Izumi editors High Temperature Ordered Intermetallic Alloys II, Materials Research Society, 1987, p.427.

33. J.A. Horton, M.K Miller, C.T. Liu, E.P. George and J.Bentley, "Effect of Aluminum Level on Boron Clustering in Ni_3Al", In C.T. Liu and A.I. Taub and N.S. Stoloff and C.C. Koch editors High Temperature Ordered Intermetallic Alloys III, Materials Research Society, 1989, p. 89.

34. D.D. Sieloff, S.S. Brenner and M.G. Burke, "FIM/Atom Probe Studies of B-Doped and Alloyed Ni_3Al", In N.S. Stoloff and C.C. Koch and C.T. Liu and O. Izumi editors High Temperature Ordered Intermetallic Alloys II, Materials Research Society, 1987, p. 87.

35. D.N. Sieloff, S.S. Brenner and H. Ming-Jian,"The Microchemistry of Grain Boundaries in Ni_3Al", In C.T. Liu and A.I. Taub and N.S. Stoloff and C.C. Koch editors High Temperature Ordered Intermetallic Alloys III, Materials Research Society, 1989, p. 155.

36. H.G. Bohn, J.M. Williams, J.H. Barrett, and C.T. Liu, "Lattice Location of Boron and Hafnium Dopants in an Ordered Nickel Aluminide by use of Ion Channeling/Nuclear Reaction Analyses", In N.S. Stoloff and C.C. Koch and C.T. Liu and O. Izumi editors High Temperature Ordered Intermetallic

Alloys II, Materials Research Society, 1987, p. 127.

37. E.M. Schulson, T.P. Weihs, I. Baker, H.J. Frost, and J.A. Horton, "Grain Boundary Accommodation of Slip in Ni_3Al Containing Boron", *Acta Metallurgica*, vol. 34, 1986, p. 1395.

38. V. Vitek, S.P. Chen, A.F. Voter, J.J. Kruisman and J.Th.M. DeHosson, "Grain Boundary Structure and Intergranular Fracture in $L1_2$ Ordered", *Materials Science Forum*, vol. 46, 1989, p. 237.

39. S.P. Chen, A.F. Voter, R.C. Albers, A.M. Borin and F.J. Hay, "Theoretical Studies of Grain Boundaries in Ni_3Al with Boron or Sulfur", *Scripta Metallurgica*, vol. 23, 1990, p. 2061.

40. T. Takasugi and O. Izumi, "Electronic and Structural Studies of Grain Boundary Strength and Fracture in $L1_2$ Ordered Alloys-I.
Binary A_3B Alloys", *Acta Metallurgica*, vol.33, 1985, p. 1247.

41. A.H. King and M.H. Yoo, "Dislocation Reactions at Grain Boundaries in $L1_2$ Ordered Alloys", In N.S. Stoloff and C.C. Koch and C.T. Liu and O. Izumi editors High Temperature Ordered Intermetallic Alloys II, Materials Research Society, 1987, p. 99.

42. C.T. Liu, C.L. White, and E.H. Lee, "Effect of Test Environment on Ductility and Fracture Behavior of Boron-Doped Ni_3Al at 600° C", *Scripta Metallurgica*, vol. 19, 1985, p. 1247.

43. M. Takeyama and C.T. Liu,"Effects of Grain Size and Test Temperature on Ductility and Fracture Behavior of a B-Doped Ni_3Al Alloy", *Acta Metallurgica*, vol. 36, 1988, 5, p. 1241.

44. M. Takeyama and C.T. Liu, " Effect of Preoxidation and Grain Size on Ductility of a Boron-Doped Ni_3Al at Elevated Temperatures", *Acta Metallurgica*, vol. 37, 1989, 10, p. 2681.

45. C.T. Liu anc C.L. White, "Dynamic Embrittlement of Boron-Doped Ni_3Al Alloys at 600° C, *Acta Metallurgica*, vol. 35, 1987, p. 643.

46. C.T. Liu and B.F. Oliver, "Effect of Grain Shape on Environmental Embrittlement in Ni_3Al Tested at Elevated Temperatures", *Journal of the Materials Research Society*, vol. 4, 1989, p. 294.

47. N.R. Bonda, D.P. Pope, and C. Laird, "Cyclic Deformation of $Ni_3(Al,Nb)$ Single Crystals at Ambient and Elevated Temperatures", *Acta Metallurgica*, vol. 35, 1987, 9, p. 2371.

48. L.M. Hsiung and N.S. Stoloff, "Electron Microscopy Study of Fatigue Crack Initiation in Ni_3Al", In C.T. Liu and A.I. Taub and N.S. Stoloff and C.C. Koch editors High Temperature Ordered Intermetallic Alloys III, Materials Research Society, 1989, p. 261.

49. S.S. Ezz and D.P. Pope, "The Asymmetry of Cyclic Hardening in $Ni_3(Al,Nb)$ Single Crystals", *Scripta Metallurgica*, vol. 19, 1985, p.741.

50. H. Pak, M. Kato and D.P. Pope, "Friction Stress and Back Stress in Cyclically Deformed Ni_3Ge Single Crystals", *Materials Science and Engineering*, vol. 100, 1988, p. 31.

51. N.R. Bonda, D.P. Pope and C. Laird, "The Dislocation Structures of $Ni_3(Al,Nb)$ Single Crystals Fatigued at Ambient and Elevated Temperatures", *Acta Metallurgica*, vol. 35, 1987, p. 2385.

52. D.D. Krueger, B.J. Marquardt and R.D. Field, "Structure and Properties of Powder Metallurgy Ni_3Al Alloys", In N.S. Stoloff and C.C. Koch and C.T. Liu and O. Izumi editors High Temperature Ordered Intermetallic Alloys II, Materials Research Society, 1987, p. 309.

53. K.M. Chang, S.C. Huang and A.I. Taub, "High Temperature Fatigue Crack Propagation in P/M Ni_3Al-B Alloys", In N.S. Stoloff and C.C. Koch and C.T. Liu and O. Izumi editors High Temperature Ordered Intermetallic Alloys II, Materials Research Society, 1987, p. 303.

54. N.S. Stoloff, G.E. Fuchs, A.K. Kuruvilla and S.J. Choe, "Fatigue of Intermetallic Compounds", In N.S. Stoloff and C.C. Koch and C.T. Liu and O. Izumi editors High Temperature Ordered Intermetallic Alloys II, Materials Research Society, 1987, p. 247.

55. W. Matuszyk, G. Camus, D.J.Duquette, and N.S. Stoloff, "Effects of Temperature and Environment on the Tensile and Fatigue Crack Growth Behavior of a Ni_3Al-Base Alloy", *Metallurgical Transactions A*, vol. 21A, 1990, p. 2967.

56. R.W. Guard and J.H. Westbrook, "Alloying Behavior of Ni_3Al (γ' Phase), *Transactions of the Metallurgical Society of AIME*, vol. 215, 1959, p. 807.

57. S.D. Antolovich and G. Webb, "Cyclic Deformation, Damage, and Effects of Environment in the Ni_3Al Ordered Alloy at Elevated Temperature", Progress Report for period 12-1-88 through 6-1-88, AFOSR-87-0162.

58. B.H. Kear and H.G.F. Wilsdorf, "Dislocation Configurations in Plastically Deformed Polycrystalline Cu_3Au Alloys", *Transactions of the Metallurgical Society of AIME*, vol. 224, 1962, p. 382.

59. V. Vitek, "From Dislocation Cores to High Temperature Strain Rate Effects in $L1_2$ Alloys", To appear in L. Johnson, J.O. Stiegler, and D.P. Pope editors High Temperature Ordered Intermetallic Alloys IV, Materials Research Society, vol. 213.

60. B.A. Greenberg and L.I. Yakovenkova, "Incomplete Cross-Slip of Superdislocations in Ordered Cu_3Au-Type Alloys", *Physical States of Solids A*, vol. 18, 1973, p. K129.

61. B.A. Greenberg and L.I. Yakovenkova, "Dislocation Barriers in Ordered Cu_3Au-Type Alloy", *Physical States of Solids A*, vol. 20, 1973, p. K53.

62. B.A. Grinberg, YU. N. Gornostryrev, and L.I. Yakovenkova, "Thermally Activated Transformations of Superdislocations in an Ordered Alloy of the Cu_3Au Type", *Physical Metal Metallurgica*, vol. 39, 1975, p. 960.

63. B.A. Greenberg and M.A. Ivanov,"On the Theory of Plastic Deformation with an Account of Dislocation Transformations of Several Types", *Physical States of Solids A*, vol. 45, 1978, p. 403.

64. B.A. Greenberg, M.A. Ivanov, YU.N. Gornostirev, and L.W. Karkina,"Phenomenological Theory of Plastic Deformation with Several Types of Mobile and Immobile Dislocations I.Theory", *Physical States of Solids A*, vol. 47, 1978, p.731.

65. Y.N. Gornostyrev, B.A. Grinberg, L.I. Yakovenkova, "Free Transformations of Superdislocations and Temperature Peculiarities of the Plastic Behavior of Ordered Alloys with $L1_2$ Structure", *Physica Metal Metallurgica*, vol. 51, 1981, 4, p. 170.

66. A. de Bussac, G. Webb, and S.D. Antolovich, "A Model for the Strain-Rate Dependence of Yielding in Ni_3Al Alloys", *Metallurgical Transactions A*, vol. 22A, 1991, p.125.

67. A. de Bussac, G. Webb, and S.D. Antolovich, "A Model for the Yield Behavior of Ni_3Al Alloys", To appear in L. Johnson, J.O. Stiegler, and D.P. Pope editors High Temperature Ordered Intermetallics IV, Materials Research Society. vol. 213.

68. S. Miura, S. Ochiai, Y. Oya, Y. Mishima and T. Suzuki, "Effect of Strain Rate on the Plastic Behavior of $L1_2$ Compounds Based on Ni_3Al", In C.T. Liu and A.I. Taub and N.S. Stoloff and C.C. Koch editors High Temperature Ordered Intermetallic Alloys III, Materials Research Society, 1989, p. 341.

69. J. Bonneville and J.L. Martin, "The Strain Rate Sensitivity of $Ni_3(Al,Ta)$ Single Crystals", To be published in L. Johnson, J.O. Stiegler and D.P. Pope editors High Temperature Ordered Intermetallic Alloys IV, Materials Research Society, vol. 213

70. K. Hemker, "A Study of the High Temperature Deformation of the Intermetallic Alloy Ni_3Al", Ph.D. Dissertation, Stanford University, 1990.

71. M. Takeyama and C.T. Liu, "Effect of Grain Size on Yield Strength of Ni_3Al and Other Alloys", *Journal of Material Research*, vol.4, 1988, p. 665.

72. C.A. Hippsley and J.H. DeVan, "Mechanisms of High Temperature Crack Growth in Nickel Aluminide", *Materials Science and Technology*, vol. 6, 1990, p. 93.

73. T.P. Weihs, V. Zinoviev, D.V. Viens and E.M. Schulson, "The Strength, Hardness and Ductility of Ni_3Al With and Without Boron", *Acta Metallurgica*, vol. 35, 1987, p. 1109.

74. E.M. Schulson, I. Baker, and H.J. Frost, "The Strength and Ductility of Intermetallic Compounds: Grain Size Effects", In N.S. Stoloff and C.C. Koch and C.T. Liu and O. Izumi editors High Temperature Ordered Intermetallic Alloys II, Materials Research Society, 1987, p. 195.

75. J.W. Eddington, Practical Electron Microscopy in Materials Science Vol 4. Defect Analysis and Characterization, Van Nostrand Reinhold Ltd., New York, 1976.

76. R. Bonnet and D. David, "Estimation des Energies de Fautes Intrinseques Dans des Phases (Ni, Al, Ti, Cr) Basees sur Ni_3Al", *Acta Metallurgica*, vol. 39, 3, 1991, p. 329.

77. PH. Lours, A. Coujou and B. De Mauduit, "On the High-Temperature Stress-Induced Spreading of Superlattice Intrinsic Stacking Faults in γ' Nickel-Based Single Crystals" *Philosophical Magazine A*, vol. 62, 2, 1990, p. 253.

78. S.P.Chen, A.F. Voter and D.J. Srolovitz, *Scripta Metallurgica*, vol. 20, 1986, p.1389.

79. R.R. Bowman, R.C. Brown, and S.D. Antolovich, "Problems Associated with Closure Load Determinations", *Engineering Fracture Mechanics*, vol. 33, 1988, p. 703.

PUBLICATIONS, PRESENTATIONS AND INTERACTIONS

I. PUBLICATIONS

1. A. de Bussac, G. Webb, and S.D. Antolovich, "A Model for the Strain-Rate Dependence of Yielding in Ni_3Al Alloys", *Metallurgical Transactions A*, vol. 22A, 1991, pp.125.

2. A. de Bussac, G. Webb, and S.D. Antolovich, "A Model for the Yield Behavior of Ni_3Al Alloys", To appear in L. Johnson, J.O. Stiegler, and D.P. Pope editors High Temperature Ordered Intermetallics IV, Materials Research Society.

3. A. de Bussac, G. Webb, and S.D. Antolovich, "A Model for Yielding in Ni_3Al", in preparation for submission to Metallurgical Transactions.

4. G.Webb and S.D. Antolovich, "Fatigue Response of Polycrystalline Ni_3Al Alloys", in preparation for submission to Metallurgical Transactions.

II. PRESENTATIONS

1. G. Webb and S.D. Antolovich, "An Investigation for the Fundamental Mechanisms of Cyclic Hardening in Ni_3Al", MRS Fall Meeting, Symposia Q, High Temperature Ordered Intermetallic Alloys, November 26 - December 1 1990, Boston, Massachusetts.

2. G. Webb and S.D. Antolovich, "Cyclic Deformation of Ni_3Al as a Function of Compostion, Temperature, and Strain Rate", Aeromat '90, May 5-8 1990, Long Beach, California.

3. G. Webb. S.D. Antolovich, and R.R. Bowman, "Fatigue Crack Propagation of Ni_3Al as a Function of Compositon and Temperature", TMS Annual Meeting and Exposition, February 19-22 1990, Anaheim, California.

4. G. Webb, S.D. Antolovich, and R.R. Bowman, "High Temperature Fatigue Response of Ni_3Al-Structure Property Relations", ASM-TMS Materials Week, October 2-5 1989, Indianapolis, Indiana.

III. INTERACTIONS

1. **OaK Ridge National Laboratory**, Dr. C.T. Liu was consulted prior to specification of alloy compositions, and he serves on the PhD committee of Mr. Webb. Several technical discussions have also been conducted with Dr. P.M. Hazzledine regarding TEM experiments and analytical modeling.

2. **Stanford University**, Dr. W.D. Nix visited Ga.Tech and had several discussions regarding the analytical modeling of anomolous yielding.

3. **NASA-Lewis Research Center**, Numerous technical discussions have been held with Dr. R.R. Bowman regarding TEM techniques employed during the course of the research. Dr. Bowman served as in a post-doctoral fellow on the project as was responsible for the specification of alloy compositions.

4. **Michigan Tech University**, Dr. W.W. Milligan visited Ga.Tech and demonstrated weak-beam imaging techniques.

IV. Personnal

All those who have participated on the project are listed below;

NAME	FUNCTION
1. Stephen D. Antolovich	Principal Investigator
2. Graham Webb	Ph. D. graduate student who carried out the bulk of experimental work and is in the process of writing Ph.D. dissertation.
3. Randy Bowman	Post-doctoral fellow. Specified the initial alloy compositions.
4. Rick Brown	Technician in the MPRL. Helped with testing and design of some experiments.
5. Pat Ledon	Senior administration secretary. Ms. Ledon administered some aspects of the project.
6. Others	Some assistance was obtained from secretaries, technicians and students in the School of Materials Engineering.

Table 3.1 Compositions of experimental alloys.

(ATOMIC PERCENT)

	Ni	Al	Cr	B
ALLOY B	76.3	23.5	0.0	0.2
ALLOY T	72.1	19.7	7.8	0.2

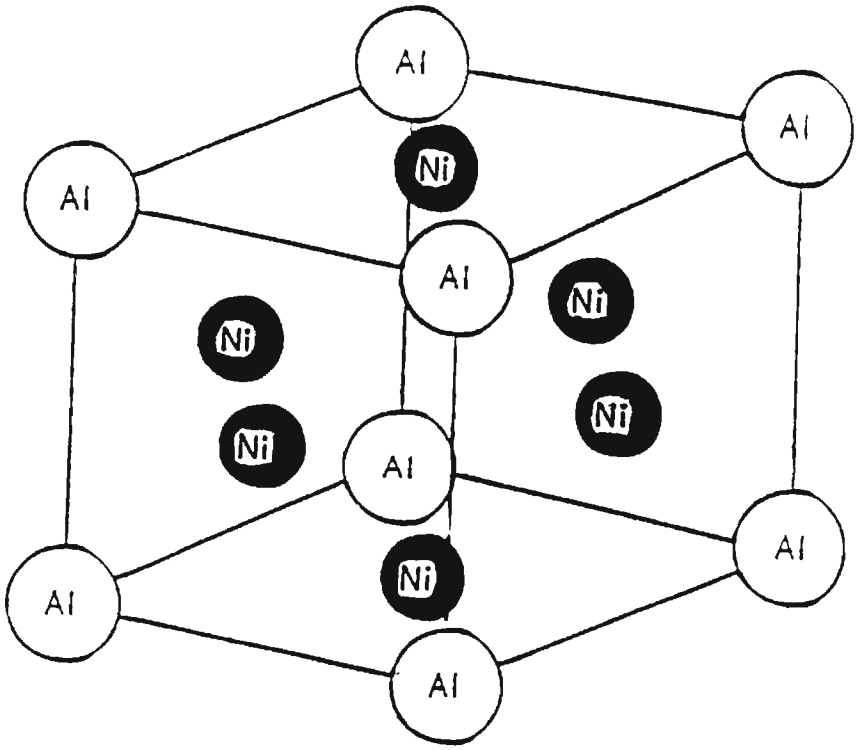

Figure 1.1 The $L1_2$ crystal structure (FCC derivative). Black circles represent Ni, White Al.

a. APB on (111)

$[\bar{1}\,0\,1] = 1/2[\bar{1}\,0\,1] + 1/2[\bar{1}\,0\,1]$

b. APB + CSF on (111)

$[\bar{1}\,0\,1] = 1/6[\bar{1}\,\bar{1}\,2] + 1/6[\bar{2}\,1\,1] + 1/6[\bar{1}\,\bar{1}\,2] + 1/6[\bar{2}\,1\,1]$

c. SISF on (111)

$[\bar{1}\,0\,1] = 1/3[\bar{2}\,1\,1] + 1/3[\bar{1}\,\bar{1}\,2]$

d. APB, CSF & SISF on (111)

$[\bar{1}\,0\,1] = 1/6[\bar{1}\,\bar{1}\,2] + 1/6[\bar{2}\,1\,1] + 1/6[\bar{1}\,2\,\bar{1}] + 1/6[1\,\bar{2}\,1] + 1/6[\bar{1}\,\bar{1}\,2] + 1/6[\bar{2}\,1\,1]$

e. SISF & SESF on (111)

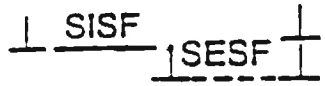

$[\bar{2}\,1\,1] = 1/3[\bar{1}\,2\,\bar{1}] + 1/3[\bar{1}\,\bar{1}\,2] + 1/3[\bar{2}\,1\,1] + 1/3[\bar{2}\,1\,1]$

Figure 2.1 Possible modes of dislocation dissociations in $L1_2$ structure. Notation described in text.

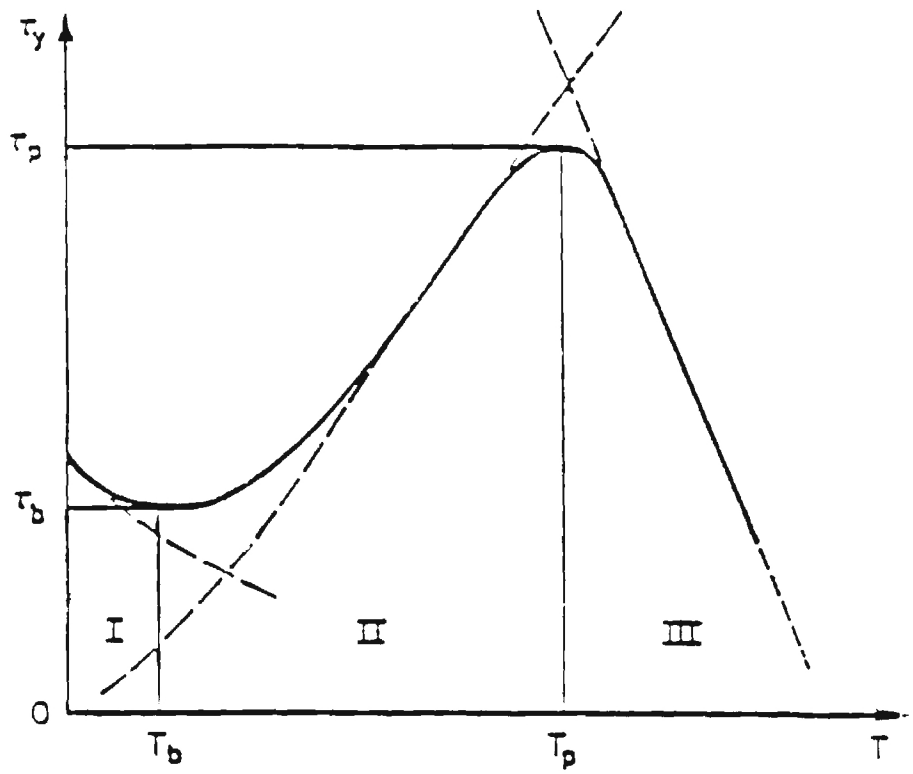

Figure 2.2 The three characteristic regions of temperature dependence of flow stress in Ni_3Al alloys.

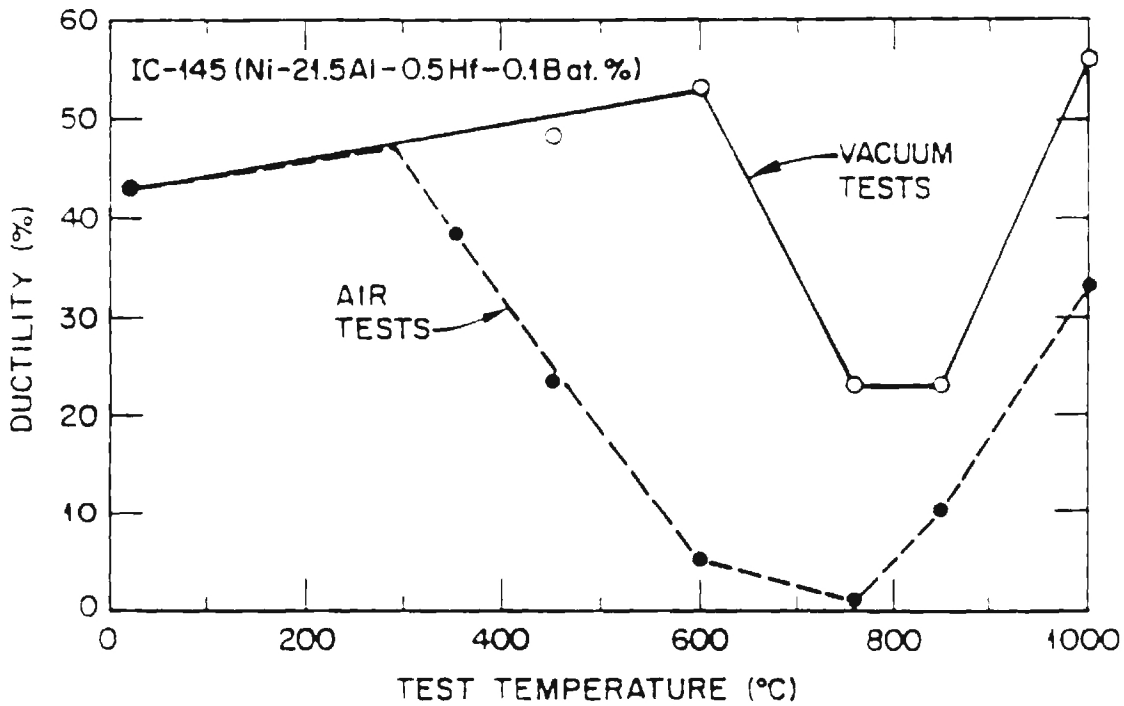

Figure 2.3 Comparison of tensile elongation of Ni-21.5 Al-0.5 Hf 0.1 B (at%) tested in vacuum and air [4].

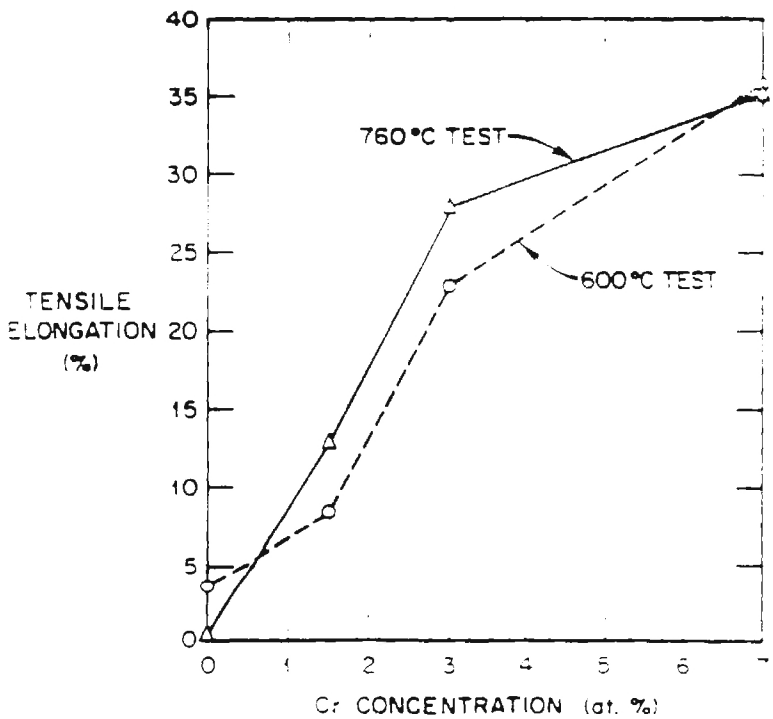

Figure 2.4 Plot of tensile elongation as a function of chromium concentration in Ni_3Al + 15.5 at.% Fe at 700° C in air [5].

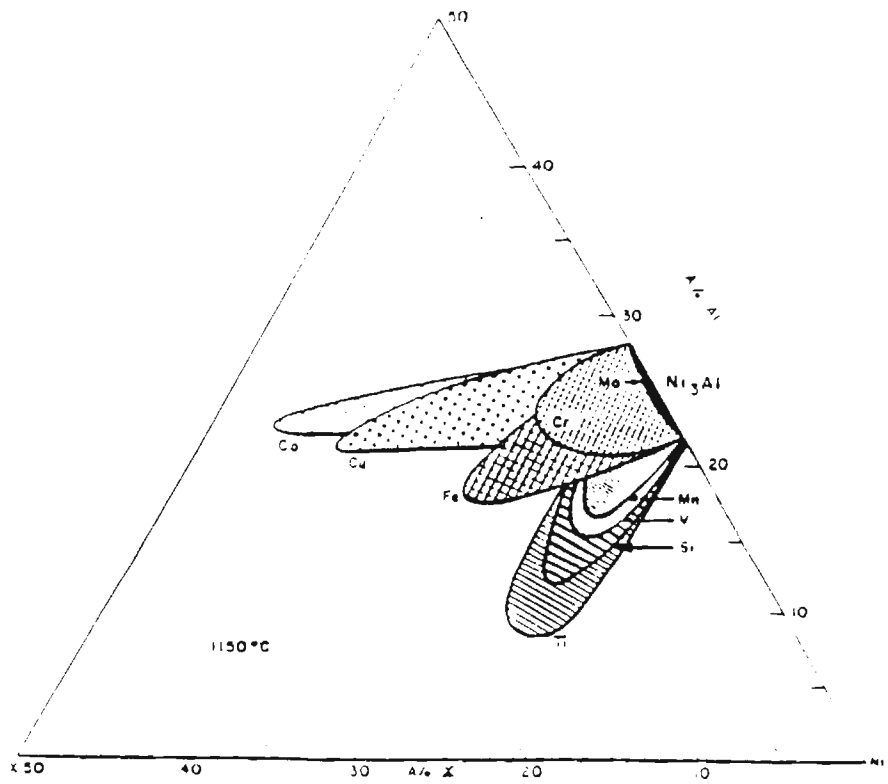

Figure 3.1 Effect of ternary element addition on phase field stability of Ni-Al-X [56]

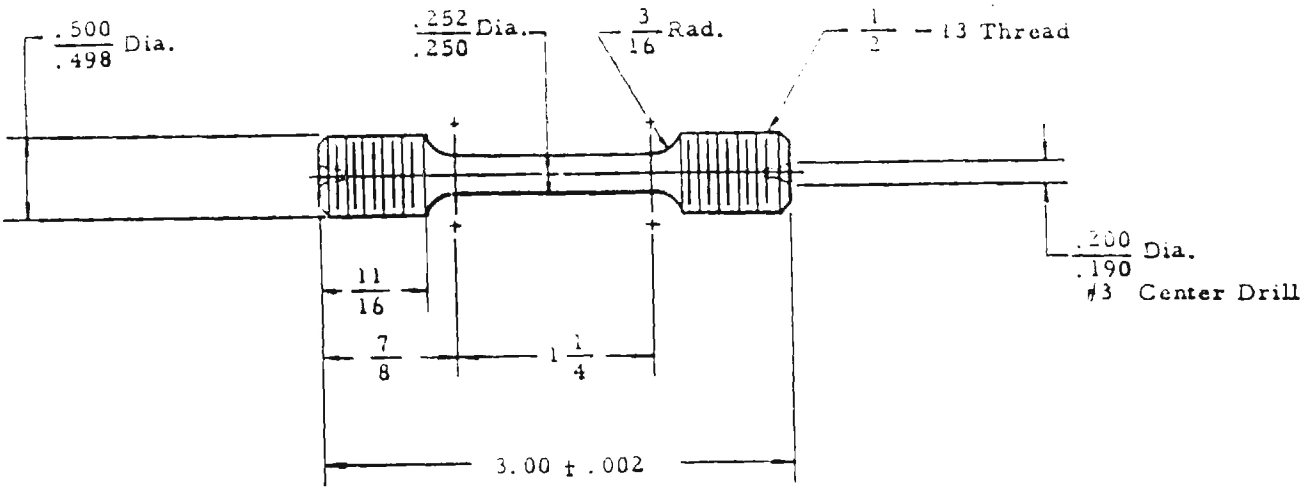

Figure 3.2 Configuration of tensile specimens utilized during the course of the research. (All dimensions in inches).

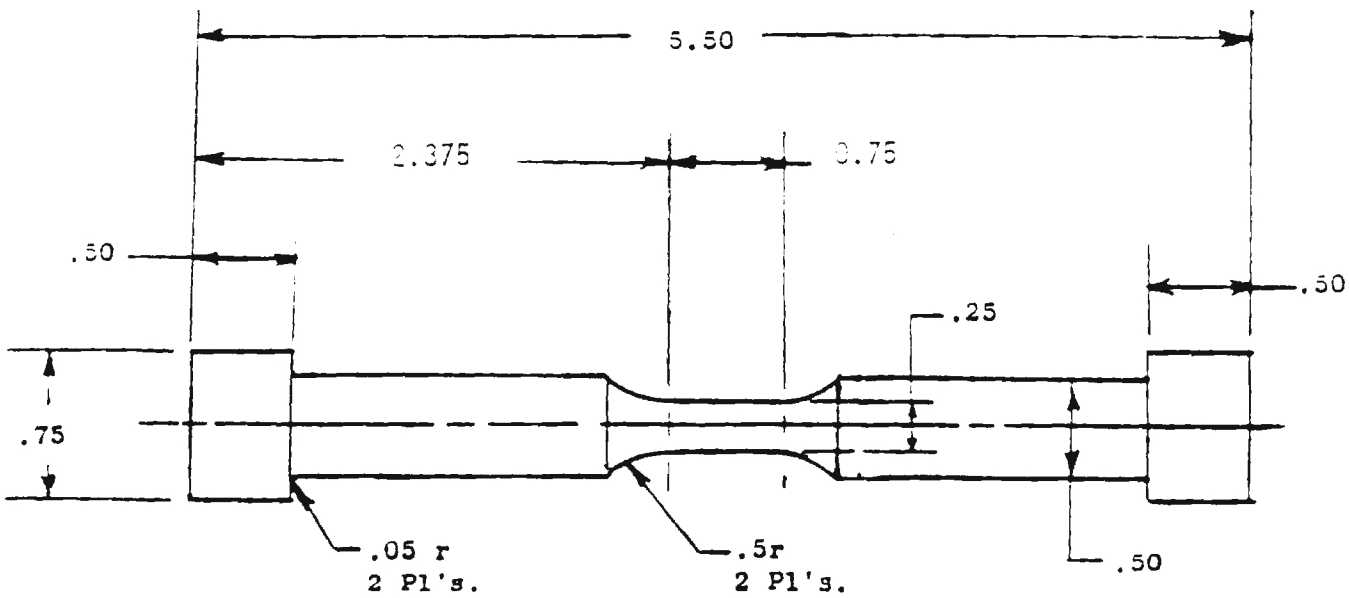

Figure 3.3 Configuration of the low cycle fatigue (LCF) specimens utilized during the course of the research. (all dimensions in inches).

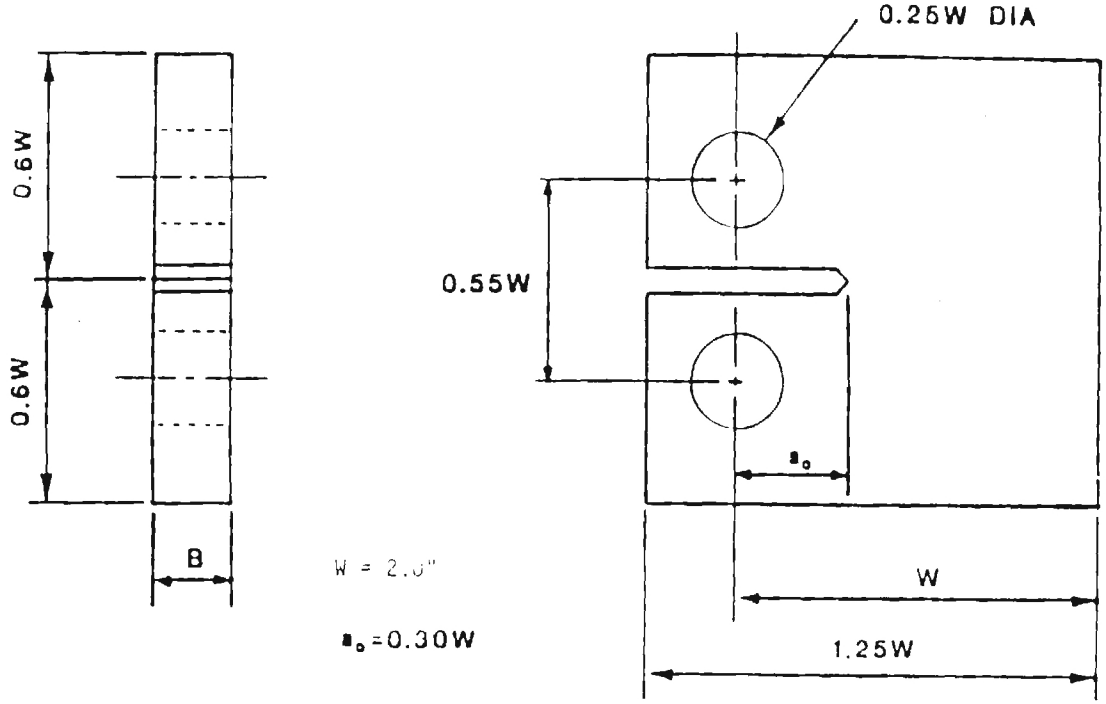

Figure 3.4 Configuration of the compact test (CT) fatigue crack propagation (FCP) specimens utilized during the course of the research.

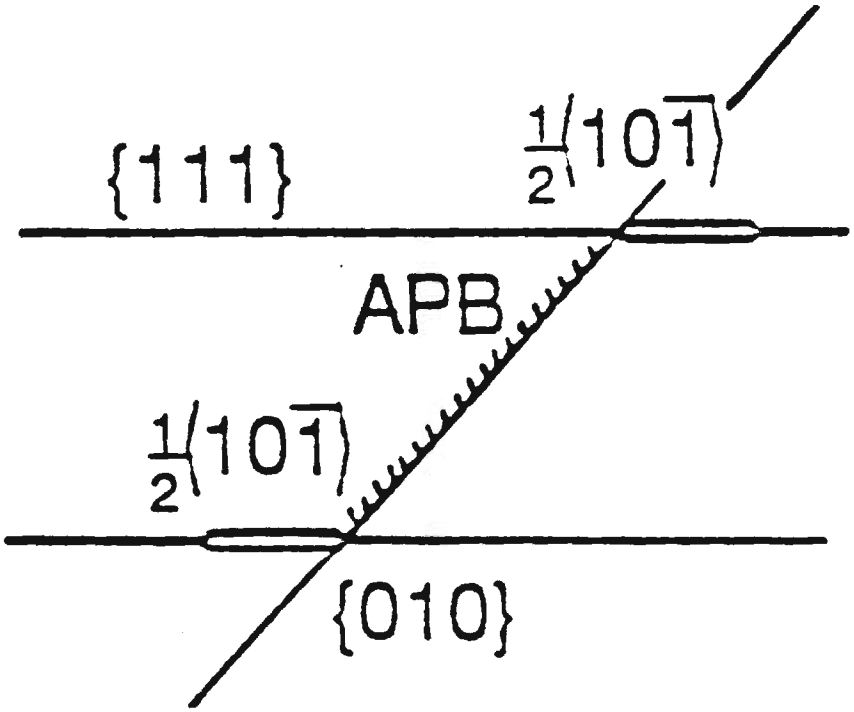

Figure 4.1 The Kear-Wilsdorf cross-slip configuration in Ni_3Al.

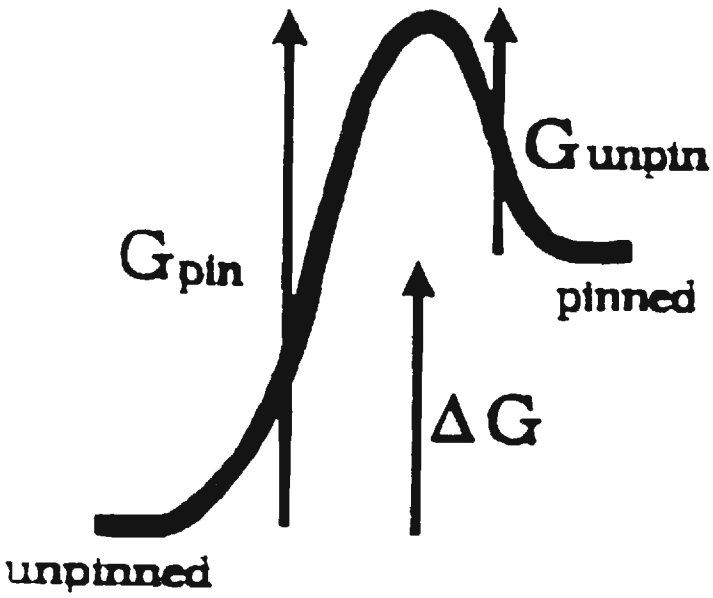

Figure 4.2 Schematic representation of the energy barriers to forward and reverse cross-slip.

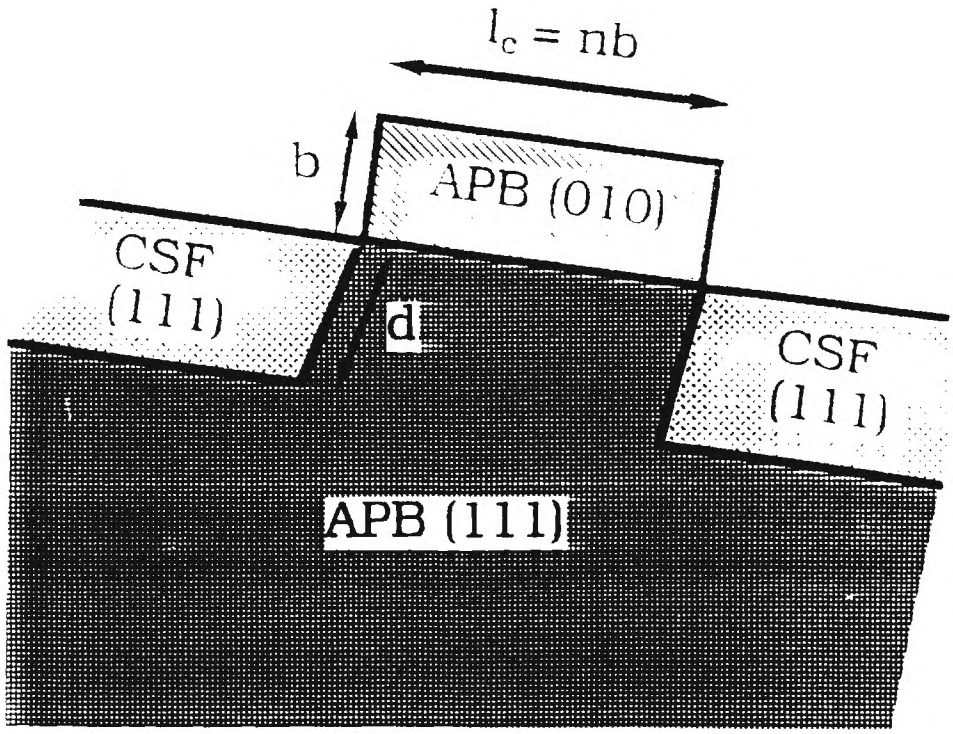

Figure 4.3 Schematic representation of the highest energy configuration of a cross-slipped segment.

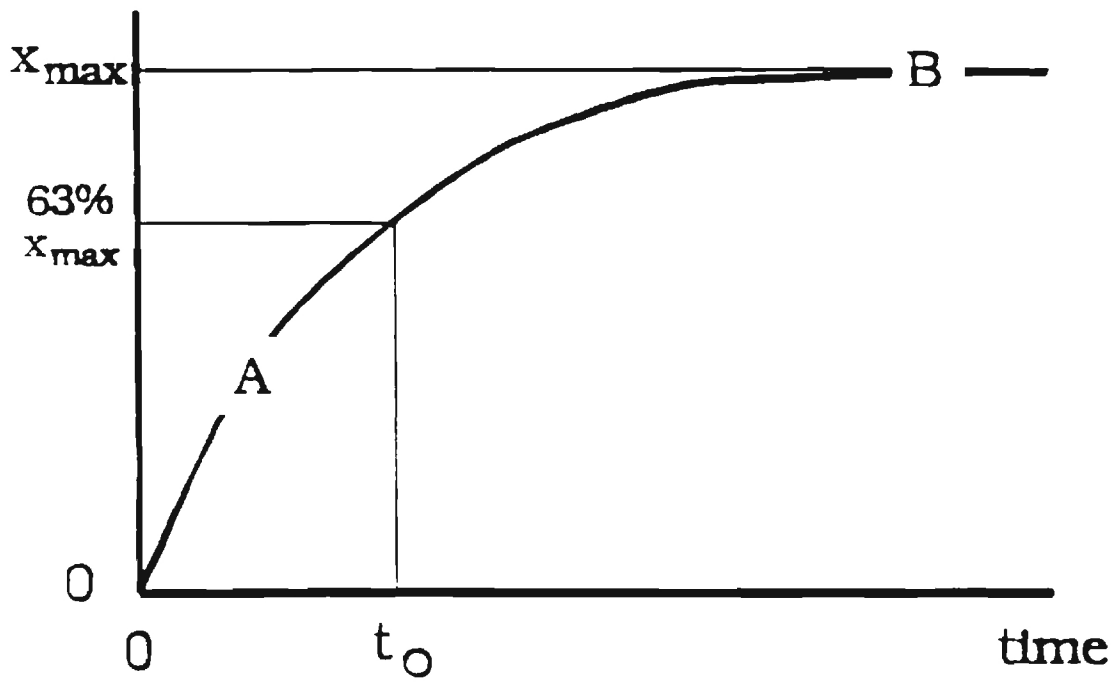

Figure 4.4 Variation in dislocation cross-slip segment accumulation with time.

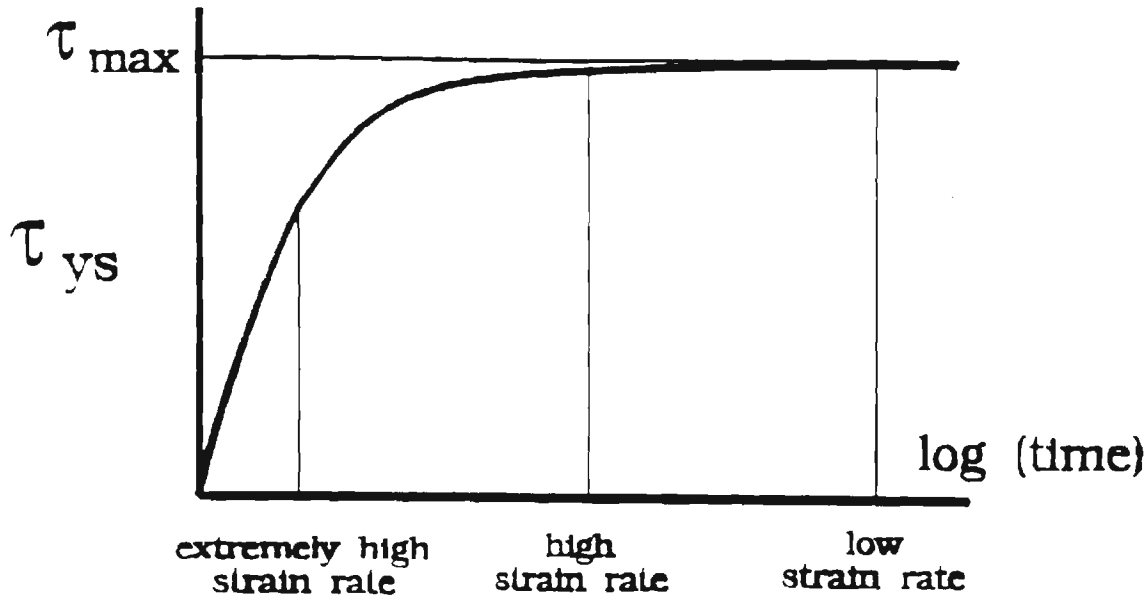

Figure 4.5 Variation in the flow stress (intrinsic resistance) as a function of time.

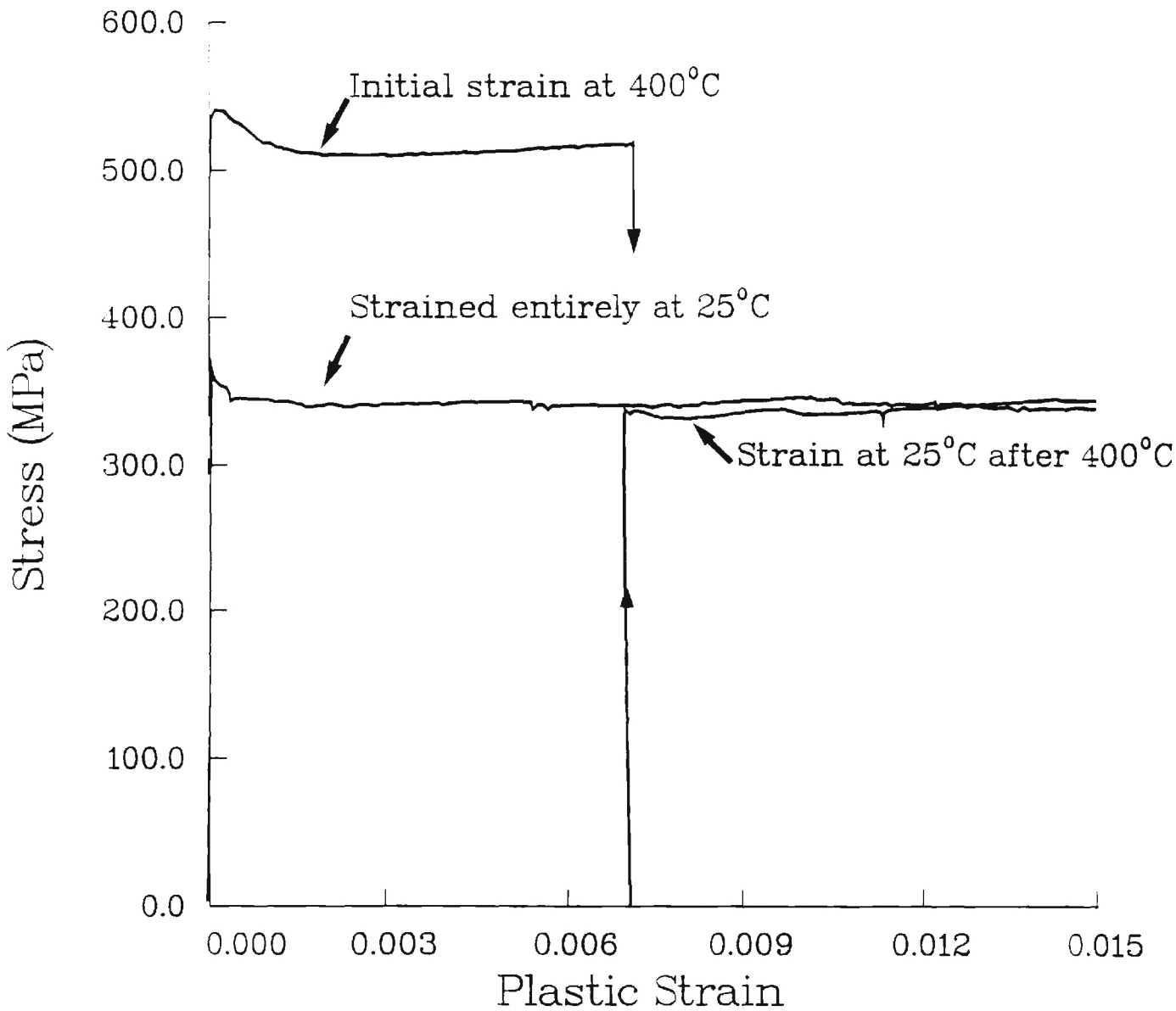

Figure 4.6 Results from Cottrell-Stokes experiment. Specimen was initially strained 1% at 400° C, then restrained at 25° C an additional 1% demonstrating complete thermal reversibility.

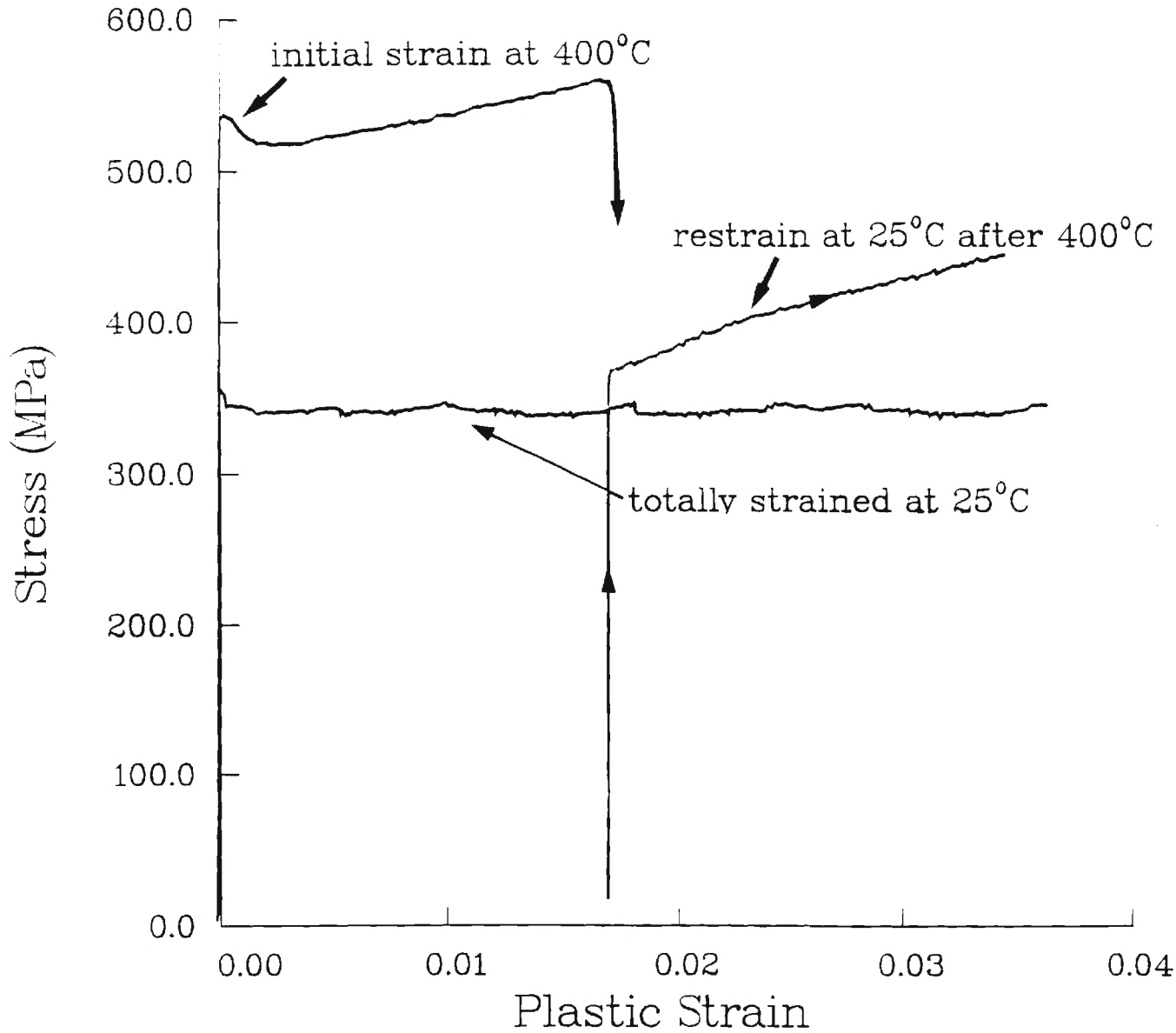

Figure 4.7 Results from Cottrell-Stokes experiment. Specimen was initially strained 2% at 400° C, then restrained at 25° C 2%. Results indicate partial irreversibility consistent with the observed increase in flow stress at 400°C.

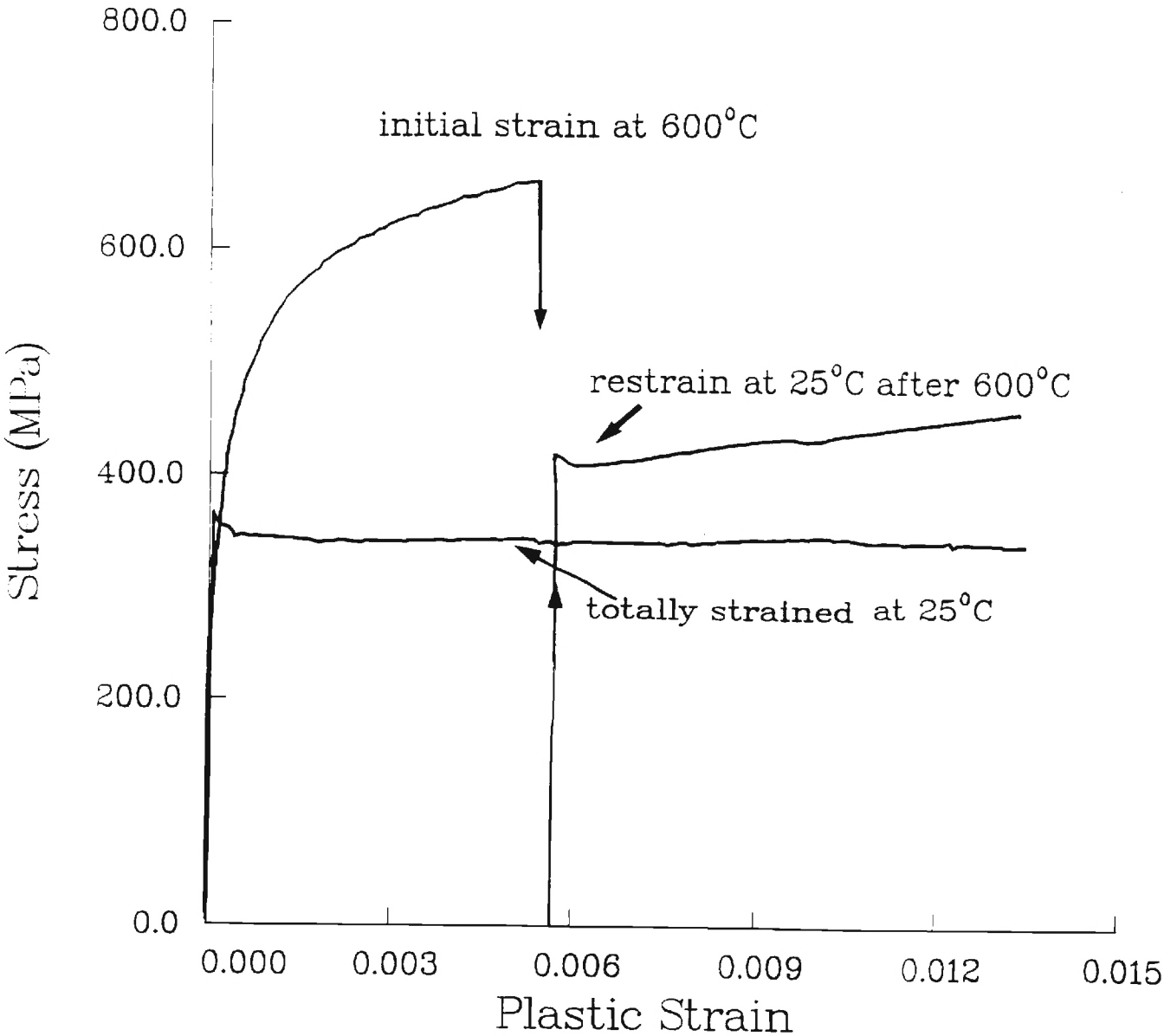

Figure 4.8 Results from Cottrell-Stokes experiment. Specimen was initially strained 1% at 600° C, then restrained 1% at 25°C. Irreversibility is related to the presence of dislocations on cube planes which gives rise to the observed irreversibility.

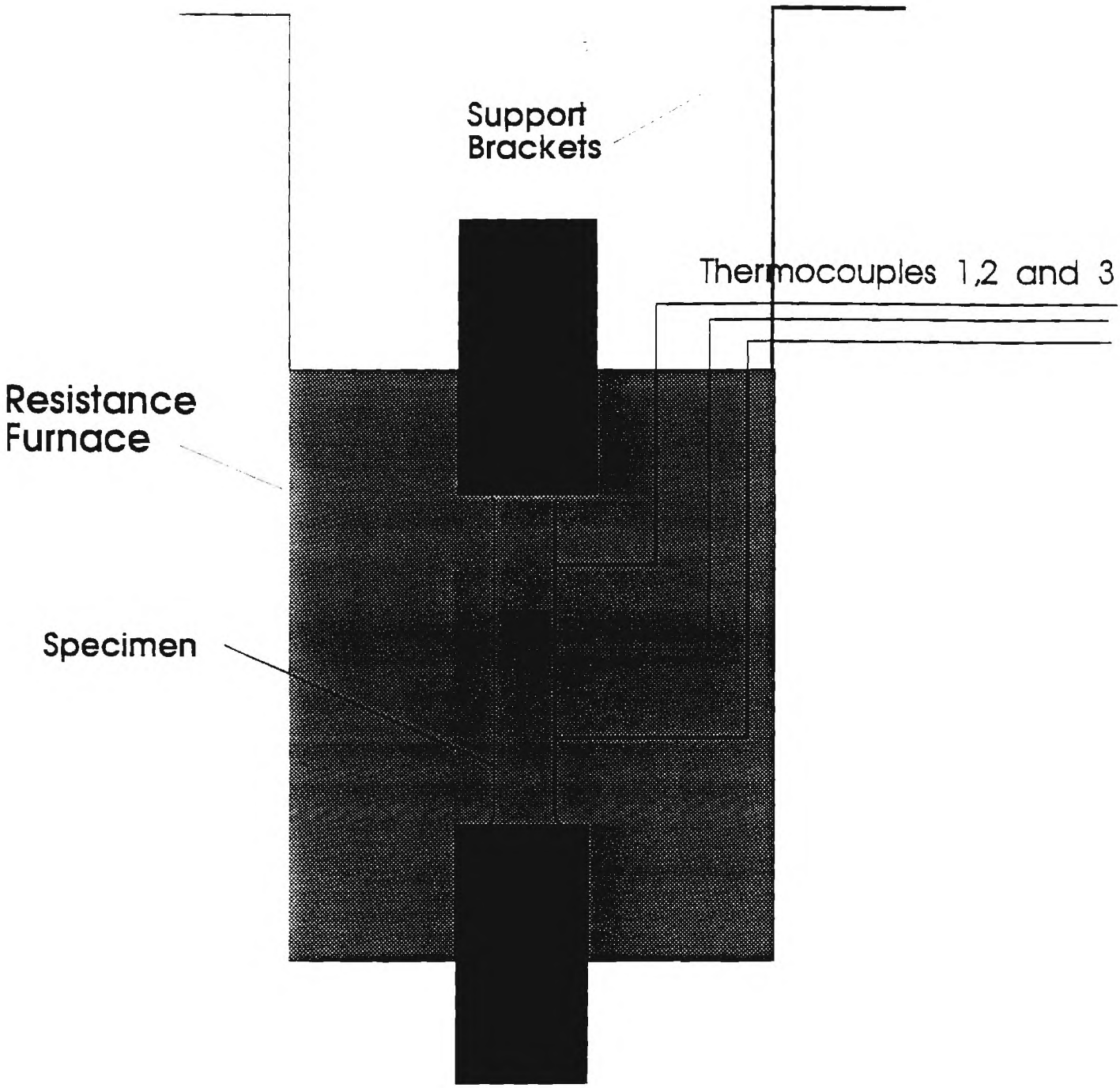

Figure 5.1 Configuration of furnace and specimen during elevated temperature tensile testing in a vacuum environment.

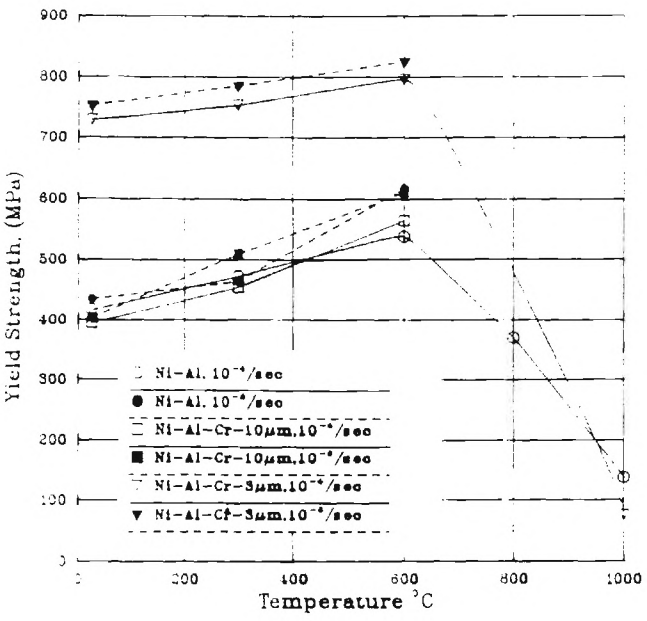

A.

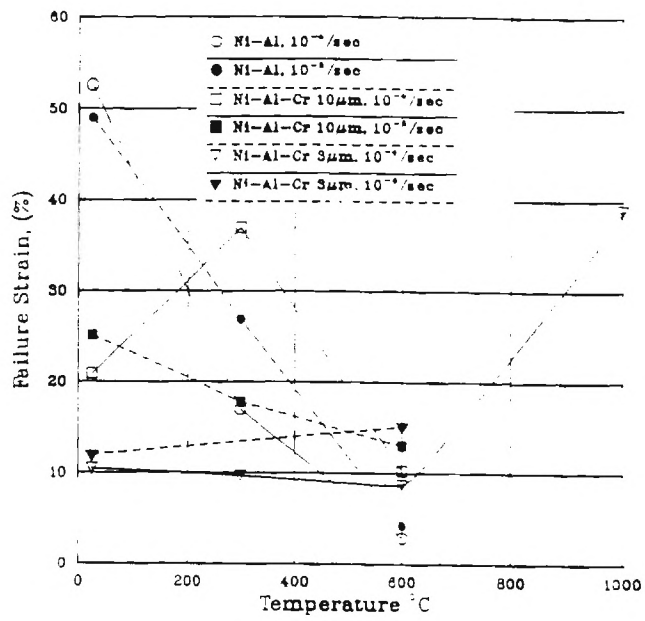

B.

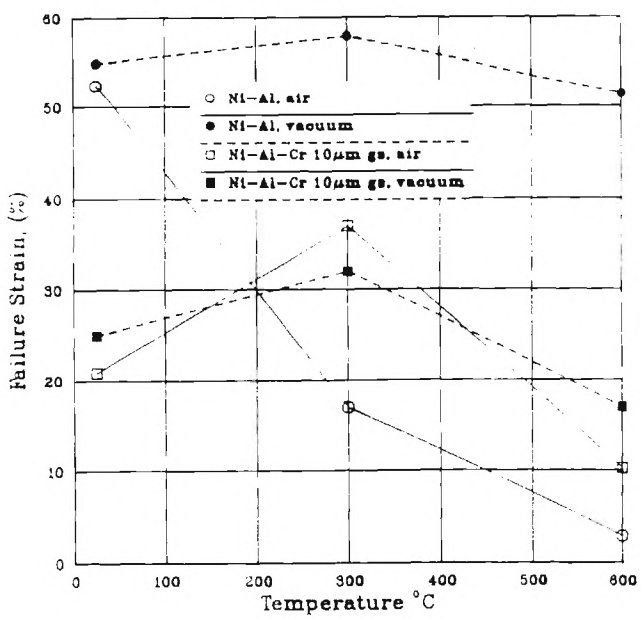

C.

Figure 5.2 Temperature dependence of monotonic properties of the experimental alloys. (a) Yield Strength (b) Elongation to failure in air (c) Elongation to failure in vacuum and air.

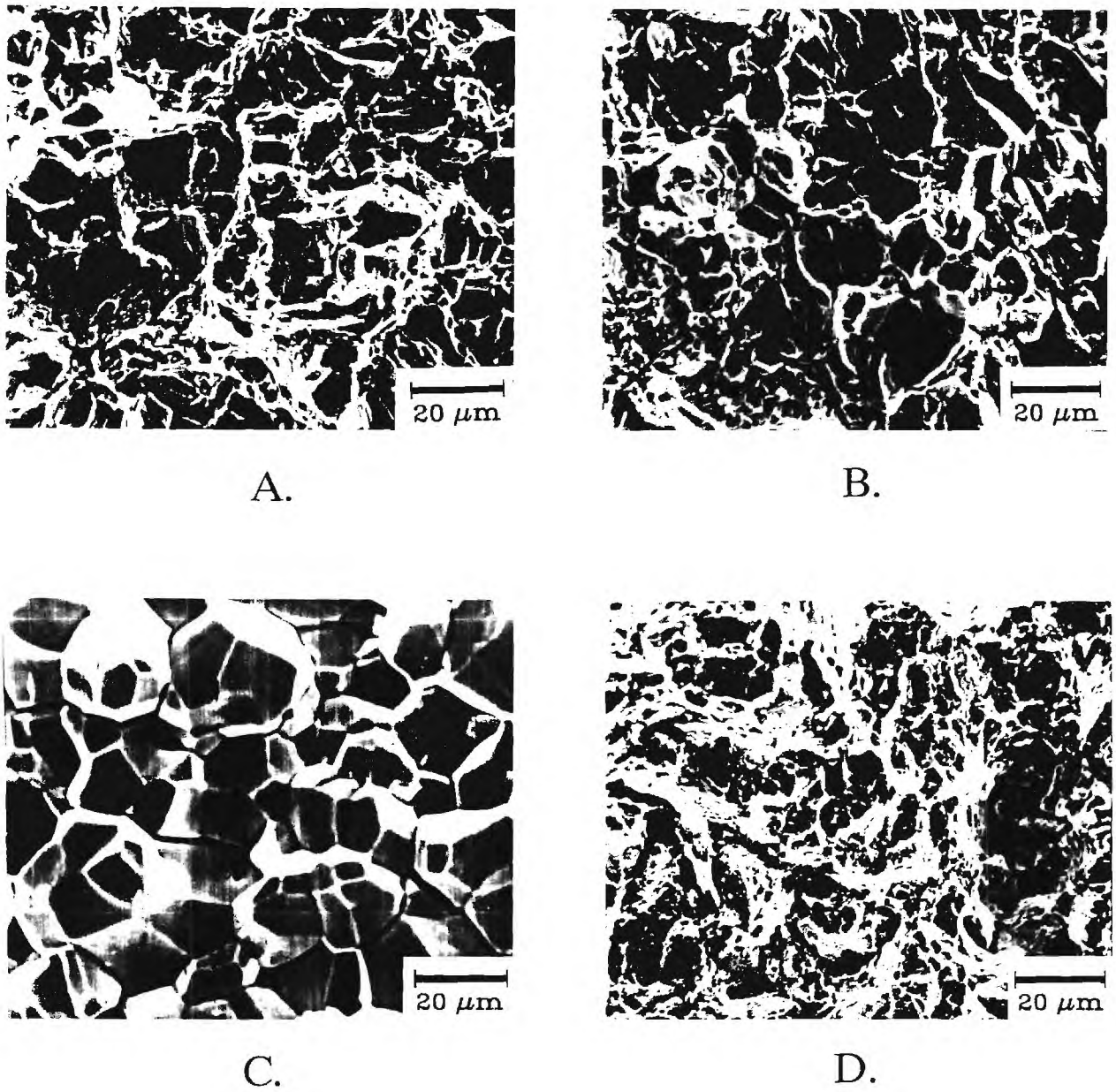

Figure 5.3 Changes in tensile fracture surface morphology of the binary alloy with temperature and environment. (a) 25°C, air (b) 300°C, air (c) 600°C, air (d) 600°C, vacuum.

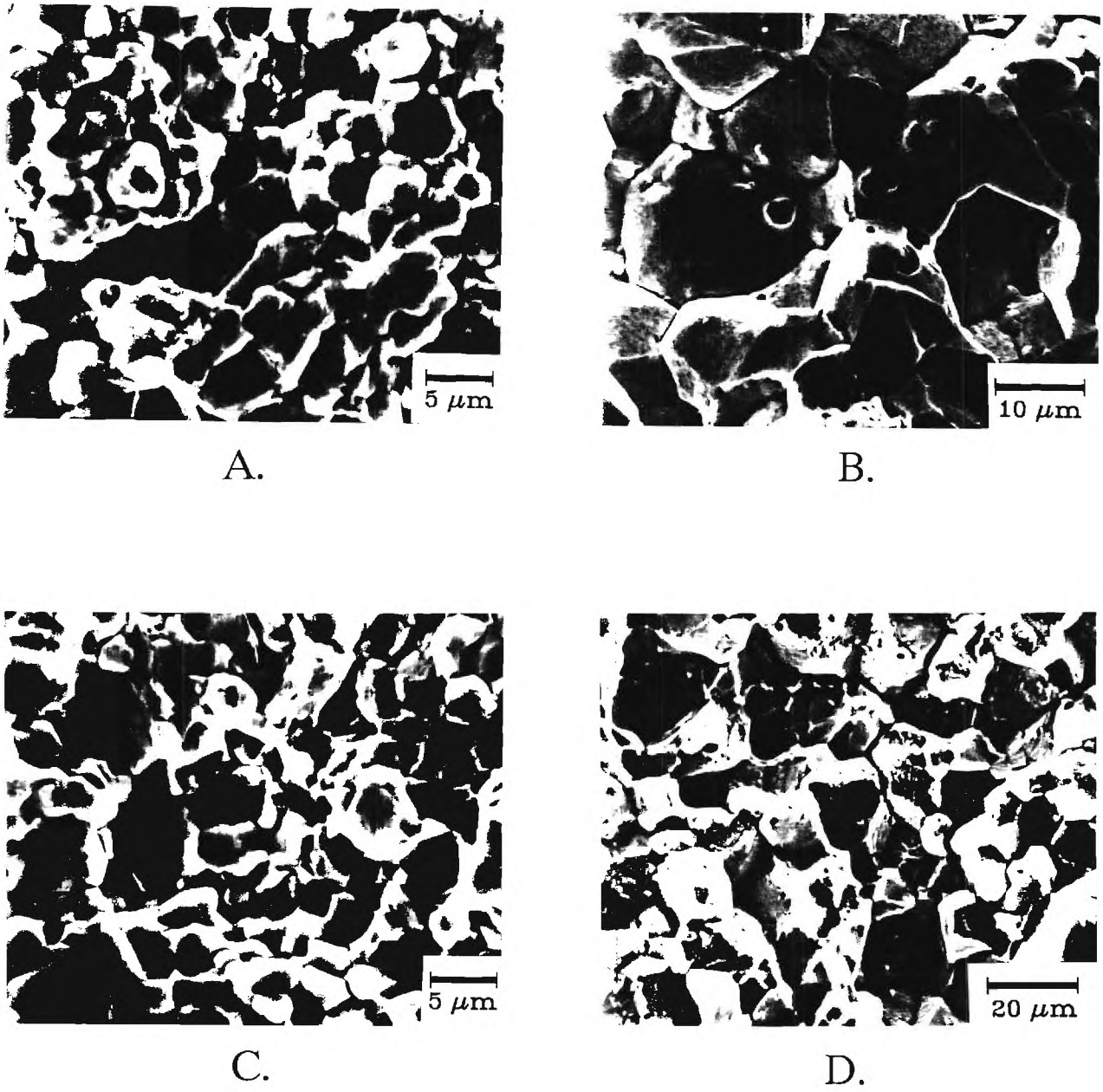

Figure 5.4 Fracture surface morphology of ternary alloys as a function of temperature and grain size. (a) 25°C, 3.5μm gs (b) 25°C, 10.1μm gs (c) 600°C, 3.5μm gs (d) 600°C, 10.1μm gs.

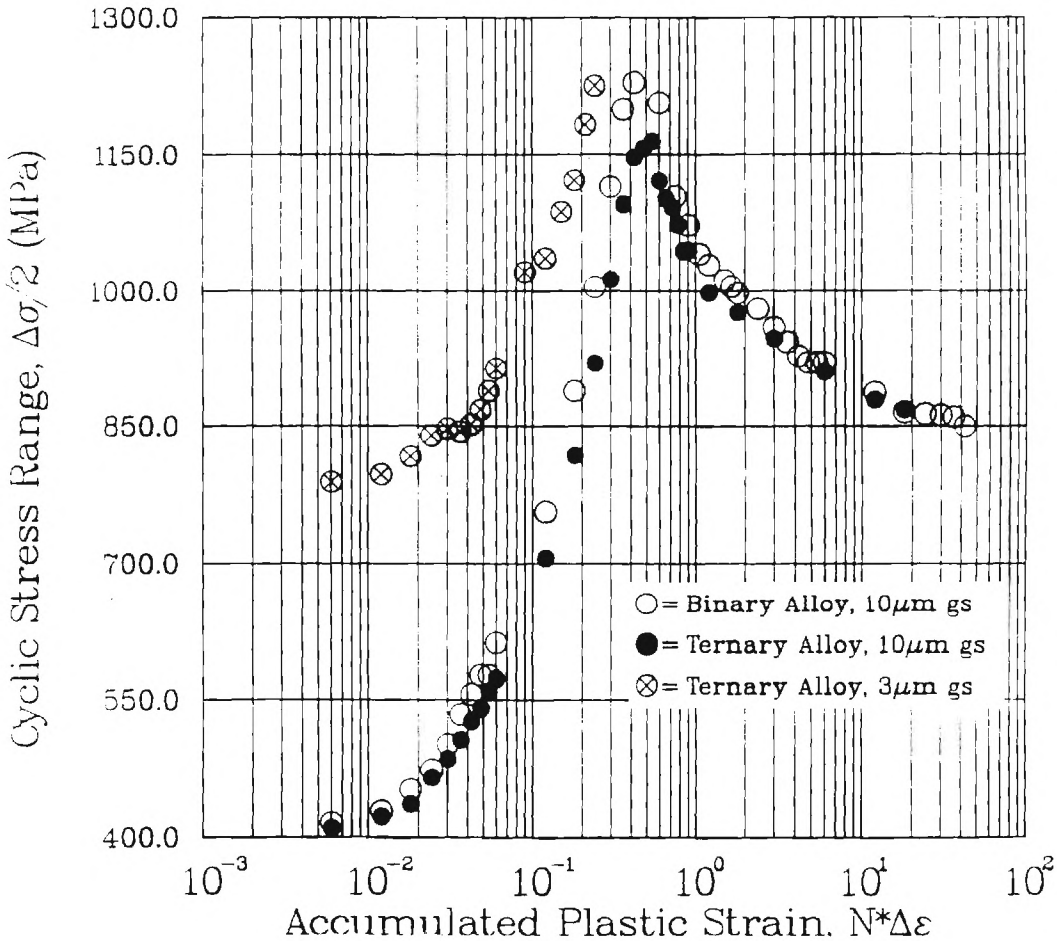

Figure 6.1 Cyclic hardening and softening characteristics at 25°C of experimental Ni_3Al alloys. The mean cyclic stress range is plotted verse the accumulated plastic strain to fracture.

1 Reversal

A.

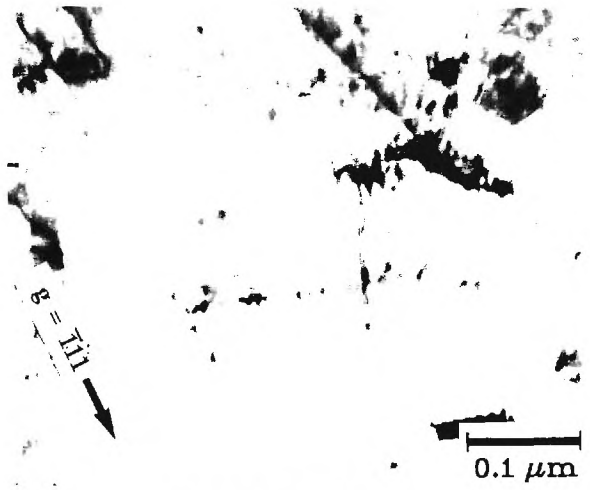

30 Reversals

B.

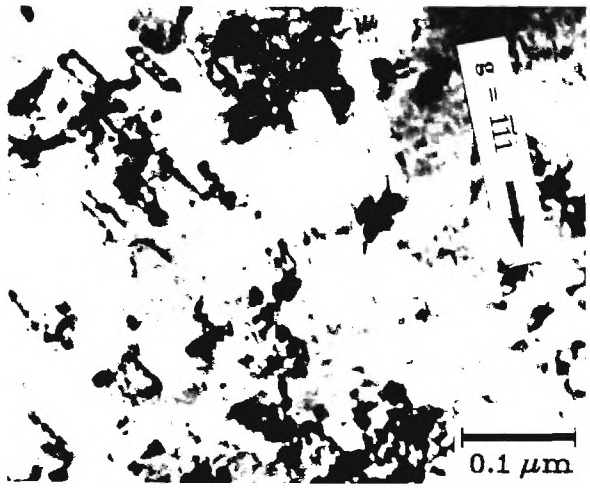

100 Reversals

C.

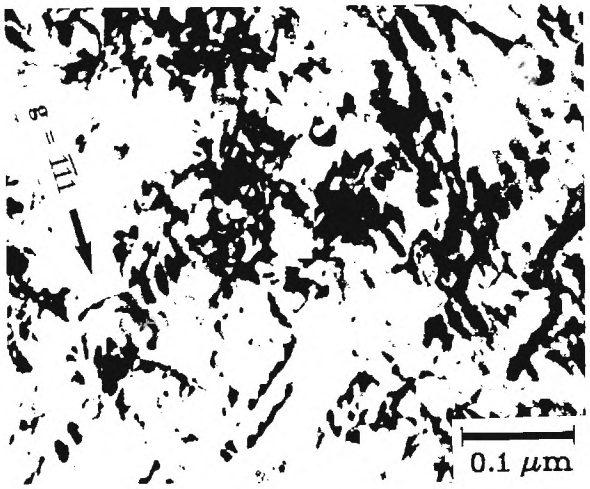

Figure 6.2 Characteristics of deformation in Ni_3Al during cyclic hardening at ambient temperature. TEM photomicrographs all utilize **g** = <111>, for maximum visibility of dislocations with **b** = <110>. Note the increasing density of faulted SISF loops (a) 1 reversal, $\Delta\epsilon_p$ = 0.006 (b) 10 reversals, $\Delta\epsilon_p$ = 0.006 (c) 100 reversals, $\Delta\epsilon_p$ = 0.006.

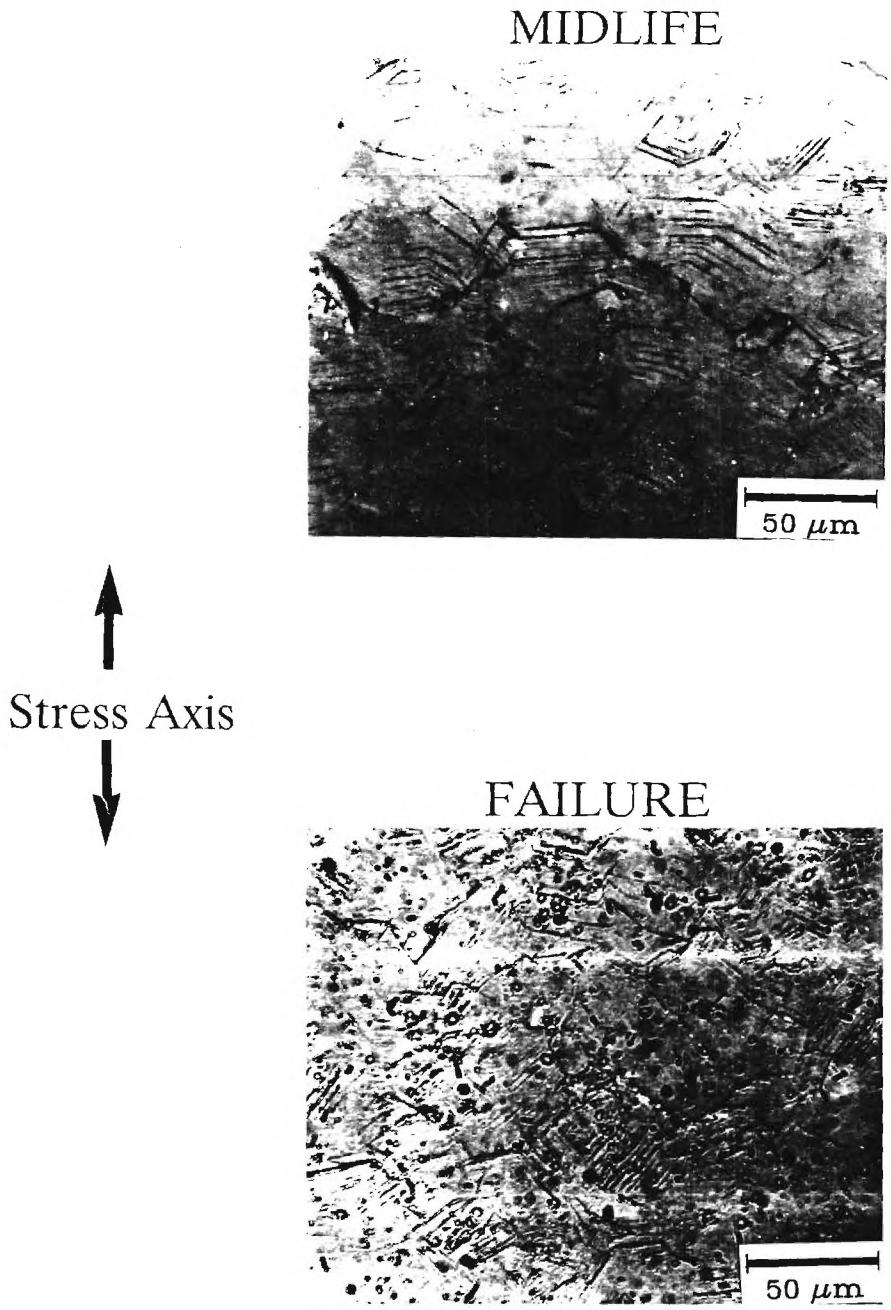

Figure 6.3 Characteristics of deformation during softening in Ni_3Al at ambient temperature. Replication of specimen surfaces at midlife and failure indicating planar slip traces which result in crack nucleation.

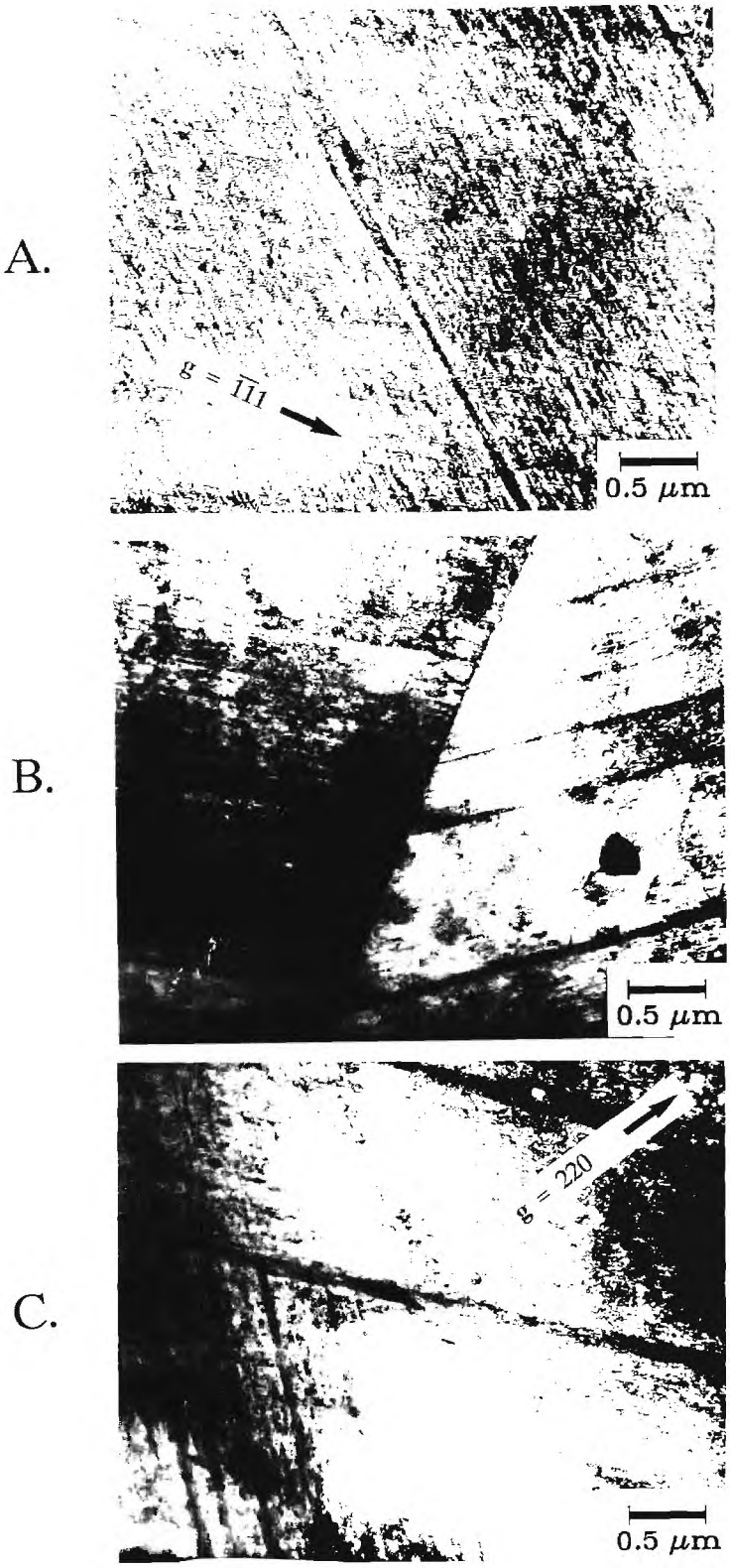

Figure 6.4 Characteristics of deformation during softening in Ni_3Al at ambient temperature. TEM investigation of slip bands reveal. (a) slip bands passing through homogeneous distribution of SISF loops (b) Slip band intersection at grain boundaries (c) Slip band intersection within grains.

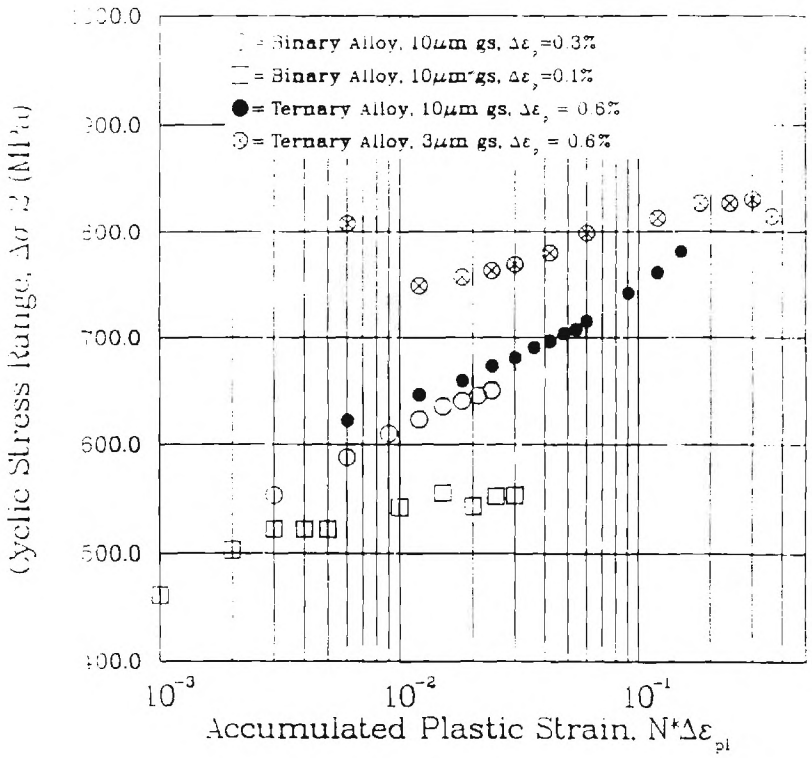

A.

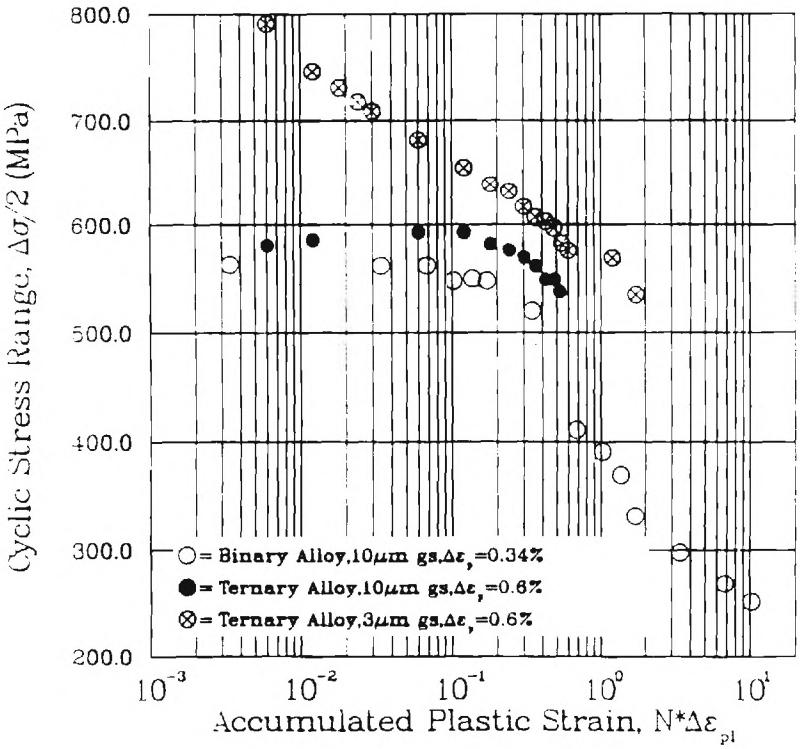

B.

Figure 6.5 Cyclic hardening and softening characteristics at 600° C of experimental Ni_3Al alloys when tested at strain rates of (a) 10^{-2}/sec and (b) 10^{-4}/sec.

A.

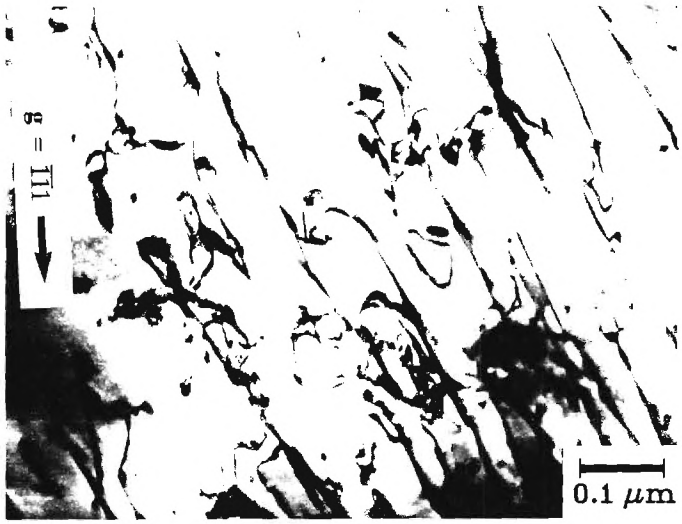

B.

Figure 6.6 Characteristics of deformation during deformation of Ni_3Al at 600° C at strain rates of (a) 10^{-2}/sec and (b) 10^{-4}/sec.

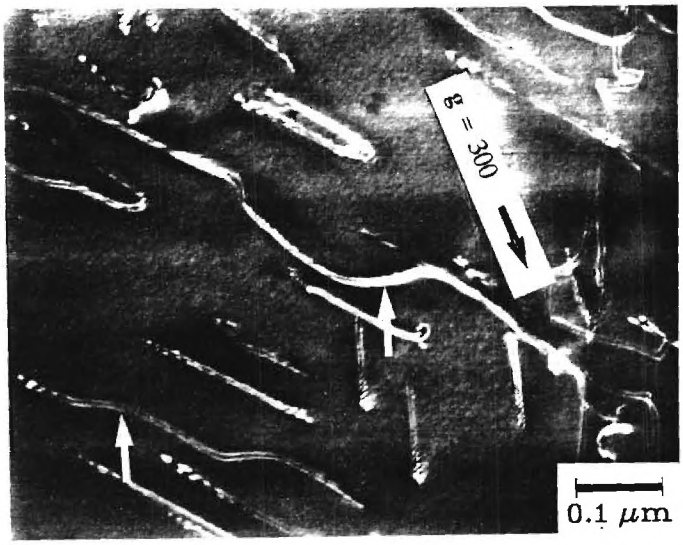

A.

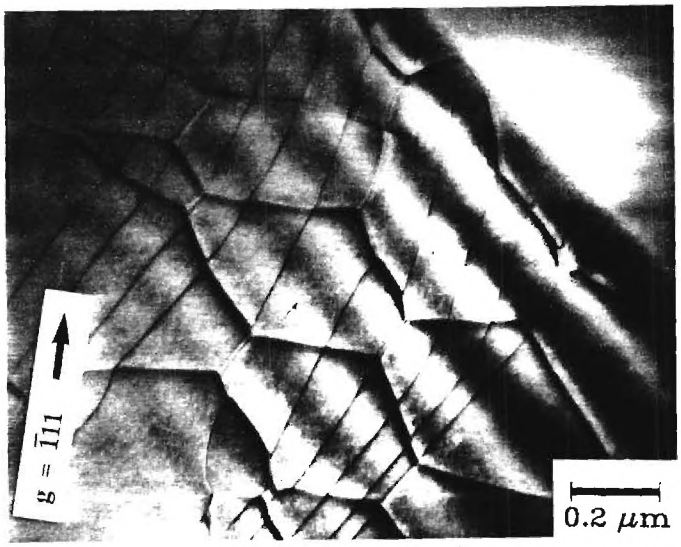

B.

Figure 6.7 Indications of thermally activated dislocation motion during deformation of Ni_3Al at 600° C at a rate of 10^{-4}/sec. (a) weak beam **g** = [100], bowing of screw dislocations onto cube planes arrows [**B** = 010]. Grain boundary dislocation networks.

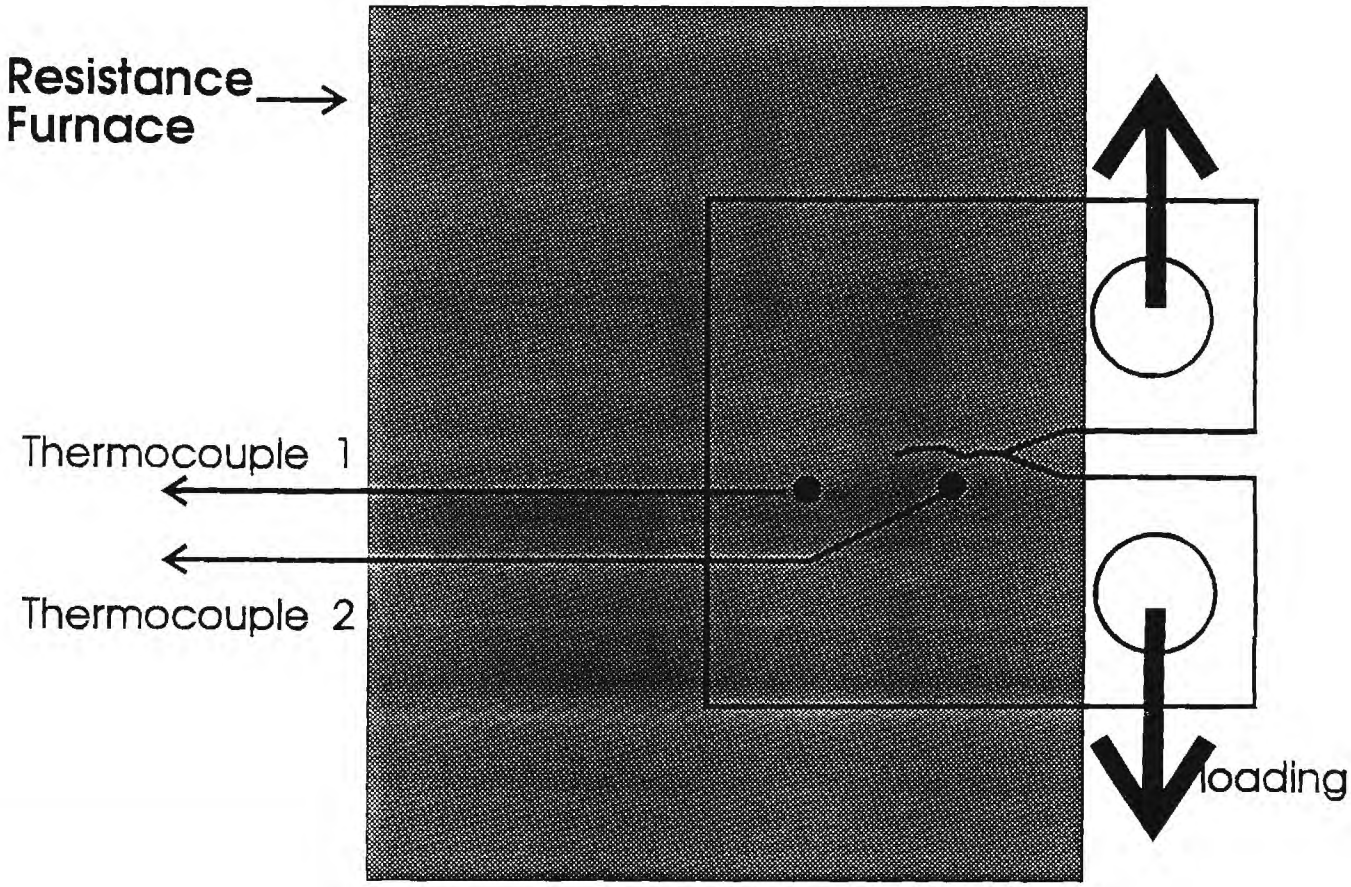

Figure 7.1 Schematic configuration of furnace, specimen and thermocouples during fatigue crack propagation testing in vacuum environments

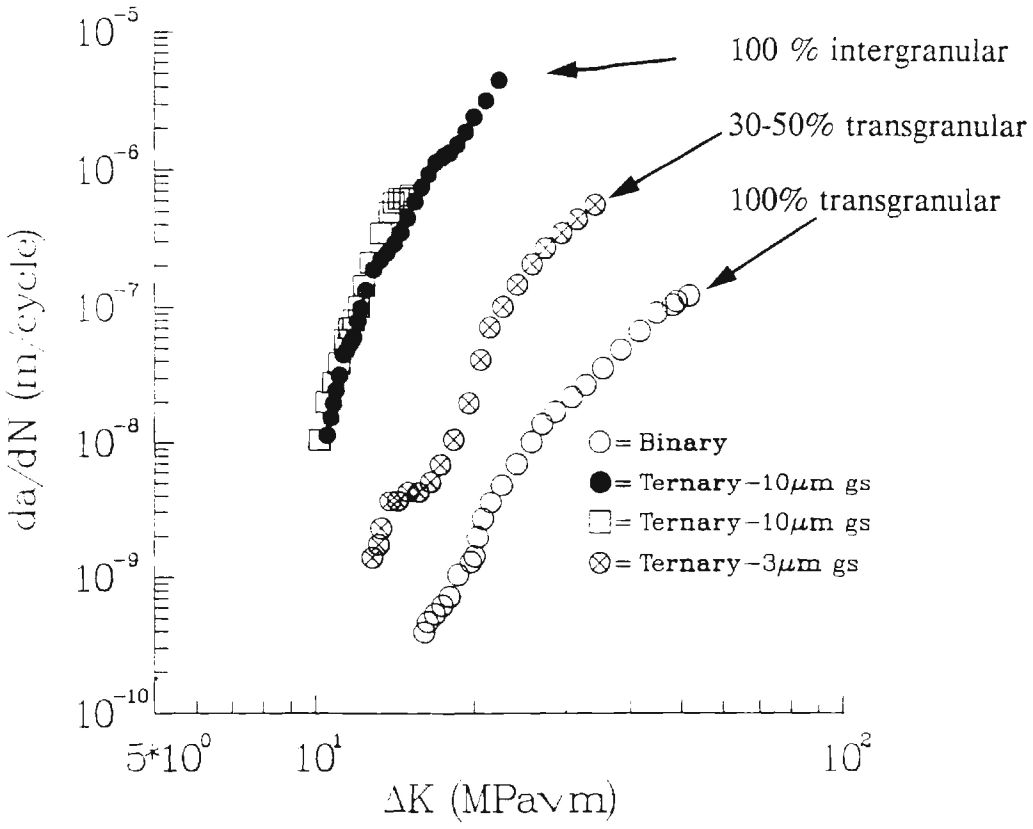

Figure 7.2 Fatigue crack growth rates of the binary and ternary alloy, 25°C, air, R=0.1, ν = 10 Hz.

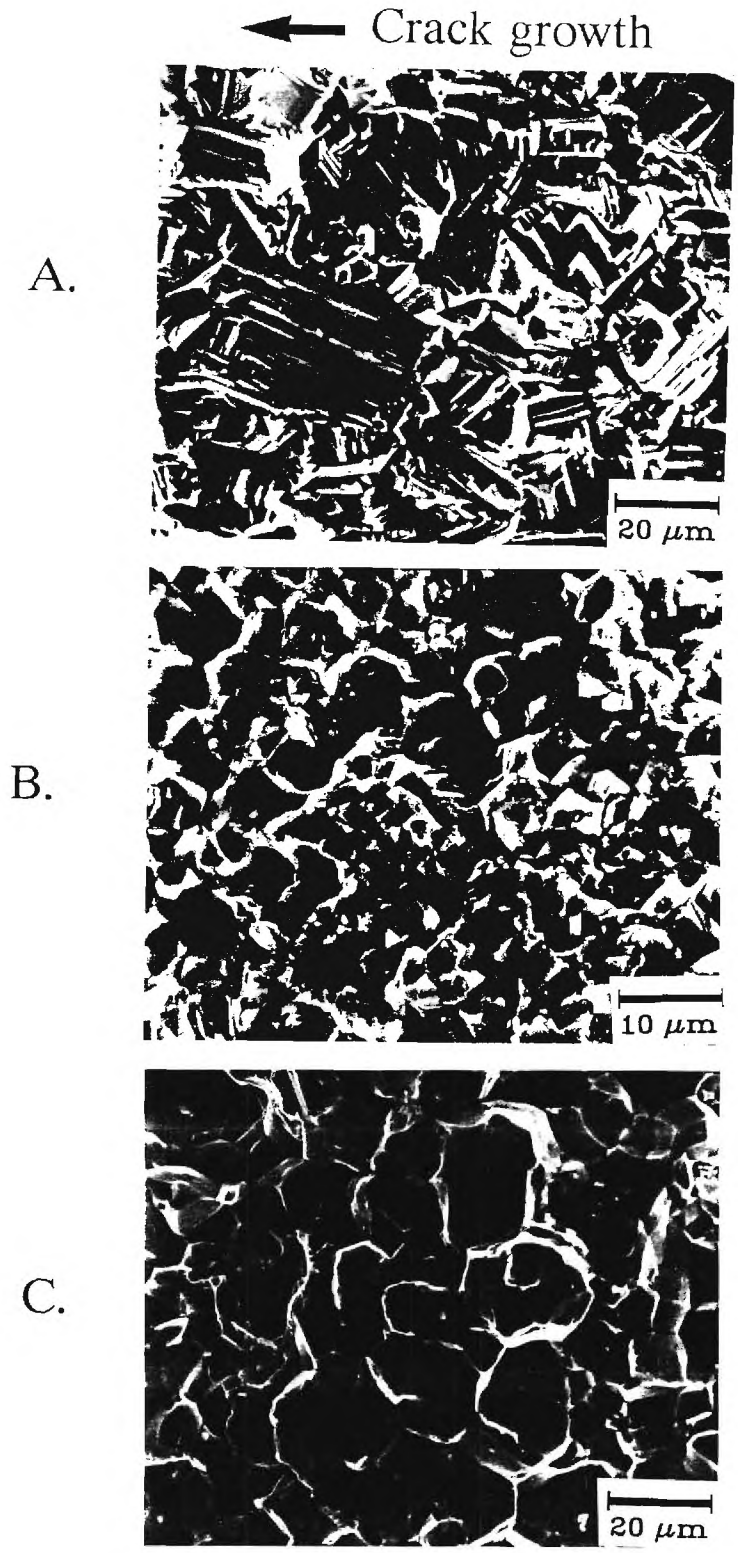

Figure 7.3 Fracture surface morphology of ambient temperature fatigue crack growth. (a). binary Ni-Al (b) ternary Ni-Al-Cr, 3.5μm grain size (c) ternary Ni-Al-Cr, 10.1μm grain size.

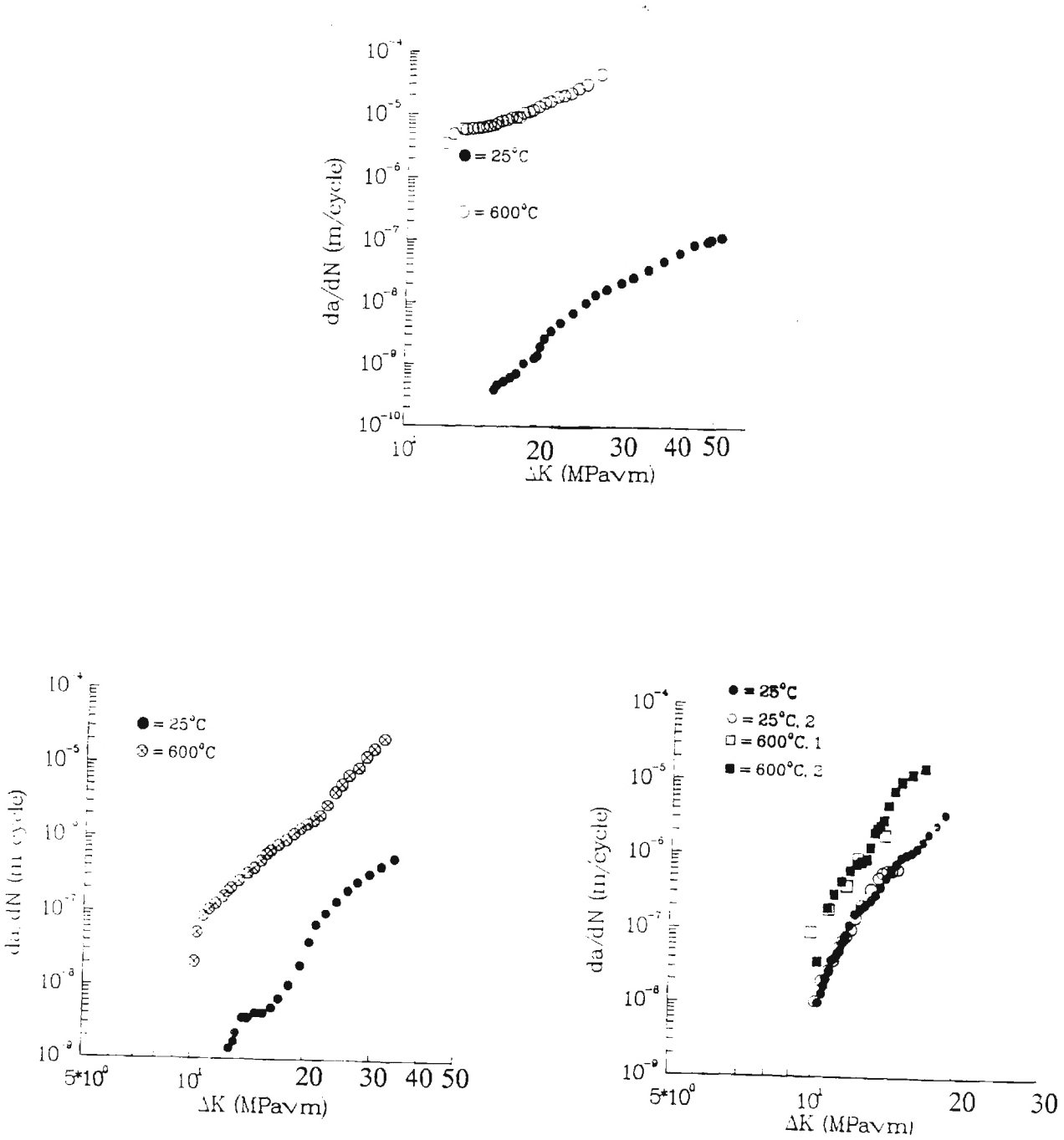

Figure 7.4 Temperature dependence of fatigue crack growth resistance in experimental binary and ternary alloys. (a) binary alloy Ni-Al, (b) ternary alloy Ni-Al-Cr, 3.5μm gs, (c) ternary alloy Ni-Al-Cr 10.1μm

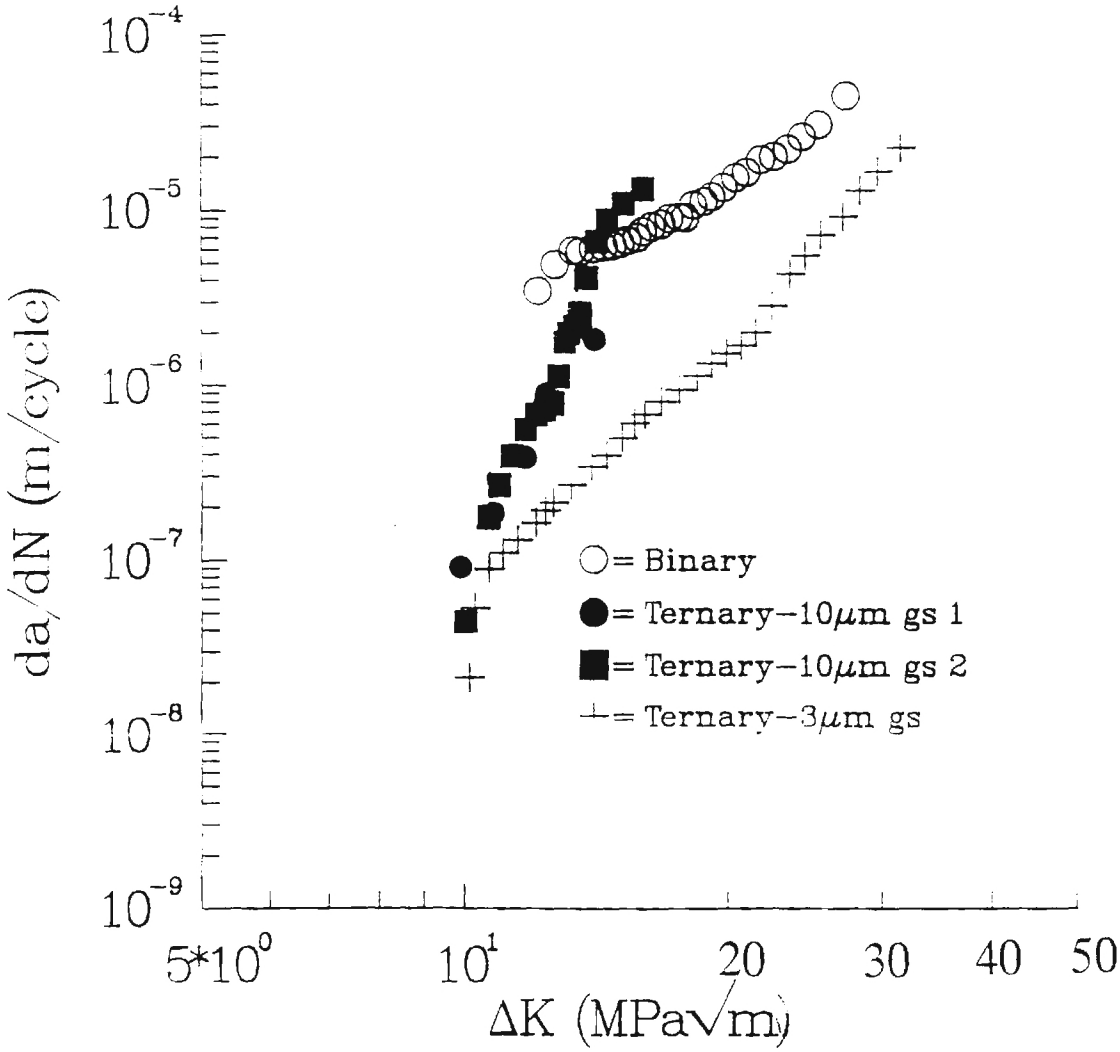

Figure 7.5 Comparison of fatigue crack growth rates at 600° C for binary and ternary alloy.

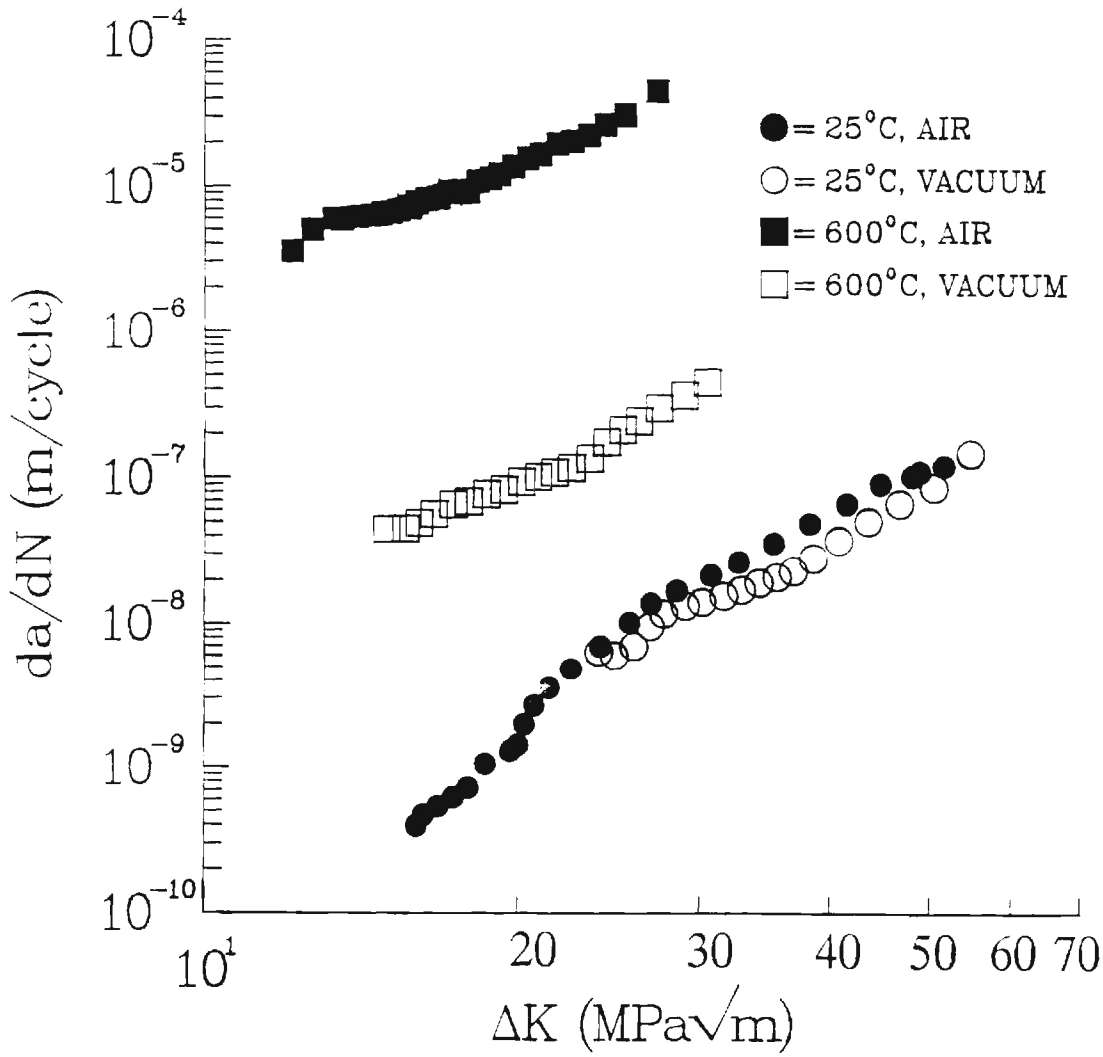

Figure 7.6 Dependence of fatigue crack growth rate on test environment and temperature for the binary alloy.

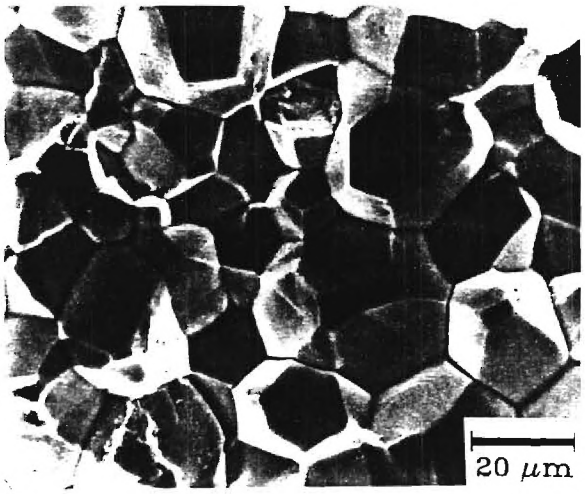

A.

← Crack Growth

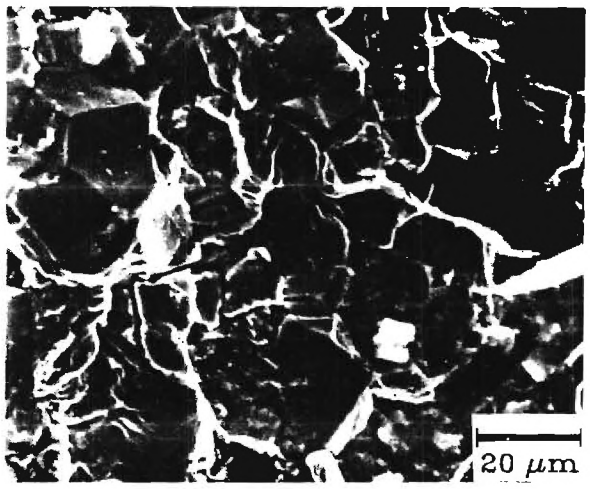

B.

Figure 7.7 Fracture surface morphology of fatigue crack growth of binary alloy at 600° C in (a) air and (b) vacuum.

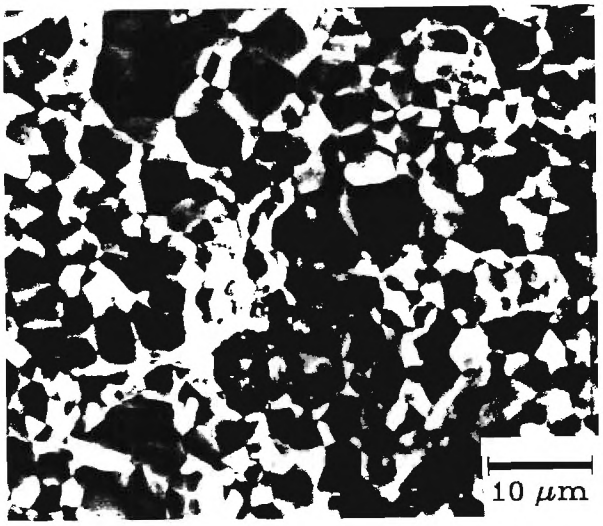

A.

Crack growth

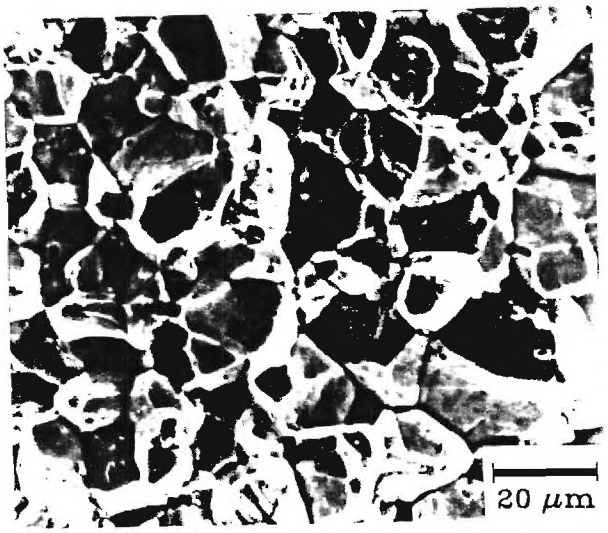

B.

Figure 7.8 Fracture surface morphology of fatigue crack growth of ternary alloy at 600° C (a) 3.5μm and (b) 10.1μm.